Universidad del País Vasco
Euskal Herriko Unibertsitatea
Instituto Biofisika Institutua

Doctoral thesis

Mechanistic details of apoptosis-regulatory proteins BAX and BFL1 at the membrane level

Hector Flores Romero

2017

Supervisor: Gorka Basañez Asua
Department of Biochemistry and Molecular Biology
Biophysics Institute (CSIC-UPV/EHU)

Acknowledgements

The candidate has been granted with a PhD fellowship from the Ministerio de Educación (2014-2017). This work has been supported by the Ministry of Science and Innovation (project BFU2011-28566/BMC).

SPEAK ONLY IF IT IMPROVES UPON THE SILENCE

INDEX

Common abbreviations and symbols:

A555	Alexa fluor-555
ANTS	8-aminonaphtalene-1,3,6 trisulfonate (ANTS)
APC	Allophycocyanin
BAK	BCL-2 Associated Killer protein
BAX	BCL-2 Associated X protein
BCL2	B-cell CLL/lymphoma 2
BCLXL	B-cell lymphoma-extra large
BFL1	Bcl-2-related protein A1
BH	BCL-2 homology domain
BID	BH3 interacting domain death agonist (full-length protein)
BIM	BCL2-interacting mediator of cell death
BSA	Bovine Serum Albumin
cBID	Caspase-8-cleaved BID (p7 (t^{n}BID) and p15 (t^{c}BID) fragments)
CD	Circular dichroism
CHAPS	3-[(3-Cholamidopropyl)dimethylammonio]-1-propanesulfonate
CHOL	Cholesterol
CL	Cardiolipin
CS	Contact sites
CuPhe	Copper (II) $(1,10\text{-fenantrolina})_3$
Cyt c	Cytochrome c
DAG	Diacylglycerol
DLS	Dynamic Light Scattering
DPX	p-xylene-bis-pyridinium bromide
FITC	Fluorescein isothiocyanate

GST	Glutathione S-transferase
GUV	Giant unilamellar vesicle
HRP	Horseradish peroxidase
IMS	Inter membrane space
KHE	100mM KCl, 10mM Hepes, 1mM EDTA, pH 7.4
LPC	Lysophosphatidylcholine
LUV	Large unilamellar vesicle
MCL	Monolysocardiolipin
mCL	Myristoylated cardiolipin
MCL-1	Myeloid Cell Leukemia-1
MIM	Mitochondrial inner membrane
MLV	Multilamellar large vesicle
MOM	Mitochondrial outer membrane
MOMP	Mitochondrial outer membrane permeabilization
NMR	Nuclear Magnetic Resonance
OG	octyl ß-D-glucopyranoside
PA	Phosphatidic acid
PBS	Phosphate Buffered Saline
PBT	Phosphate-buffered saline with Tween 20
PC	Phosphatidylcholine
PE	Phosphatidylethanolamine
PEGMAL	Methoxypolyethylene glycol maleimide
PI	Phosphatidylinositol
PS	Phosphatidylserine
PUMA	p53 up-regulated modulator of apoptosis

Rh	Rhodamine
SD	Standard Deviation
SE	Standard Error
SEC	Size exclusion chromatography
SUV	Small Unilamella Vesicle
TA	Tail anchored
tBID	Truncated-BH3 interacting domain death agonist (p15 active fragment, also known as t^cBID)
TCEP	Tris (2-carboxyethyl) phosphine
TX100	Triton-X 100
$\Delta\pi$	Increase in the surface pressure
λ	Wavelength
π	Surface pressure
π_0	Initial surface pressure
π_c	Critical pressure

CHAPTER 1:

Introduction and Objectives

1 Introduction and Objectives

1.1 MITOCHONDRIA

Mitochondria are essential organelles for eukaryotic cells. They are partially autonomous organelles, as they harbor their own DNA, RNA and protein synthesizing machinery. Furthermore, mitochondria are also capable of synthetizing some lipids on their own (Horvath & Daum, 2013). The mitochondrion is thought to have a bacterial evolutionary origin and it has become perhaps in the ultimate symbiont. This hypothesis is backed by substantial experimental evidence, including the similarities between the bacterial and mitochondrial DNA and the translational apparatus (Kutik et al, 2009). In addition, mitochondria also have a unique and quite complex membrane system, which is the basis for their numerous intricate functions (Harner et al, 2011). Concretely, these organelles are surrounded by an envelope composed by the outer (MOM) and inner (MIM) mitochondrial membranes.

The MOM has been assumed to be relatively permeant to small molecules and ionic species. In contrast, the MIM is largely impermeable and forms the mayor barrier between the cytosol and the mitochondrial matrix. The MIM is considered to be the most protein-rich cellular membrane, containing proteins and protein complexes that are essential for the normal mitochondrial function. This MIM can be further divided into the inner boundary membrane (IBM), which is in continuous and close apposition to the MOM, and the cristae membrane (CM). Cristae are invaginations of the IBM that protrude to the matrix. Cristae and IBM are connected by narrow tubular structures called cristae junctions (CJ) (Reichert & Neupert, 2002). The space between the MOM and the MIM is called intermembrane space (IMS), and it is rather narrow in comparison to the space between cristae sheets, also called intracristae space (ICS). Furthermore, there are sites of firm interaction between MOM and IBM that may be necessary for the structural organization of mitochondrial membranes. These connections have been termed mitochondrial contact sites (CS) (Figure 1.1).

With the appearance of the first transmission electron microscopy TEM-images of mitochondria, it was observed these organelles can assume a wide variety of morphologies. After some extensive studies, it was suggested that these mitochondrial membrane shape changes might not be random, but rather might reflect a novel regulatory mechanism of the organelle. Indeed, it is now assumed that mitochondrial functions can be affected by changes in mitochondrial membrane topology (Mannella, 2006a; Mannella, 2006b). Moreover, (Scorrano et al, 2002) proposed that the MIM topology could also be implicated in the apoptotic process.

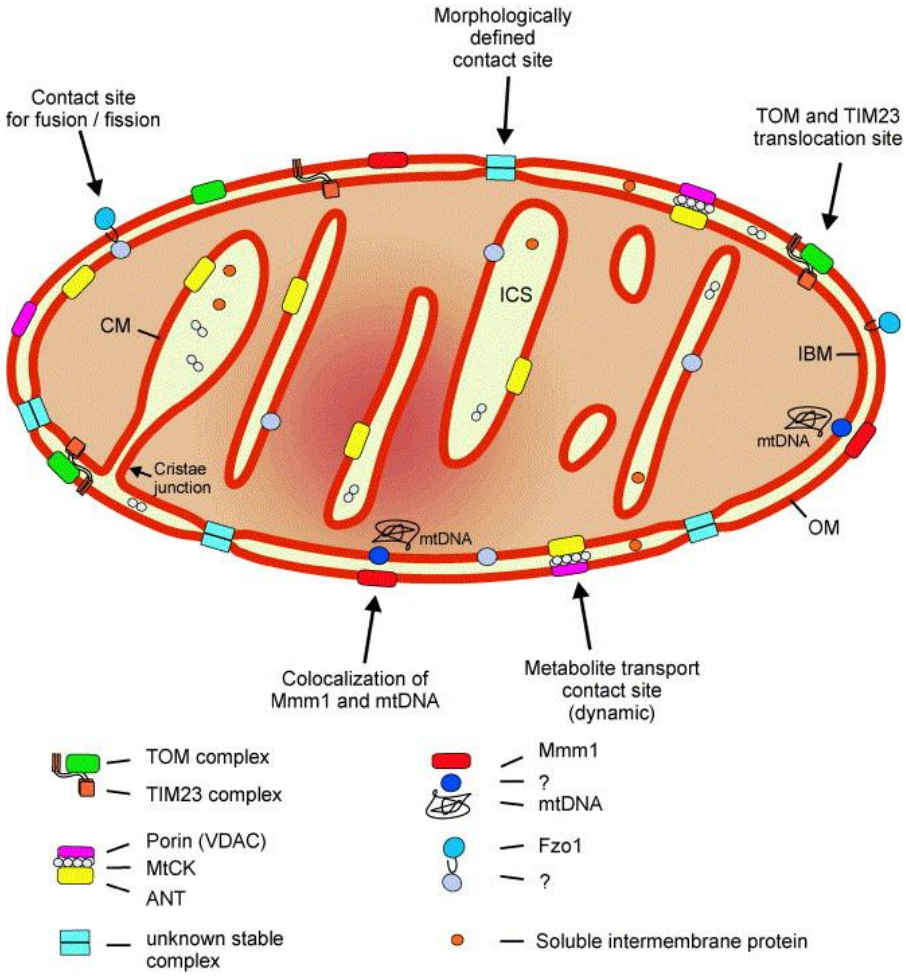

Figure 1.1 Different components of mitochondria. This represents a cross section of a (non-existing) composite mitochondrion based on data from different organisms. Cristae are connected to the inner boundary via narrow tubular structures, called cristae junctions—only one of them is visible in this cross-section. OM, outer membrane; IBM, inner boundary membrane; CM, cristae membrane; ICS, intracristal space. Image taken from (Reichert & Neupert, 2002).

Specifically, they showed that tBID, a BCL2 family member protein (see at section 1.4), causes a rapid remodeling of the MIM, increasing the number of CJ and inverting the MIM curvature. This dramatic change in the MIM topology coincides with the enhanced mobilization of the internal cytochrome c (cyt c), a molecule that in the cytosol is directly associated with apoptotic cell death. Furthermore, it has been proposed that most of the cyt c is locked inside the cristae by the OPA1(Optic atrophy 1)-containing complexes located at the neck of the cristae and thus, disassembly of OPA1 complexes may be critical for the majority of cyt c to gain access to the IBM (Frezza et al, 2006). In this regard, it has been reported that the proapoptotic BCL2 family members BAX and BAK interact with mitochondrial CS during apoptosis to affect MOM permeability and induce activation of a novel MIM protease termed OMA1. These interactions between BAX/BAK and CS leads to enhanced OMA1 protease activity, resulting in accelerated autodegradation of OPA1 and thereby facilitating cyt c release and apoptotic pathway (Jiang et al, 2014).

1.2 MITOCHONDRIAL DYNAMICS

Mitochondria are reticular organelles that have high plasticity for their dynamic structures and constantly undergo fission and fusion as well as movement through the cytoskeleton. As previously mentioned, mitochondrial morphology changes are determined by a balance between mitochondrial fusion and fission events, collectively known as mitochondrial dynamics. Perturbations on mitochondrial dynamics can have tremendous consequences on cell metabolism and therefore on cell life. Indeed, the importance of fission and fusion homeostasis has been highlighted by a number of diseases linked to an imbalance between these two processes. Mitochondrial fusion allows mitochondria to exchange their content including the mtDNA and proteins between individual mitochondria, whereas mitochondrial fission allows for mitochondrial biogenesis, and the segregation of damaged and inactive mitochondria by autophagic clearance (Diaz & Moraes, 2008). The main components of the mitochondrial fission and fusion machinery belong to the Dynamin superfamily. In mammals, outer membrane fusion is regulated by Mitofusins 1 and 2 (MTF1 and MTF2), while inner membrane fusion process is controlled by OPA1 and organelle division or fission is mediated by DRP1 (Figure 1.2).

Interactions between mitochondria and the cytoskeleton are essential for normal mitochondrial morphology, motility and distribution. While microtubules and their motors have been established as important factors for mitochondrial transport, emerging evidence indicates that mitochondria interact with the actin cytoskeleton in many cell types (Boldogh & Pon, 2006). Moreover, close appositions between mitochondria and the ER have been observed by electron microscopy. The close contacts between these organelles are referred as mitochondria-associated ER membranes (MAM) (Giorgi et al, 2009; Vance, 1990). These contiguous membranes contain multiple phospholipid- and glycosphingolipid- synthesizing enzymes and support direct transfer of lipids between ER and mitochondria (Stone & Vance, 2000). MAMs play important roles in mitochondrial morphology and in many cellular functions ranging from lipid metabolism, to calcium signalling and apoptosis (Doghman-Bouguerra & Lalli, 2017). MAM regions are zones enriched in Inositol Triphosphate Receptors (IP3Rs), and are thus considered “hotspots” of Ca^{+2} transfer from ER to mitochondria (Rizzuto et al, 1998). Remarkably, mitochondrial Ca^{+2} accumulation may play a role in determining the outcome of the cell (Duchen et al, 2008) (Figure 1.2). Indeed, studies several organisms have revealed that mitochondrial dynamics appear to be subject to regulation by the same proteins that regulate apoptosis, including BCL2 family proteins (Aouacheria et al, 2017).

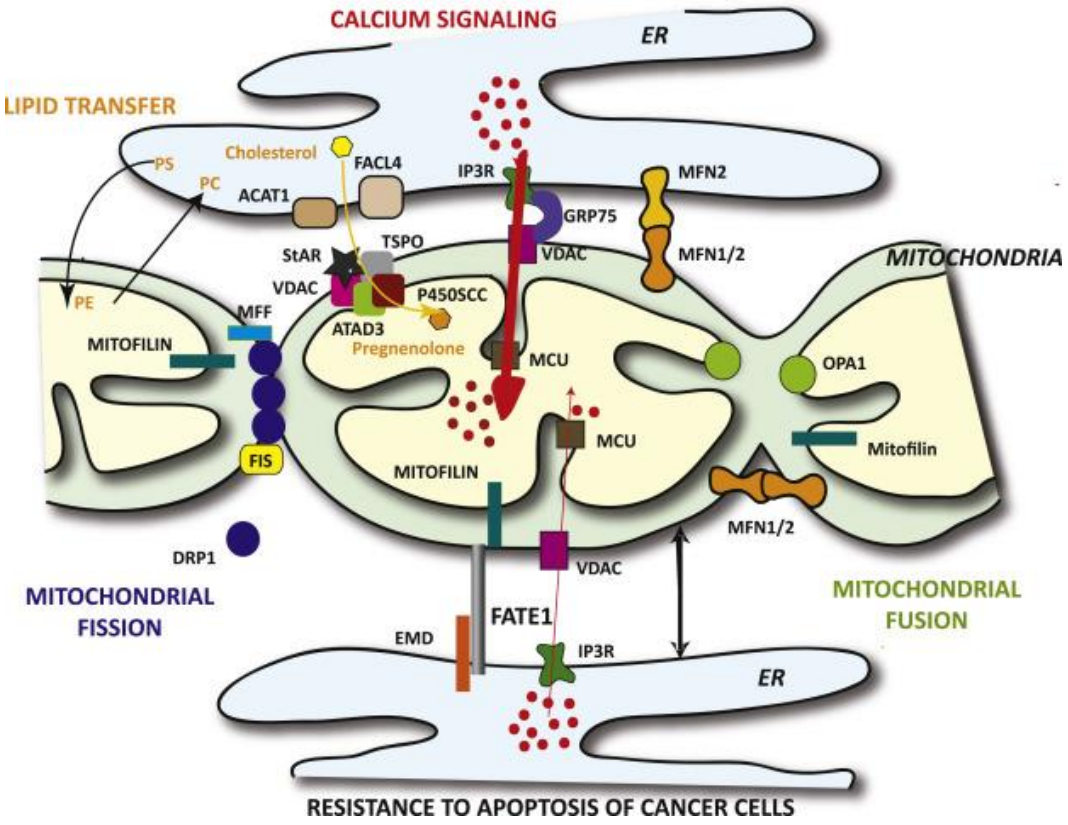

Figure 1.2 MAM proteins involved in ER-mitochondria Ca^{2+}signaling, lipid transfer and mitochondrial morphology. Some proteins localized in MAMs (IP3R, VDAC, GRP75) regulate Ca^{2+} release from the ER for an efficient mitochondrial Ca^{2+} uptake. MAMs play an important role in phospholipid shuttling between ER and mitochondria such as Cholesterol, PS, PE and CL. Mitochondrial morphology is regulated by Mitofusins 1/2, OPA1 and DRP1. Taken from (Doghman-Bouguerra & Lalli, 2017).

1.3 ROLE OF MITOCHONDRION IN CELL DEATH

As described above, in healthy cells, the main function of mitochondria is the production of energy by oxidative phosphorylation and the maintenance of Ca^{+2} homeostasis. However, mitochondria are also actively implicated in cell death closely involved, among others, in necrotic and apoptotic processes.

1.3.1 Necrotic cell death

During classical necrotic death, the cell becomes physically or chemically stressed until the point that it cannot maintain its integrity and it finally swells, bursts and decomposes in a passive and unorganized manner. As a consequence, necrosis is typically associated with disruption of the plasma membrane, major organellar structural changes including mitochondrial swelling, release of intracellular contents and inflammation of the surrounding tissue. Thus, this type of cell death

is usually considered "non-programmed" and does not present specific biochemical markers (Kroemer et al, 2009). However, recent investigations have shown that under specific conditions necrotic death can occur in a genetically encoded and organized manner, rather than being an accidental process (Christofferson & Yuan, 2010; Galluzzi & Kroemer, 2008). This programmed necrosis process has also been termed necroptosis and involves activation of death receptors such as FAS or TNF, calcium cross-talk between ER and mitochondria, mitochondrial depolarization and ATP depletion, among other regulated events. Interestingly, certain BCL2 family members have been implicated in necroptosis regulation (Dorn, 2013; Whelan et al, 2010).

A high m[Ca^{+2}] in combination with other characteristics, such as, oxidative stress, high inorganic phosphate concentration (ATP depletion) and mitochondrial depolarization can lead to the opening of the mitochondrial permeability transition pore (mPTP). The mPTP is a pore whose exact structure is unknown, but it is thought to be composed by the adenine nucleotide translocator (ANT) in the MIM, the voltage dependent anion conductance (VDAC) in the MOM, and cyclophilin D, in the matrix, which confers sensitivity to the complex to cyclosporine A. Under pathological conditions, the mPTP is opened leading to a destruction of the mitochondrial potential, ATP consumption and energetic collapse, normally ending in a necrotic cell death (Duchen, 2000; Duchen, 2004; Krieger & Duchen, 2002; Osellame et al, 2012).

1.3.2 Apoptotic cell death

In addition to the role of mPTP in necrotic cell death, mitochondria are also actively implicated in apoptotic cell death. Apoptosis is a fundamental process of the entire animal kingdom (Metazoan), with millions of cells dying by apoptosis in the adult human body every second (Adams & Cory, 2007). Importantly, research done in apoptosis has also lead to the discovery that this type of cell death is not only essential for normal physiological developmental and homeostatic processes, but it is also crucial as a defensive strategy to remove infected, mutated, or damaged cells (Miura, 2011). Accordingly, defective apoptotic processes have been implicated in an extensive variety of human diseases (Adams & Cory, 2007; Strasser et al, 2011).

Morphologically, a cell dying via apoptosis is characterized by rounding-up of the cell, cell shrinking (pyknosis), nuclear condensation and fragmentation (karyorrhexis), membrane blebbing (maintaining its integrity until the final stages of the process) and finally, the separation of the cellular components into apoptotic bodies. Another typical feature of an apoptotic cell is the redistribution of phosphatidylserine (PS) from the inner to the outer leaflet of the plasma membrane, serving as a 'come and- get-me' signal to attract phagocytes to engulf the fragmented cell (Kroemer et al, 2005; Kroemer et al, 2009). The latter process allows rapid removal and clearance of apoptotic cells thereby avoiding immune activation and inflammation of surrounding tissue (Bevers & Williamson, 2010; Elliott & Ravichandran, 2010; Lauber et al, 2003).

In vertebrates, apoptosis can occur through two main pathways: the “extrinsic” or death receptor pathway and the “intrinsic” or mitochondrial pathway (Figure 1.3). Although the initial death signals are heterogeneous, both pathways ultimately lead to the activation of the executioner caspases (mainly caspases 3/7) that are responsible of the proteolytic cleavage of hundreds of different proteins within the cell, leading to the morphological features that define the apoptotic process (Green, 2005; Strasser et al, 2011).

The extrinsic apoptotic pathway is triggered upon binding of extracellular death ligands of the tumour necrosis factor (TNF) superfamily (TNF α, Fas/CD95-L, TNF-related apoptosis-inducing ligand (TRAIL)) to their cognate cell surface receptor (TNF receptors), Fas, TRAIL receptor (TRAILR1 and TRAILR2)) (Fulda & Debatin, 2006; Lavrik et al, 2005; Walczak & Krammer, 2000). Of note, in some cells, the extrinsic and intrinsic pathways are independent (Type I cells, for example lymphocytes), whereas in others, both pathways converge at the mitochondria (Type II cells, for example hepatocytes) through caspase-8-mediated cleavage of BH3-interacting domain death agonist (BID) (Czabotar et al, 2014; Fulda et al, 2002; Lee et al, 2016; Li et al, 1998; Scaffidi et al, 1998)(Figure 1.3).

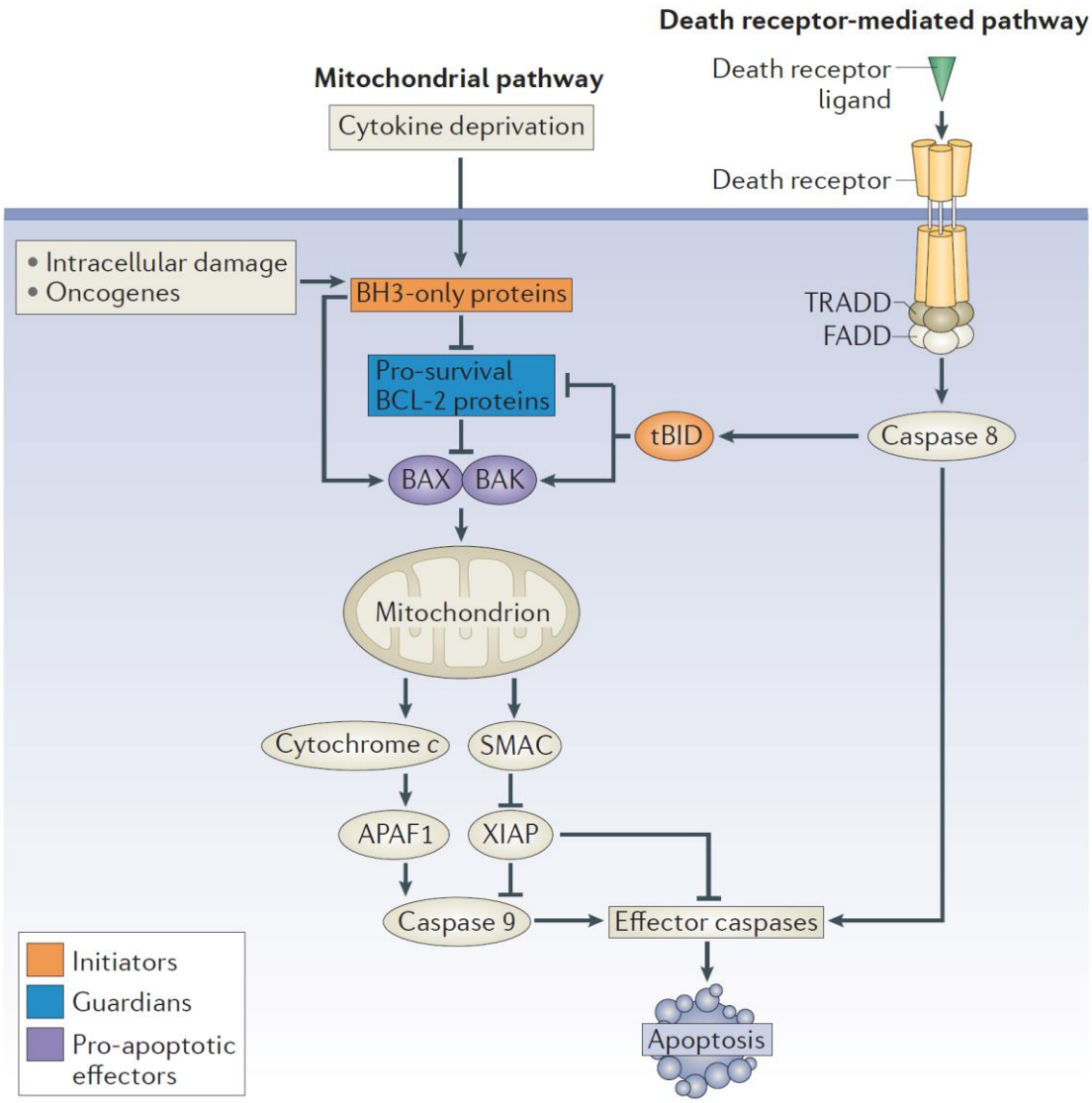

Figure 1.3 The mitochondrial and death receptor-mediated pathways to apoptosis. Diverse cytotoxic stimuli, including oncogenic stress and chemotherapeutic agents, as well as developmental cues, engage the mitochondrial pathway, which is regulated by BCL-2 family members. These stimuli activate BH3-only family members (initiators), which inhibit the pro-survival BCL-2-like proteins (guardians), thereby enabling activation of the pro-apoptotic effectors BAX and BAK, which then disrupt the mitochondrial outer membrane. The death receptor-mediated (or extrinsic) pathway of apoptosis is activated when certain death receptor ligands of the tumor necrosis factor (TNF) family (such as FAS ligand and TNF) engage their cognate death receptors (FAS and TNFR1, respectively) on the plasma membrane, leading to caspase 8 activation via FAS-associated death domain protein (FADD) and TNFR-associated death domain protein (TRADD). The two pathways converge at activation of the effector caspases (caspase 3, caspase 7 and caspase 6). In addition, the truncated form of BID (tBID), which is generated by caspase 8-mediated proteolysis of BID in the death receptor-mediated pathway, can engage the mitochondrial pathway to amplify the apoptotic response. Taken from (Czabotar et al, 2014).

1.3.3 Mitochondrial apoptotic pathway

Most of cell death in vertebrates proceeds via the intrinsic or mitochondrial pathway (Green & Kroemer, 2004). This pathway can be activated by a variety of stress stimuli including radiation (UV and gamma), heat, viral virulence factors, growth-factor deprivation, DNA-damage, oxidative stress and the activation of some oncogenic factors (Plati et al, 2011).

The crucial event in the intrinsic mitochondrial pathway is mitochondrial outer membrane (MOM) permeabilization (MOMP) that allows the release of apoptogenic factors sequestered in the IMS. In vertebrates, this event usually constitutes "the point of no return" of the apoptotic cascade (Green & Kroemer, 2004; Kroemer et al, 2007). So, MOMP typically leads to cell death irrespective of caspase activity by causing a progressive decline in mitochondrial function, although cells can survive this under certain circumstances, which may have pathophysiological consequences (Tait et al, 2010). MOMP is regulated by the BCL-2 family proteins, which establish a complex interaction network within themselves and with other cellular factors to dictate whether or not MOMP ensues and therefore a cell dyes by apoptosis (Chipuk et al, 2010; Youle & Strasser, 2008). Other important apoptosis-related mitochondrial processes have been described to occur previous or in parallel to the MOMP, such as dissipation of membrane potential ($\Delta\psi_m$) (Zamzami et al, 1995) and alterations in mitochondrial structure and function (Petit et al, 1995).

The apoptogenic factors released from IMS play different roles in the intrinsic apoptotic pathway. Cyt c release, a small protein (12 kDa) loosely associated to the mitochondrial lipid cardiolipin (CL) in the MIM, is one of the key events of the mitochondrial-dependent apoptosis. Upon CL oxidation and MOMP, Cyt c can diffuse into the cytosol, where it promotes the assembly of the apoptosome, a molecular platform that includes: Cyt c, apoptosis protease activating factor (APAF-1), initiator caspase 9 and ATP/dATP. This multiprotein complex activates caspase-9 resulting in the downstream caspase cascade activation (Garrido et al, 2006; Li et al, 1997; Liu et al, 1996; Ott et al, 2002; Saelens et al, 2004; Zou et al, 1997). In addition to Cyt c, MOMP allows intracytoplasmic release of two larger apoptogenic proteins termed SMAC/DIABLO (25kDa) and Omi/HtrA2 (37kDa). SMAC/Diablo and Omi/HtrA2 bind to and neutralize endogenous inhibitors of caspases (IAPs), thus favouring caspase activation (Saelens et al, 2004). Furthermore, Omi/HtrA2 has also been implicated in caspase-independent cell death due to its proteolytic activity (Saelens et al, 2004). Two additional apoptogenic proteins that are released from mitochondria as a consequence of MOMP are AIF (62 kDa) and Endo G (23 kDa) that, once released to the cytosol, translocate to the nucleus and mediate chromatin condensation and DNA fragmentation (Daugas et al, 2000; Li et al, 2001; Susin et al, 1999).

The timing of the release of these multiple proteins from the IMS to the cytosol is under debate and depending on the cell type or apoptotic stimuli, the redistribution order of these apoptogenic factors can be different. In some studies, a differential release of Cyt c, SMAC/DIABLO and AIF

has been reported (Arnoult et al, 2002; Chauhan et al, 2001; Daugas et al, 2000; Modjtahedi et al, 2006). However, other studies showed that Cyt c and SMAC/DIABLO are released simultaneously (Munoz-Pinedo et al, 2006; Rehm et al, 2003; Zhou et al, 2005).

One potential explanation for the differences in apoptogenic protein release from mitochondria has been attributed to differences in their retention mechanisms within the mitochondria, processes closely related with the mitochondrial dynamics. For example, it has been proposed that 90% of the Cyt c is sequestered within the mitochondrial cristaes where it binds to the mitochondrial specific lipid CL. Thus, in order to induce Cyt c release, mitochondrial cristae has to be remodelled (Scorrano et al, 2002) and Cyt c has to be freed from CL (Ott et al, 2002). In the case of AIF, a non-caspase protease, it has to be cleaved to remove its anchorage-point from the MIM (Polster et al, 2005). In addition, or alternatively, the different timing of mitochondrial apoptogenic factors release could be due to creation of specific MOM pores selective for each (or some, but not all) apoptogenic protein(s) (Saito et al, 2000). Another controversial issue is that with the exception of Cyt c, genetic ablation of other mitochondrial proapoptotic factors has shown little effect on the apoptotic process (Irvine et al, 2005; Okada et al, 2002) (Figure 1.4).

Of note, defects in mitochondrial apoptotic pathway have the potential to confer a survival advantage to cancer cells, contributing to the resistance of cancer cells to chemotherapy and radiotherapy (Hanahan & Weinberg, 2011).

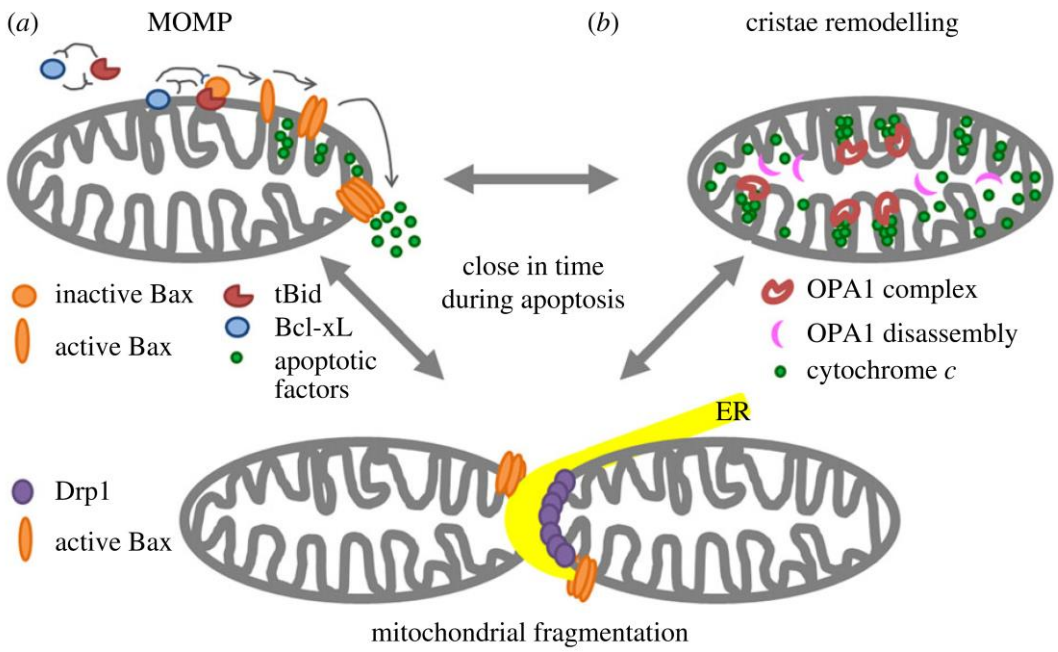

Figure 1.4 Scheme of structural changes in mitochondria during apoptosis: (a) MOMP, **(b)** cristae remodeling and **(bottom)** mitochondrial fragmentation. Taken from (Ugarte-Uribe & Garcia-Saez, 2017).

1.4 THE BCL-2 PROTEIN FAMILY

***Bcl**-2* gene was the first apoptotic regulator to be identified in human follicular **B**-**c**ell **l**ymphoma and established the family name (Bakhshi et al, 1985). Since then, more than 20 BCL-2 related proteins have been identified in mammals, all of which share amino acid sequence homology in one to four regions designated BCL-2 homology domains (BH1, BH2, BH3, and BH4) (Chipuk et al, 2010; Youle & Strasser, 2008). In addition to BH domains, many BCL-2 family members possess C-terminal hydrophobic regions that serve to target and/or anchor them to intracellular membranes.

Interestingly, BCL2 family proteins have been involved in several cellular processes such as mitochondrial dynamics (Aouacheria et al, 2017; Martinou & Youle, 2011), metabolic efficiency/cellular respiration (Alavian et al, 2011), calcium homeostasis (Szegezdi et al, 2006) and autophagy (Heath-Engel et al, 2008) among others. However, as previously mentioned, the main function of BCL-2 family proteins is MOMP regulation, which establish a complex interaction network within themselves and with many other cellular factors to dictate the cell fate (Chipuk et al, 2010; Youle & Strasser, 2008). Classicaly, depending on functional criteria and on their content of BH domains, BCL-2 family members were classified in three subgroups (Figure 1.5):

- **Antiapoptotic BCL2-type proteins**: contain all four BH domains and primarily inhibit apoptosis by preventing MOMP. They include BCL-2 itself, BCL-XL (B-cell lymphoma-extra-large), MCL-1 (myeloid cell leukemia-1), BCL-2-L2 (Bcl-2-like protein 2) commonly known as BCL-w, BCL2-A1 (Bcl-2-related protein A1) also known as A1(mouse)/BFL1(human) and BCL-B (Bcl-2-like protein 10).

- **Proapoptotic multidomain BAX-type proteins**: These proteins contain BH1-3 domains and directly cause MOM. They include BAX (BCL-2 Associated X protein), BAK (BCL-2 Associated Killer protein) and perhaps BOK (BCL2-related ovarian killer)/MTD (Matador).

- **Proapoptotic BH3-only proteins**: Contain only the BH3 domain and promote MOMP by activating BAX-type proteins. They include BID, BIM (BCL-2-interacting mediator of cell death), PUMA (p53 up-regulated modulator of apoptosis), BAD (BCL-2 antagonist of cell death), BIK (BCL-2-interacting killer), BMF (BCL.2-modifying factor), PMAIP1 (Phorbol-12-myristate-13-acetate-induced protein) commonly known as NOXA, and HRK (harakiri).

Importantly, although the above classification is useful, it does not take into account the switch in phenotype observed for a number of BCL-2-type and BAX-type proteins under certain cell and environmental contexts (Basanez et al, 2001; Clem et al, 1998; Fannjiang et al, 2003; Landeta et

al, 2014; Lewis et al, 1999; Qi & Hardwick, 2008). Indeed, despite showing a high level of sequence and structure similarities, different members within the same subgroup of the BCL-2 family can fulfill dissimilar physiological functions (Hardwick et al, 2012). Moreover, despite it is widely assumed that the BH4 distinguishes all anti-apoptotic BCL-2 family proteins from pro-death members that lack a BH4, most multiple alignment programs fail when their BH4 domain of the original triumvirate (BCL-2, BCL-XL and BCL-W) is align with the putative BH4 of their anti-apoptotic homologs Mcl-1 and Bfl-1/A1 (Aouacheria et al, 2013). Of note, in this thesis the terms domain and motif, referring to the BCL2 homology sequences, are used indistinctly. However, some authors argue that as a domain is associated with an autonomous folding unit of protein structure, and a motif is a sequence of conserved aminoacids that differentiates one family of proteins from another, BH domains should be redefined as a BH motifs (Aouacheria et al, 2015).

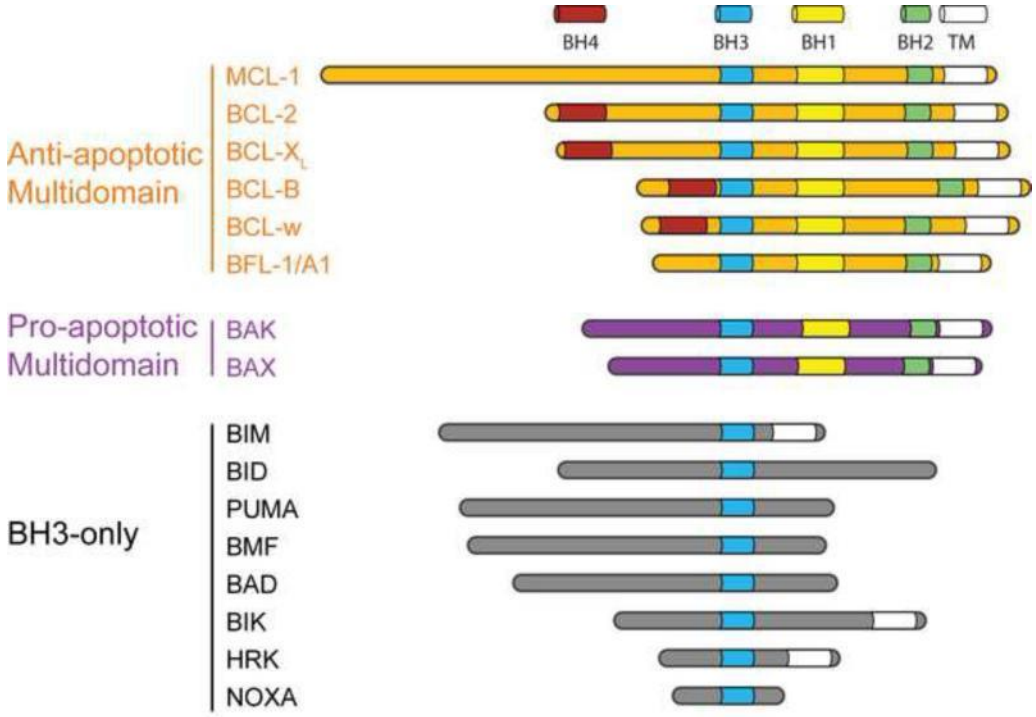

Figure 1.5 The BCL-2 protein family. Representation of the structural domains of representative members of each subfamily is shown. The BCL-2 family members can be classified as prosurvival proteins and proapoptotic members, in which there are two subgroups: multidomain effectors (BAX, BAK and perhaps BOK) and BH3-only proteins. Image taken from (Gimenez-Cassina & Danial, 2015).

1.4.1 Solution Structures of BCL-2 family proteins

Given the difficulty of applying conventional structural techniques to study membrane proteins, most detailed structural information available to date corresponds to BCL2 family members in an aqueous environment. During the last two decades, X-ray crystallography and Nuclear Magnetic Resonance (NMR) have been applied to gain atomic-level structural information of BCL2 family proteins conformations.

1.4.1.1 Multidomain-type folding

Despite their functional heterogeneity all 3D structures of multidomain BCL2 family proteins solved to date revealed the same globular helical fold, with a central predominantly hydrophobic hairpin that is flanked on both sides by pairs of amphipathic helices. This peculiar folding is strikingly similar to the pore-forming domain of bacterial toxins such as the colicins and diphtheria toxin (Muchmore et al, 1996; Petros et al, 2004). Another important common feature is the presence of BH1, BH2 and BH3 domains shape a hydrophobic groove, which acts as the docking site for the BH3 domains of other BCL2 protein-binding partners (Liu et al, 2003b; Sattler et al, 1997).

The first 3D structure resolved was the structure of a C-terminal truncated version of antiapoptotic BCLXL in complex with a long helical fragment of proapoptotic BIM (Figure 1.6A). Based on this structure, the canonical BH3 into groove interaction was firmly demonstrated, which has been particularly informative concerning how these two subfamilies engage in protein:protein interactions (Liu et al, 2003b). This interaction consists on, the hydrophobic match between four conserved hydrophobic residues (termed hereafter h1, h2, h3, and h4) localized in one side of the proapoptotic BIM BH3 peptide and in the canonical groove. In addition, BIM BH3 peptide contains several polar residues that interact with polar residues localized in the vicinity of the BCLXL hydrophobic groove (Figure 1.6B-C). According to the atomic structure, appeared to be particularly important a salt bridge established between an aspartate residue of the proapoptotic BH3 domain (D99 in BIM BH3) and an arginine residue of the antiapoptotic hydrophobic groove (R139 in BCL-XL). Thus, combination of hydrophobic and polar forces (including the salt bridge) triggers the BH3-into-groove interaction. Importantly, subsequent studies demonstrated that experimentally determined binding-specificities could be explained attending to sequence and structural diversities of the proapoptotic BH3 domains and hydrophobic grooves (Certo et al, 2006; Chen et al, 2005; Dutta et al, 2010; Kuwana et al, 2005; Petros et al, 2004).

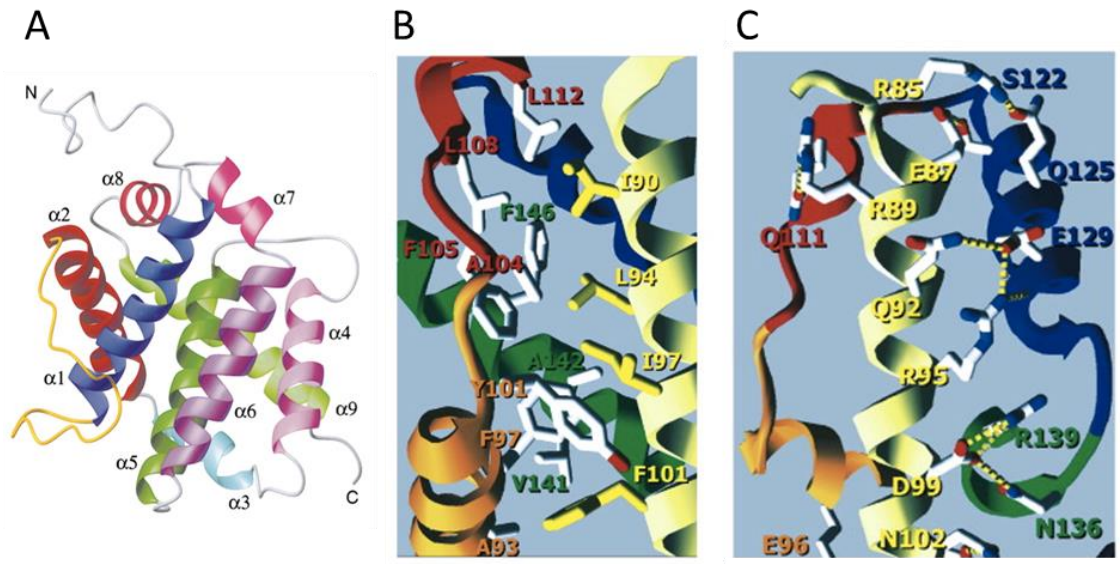

Figure 1.6 Details of the Interaction of BCLXL with BIM (PDB:1MAZ) (A) Structure of BIM BH3 peptide in complex with C-terminal truncated BCLXL. **(B)** Hydrophobic interactions between BCLXL and BIM. The side chains of the conserved four BH3 hydrophobic residues from BIM are shown in yellow. The side chains of the BCLXL hydrophobic residues that interact with BIM are shown white. **(C)** Hydrophilic interactions between BCLXL and BIM. Side chains of BCLXL and BIM involved in H bonds and salt bridges are shown in white. Taken from (Liu et al, 2003b).

In this scenario, BCL2-type and BAX-type proteins are sharing both similar folding and interaction with their BH3-only counterparts, but the effect elicited upon BH3-ligand interaction is dissimilar. In 2013, Coleman and colleagues unearthed the termed "holy grail of BCL2 family proteins" revealing for the first time the atomic structure of truncated version of BAX bounded to BH3 peptide (Czabotar et al, 2013). Here, a new surface of interaction between BAX and BH3-ligand was described (termed hereafter as "h0"), which is not present in the structured solved of BCL-2 type proteins (Figure 1.7). Remarkably, in this work was also described a cavity in BAX that is absent in its antiapoptotic family members, which according to the authors, explains the sequence of events that BAX-type proteins experiment to develop their pore forming activity including the separation of core (α2-α5) and latch (α6-α8) domains, oligomerization and membrane insertion (see also 1.7 and 1.8 sections).

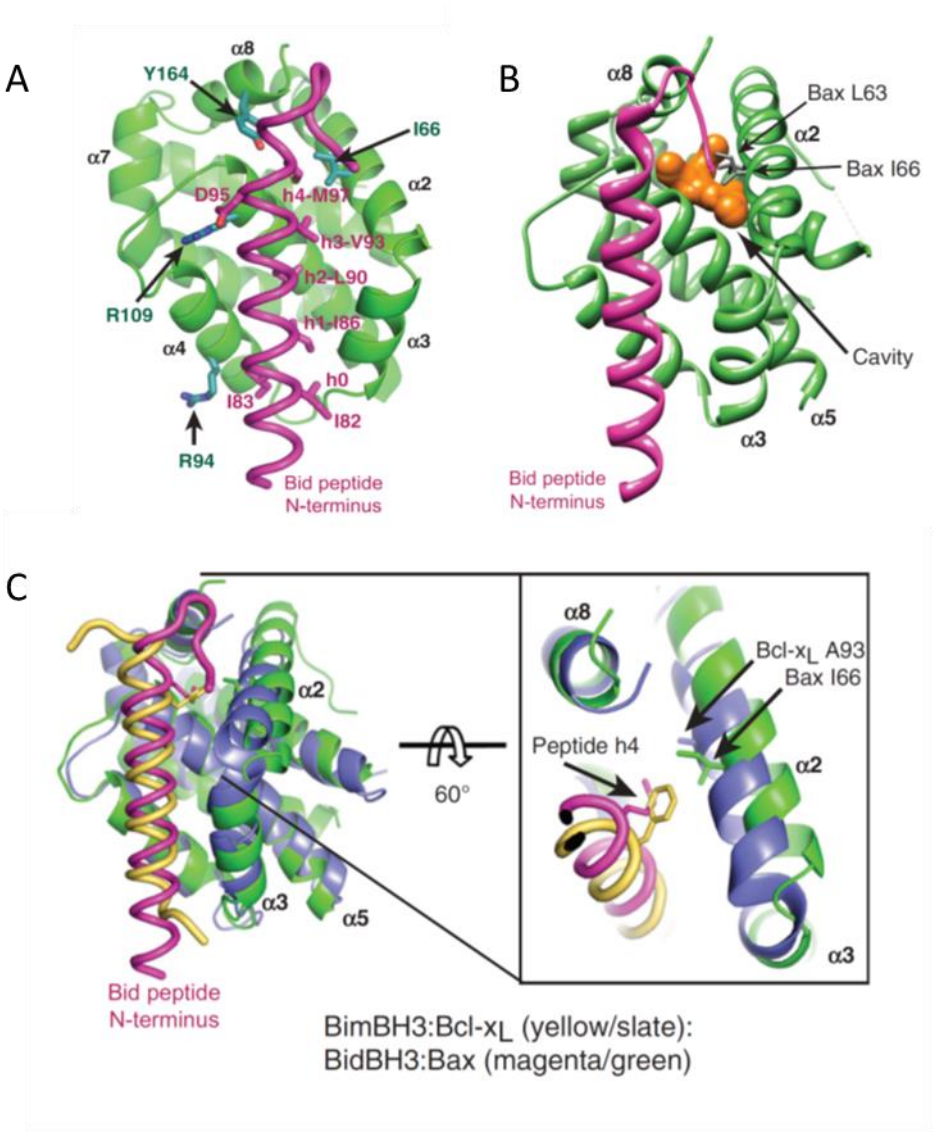

Figure 1.7 BidBH3 peptide (magenta) projects four canonical hydrophobic residues (h1 through h4) into the canonical binding groove of BAX (green). (A) The h0 residues I82 and I83 make additional interactions with the BAX groove. Bid D95 forms a salt link to BAX R109 (cyan). Other BAX side-chains shown (cyan) are R94 (close to Bid I83) and I66 and Y164 (both close to Bid M97). **(B)** Cavity (orange, 140A ° 3) in the hydrophobic core of BidBH3:BAX complex between α2, α5, and α8. The cavity is adjacent to BAX a2 residues L63 and I66 (side chains shown in gray). **(C)** Overlay of BidBH3:BAX with BimBH3:BCL-XL and zoom showing relative displacement of the BAX α2 and the contacts between hydrophobic residues on the BH3 domains of protein (h3 residues BCL-XL A93/BAX I66) and peptide (h4 residues Bid M97/Bim F159). PDB:4BD2, BH3:BAX and PDB:1MAZ, BH3:BCL:-XL. Adapted from (Czabotar et al, 2011).

Importantly, the results obtained with this BAX variant lacking its TM domain could not reassemble, efficiently or completely, what is happening with full length protein. In the case of BAX, the helix 9 is located in the hydrophobic groove modulating its availability to BH3-ligands and therefore the TM must be dislodged to enable this canonical interaction (Suzuki et al 2000). Starting out from this premise, it was postulated that BAX, in the opposite side of the canonical

interaction site, has also a non-canonical groove or binding surface for BH3-ligands (Edwards et al, 2013; Gavathiotis et al, 2008; Leshchiner et al, 2013), that comprises mainly helices α3, α4 and α5, forming a cleft between α1-α6. According to this model, full length BAX binds first BH3-ligand in the non-canonical surface, which enables the release of TM domain and membrane targeting, and once in the membrane, it is the canonical groove which triggers BAX oligomerization and pore formation. Moreover, recently has been identified a compound that binds BAX in the junction of the α3–α4 and α5–α6 and sensitizes its activation allosterically, mobilizing the α1– α2 loop and BH3 motifs which are implicated in the activation and oligomerization of BAX, respectively (Pritz et al, 2017). In addition, same group have reported that the α1 of the antiapoptotic BCL2 is a non-canonical binding surface for BAX (Barclay et al, 2015), adding an extra degree of complexity to anti/pro heterodimerization (Figure 1.8).

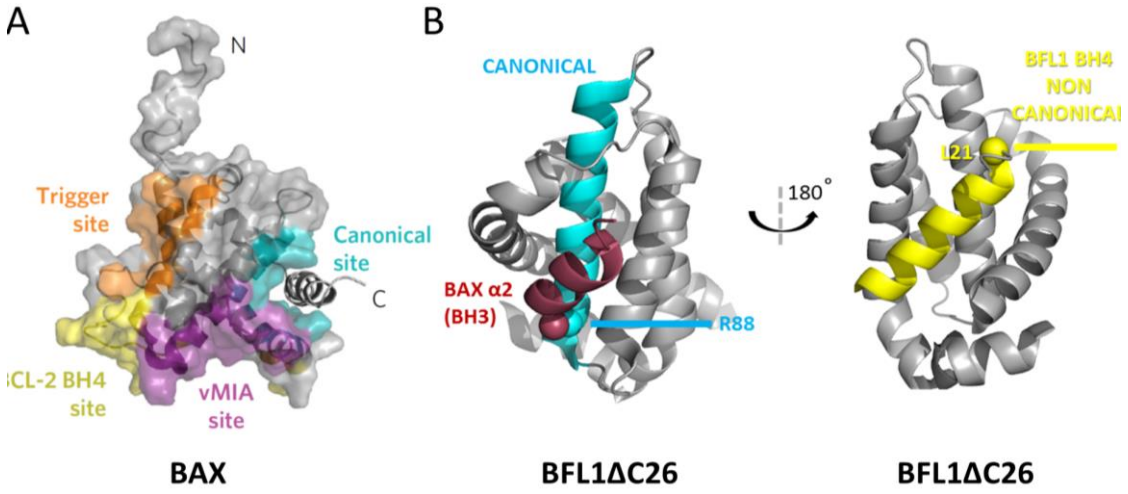

Figure 1.8 BH3 binding sites: (A) BAX contains a series of surface grooves that regulate its proapoptotic activity, including the activating BH3 trigger (orange) and canonical (cyan) sites and the inhibitory BCL -2 BH4 (yellow) and vMIA (purple) interaction pockets. **(B)** BFL1 (PDB= 2VM6) interacts with BAX-BH3 via canonical site (cyan, left) and the analogous position of the non-canonical site (right, yellow). Adapted from (Pritz et al, 2017).

1.4.1.2 BH3-only proteins

Because recombinant mutant versions of most BH3-only proteins (e.g. BIM, BMF, PUMA and BAD) lacking their C-terminal regions do not have a well-defined 3D structure under physiological conditions, they have been classified as Intrinsically Unstructured Proteins. However, it has also been shown that these BH3-only proteins undergo a significant conformational transition upon binding to antiapoptotic members, where their BH3 domain switches from adopting an unstructured or partially structured to a well-ordered helix. This is consistent with the fact that synthetic peptides representing BH3 domains of almost all BH3-only proteins have been crystallized bound to antiapoptotic members (Day et al, 2005; Day et al, 2008; Hinds et al, 2007; Liu et al, 2003b; Petros et al, 2000).

Exceptionally, the BH3 only protein BID, shares multidomain folding with one central hydrophobic helix (α6) being surrounded by the remaining seven amphipathic helices (Chou et al, 1999; McDonnell et al, 1999). BID also contains a large unstructured loop between helices α2 and α3 wherein a consensus sequence for caspase-8 cleavage is localized. The latter posttranslational modification markedly stimulates mitochondrial BID localization, BAX/BAK activation and MOMP (Gross et al, 1999).

1.5 MECHANISM OF ACTION OF BCL-2 FAMILY PROTEINS DURING APOPTOTSIS: CONTENTIOUS ISSUES

1.5.1 General overview of the MOMP process regulated by BCL-2 family proteins

Despite extensive research effort, many important mechanistic questions regarding apoptosis regulation mediated by BCL-2 family proteins remain to be answered: (i) How do different BCL-2 family proteins target the MOM?; (ii) How do BH3 only proteins and BCL2 type proteins regulate BAX-type proteins?; (iii) What is the role of the membrane and/or specific lipids in BCL-2 family protein function?; (iv) What is the precise molecular pathway for BAX/BAK functional activation? and (v) What is the nature of the BAX/BAK-driven pore and how is it regulated?

1.5.2 How do different BCL-2 family proteins target the MOM?

In healthy cells, many BCL-2 family proteins are found not only in the mitochondria but also in the cytosol, the ER and the nucleus. During apoptosis, most BCL-2 proteins translocate to or become enriched at the MOM, apparently to regulate its permeability. Additionally, non-MOM localizations of BCL-2 family members have also been connected to MOMP regulation, as well as to non-apoptotic functions of BCL-2 family proteins (Aouacheria et al, 2017; Hardwick et al, 2012) .

1.5.2.1 Cellular distribution of BCL2 multidomain family members

BCL-2 family proteins have a heterogeneous distribution, that depends on the intrinsic nature of each specific family member, cell type and cellular conditions. Under healthy conditions, BCL2 is an integral protein present in mitochondria, ER and nucleus (Hausmann et al, 2000; Hsu et al, 1997; Lithgow et al, 1994). In the case of BCL-XL (Hausmann et al, 2000; Hsu et al, 1997) and BCL-W (Wilson-Annan et al, 2003), both exist partly in the cytosol and in the membrane and translocate to mitochondria during apoptosis. In particular, BCL-W is loosely associated to the

membrane, and its anchoring to the MOM is only triggered when a BH3-only protein binds to the hydrophobic groove of BCL-W (Wilson-Annan et al, 2003). The subcellular localization of MCL-1 is even more complex: depending of the physiological cellular status and cell-type, MCL-1 has been localized to the mitochondria, the cytoplasm and the nucleus (Thomas et al, 2012). Concretely, BFL1 which does not contain a well-defined C-terminal transmembrane domain (TM), has a cytosolic fraction in healthy cell lysates and become inserted into the mitochondrial fraction in response to various apoptotic stimuli, following displacement of the C-terminal region by BH3-only proteins (Brien et al, 2009; Herman et al, 2008; Kucharczak et al, 2005).

In the case of the multidomain proapoptotic proteins, BAX is mostly cytosolic (Suzuki et al, 2000) while BAK is inserted constitutively in the MOM and the ER (Breckenridge et al, 2003; Griffiths et al, 1999). This issue has been usually addressed to the nature of their TM domain. BAX possessed an amphipatic C-terminal domain, which tends to bind preferentially to its hydrophobic pocket rather than to insert in the membrane, whereas BAK has a hydrophobic one, with high tendency for MOM anchoring. Consistently, BAXTM-like mutations in the C terminal of full-length BAK, becomes this protein much more soluble but still preserving its ability to translocate to MOM or liposomal membranes (Leshchiner et al, 2013).

Many different mechanisms have been proposed to explain mitochondrial targeting of BCL-2 multidomain proteins : 1) Anchorage of the hydrophobic C-terminal helix into the MOM; 2) Interaction with other BCL-2 family partners; 3) Interaction with non-BCL-2 family proteins, including TOM/TIM complexes and enzymes that produce post-translational modifications and 4) Interaction with mitochondrial lipids such as CL (Dorn & Maack, 2013).

1.5.2.2 Anchorage of the hydrophobic C-terminal helix

Among BCL-2 family members, the hydrophobicity of their C-terminal sequences has been frequently associated with their membrane targeting. Despite there is not a common feature the antiapoptotics BCL-2, BCL-XL, BCL-W and the proapoptotic BAK have a well-defined hydrophobic TM domain that constitutively target those proteins to the membrane. This hydrophobic tail is often flanked by basic residues that contribute to MOM localization, as it is observed for BCL-XL, whereas fewer basic residues favours ER localization as it is the case of BCL-2 (Kaufmann et al, 2003; Zhu et al, 1996).

However, the hydrophobicity of the C- terminal cannot drive exclusively membrane targeting as MCL1 and BAX with an amphipatic TM domain, or BFL1, BOK and some BH3-only proteins which do not meet general criteria of TM sequences, still translocate to the membrane upon certain cellular conditions (Lindsay et al, 2011).

1.5.2.3 Interaction with other BCL-2 family partners

BAX translocation to the MOM is particularly important in the apoptotic pathway regulation, as traditionally has been considered an early step in the process of functional activation of the protein (Antonsson et al, 2001; Mikhailov et al, 2001; Nechushtan et al, 1999; Nechushtan et al, 2001; Valentijn et al, 2008). To date, three contrasting but not necessarily mutually exclusive models have been proposed to explain the mechanistic underpinnings of this process.

The *Cytosolic BH3-only interaction model* postulates that selected BH3-only proteins such as BIM and PUMA, first bind to BAX non-canonical groove (α1/α6) at the cytosol. This protein:protein interaction triggers the release of BAX α9 from the canonical groove, thereby simultaneously allowing BAX translocation to the MOM together with exposition of BAX canonical BH3 binding-groove (Figure 1.8) (Edwards et al, 2013; Gavathiotis et al, 2010; Gavathiotis et al, 2008; Leshchiner et al, 2013; Walensky, 2013).

The *Combined BH3-only and MOM interaction model*: Here, first BH3-only proteins bind to the MOM, and this protein:lipid interaction is a pre-requisite for BAX recruitment to the mitochondria. Interaction of BH3-only proteins with BAX at the MOM level leads to disengagement of BAX´s C-terminal helix from the hydrophobic groove (Lovell et al, 2008; Wilfling et al, 2012).

The *Dynamic MOM interaction model* or retrotranslocation postulates that in healthy cells, BAX is not only in the cytosol but it is also constitutively targeted to the MOM, maintaining a dynamic equilibrium between the two subcellular compartments. Some studies suggest that BAX is actively retrotranslocated from the MOM by several antiapoptotic proteins such as BCL2 or BCL-XL (Edlich et al, 2011b; Todt et al, 2013), while others suggest that BAX retrotranslocation may occur independently to the presence of antiapoptotic and BH3-only proteins (Schellenberg et al, 2013). Recently, has been demonstrated that BAX-homolog, BAK, is also in a antiapoptotic-regulated dynamic equilibrium, but its hydrophobic C-terminal displaced the equilibrium to the membrane targeting (Todt et al, 2015).

Within this last framework, it is conceivable that specific non BCL-2 related proteins or lipid factors present at the MOM may play a role in the reversible disengagement of BAX C-terminal hydrophobic helix. However, as some authors have been able to reproduce BAX`s retrotranslocation *in vitro* by using recombinant proteins and model membranes, the presence of other non-BCL2 proteins cannot be an essential requirement (Bleicken et al, 2017). Moreover, although the precise extent of BAX insertion in the MOM remains not well defined, this retrotranslocation process must require the removal of protein–lipid interactions, which theoretically should be thermodynamically unfavourable. Unless a molecular mechanism that provides energy for retrotranslocation is discovered, one could also reason that the dissociation of BAX from the membrane could proceed spontaneously via a low energy barrier accessible by thermal fluctuations (Cosentino & Garcia-Saez, 2017).

Regarding mitochondrial targeting of BH3-only proteins, one possibility is that they translocate to the MOM by binding to resident multidomain BCL-2 proteins (i.e. via protein:protein interactions) (Schinzel et al, 2004). Alternatively, considering that most BH3-only proteins contain a C-terminal hydrophobic domain similar to that found in multidomain proteins, BH3-only proteins could also be targeted to the MOM via direct interaction with MOM lipids (Wilfling et al, 2012) and once in the MOM, the BH3 only proteins could attract to the multidomain family members. Remarkably, CL-binding domains have been identified in tBID and BAD (Gonzalvez et al, 2005; Gonzalvez et al, 2010; Hekman et al, 2006; Lutter et al, 2000; Petit et al, 2009). See also 1.6.2 section or lipid:BCL2-proteins interaction section.

Of note, each type of BH3-only protein displays a distinct tissue distribution, and usually is the target of a particular signal transduction pathway. For example, in the case of BID, it is located in the cytosol adopting an inactive form (Chou et al, 1999; McDonnell et al, 1999; Wang et al, 1996), then its cleavage by caspase-8 exposes a previously buried hydrophobic surface and reduces its negative molecular charge prompting its membrane targeting (Gross et al, 1999). BIM and BMF seem to be bound to cytoskeletal structures under healthy conditions, however during apoptosis, are translocated to the MOM (Puthalakath et al, 1999; Puthalakath et al, 2001). BAD is sequestered in the cytosol by 14-3-3 scaffold proteins, while upon dephosphorilation it is targeted to the MOM- or stays in cytosolic forming a complex with BCL-XL (Datta et al, 2002).

1.5.3 Regulation of BAX/BAK permeabilization function

The complex level of regulation needed to decide the cell fate of the cell is associated with an intricate interaction network of BCL-2 family proteins, among themselves, as well as with other cellular components. It is well known that BH3-only proteins discharge their pro-apoptotic functions through BAX-type proteins, while their activity is suppressed by anti-apoptotic BCL-2-type proteins (Cheng et al, 2001; Zong et al, 2001). However, the exact hierarchy of these interactions and the role of other MOM factors remain controversial.

Historically, largely based on solution binding studies between pro- and antiapoptotic family members, two seemingly opposing models emerged: the indirect and the direct activation models. Then, the MOM itself has been considered as one of the main regulators of BCL-2 family member interactions and functions. Thus, at least three non-mutually exclusive models exist to explain how interactions among the BCL-2 family proteins regulate MOMP and apoptosis (Figure 1.9).

1.5.3.1 Indirect activation model

In the indirect activation model or derepression model, the BCL-2 type proteins are continuously bounded to BAX-type proteins, and BH3-only proteins act by binding to and neutralizing BCL-2 type proteins, thereby freeing BAX-type proteins to elicit MOMP (Chen et al, 2005; Willis et al, 2005). The different affinities of soluble BH3 domain peptides for anti-apoptotic BCL-2 type proteins offered a potential explanation for the dissimilar lethality observed in BH3-only proteins.

Whereas BIM, PUMA and tBID bind avidly to all the pro-survival proteins, the rest of BH3-only proteins associate only with specific antiapoptotic. For example, NOXA binds only to MCL-1 and BFL1, while BAD binds only to BCL-2, BCL-XL and BCL-W. Importantly, the promiscuous binders (e.g. BIM, BID and PUMA) are much more potent killers than those that cannot engage all the pro-survival proteins, but the combination of NOXA and BAD potently induces cell death (Chen et al, 2005). Indeed, based on the specific derepressors BAD and NOXA, BH3-like or BH3 mimetic anticancer drugs have been designed. These structurally equivalent molecules, BAD-like ABT737 and NOXA-like S63845(Kotschy et al, 2016), retain the specific ability to block certain antiapoptotic proteins, which are one of the main reasons for chemotherapy resistance (Opydo-Chanek et al, 2017a; Opydo-Chanek et al, 2017b; Vela & Marzo, 2015).

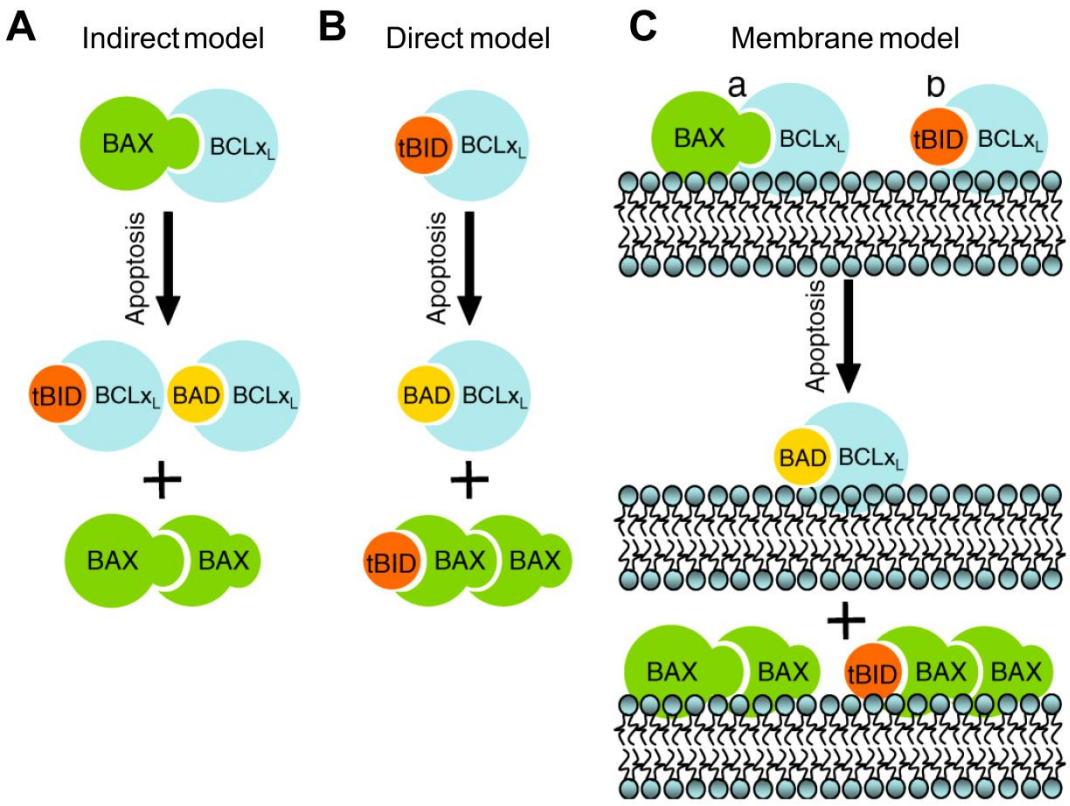

Figure 1.9 Scheme of the models proposed to describe the regulation of the BAX/BAK permeabilization function. Antiapoptotic proteins are represented by BCL-XL (*blue*), multidomain proapoptotic proteins by BAX (*green*) and BH3 only proteins, sensitizers by BAD (*yellow*) and activators by tBID (*red*). (**A**) In the "Indirect model", BH3-only proteins bind BCL-XL, releasing bound BAX that could self-activate in the absence of any other protein. (**B**) The direct model states that BH3 only proteins comprise two classes: the *activators* (here tBID) that are bound to antiapoptotic proteins, but once displaced by the *sensitizers* (BAD) could lead to activate directly BAX or BAK. (**C**) In the membrane model, the membrane is a regulating parameter of the interaction of the three subgroups of proteins. Taken from (Basanez & Hardwick, 2008).

Another postulate of the indirect activation model is that BAX-type proteins are structurally active but remain inhibited under non-apoptotic conditions due to binding to antiapoptotic proteins.

Thus, once BAX-type proteins are liberated from their inhibitory interactions with BCL-2 type proteins they can lead to MOMP. Consistent with this view, in the absence of any other BCL2 proteins, heat-activated BAX can promote cyt c release in isolated mitochondria or in MOM-like vesicles. In addition, BAX mutants harbouring specific substitutions in their BH3 domain that prevent their sequestration by BCL-2-type proteins, but not their homodimerization activity, provoke unrestrained apoptosis (Czabotar et al, 2011; Fletcher et al, 2008).

However, the indirect activation model cannot explain the fact that only a minor portion of BAX/BAK is sequestered by antiapoptotic proteins *in vivo*. Moreover, mutants of BCL-2-type proteins that fail to bind BAX and BAK can be fully protective against cell death (Cheng et al, 1996). Furthermore, we cannot exclude the possibility that other non BCL2 proteins are involved in BAX-mediated apoptosis and pore formation.

1.5.3.2 Direct activation model

The direct activation model states that BAX-type proteins are activated by binding to certain BH3-only proteins such as tBID, and the BCL-2-type proteins primarily function by sequestering these activators from BAX/BAK. This model was first proposed to address the experimental observation that peptides representing the BID BH3 and BIM BH3 domains, unlike other BH3 peptides (e.g. BAD and NOXA), seemingly suffice to activate the mitochondria-permeabilizing function of BAX/BAK (Kuwana et al, 2005; Letai et al, 2002; Wei et al, 2000). Therefore, BH3 only proteins comprise two classes: those that directly activate BAX/BAK named "direct activators" such as tBID, BIM and PUMA; and those that displace the activator proteins from antiapoptotic proteins and activate BAX/BAK indirectly, known as "sensitizers" or "de-repressors" such as BAD, NOXA or BMF. In agreement with this model, several groups showed that tBID efficiently activates the permeabilizing function of BAX and BAK in pure lipid membranes (Bleicken et al, 2010; Etxebarria et al, 2008; Kuwana et al, 2002; Lovell et al, 2008; Oh et al, 2010; Terrones et al, 2004).

In this context, the main function of the anti-apoptotic proteins is to sequester the activator BH3 only proteins BIM, BID and PUMA, thereby blocking their activation of BAX/BAK. In contrast to the well-established binding of the BH3-only protein to antiapoptotic members, the main caveat for the direct model was the difficulty to detect an interaction between the BH3-only proteins and BAX-type members. These and other observations led to a "hit-and-run" mechanism for BAX/BAK activation by selected BH3-only proteins (Dai et al, 2011; Eskes et al, 2000; Lovell et al, 2008; Wei et al, 2000), based on a transient interaction between BH3-only "ligands" and BAX-type "receptors".

Nevertheless, fluorescence resonance energy transfer (FRET) spectroscopy and fluorescence biocomplementation studies showed steady-state interaction between BAX and tBID measured in liposomes (Lovell et al, 2008) and in cells (Vela et al, 2013). In addition, recent structural studies provide strong support for a direct physical interaction between BH3 domains of selected

BH3-only proteins and BAX-type proteins. On the one hand, NMR studies of BIM and PUMA SABH peptides bound to full-length BAX in non-canonical surface between α1-α6 (Gavathiotis et al, 2010; Gavathiotis et al, 2008; Leshchiner et al, 2013; Walensky, 2013). On the other hand, X-Ray crystal structure of synthetic BID BH3 peptide bound to the canonical groove of BAXΔC21 (BAX lacking the tail-anchor sequence) (Czabotar et al, 2013) and BIM BH3 peptide bound to the canonical groove of truncated version of BAX-homolog, BAK (Moldoveanu et al, 2013) were reported firmly confirming a canonical BH3-into-groove interaction. Importantly, from these studies an additional hydrophobic interaction (h5) was described near the N-terminus which could be the signature amino acid for distinguishing activator and sensitizer BH3 domains (Czabotar et al, 2013). In addition, combining size exclusion chromatography, double-electron resonance (DEER) and CHAPS, the oligomerization of BAX in solution upon BIM BH3 activation has been reported, providing a functional activation of BAX in the absence of MOM or MOM-like membranes (Sung et al, 2015).

Several caveats have been raised to this model. First, non-canonical BH3-binding site in BAX involves several specific residues (K21, R134, Q28, Q32 and E131) surrounding the hydrophobic surface. According to the authors, the SABH:BAX binding was shown to be specifically disrupted by K21E mutagenesis (Gavathiotis et al, 2010; Gavathiotis et al, 2008; Kim et al, 2009), but however, knock-in studies showed that BAXK21E mutant induces apoptosis as efficiently as wt BAX does in BAX/BAK DKO cells. Second, it remains to be proven that putative BH3-only activators other than BIM (Gavathiotis et al, 2008) and PUMA (Edwards et al, 2013), such as tBID, also bind the non-canonical groove of BAX to trigger its functional activation. Third, it remains to be rigorously shown that the binding interactions observed between the chemically modified BIM or PUMA SABH peptides and BAX in solution mirror the binding interactions occurring at the MOM level between the entire BIM or PUMA protein and BAX. Despite these caveats, Walensky L.D. and colleagues proposed a new model for BAX activation. The first step would consist in the union of BIM to the non-canonical groove of BAX at the cytosol, followed by release of BAX C-terminal domain allowing BAX MOM translocation, and enabling another BH3 interaction through the BAX canonical groove (Edwards et al, 2013; Leshchiner et al, 2013; Walensky, 2013).

Finally, the structures obtained by X-Ray crystallography described above does not explain how direct activators might bind the full-length BAX, as its canonical groove is occupied by the C-terminal helix 9. Alternatively, as mentioned before, BAX may be in dynamic equilibrium between cytosol and membrane with the C-terminal anchorage being only transient (Schellenberg et al, 2013), thus, the canonical hydrophobic groove will be free for BH3 only binding. However, even if in the studies where the helix 9 is included (Sung et al, 2015), BAX activation requires a detergent (in order to mimic membrane lipophilic conditions) to dimerized.

1.5.3.3 Membrane models

More recent models emphasize the role of the MOM in the BCL-2 family proteins interactome during apoptosis (Basanez & Hardwick, 2008; Billen et al, 2008; Leber et al, 2007; Leber et al, 2010). According to the "Membrane-Embedded Model", the association of BCL-2 proteins to the MOM causes conformational changes in these molecules that affect their binding interactions. Recent findings based on advance fluorescence microscopy techniques indicate that BCL-XL affinity for tBID is higher at the membrane level than in solution or that the presence of a membrane is necessary for tBID to interact with BAX (Garcia-Saez et al, 2009; Liu et al, 2012).

Moreover, even if has been very controversial and nowadays has lost impact, some authors postulated that BH3 only proteins function as direct activators of BAX/BAK and can both activate or inhibit the role of the antiapoptotic proteins. In this way, BH3 only sensitizer proteins could bind to the hydrophobic groove of the antiapoptotic proteins inhibiting its prosurvival function. On the other hand, in some conditions interaction of BH3 only proteins with BCL-2 type proteins leads to membrane insertion of α5 of the latter proteins (Dlugosz et al, 2006; Leber et al, 2010; Peng et al, 2006). Based on these observations, it has been proposed that BCL-XL actually needs to be activated similarly to BAX to perform its antiapoptotic function, and BCL-XL and BAX compete with each other at different steps along the molecular pathways leading to their functional activation. In other words, BCL-XL would inhibit apoptosis by acting as a dominant-negative version of BAX (Billen et al, 2008; Shamas-Din et al, 2013).

On the other hand, a "Unified Model" was proposed based on the relative affinities of different BH3 domain chimeras for BCL-2 type proteins. Two types of inhibition interactions between MOM-localized antiapoptotic proteins and proapoptotic partners were proposed: interactions with BH3-only direct activator proteins (MODE 1) or interactions with activated effectors BAX/BAK (MODE 2). Both mechanisms could inhibit MOMP, but antiapoptotic binding to BAX/BAK is more efficient than binding BH3 only activators (Llambi et al, 2011). Since activated BAX/BAK can activate another BAX/BAK molecules (Gavathiotis et al, 2010), therefore inhibiting this auto-activation process seems more efficient than sequestration of all the direct activator BH3 only proteins (Llambi et al, 2011). However, this assumption is on debate, as recently published *in vitro* studies by combining model membranes and recombinant proteins reveal that the inhibition interaction of BH3 only proteins by the BCL2-type proteins is much more efficient (Bleicken et al, 2017; Landeta et al, 2014).

Finally, another increasingly recognized aspect that determines the binding interactions and functions of BCL-2 family proteins is the lipid composition of the MOM (Chipuk et al, 2012; Terrones et al, 2004; Terrones et al, 2008). Building in those observations, a "Lipid-Centric Model" has been proposed, where apoptosis-related lipids modulate the activation and action of BCL-2 family members, either through a direct and stereoselective interaction (Chipuk et al, 2012), or via a bilayer-mediated effect (Basanez et al, 2012). Regarding the latter, it is conceivable

that the BH3-only protein cBID stimulates BAX permeabilizing function not only by direct binding via BH3-into-groove interactions, but also by altering the physical properties of the host bilayer via cBID:lipid interactions (Basanez et al, 2002; Bleicken et al, 2016; Terrones et al, 2004). Upon protein adsorption at the bilayer/solution interface, these amphipathic helices can change lipid bilayer properties such as the intrinsic curvature and elasticity, which may alter the bilayer deformation energy associated with protein conformational changes (McIntosh & Simon, 2006). Of note, lipid-mediated modes of BCL-2 family protein action could also be linked to mitochondrial dynamics (Basanez et al, 2012; Etxebarria et al, 2009; Montessuit et al, 2010). In stark support of the membrane relevance, recently, Oneil et al 2016 demonstrated in a study using a new cell line, knocked out for the most abundant BCL2 proteins, that BAX overexpression is sufficient to promote apoptosis (O'Neill et al, 2016). Moreover, in our group we have shown that membrane could modulate the interactome among BCL2 proteins as its composition can alter the activity of MCL1, which can inhibit BAX pore formation or promote itself a pore formation depending on the CL content (Landeta et al, 2014).

1.6 THE MITOCHONDRIAL LIPID-FINGERPRINT AS A CELL FATE INDICATOR

1.6.1 Mitochondrial lipids

Mitochondria play a critical role in lipid metabolism and dynamics. Key steps as lipid degradation, fatty acid synthesis, together with essential reactions for the biosynthesis of significant levels of lipids occur in the mitochondria. Under normal conditions, the major components of mitochondrial membranes are glycerophospholipids and to a lesser extent sphingolipids and sterols which are important components of plasma membrane, Golgi apparatus, and lysosomal compartments, and are only found in trace amounts in mitochondrial membranes (van Meer et al, 2008). Of note, in cells involved in the biosynthesis of steroid hormones, mitochondria have a higher content of sterols (Strauss et al, 2003).

The glycerophospholipid composition of mitochondrial membranes has been determined in yeast and mammalian cells, and although the exact composition determined in different studies varies (most likely because of differences in the growth conditions or in the purity of the analysed fractions), the relative abundance of different phospholipids remains within a relatively narrow range (Fleischer et al, 1967; Osman et al, 2011; van Meer et al, 2008). Thus, even if mitochondria are highly dynamic organelles, its lipid composition varies little among different cells, suggesting that major changes cannot be tolerated (Figure 1. 10).

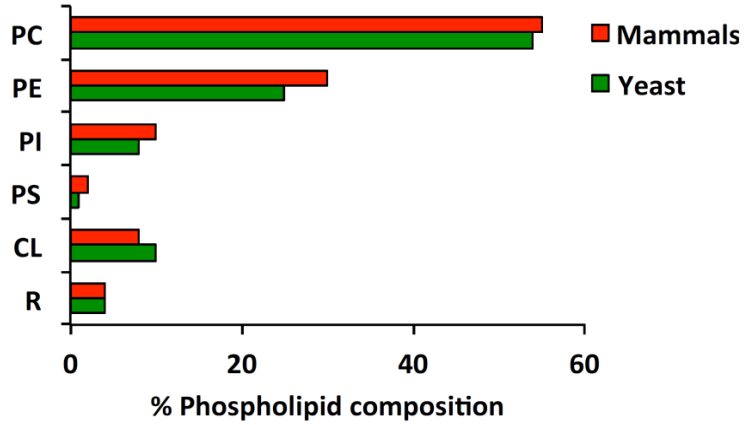

Figure 1.10 Lipid composition of mitochondria in healthy cells. The lipid compositional data are expressed as a percentage of the total phospholipid in mammals (red) and yeast (green) mitochondria. PC: Phosphatidylcholine; PE: Phosphatidylethanolamine; PI: Phosphatidylinositol; PS: Phosphatidylserine; CL: Cardiolipin and R: remaining lipids Adapted from (van Meer et al, 2008).

Regarding the relative abundance of glycerophospholipids at the MOM and MIM, a consensus exists for phosphatidylcholine (PC), phosphatidylethanolamine (PE), and phosphatidylinositol (PI). Moreover, it should be noted that the only asymmetrically distributed lipid is the CL. Originally, CL was thought to be present almost exclusively within the MIM, representing on average approximately ≈ 5% of the total lipid content of the MOM. However, subsequently it was shown that local CL concentrations at specific MOM domains known as the mitochondrial membrane contact sites (CS) can be as high as ≈25% (Ardail et al, 1990). Moreover, a recent study in yeast corroborates this CL-patches in the MOM lipid composition (Gebert et al, 2009).

Because CL is the signature glycerophospholipid of mitochondria it is not surprising that CL is implicated in many mitochondrial functions in healthy cells, including maintenance of normal organelle ultrastructure, energy metabolism, protein import processes, and mitochondrial dynamics (Schlame & Ren, 2009; Tamura et al, 2009). However, as commented previously, far from being inert structural elements mitochondrial lipids can affect the function of specific mitochondrial proteins that are implicated in the apoptotic pathway, either through specific binding interactions or via changes in the physical properties mitochondrial membrane.

1.6.2 BCL2-mediated apoptosis-related mitochondrial lipids

MOM lipid composition is critical for the BCL-2 family proteins function, and therefore perturbation of the lipid composition in the mitochondria can lead to phenotypes associated with deregulated cell death (Canals & Hannun, 2013; Claypool & Koehler, 2012; Van Brocklyn & Williams, 2012). In this section, we describe the main characteristics of mitochondrial lipid

composition as well as proposed roles of apoptosis-related lipids in regulating the function of selected proapoptotic BCL-2 family members and mitochondrial proteins.

1.6.2.1 Cardiolipin

CL is the most specific lipid constituent of the mitochondrial membranes. CL is a unique phospholipid for at least three reasons. First, it is almost exclusively found in association with the MIM, the compartment in which it is synthesized. Second, CL is a double phosphoglycerolipid composed by two phosphatidyl residues bridged by a glycerol. Thus, it has two phosphate headgroups and four attached fatty acyl chains. Third, CL is a so-called structural phospholipid capable of acquiring lamellar and hexagonal structures (Figure 2.2, page 64).

Structure

CL is a phospholipid composed of two phosphatidyl moieties linked to a central glycerol group (Figure 1.11). The two phosphatidyl moieties are stereochemically non-equivalent, because one is in pro-R and the other is in pro-S position with respect to the central carbon atom of the glycerol bridge. The presence of two phosphate groups confers two negative charges, a fact that could be of importance for protein interactions (Claypool et al, 2008).

Molecular species of CL derive from permutations of the four acyl chains. Eukaryotic CL have a unique fatty acid pattern, which is essentially restricted to C18 chains. However, there is an exception found in the yeast Saccharomyces cerevisiae, in which CL contains about equal amounts of oleoyl (18:1) and palmitoleoyl (16:1) residues. In the case of mammals, the dominant C18 chain is the linoleoyl (18:2). On the contrary, in bacteria CL containing mostly saturated and monoenoic acyl groups with 14-18 carbon atoms can be found (Schlame & Ren, 2009; Schlame et al, 2000).

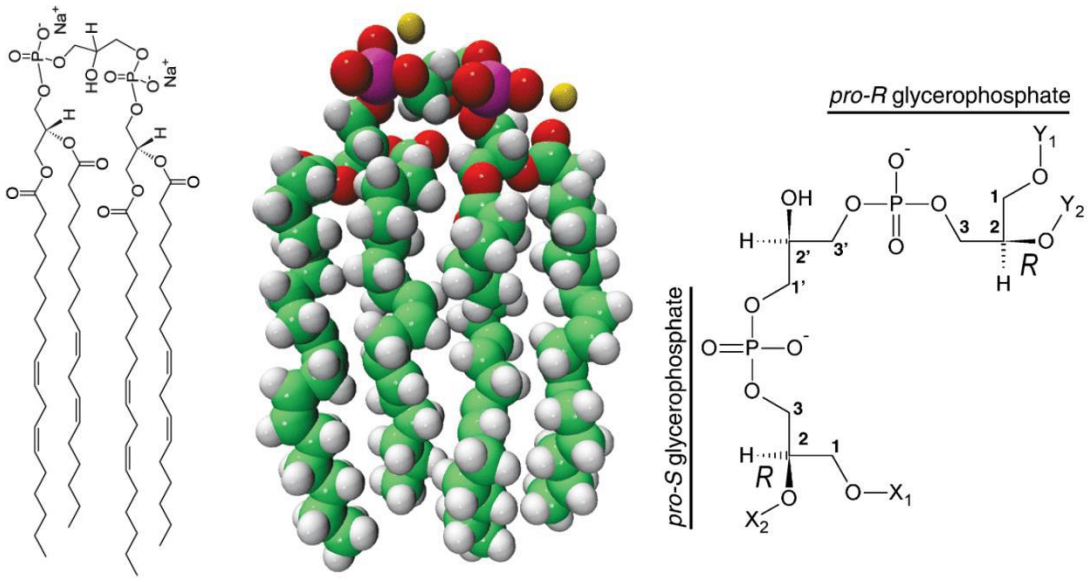

Figure 1.11. Cardiolipin structure. The molecule consists of two sn-glycero-3-phosphate moieties linked by a glycerol group. Four acyl groups (X1,X2,Y1,Y2) are attached to the glycerophosphates. Both glycerophosphates carry obligate chiral centres in R conformation. The central glycerol carries a prochiral center (if X1=Y1 and X2=Y2) or a true chiral centre (if X1≠Y1 and X2≠Y2). As a result, the two glycerophosphates occupy different estereochemical positions. Image adapted from avatilipids.com and (Schlame & Ren, 2006).

CL displays characteristic phase polymorphism, being able to form micellar, lamellar and hexagonal structures. Phase transitions from micellar to lamellar, and lamellar to hexagonal are favoured by the presence of divalent cations, low pH, high ionic strength and a high number of acyl groups. The importance of head group charges for phase behaviour are visible by the fact that ionic strength and the pH induce hexagonal structures. Another determining factor seems to be the volume of the hydrophobic moiety. For instance, dilysocardiolipin, which only contains two acyl chains, may form micellar and lamellar structures, whereas acylcardilipin, which contains an extra acyl chain compared to CL, always exists in hexagonal state. Hexagonal CL may play a role in membrane contact zones and other areas where the bilayer structure is perturbed (Ortiz et al, 1999).

Biosynthesis and degradation

The biosynthesis of CL begins with the formation of phosphatidic acid from glycerol-3-phosphate and activated fatty acids. Then, phosphatidic acid reacts with CTP to form the high-energy phosphoanhydride intermediate CDP-diacylglycerol, by the enzyme CDP-diacylglycerol synthase. This enzyme is localized to the ER, but can be also found in mitochondria. The activated phosphatidyl group is subsequently transferred to the sn-1 hydroxyl group of glycerol-3-phosphate to yield phosphatidilglycerolphosphate (PG-P). The enzyme responsible to catalyse the formation of the PG-P is the phosphatidylglycerolphosphate synthase (Pgs1). It has been

observed, that deletion of the gene encoding this enzyme is not lethal, but seriously compromise mitochondrial function. Then, the PG-P is dephosphorylated to phosphatiydlglycerol by phosphatidylglycerolphosphatase enzymes. These enzymes are Gep4 in yeast and PTPMT1 in mammals. These enzymes are both anchored to the matrix side of the MIM. Loss of this enzymes leads to PG-P accumulation, destabilization of the respiratory chain supercomplexes and impaired cell growth. From here, the pathway diverges into prokaryotic and eukaryotic branches. In prokaryotes, phosphatidylglycerol receives a phosphatidyl group from another phosphatidylglycerol by transesterification. In eukaryotes, phosphatidylglycerol receives an activated phosphatidyl group from phosphatidyl-CMP, which is catalysed by CL synthase, which is a phosphatidyltransferas (Claypool & Koehler, 2012; Horvath & Daum, 2013; Schlame, 2008) (Figure 1.12).

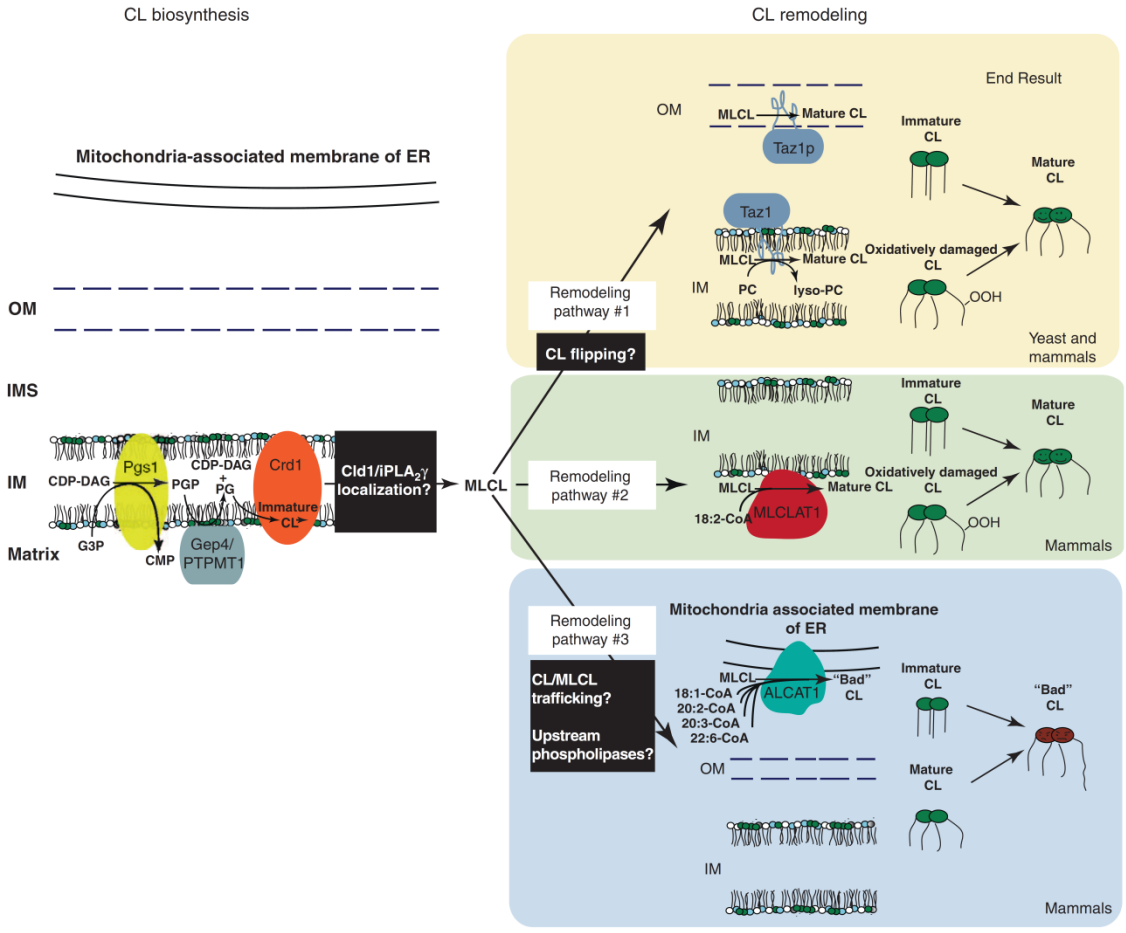

Figure 1.12. Overview of CL biosynthesis and remodelling. Image taken from (Claypool & Koehler, 2012).

CL requires continuous turnover to maintain the steady state. CL can be degraded by at least two enzymes; phospholipase A and phospholipase D. In 2006 a novel mitochondrial phospholipase D specific for CL and implicated in mitochondrial fusion was described (Choi et al., 2006). In this case, the product of CL hydrolysis is the fusogenic phospholipid phosphatidic acid (PA). Thus, mitochondrial phospholipase D could link mitochondrial dynamics to the CL metabolism. During

apoptosis the degradation of CL is linked to its oxidation. The mitochondrial respiratory chain is the main source of reactive oxygen species (ROS) and CL is a prime target due to its proximity to the ROS source and to its highly unsaturated acyl chains. Indeed, selective ROS-mediated CL peroxidation has been demonstrated to precede mitochondrial cyt c release during apoptosis (Kagan et al., 2005; Ott et al., 2007).

CL during apoptosis

Different lines of evidence indicate that during apoptosis the net content of CL at the MOM increases. Phospholipid transport between MOM and MIM has been proposed to occur at CS between both membranes (Ardail et al, 1991; Simbeni et al, 1991). Although the mechanism responsible for CL translocation from the MIM to the MOM during apoptosis is still unsettled, mitochondrial phospholipid scramblase-3 (PLS3) (Liu et al, 2003a; Liu et al, 2008), mitochondrial kinases (Epand et al, 2007) as for example nucleoside diphosphate kinase Nm23-H4/NDPK-D (Schlattner et al, 2013), and specific BCL-2 family proteins such as tBID could be also implicated in this process due to a membrane remodelling and reordering of CL at the CS (Esposti et al, 2001; Gonzalvez et al, 2005; Gonzalvez et al, 2010; Heit et al, 2011; Jalmar et al, 2013; Scorrano et al, 2002; Tyurin et al, 2007). In fact, the first set of evidence linking CL to apoptosis induction was the discovery that MOM-localized CL acts as a mitochondrial receptor for tBID (Lutter et al, 2000). Alternatively, considering that in the presence of Ca^{++} CL forms highly-curved inverted hexagonal H_{II} structures (Gonzalvez & Gottlieb, 2007; Grijalba et al, 1999; Killian et al, 1994; Ortiz et al, 1999), calcium accumulation could cause significant stress in CL-enriched regions of mitochondrial membranes, promoting the redistribution of CL itself to the surface of the mitochondria via CS (Schug & Gottlieb, 2009).

In pure lipid model membranes, CL promoted association of tBID to the liposomes in a dose-dependent manner (Lutter et al, 2001), and independently of BAX translocation (Gonzalvez et al, 2010). In a cell line carrying a temperature-sensitive CL synthase gene, reduction of mitochondrial CL levels via temperature changes inhibited tBID targeting to the MOM (Lutter et al, 2000). Subsequently, tBID was found to localize preferentially at MOM CS by immunoelectron tomography and mitochondrial subfractionation (Lutter et al, 2001). On the other hand, caspase-8, the proteolytic enzyme that generates tBID, targets the mitochondria via interaction with CL, mediating BID cleavage, which also translocates to mitochondria (Gonzalvez et al, 2008; Jalmar et al, 2013). Indeed, masking CL is sufficient to block the accumulation of caspase-8 and tBID on apoptotic mitochondria, preventing Cyt c release (Heit et al, 2011)(Figure 1.13).

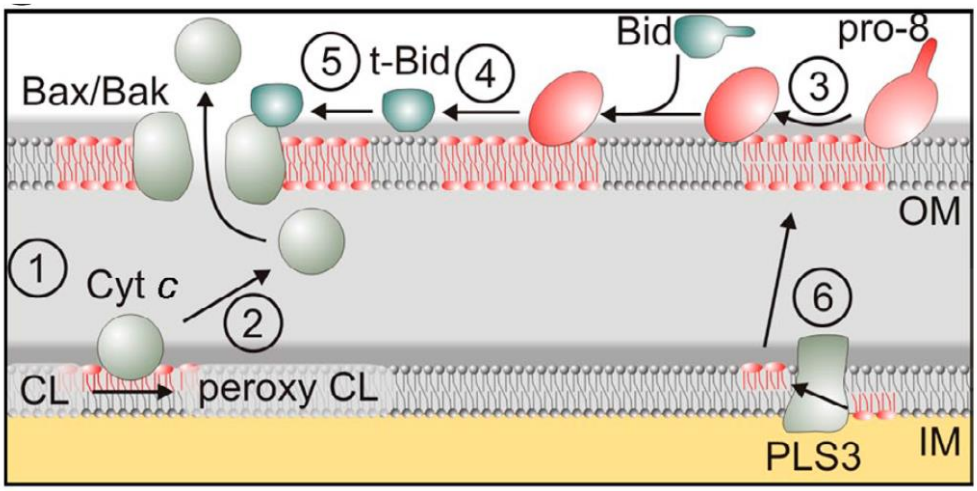

Figure 1.13 Manifold roles of CL during apoptosis. (**1**) Cyt c binds to CL in the inner membrane. (**2**) Release of cytochrome c upon oxidation of CL. (**3**) Pro–caspase-8 (pro-8) binds to the surface of mitochondria and undergoes autocatalytic processing in a CL-dependent manner. (**4 and 5**) BID cleavage to truncated BID (tBID) by caspase-8 (**4**) and activation and oligomerization of BAX/BAK is stimulated by CL (**5**). (**6**) PLS-3 allows export of CL from the inner to the outer mitochondrial membrane (Osman et al, 2011).

Additionally, accumulation of anionic lipids in certain cellular membranes can target polycationic motifs of proteins (Yeung et al, 2006). It is therefore conceivable that an increase in the anionic charge (principally CL) in the MOM during early stages of apoptosis (Heit et al, 2011), could lead to the recruitment of BCL-2 family proteins. Noteworthy, a specific binding pattern for CL has been proposed. Due to the observation of tight binding interactions with three residues (KKY, RKY, and HRN) in different crystal structures of proteins bound to CL, a "XXY" motif, where X is a positively charged and Y a polar residue, can be suggested as a preliminary CL binding motif. It is important to point out that these suggested motifs are nonlinear in amino acid sequence, so that residues from different subunits may contribute to CL binding (Palsdottir & Hunte, 2004). Also, due to the limited number of CL: protein structures available to date, caution should be exercised when assuming that the XXY motif constitutes a common CL-binding motif in mitochondrial proteins.

In this regard, a putative CL-binding domain has been proposed for tBID consisting of lysines 157 and 158 which might establish electrostatic interactions with the CL headgroup (Gonzalvez et al, 2010; Petit et al, 2009). Of note, it has also been described that other phospholipids as PC (Garofalo et al, 2003), PG and PE (Esposti et al, 2001) allow membrane translocation of tBID. Furthermore, it has also been proposed that CL promotes tBID association with the MOM by changing the physical properties of its lipid bilayer, rather than via a direct and specific tBID: CL interaction (Lutter et al, 2000).

Different types of CL modifications have also been linked to apoptosis. For example, peroxidation of CL facilitates Cyt c detachment from the MIM, thereby allowing the presence of a "free" pool

of Cyt c at the intermembrane space, which can be released from mitochondria upon MOMP triggering (Kagan et al, 2005; Ott et al, 2002). CL peroxidation promotes BAX-driven liposome permeabilization and MOMP as well, apparently by changing membrane curvature (Mari et al, 2008). During apoptosis, mitochondria accumulate monolysocardiolipin (MCL), a metabolic product of CL, which can interact with tBID and elicit membrane curvature changes (Esposti et al, 2003; Liu et al, 2005). In addition, a peptide representing the α6 helix of cBID has been described to (i) bind to mitochondria and CL-containing model membranes, and (ii) induce mitochcondrial lipid peroxidation and ROS production (Gonzalvez et al, 2010).

During apoptosis, two other glycerolipids that accumulate in mitochondria before MOMP showing potential to induce membrane curvature changes are lysophosphatidylcholine (LPC) and diacylglycerol (DAG) (Crimi & Esposti, 2011). Interestingly, LPC and DAG have been shown to modulate the membrane-permeabilizing function of BAX by altering the energetic proclivity for proteolipidic pore formation (Basanez et al, 2002; Terrones et al, 2004).

1.6.2.2 Sphingolipids

To date, much of the work on sphingolipids aimed to deciphering the complex biology of sphingolipids as glycosphingolipids and sphingomyelin, which play an important role in diverse processes, e.g. cell adhesion or signal transduction. More recently, ceramide (CER), ceramide-1-P (CER-1P), sphingosine (Sph) and sphingosine-1-P (S1P) have been recognized as playing relevant physiological functions in the regulation of cell proliferation, migration and differentiation, regulation of angiogenesis and in the pathobiology of some diseases as autoimmune diseases, neurodegenerative diseases and cancer (Van Brocklyn & Williams, 2012)(Gomez-Munoz, 2006).

CER and CER-1P are antagonist molecules that can be interconverted by phosphorylation and dephosphorilation. Importantly, an appropriate balance between them seems to be crucial for tissue homeostasis, thus their dysregulation could end in pathological situations (Gangoiti et al, 2010). CER have been reported to be involved in apoptosis, although these lipids are minor components of MOM under normal conditions (Goonesinghe et al, 2005; Obeid et al, 1993; Sandra et al, 2005; Siskind, 2005; Sorice et al, 2009). However, it is now well established that cellular CER levels increase in response to a variety of apoptotic stimuli as TNFα, FAS ligand or DNA damage (Cremesti et al, 2001; Obeid et al, 1993), with CER generation occurring prior to the activation of the apoptotic machinery (Selzner et al, 2001). CER has also been reported to produce alteration in bioenergetics, ROS production and permeabilization of MOM (Birbes et al, 2001; Colombini, 2010; Siskind, 2005). The latter process could occur through formation of MOM channels exclusively composed of CER molecules, although this model has not gained general acceptance (Siskind, 2005; Siskind et al, 2002; Stiban et al, 2006).

Regarding BCL-2 family proteins, CER production increases BAX translocation to mitochondria (Birbes et al, 2005) and stimulates MOMP driven by BAX/BAK, but the underlying mechanisms

are still under debate. On the one hand, the possibility has been raised that during apoptosis CER and BAX may form composite channels directly responsible for enabling the release of mitochondrial apoptogenic factors (Ganesan et al, 2010). BAK (but not BAX) has also been suggested to activate CER synthesis and the increase in CER levels would result in subsequent synergistic channel formation at the MOM by CER and BAX/BAK, implying a non-redundant function for BAX and BAK in apoptosis and metabolism (Beverly et al, 2013; Siskind et al, 2010).

On the other hand, it has been shown that sphingolipid metabolites other than CER cooperate with BAX-type proteins in promoting MOMP. Specifically, transfer of ER-localized CER to the mitochondria leads to production of S1P and hexadecenal (HEX), which in turn, are implicated in functional activation of BAK and BAX, respectively (Chipuk et al, 2012). Experiments using pharmacological inhibitors of sphingolipid enzymes together with reconstitution studies on isolated mitochondria suggest that the mitochondrion-specific sphingosine kinase 2 (producing S1P) and S1P lyase (producing HEX) stimulate apoptosis driven by BAK and BAX, respectively.

Finally, the last group of apoptosis-related sphingolipids is that represented by gangliosides. GD3, a CER-based glycolipid, has been reported to accumulate in mitochondria in several cell lines in response to CER or TNFα treatment suggesting that GD3 contributes to the mitochondrial apoptotic pathway. In fact, exogenous addition of GD3 leads to caspase activation in intact cells, and treatment of isolated mitochondria with GD3 induces cytochrome-c release (Rippo et al, 2000). However, little is known about the impact of this particular ganglioside on BCL-2 protein family function.

1.6.2.3 Cholesterol

Cholesterol (CHOL) plays an important role in the structure, physical properties and function of biological membranes. The CHOL/phospholipid mass ratio of MOM is normally kept between 3% and 24% (Daum, 1985), although different tumour cells were reported to have higher levels of CHOL in their mitochondrial membranes (Baggetto et al, 1992; Crain et al, 1983). However, CHOL has been described to have dual roles in cell death regulation. This dual role apparently depends on the regulation of mitochondrial GSH (mGSH) stores, which in turn play a fundamental role in oxidative stress, CL maintenance and cell death susceptibility (Baulies et al, 2017; Montero et al, 2010).

Mitochondrial CHOL is emerging as an important regulatory factor of MOMP and cell death (Garcia-Ruiz et al, 2009). Different mechanisms have been proposed to explain the antiapoptotic effect of CHOL. First, high levels of CHOL have been shown to protect mitochondria from large amplitude swelling (Graham & Green, 1970) and proton leaking across the MIM, as well as to modify the activities of a number of mitochondrial membrane proteins implicated in apoptosis (Colell et al, 2003). Second, evidence was gathered supporting that CHOL inhibits BAX membrane insertion, oligomerization, and Cyt c release (Lucken-Ardjomande et al, 2008; Montero et al, 2008), either by changing lipid lateral organization or through changes in the

membrane elastic properties (Garcia-Ruiz et al, 2009; Montero et al, 2008). The ability of CHOL to form ordered microdomains in mitochondrial membranes has been linked to both regulation of BCL-2 protein function and apoptosis modulation in intact cells (Garofalo et al, 2005). A putative CHOL recognition amino acid consensus (CRAC) motif has also been identified in BAX, corresponding to residues 113 to 119 of the BAX α5-helix (Martinez-Abundis et al, 2011). However, the CRAC motif is a relatively poor conserved sequence. In addition, BAK does not contain a well-defined CRAC motif.

1.6.3 Lateral segregation of mitochondrial lipids

In addition to specific lipid moieties, lipid may also form lipid domains in mitochondria functioning as signalling platforms for BAX-type protein insertion, oligomerization and pore formation at the MOM. Little is currently known about the lateral distribution of phospholipids in mitochondrial membranes. The non–bilayer forming lipids PE and CL laterally segregate into distinct domains in bacterial membranes lacking sterols and sphingolipids (Kawai et al, 2004; Mileykovskaya & Dowhan, 2000; Nishibori et al, 2005). In the case of CL, clusters of certain size but not individual CL molecules may stabilize the geometry of highly curved regions of the membrane (Schlame & Ren, 2009). In consequence, the high membrane curvature at cristae tips may impose geometric constraints that could lead to an enrichment of CL and PE (Osman et al, 2011), which are also enriched in CS (Ardail et al, 1990; Simbeni et al, 1991). Moreover, recently was reported that the fluidity of the lipid bilayer increased and its mechanical stability decreased with CL concentration, indicating that CL decreases the packing of the membrane and CL promotes the formation of membrane areas with apposed double bilayers or nonlamellar structures, similar to those proposed for mitochondrial contact sites. Altogether, goes in favour that CL induces membrane alterations that support the role of CL in facilitating bilayer structure remodelling, deformation, and permeabilization (Unsay et al, 2013). In addition, BID or tBID may facilitate the assembly of CL-enriched microdomains by segregating together with CL or MCL (Esposti et al, 2003; Gonzalvez et al, 2005; Gonzalvez et al, 2010; Gonzalvez et al, 2008; Kudla et al, 2000; Manara et al, 2009).

Consistent with these ideas, it has been recently proposed that CL provides an anchor and an activating platform for caspase-8/BID, resulting in a change in the fluidity of the membrane when these three components are present together (Gonzalvez et al, 2008; Jalmar et al, 2013). In sum, these data support the existence of spatially CL-enriched microdomains in mitochondria that could act as platforms for recruitment of BCL-2 proteins and could also affect other mitochondrial processes, such as fusion or fission, as well as the insertion or extraction of membrane proteins (Figure 1.14).

Alternatively, or in addition, mitochondria may also contain lipid microdomains reminiscent of the lipid rafts of the plasma membrane (Garofalo et al, 2003). Under pro-apoptotic stimulation, raft-like microdomains were detected on mitochondria that apparently contribute to apoptosis-

associated modifications and to late apoptogenic events (Garofalo et al, 2005; Garofalo et al, 2003; Malorni et al, 2007). These raft-like domains were enriched in gangliosides (GD3, GM3) and CL, while showing a relatively low content of CHOL (Malorni et al, 2007; Sorice et al, 2009). Disruption of such raft-like microdomains by methyl-β-cyclodextrin prevented mitochondria depolarization, Cyt c release and apoptosis execution. Depending on the physiological status of the cells, these raft-like microdomains seem to be enriched in specific mitochondrial proteins, including the voltage-dependent anion channel-1 (VDAC-1), the fission protein hFis1, and BCL-2 family proteins such as tBID and BAX (Morales et al, 2007).

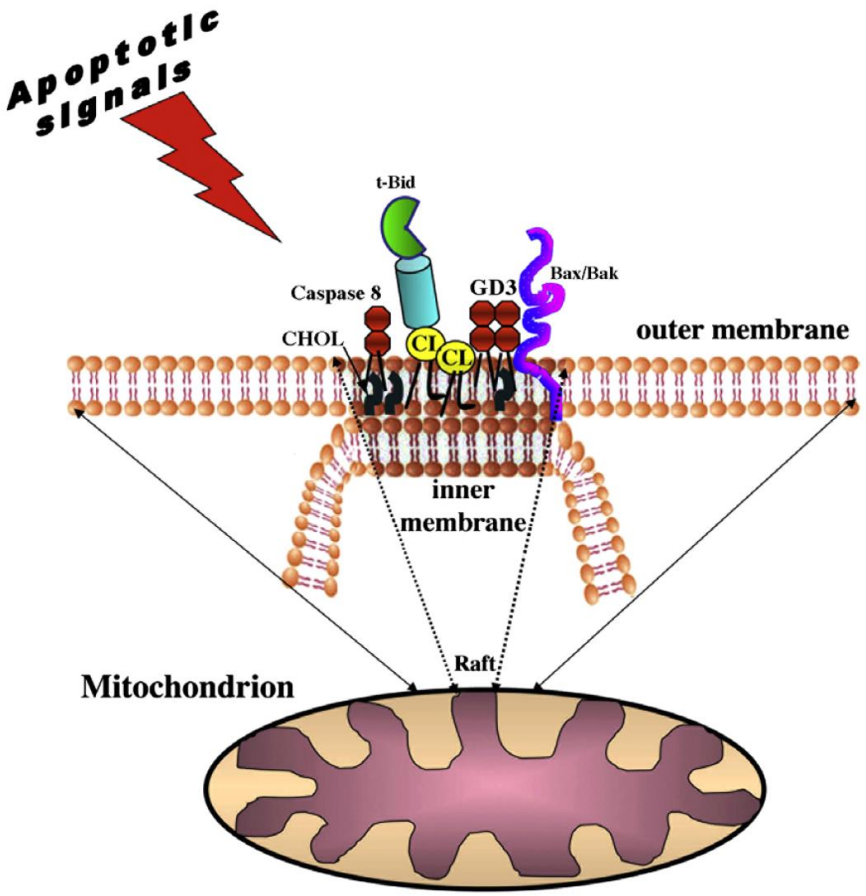

Figure 1.14 Schematic drawing illustrating how cardiolipin-enriched raft-like microdomains are essential activating platforms for apoptotic signals on mitochondria. CL-enriched microdomains, between the mitochondrial inner and outer membranes, represent specialized of mitochondrial membrane tBID is recruited and causes BAX/BAK oligomerization (Sorice et al, 2009).

1.7 MEMBRANE-ASSOCIATED STRUCTURES OF BAX

BAX and its homolog BAK are key regulators of the mitochondrial pathway of apoptosis. On cell stress BAX and BAK accumulate at distinct foci on the mitochondrial surface where they undergo a conformational change, oligomerize, and mediate cytochrome c release, leading to cell death. The molecular mechanisms of BAX and BAK assembly and mitochondrial permeabilization have remained a long standing question in the field. Recent structural and biophysical studies at several length scales have shed light on key aspects of BAX and BAK function that have shifted how we think this process occurs. These discoveries reveal an unexpected molecular mechanism in which BAX (and likely BAK) dimers assemble into oligomers with an even number of molecules that fully or partially delineate pores of different sizes to permeabilize the MOM during apoptosis.

Given the difficulty of applying conventional structural techniques to study membrane proteins, most detailed structural information available corresponds to BCL-2 family members in aqueous environments. So that, the first puzzle with mechanistically relevant information describing BCL2 family proteins interactoma is mainly based on studied that lack in the presence of the membrane. However, the complexity and heterogeneity of the membrane, including curvature, lipid composition etc., has been considered particularly relevant. Indeed, as was described above, membranes are one of the main regulators of the targeting and function of these family proteins, and therefore the study of BCL2 proteins in a membrane environment seems to be compulsory. In the last decade structural information on these molecules in their membrane-associated states has started to emerge, providing fundamental insight about the structural changes accompanying membrane translocation and insertion of BCL-2 proteins during apoptosis.

1.7.1 Conformational changes of BAX during activation.

Understanding the structural changes driving BAX-type proteins from an apoptosis-inactive conformation to a fully activated structure responsible for MOMP has been considered the “holy grail” of the apoptosis research (Youle & Strasser, 2008). In the following sections, the recent progress made in elucidating structurally how BAX mediate MOMP in apoptosis is explained. Proving information, from the conformational changes of BAX needed for its activation in the membrane, through its molecular assembly into oligomers, to the most recent findings about the supramolecular organization of BAX in model systems and cells, and finally their implication in the apoptotic pore formation. These events, are usually encompassed in the following subsections: 1) Early activation steps (N-terminal and BH3 exposure), 2) Membrane insertion, 3) Oligomerization and 4) Supramolecular Structures and Pore Formation.

1.7.1.1 Early activation steps

Biochemical and structural studies have shown that upon apoptosis induction, BAX and BAK undergo profound structural rearrangements, including N-terminus and BH3 domain exposure.

Of note in order to enable this restructuration, the C-terminus must be released from the hydrophobic groove (Figure 1.15).

N-terminal exposure and C-terminal insertion

The N-terminus of BAX and BAK contains two regions, the N-segment (residues 1-15 and 1-23 for BAX and BAK respectively) and the α1 helix. The N-segment in BAX is flexible and exposed to the solvent (Suzuki et al, 2000). During apoptosis the N-terminus of BAX undergoes conformational changes, accompanied by different ellipticity and partial rotation of the α1 helix. This conformational change has commonly been used as a marker in cellular assays to detect early steps in BAX/BAK activation (Dewson & Kluck, 2009; Dewson et al, 2009; Dewson et al, 2008; Griffiths et al, 2001; Kim et al, 2009; Lalier et al, 2007; Nechushtan et al, 1999). Most data come from studies based on the conformation-specific antibodies that recognized the exposure of the hidden epitope: 6A7/49F9 antibody for BAX and Ab-1 antibody in the case BAK (Czabotar et al, 2013; Dewson et al, 2008; Griffiths et al, 2001; Kim et al, 2009; Peyerl et al, 2007). These structural rearrangements have also been addressed by structural studies in active BAX/BAK conformation, showing that upon tBID activation helix α1 is liberated from the remaining structure of BAX/BAK along with the loop that interconnects α1-α2 (Bleicken et al, 2010; Oh et al, 2010).

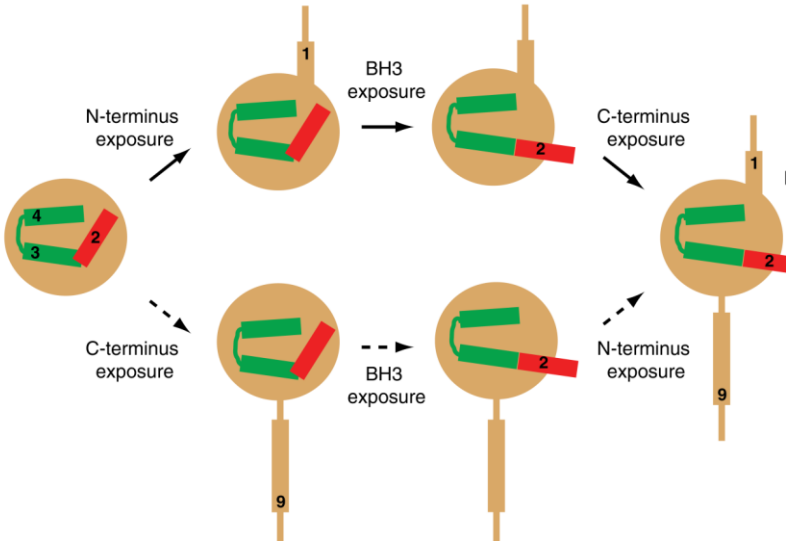

Figure 1.15. Two proposed sequences of BAX conformation change during early activation steps during apoptosis. The non-activated form of BAX is represented as a globular molecule (orange) containing a hydrophobic surface groove (α3/α4; green) and a buried BH3 domain (α2; red). A BH3-only protein binds BAX to its non-canonical groove (solid arrow) and initiates BAX conformational changes. In this model, first, BAX exposes its N-terminal (α1) and then the BH3 domain. Finally, the exposure of these domains leads to the dislodgement of the C-terminal domain (α9). By contrast in the other model (dashed arrow), the sequence is the opposite. First, the C-domain in BAX is released from the canonical groove; in this manner BH3-only proteins could bind this groove. Once BAX is activated the BH3 domain is exposed and then the N-terminal region. In this drawing the insertion of the α5-α6 central hairpin has not been taken into account. Taken from (Westphal et al, 2011).

In the specific case of BAX, it has also been described that the α1 helix stabilizes helix 9 engagement into the hydrophobic groove, concluding that the N-terminal exposure is correlated with insertion of the protein into the MOM (Kim et al, 2009; Nechushtan et al, 1999). However, recent studies suggest that BAX tail-anchoring to the MOM precedes the conformational change leading to exposure of BAX N-terminal epitope (Schellenberg et al, 2013). In stark contrast, BAX bound to liposomes led to N-terminal exposure but without membrane insertion (Yethon et al, 2003). This controversial issue is particularly important in the understanding of BAX membrane activities and the mode of inhibition exercised by the antiapoptotic members.

BH3 domain exposure

Solution structures of BAX, BAK, BID and BCL-2 type proteins revealed that in all these molecules the hydrophobic face of helix α2 (BH3 domain) is oriented towards the protein interior (Moldoveanu et al, 2006; Suzuki et al, 2000). Complementarily, solution structures of synthetic peptides representing proapoptotic BH3 domains complexed with BCL-2 type or BAX-type proteins revealed that the same hydrophobic face of such peptides makes crucial interactions with the hydrophobic groove of multidomain binding partners. From here, it is reasonable to assume that if BH3-into-groove interactions are the core mechanism by which BCL-2 family proteins modulate MOMP, BAX/BAK/BID need to change conformation to expose their BH3 domains in order to engage in homo- or hetero-dimerization reactions (Cartron et al, 2005; Dewson et al, 2008; Dewson et al, 2012; George et al, 2007; George et al, 2010; Munoz-Pinedo, 2012; Sattler et al, 1997; Simonen et al, 1997; Whelan et al, 2012; Willis et al, 2005). Consistently, the blockade of BAX/BAK BH3 domain by epitope-specific antibodies prevents BAX/BAK oligomerization and Cyt c release (Bleicken et al, 2010; Czabotar et al, 2013; Dewson et al, 2008; Dewson et al, 2012; Moldoveanu et al, 2013).

1.7.1.2 Membrane insertion of BAX

Another aspect that has received considerable attention regarding the activation of BAX-type proteins is the insertion of distinct helical fragments into the membrane lipid bilayer. Glycosylation assays *in vitro* using BAX fragments and microsomal membranes showed that helices α1, α5, α6, and α9 are all inserted into the membrane adopting a transmembrane orientation, although α6 alone did not insert into the membrane (Garcia-Saez et al, 2004). Cysteine accessibility experiment using mitochondria isolated from cells overexpressing BAX indicated that BAX α5, α6, and α9 are inserted into the membrane, although this process was shown to be insufficient for MOMP induction (Annis et al, 2005). In addition, the sequence of events leading to this insertion remains unknown, although evidences suggest that BAX α5α6 membrane insertion occurs prior to oligomerization and membrane permeabilization but after BAX:tBID interaction (Annis et al, 2005; Lovell et al, 2008; Weber et al, 2013). On the other hand, cross-linking studies with overexpressed BAX/BAK suggest that during MOMP the two

proteins only insert their C-terminal α9 helix into the membrane, while the rest of the molecule (including α5α6) maintains the solution globular fold (Dewson & Kluck, 2009).

By contrast, rather than maintaining its globular fold, as previously said recently it has been proposed that BAX α5α6 separates from the core of the protein during the early activation step of the protein. Crystallographic data for truncated BAX in detergent solution have disclosed a novel conformational change on BAX activation that generates a 'core' (α2– α5) and a 'latch' (α6– α8) domain and induces transient exposure of the α2/BH3 domain. This rearrangement proceeds via partial unfolding of the hairpin comprising helices α5 and α6 and seems to be essential for BAX function (Czabotar et al, 2013) (Figure 1.16).

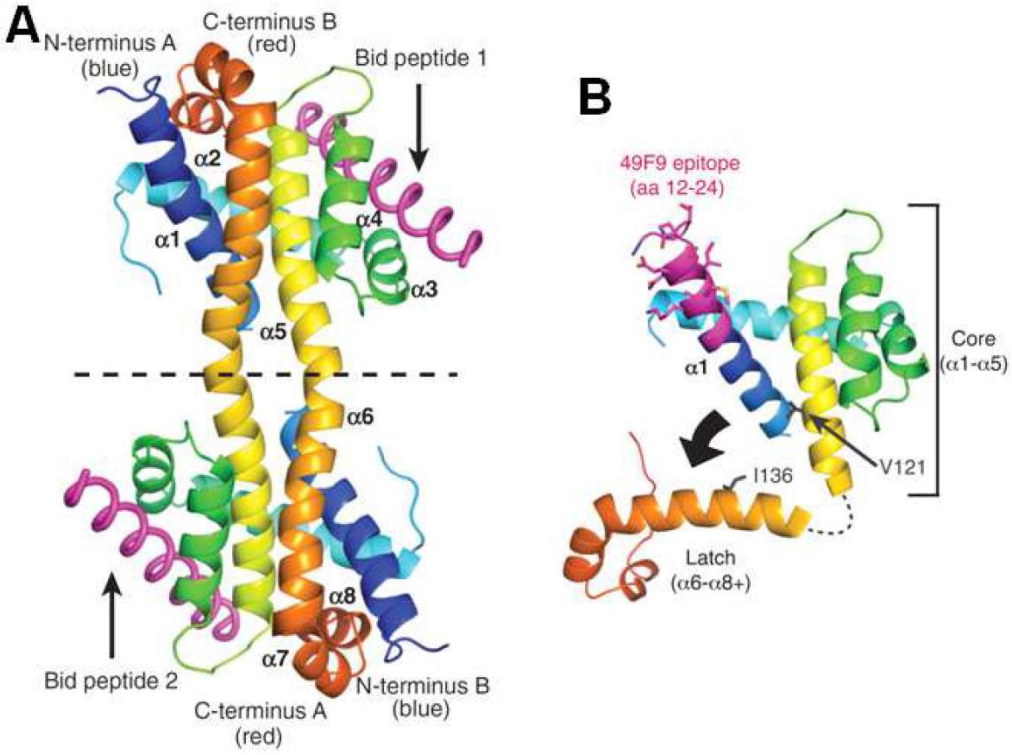

Figure 1.16 Early activation steps in BAX-type proteins. (**A**), dimer of BAXΔC21, rainbow coloured (blue N terminus to red C terminus) in complex with BIDBH3 (magenta), illustrating domain swapping of helices α6–α8 (coloured orange and red) across the dotted line (PDB: 4BD2). (**B**), Putative intermediate in transition from monomeric BAXΔC21 to the structure in the left. Taken from (Czabotar et al, 2013).

In the dimer the α2/BH3 domain of a BAX molecule binds to the canonical groove of another BAX and viceversa (BH3-in-groove interaction) (Figure 1.17). This allows the formation of a stable 'symmetric' dimerization domain, which supports a model initially proposed based on crosslinking and low-resolution structural studies (Bleicken et al, 2010; Dewson et al, 2012). This symmetric model was also confirmed using double electron–electron resonance (DEER) studies of the full-length protein, in solution (Sung et al, 2015) in a membrane environment (Bleicken et al, 2014) and by FRET microscopy in living cells (Gahl et al, 2014).

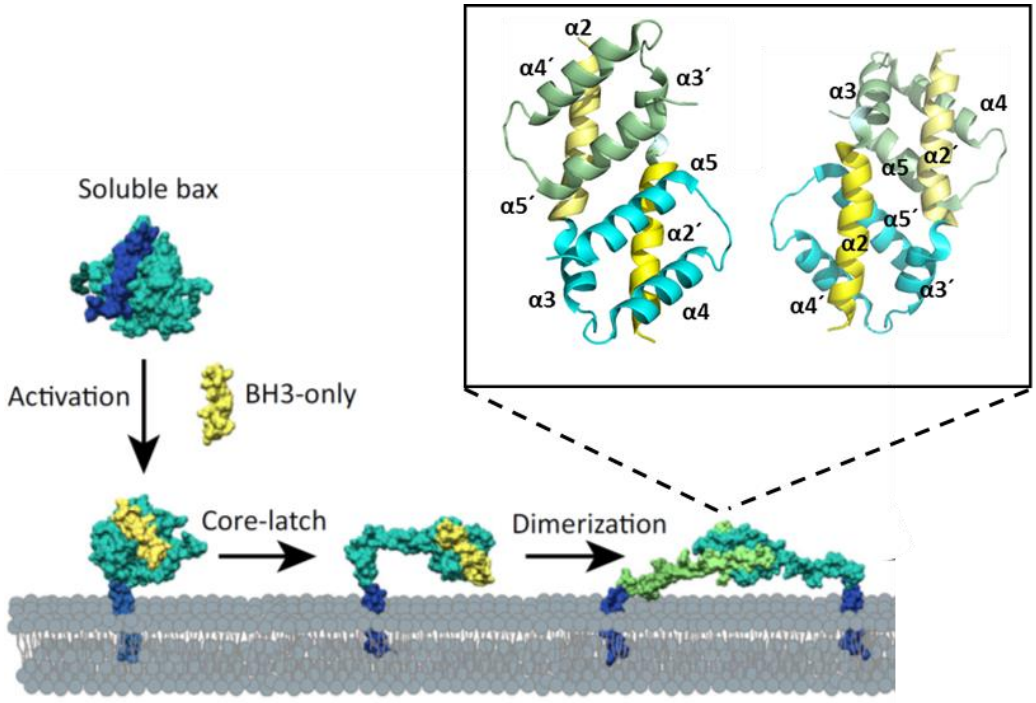

Figure 1.17. Model for BAX Activation and Dimerization at the Membrane. Proteins are illustrated in their surface representations. In its soluble form, BAX (cyan) retains a globular conformation where its transmembrane domain (α9 helix, blue) is kept in the BAX hydrophobic groove (α2–α5). On activation by BCL2 homology (BH)3-onlyproteins (yellow), BAX undergoes a series of conformational changes displacing α9 from the groove, which inserts in the membrane (grey), and dissociating in a core (α2–α5) and a latch (α6–α9) domain by unfolding of helices α5 and α6. Following activation, BAX engages in BH3-in-groove dimerization with another activated BAX molecule (light green) while displacing the BH3-only activator from the hydrophobic groove. This leads to the formation of a symmetric dimer. Zoomed in cartoon representation appears the core domains PDB (4BDU), one monomer (M) coloured in yellow (BH3/α2) and in pale cyan (α3- α5) and a second monomer (M´) coloured in pale yellow (BH3/α2) and in cyan (α3- α5). Adapted from (Cosentino & Garcia-Saez, 2017; Czabotar et al, 2013).

Since this model was proposed, same group proposed a mechanism in which apoptotic pore formation requires the insertion of BAX central helices into the mitochondrial outer membrane (Cosentino & Garcia-Saez, 2017; Subburaj et al, 2015; Westphal et al, 2014a; Westphal et al, 2014b).This new approach rejected a longstanding 'umbrella' model, inferred on the grounds of structural similarities between soluble BAX and other α-pore-forming proteins like colicin and diphtheria toxin (Petros et al, 2004). In the umbrella model, α5 and α6 helices were assumed to insert as a transmembrane hairpin perpendicularly to the membrane while the other helices would lie on the membrane surface in an umbrella-like configuration. In the "in-plane model" α9 is a TM domain and other helices (including α5 and α6) insert only shallowly into the bilayer (Figure 1.18A-B). However, the interpretation of how BAX domains are arranged with respect to such a membrane pore is unclear in this model. Complementarily, with small peculiarities but sharing the same tendency, DEER studies of membrane-bound full-length BAX provided additional information about the structure of active BAX dimers in the membrane (Bleicken et al, 2014).

While the α2– α5 core helices of BAX dimers retain a well-defined structure similar to the soluble one, helices α6–α9 adopt a more flexible conformation, which may play a role in membrane destabilization. This is the basis for a model where partial opening of helices α5 and α6 is essential for membrane permeabilization; these two pairs of helices assemble in the dimer as a 'clamp', with the dimerization domain (helices α2–α5) at the rim of a lipidic pore and the amphipathic α6 helices lying on the surface, parallel to each other, on opposite sides of the membrane (Bleicken et al, 2014) (Figure 1.18C-D). In this "symmetric" model it is unclear how the C-terminal α9 helices are oriented. They could be antiparallel, unless the structural symmetry of the dimer is broken. Despite this, if confirmed, this model would provide a firm explanation for how BAX molecules stabilize open pores at the membrane.

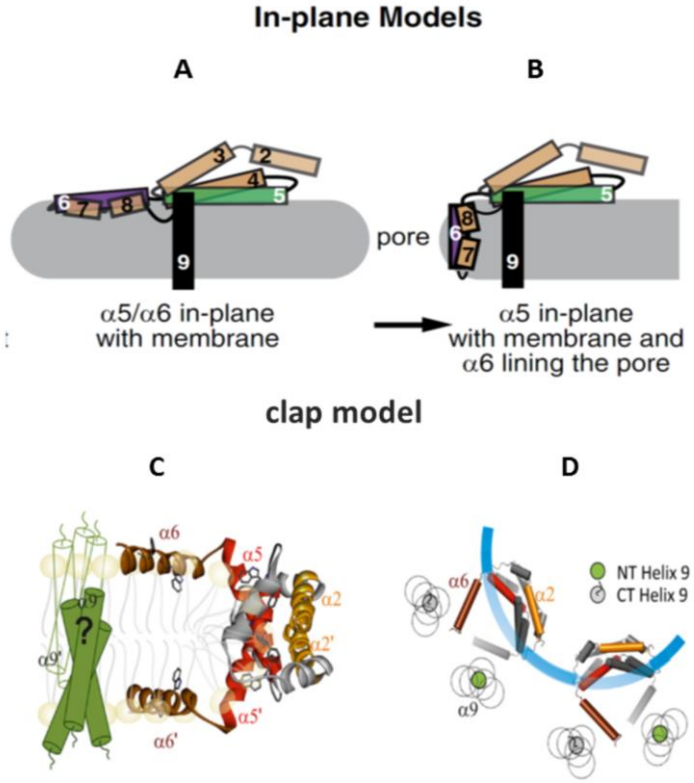

Figure 1.18 Models of active dimeric BAX in the membrane. (A) In the in-plane models, α5 remains with α2–α4 in the core, where it contributes one face to a BH3:groove interface and the opposite to the membrane, whereas α6 disassociates from the α2–α5 core and collapses onto the membrane, presenting its polar face to the cytosol and its nonpolar face to the membrane. **(B)** Several of the in-plane helices may then slide into a nascent pore to promote its development or stabilize its wall. **(C)** Hypothetical clamp model for the topology of active BAX dimers at the MOM: the dimerization domain is at the rim of a pore induced by BAX in the membrane, with helices 5 and 6 lying on the membrane surface. The hypothetical symmetric and transmembrane location of the dynamic helices 9 is sketched. **(D)** Schematic top view of two adjacent BAX dimers in the pore based on the proposed structural model (C) and compatible with a transmembrane orientation of the dynamic helices 9. The coloured helix α6 in the dimer is above the membrane, while the α6 depicted in grey is laying spatially below the one coloured, so that the corresponding helix 6 is below the membrane plane. The possible locations of the dynamic N and C termini (NT, CT) of helices 9 are shown (D). Adapted from (Bleicken et al, 2014; Westphal et al, 2014a).

1.7.1.3 Oligomerization

Some studies raise the question if oligomerization is essential for permeabilization. Based on a reconstituted system, Newmeyer and colleagues indicated that BAX oligomerization is not a pre-requisite for BAX pore formation (Kushnareva et al, 2012). In agreement with this idea, Xu and colleagues found that a single molecule of BAX inserted in a nanodisc can form a small pore (Xu et al, 2013). However, multiple studies have suggested that that MOMP is accompanied by BAX and BAK homo-oligomerization, even if some aspects of this process are still controversial. It has been proposed that higher-order multimers of BAX/BAK are formed through engagement of other interaction surfaces, most prominently BAX/BAK α6 (Dewson et al, 2009; Ma et al, 2013). Another model for BAX oligomerization is the "head-to-tail" or asymmetrical model (Bogner et al, 2010; Zhang et al, 2010). Here, an activated BAX molecule with an exposed BH3 domain would bind to a second BAX molecule in the non-canonical groove pocket thereby explaining formation of higher-order BAX oligomers (Figure 1.19).

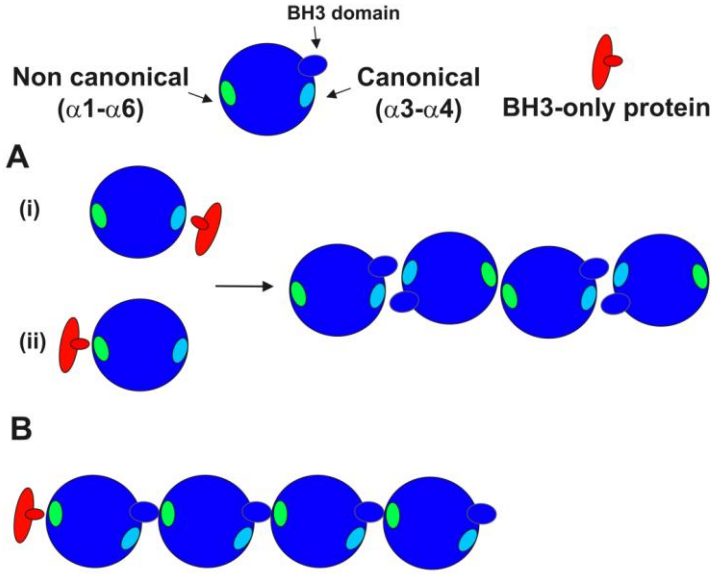

Figure 1.19 Proposed models for BAX activation and oligomerization. BAX is represented as a globular blue molecule; the non-canonical groove is in green, the canonical groove in light blue and the BH3 domain as a small square in blue. **(A)** "BH3 in groove" or symmetric dimer. The BH3-only protein (red) can bind the non-canonical or the canonical groove and BAX molecule exposes its BH3 domain; this now could bind to the canonical groove of another activated BAX molecule. Thus, this model is based in the interaction of the BH3 domain into the canonical groove. In addition, it has been proposed that higher order oligomers could be formed by interactions of the α6 helix. **(B)** "Head-to-tail" or asymmetrical model**.** Here, a BH3 only protein activates a BAX molecule that exposes its BH3 domain; This BAX BH3 domain is able to activate another BAX molecule by the non-canonical groove thereby allowing the formation of higher order oligomers.

However, as explained before, according to the currently popular view, once the BH3 domain of a BAX/BAK molecule is exposed it engages the canonical binding groove of another activated BAX/BAK molecule, forming ‘‘BH3-in-groove’’ “symmetric” dimer (Bleicken et al, 2010; Bleicken et al, 2014; Dewson et al, 2009; Dewson et al, 2008; Dewson et al, 2012; Oh et al, 2010; Westphal et al, 2014a). Here, the existence of an additional interface would provide a rationale for how symmetric BAX and BAK dimers further assemble in higher-order oligomers. Several studies have implicated a role for helices α6 and α9 in BAX oligomerization (Dewson et al, 2012; Zhang et al, 2015). Dimerization via α9 (and probably α6) occurs downstream of BH3-in-groove dimerization, suggesting that it might represent the interaction site of symmetric dimers needed to form higher-order oligomers. Since α9 dimerization is not required for the passage of small molecules like cytochrome c but only for bigger ones like SMAC, the relative importance of interdimer contacts via helices α6 versus α9 remains unclear (Zhang et al, 2016). Recently, crosslinking and DEER results have reported a novel oligomerization site for BAK in isolated apoptotic mitochondria involving the α3/α5 interface, which, together with α6 (and hypothetically α9), stabilizes interactions of neighbouring BAK homodimers (Mandal et al, 2016).

1.7.1.4 Supramolecular structures formed by BAX (and BAK)

Historically and currently back in vogue, the formation of BAX/BAK clusters has been linked with apoptotic phenotype (Figure 1.20 A-B), (Nasu et al, 2016; Nechushtan et al, 2001; Uren et al, 2017) and recently, in the edge of these clusters, has been reported the formation of BAX assemblies associated with its apoptotic activity, in form of semi-arcs, arcs and rings (Grosse et al, 2016; Salvador-Gallego et al, 2016)(Figure 1.21 A-B). In agreement with experiments on model membranes, BAX oligomers displayed a wide distribution of sizes (ranging from a few tens of nanometres to 100nm in diameter) and shapes, indicating that BAX-mediated MOMP involves flexible and diverse pores structures.

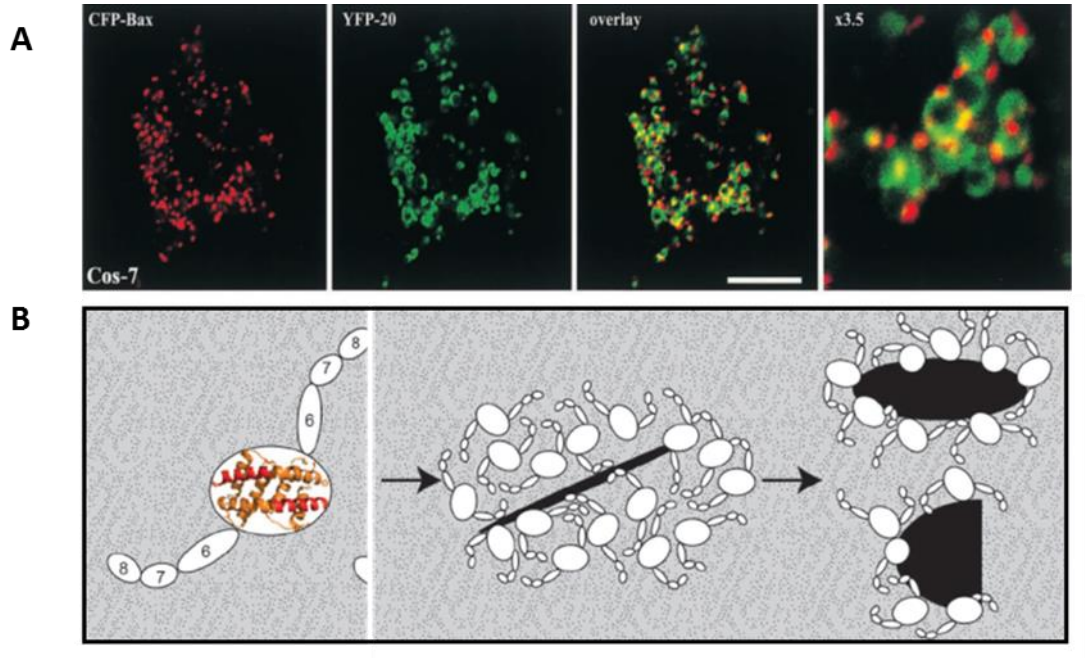

Figure 1.20 BAX/BAK supramolecular structures (I). Apoptotic clusters-A-B: **(A)** Cos-7 cells transiently expressing CFP-BAX together with the outer mitochondrial membrane marker, YFP-20, were treated with 1 μM STS for 5 h to induce apoptosis and then were examined by laser scanning confocal microscopy. CFP-BAX(red) was located in small punctate structures, whereas YFP-20 (green) was located in larger round mitochondrial-shaped structures. In overlay images, the BAX clusters appeared to be located next to or on top of the YFP-20–labelled structures. Bars, 25 μm . Taken from (Nechushtan et al, 2001). **(B)** Hypothesis of how growing clusters of BAK dimers induce membrane tension to rupture mitochondria. The top view of BAK dimers lying in-plane on the mitochondrial surface. The α2-α5 core is bounded by the large oval. Extending from the core are the membrane anchored C-terminal helices α6, α7 and α8. For simplicity, the α9 transmembrane domains that project into the membrane plane, and the flexible, solvent exposed N-termini of each dimer are not shown(left). Lipids and Bak dimers rearrange to bury exposed hydrophobic surfaces, yielding a variety of proteolipid (toroidal) 'pores′(right). Taken from (Uren et al, 2017).

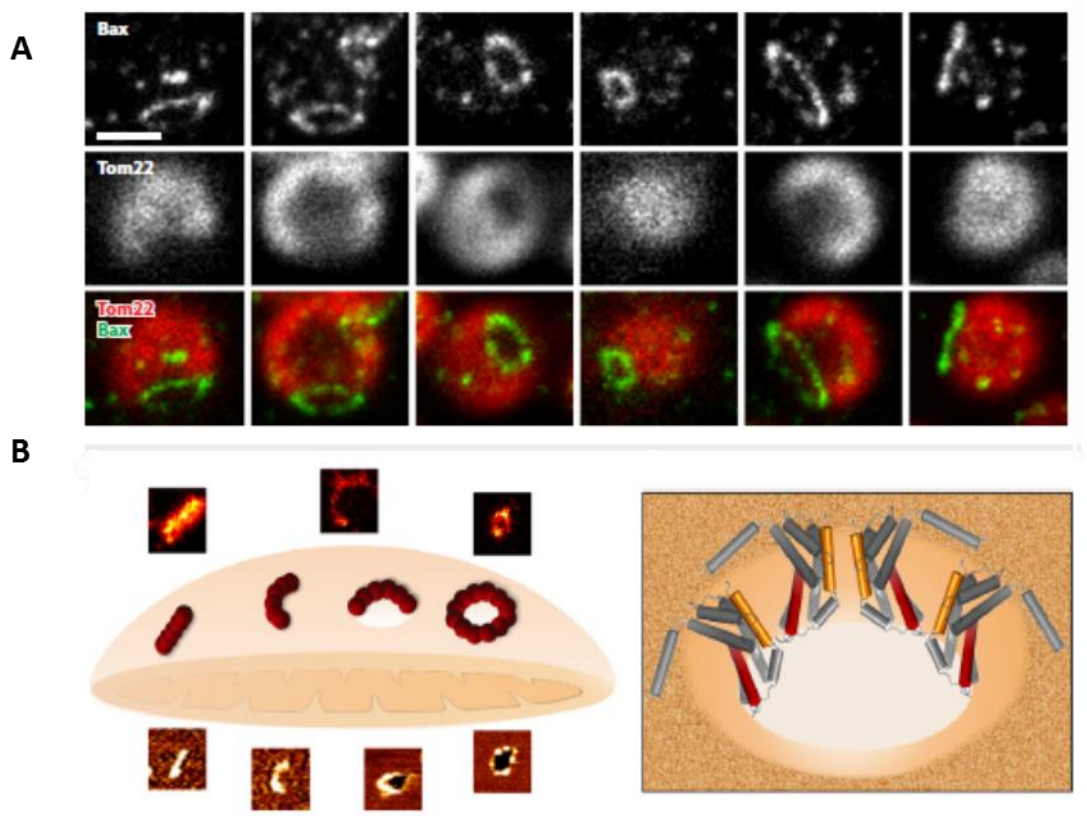

Figure 1.21 BAX/BAK supramolecular structures (II). Apoptotic rings A-B. **(A)** Apoptotic mitochondria were decorated with antibodies against BAX (green) and Tom22 (red). The BAX signal was recorded in the STED mode. Shown are the individual colour channels as well as an overlay (from top to bottom) of several apoptotic mitochondria. We used Lagrange interpolation to double the number of pixels. Note that throughout this manuscript except for contrast stretching, no image manipulation was applied. Scale bar: 0.5 µm (C). Taken from **(**Grosse et al, 2016). **(b)** ***left:*** Illustration of the possible roles for the BAX non-random assemblies revealed by SMLM and AFM during apoptosis. Linear and arc clusters not perforating the membrane could correspond to BAX at initial stages of gathering on healthy mitochondria. They would evolve toward opening of membrane pores, where the protein is covering completely (full rings) or partially (arcs) the pore rim. We cannot exclude that a fraction of the linear and arc-shaped assemblies corresponds to BAX pores observed from different perspectives. The number of red spheres (BAX dimers) is illustrative and does not need to correlate with the actual number present in the structures. ***right:*** The mechanism by which BAX permeabilizes the membrane is mainly by releasing the curvature stress at the membrane edge. Full as well as partial coverage of the pore rim by BAX molecules could reduce line tension enough to stabilize the open pore state. The illustration shows an incomplete ring assembly of active BAX dimers adopting a clamp-like structure at the pore interface (Bleicken et al, 2014). Taken from (Salvador-Gallego et al, 2016).

However, despite all the structural and apparently biologically relevant information, the question about the minimum number of BAX molecules able to form a functional pore at the MOM remains open. As previously commented, data from lipid nanodisks suggest that monomers or dimers are sufficient to stabilize membrane openings (Xu et al, 2013), which could grow with

additional BAX molecules. Moreover, due to the apparent impossibility of decoupling apoptotic process (loss of membrane potential, cyt c release, mitochondrial cristae remodelling etc.) the direct link between these structures and MOMP remains ill defined. Furthermore, another issue is the contribution of other MOM components to BAX-pore structures, including BAK (Zhou & Chang, 2008) and proteins involved in mitochondrial dynamics such as Drp1 and Mitofusins (Karbowski et al, 2002) MOMP have to be considered.

1.7.2 Insights into the Assembly of BAX oligomers

Deep structural changes induce a conformation of BAX that inserts extensively into the lipid bilayer and perforates it (Czabotar et al, 2014). This step is concomitant with BAX assembly into oligomers. Crosslinking and gel filtration studies have detected diverse oligomeric forms of BAX (Annis et al, 2005; Antonsson et al, 2001). However, none of these experimental approaches allowed precise determination of the oligomeric state of BAX during its activation and function in the membrane.

Single-molecule imaging studies have recently elucidated key aspects of the molecular mechanism of BAX assembly in the membrane. Initially, BAX inserts in to the bilayer as a monomer, suggesting that BAX activation involves conformational changes that allow its membrane insertion but precede its dimerization, supporting a two-step activation process for BAX. However, probably due to the instability of this monomeric structure, BAX molecules quickly self-assemble into higher-order oligomers (Subburaj et al, 2015). Importantly, in equilibrium, BAX in the membrane is present as a mixture of species based on dimer units. In this scenario, the interdimer interactions are weaker than intra dimer ones, in line with a dynamic vision of BAX assembly where oligomerization is a reversible process that can be modulated, for example, by protein density at the membrane. Interestingly, same group have reported that BCL-XL is able to disassemble preformed complexes (Subburaj et al, 2015). Although the exact molecular mechanism is not understood, this suggests that the assembly pathway of BAX can be a reversible process that can be regulated by other BCL2 members. This issue would explain the variety of oligomeric species found in previous studies and would be consistent with the formation of membrane pores that are tunable in size (Bleicken et al, 2013a; Bleicken et al, 2013b; Gillies et al, 2015).

1.8 PORE FORMATION

Since decades it is well established that BAX, BAK and perhaps BOK are the executioners of MOMP, but the nature of the membrane openings exerted by activated BAX/BAK has been a highly controversial issue. Different models have been proposed to explain how BAX-type proteins lead to MOMP. However, in the last 5 years the field converge in a pore constituted mainly, if not solely, of BAX (and BAK) dimmers with a proteolipidic nature and tunable size. However, there are still open question discussed below. These models can be divided in two groups: Indirect Models and Direct Models.

1.8.1 Indirect models

According to this view, BAX-type proteins induce MOMP by regulating the activity of endogenous mitochondrial channels. This model postulates that BAX permeabilizes MOM via a physical interaction with the components of the mPTP (Permeability Transition Pore) found at mitochondrial contact sites (Kroemer et al, 2007). The mPTP is thought to be composed by the adenine-nucleotide translocator (ANT, located in the MIM), the voltage-dependent anion channel (VDAC, located in the MOM) and the cyclophilin-D (CyP-D, located into the matrix surface of the MIM) (Baines et al, 2005; Schinzel et al, 2004). mPTP opening allows the free flux of ions and water into the mitochondrial matrix, causing swelling of the organelle and rupture of the MOM; a phenomenon that is not usually detected in a cell dying by apoptosis. Moreover, mPTP-induced cell death is generally considered to be necrotic rather than apoptotic (Nakagawa et al, 2005; Tsujimoto et al, 2006).

This hypothesis has been questioned and nowadays is almost totally relegated mainly due to knock-out studies showing that each one of the postulated mPTP components (VDAC, ANT and Cyp-D) are not dispensable for MOMP and apoptotic cell death (Baines et al, 2005; Baines et al, 2007; Kokoszka et al, 2004; Nakagawa et al, 2005; Whelan et al, 2012). In 2013, some authors suggest that the true component of the mPTP is dimeric ATPase, and therefore, it cannot be completely ruled out the mPTP, at least under some conditions (Giorgio et al, 2013). However, recent results describing supramolecular structures in both cellular and *in vitro* conditions support the idea that BAX (and BAK) are sufficient for the apoptotic pore formation.

1.8.2 Direct models

This model originated from the structural similarities found between BCL-2 proteins and bacterial pore-forming toxins (Petros et al, 2004). Furthermore, different groups have shown that activated BAX and BAK can permeabilize pure lipid membranes in the absence of other mitochondrial components (Basanez et al, 1999; Basanez et al, 2002; Bleicken et al, 2010; Bleicken et al, 2013b; Kuwana et al, 2002; Martinez-Caballero et al, 2009; Roucou et al, 2002; Saito et al, 2000; Schafer et al, 2009; Terrones et al, 2004; Xu et al, 2013).

As mentioned before, different lines of evidence suggest that the central hairpin (α5α6) is responsible for its pore forming activity. Deletion of BAX α5α6 abolished BAX driven Cyt c release (Heimlich et al, 2004) and peptides corresponding to BAX α5 or α6 form pores similar to those elicited by activated full length BAX (Fuertes et al, 2010a; Garcia-Saez et al, 2005; Garcia-Saez et al, 2006; Valero et al, 2011).

Despite intense research, the nature and the exact mechanism by which BAX/BAK mediate MOM permeabilization remain controversial. Two distinct models have been proposed for the BAX/BAK pore; (i) a proteinaceous barrel-stave channel, and (ii) a proteolipidic pore (Figure 1.22).

1.8.2.1 Proteinaceous channels

Proposed two decades ago and nowadays almost discarded, this model postulates that BAX or BAK induces MOMP generating a purely proteinaceous channel, as in the case of the peptide alamethicin or β-pore forming toxins (PFT). In the alamethicin channel, its helices adopt a transmembrane configuration and interact with each other as in the staves of a barrel, so that the lumen of the aqueous channel is formed by the peptide (He et al, 1996; Qian et al, 2008a) (Figure 1.22A/C). In a similar way, pore-forming toxins such as pneumolysin or tetanolysin first oligomerize in the membrane in a structure named pre-pore and then, they insert a β-hairpin of each oligomer unit in a transmembrane fashion. In this PFT induced channel, the lumen of the pore is exclusively constituted by a huge β-barrel (Anderluh & Lakey, 2008).

Following this line of reasoning, BAX has been proposed to be a component of a purely proteinaceous Mitochondrial Apoptosis-induced Channel (MAC) (Dejean et al, 2005). In kinetic and conductance studies it was estimated that MAC channel contains up to nine molecules of BAX (Martinez-Caballero et al, 2009), with a diameter in the range of 2.9 to 7.6 nm. MAC channel has been shown to be permeable to 10 and 17 kDa, but not 45 and 71 kDa Dextran (reviewed in (Dejean et al, 2010). By contrast, liposome permeabilization experiments indicated that a tetrameric BAX channel is the minimal stoichiometry required to allow Cyt c passage across liposomal membranes in the absence of any additional mitochondrial protein (Saito et al, 2000). However, neither the tetrameric BAX channel nor the MAC channel explains that BAX-driven MOMP allows the release of multiple, differently-sized mitochondrial proteins.

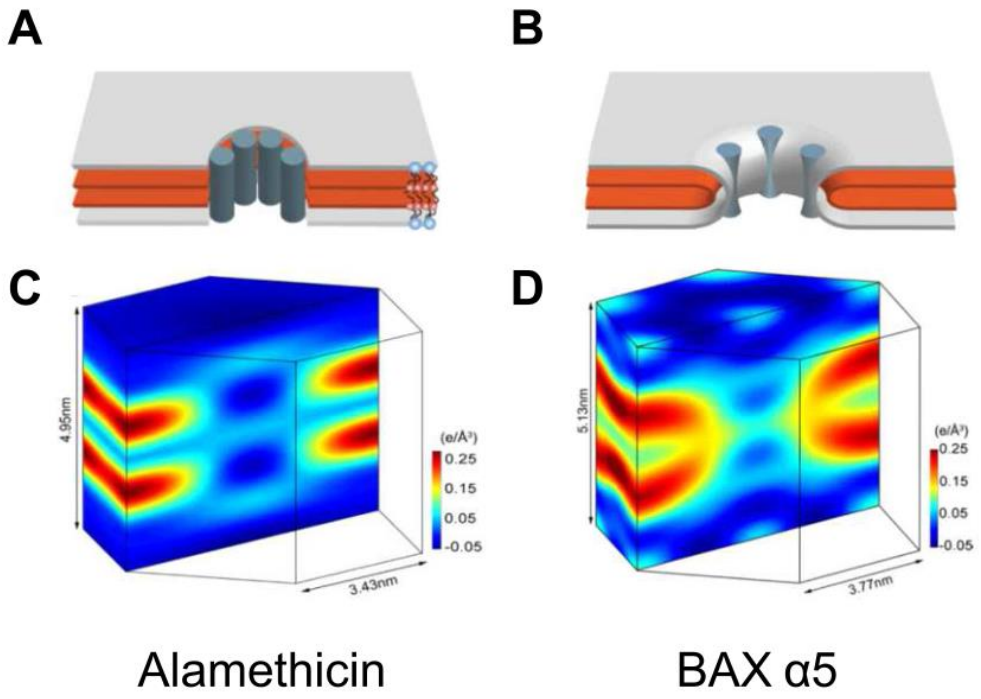

Figure 1.22 Barrel-stave vs. Proteolipidic pore model. Schematic representations of barrel-sate model (**A**) and proteolipidic model (**B**) are shown in a 3D view cut through the pore. Grey layers represent lipid headgroups of the bilayer, Br atoms located in the acyl chains are shown in red and protein helices by dark cylinders. The corresponding normalized electron density distributions of Br atoms of lipid bilayers containing alamethicin (**C**) and BAXα5 (**D**). Br atoms are distributed in the high-density region (yellow-red-black). Note that unlike in a proteinaceous channel, in a proteolipidic pore: (i) the surface of the pore is lined by lipid headgroups, (ii) membrane monolayers are bent at the edge of the pore, and (iii) the two leaflets of the bilayer become continuous. Taken from (Qian et al, 2008b).

1.8.2.2 Proteolipidic pore

The proteolipidic pore model was first proposed to explain the mode of action of magainin, a 23-residue antimicrobial peptide (Ludtke et al, 1996; Matsuzaki et al, 1996). From a structural viewpoint, the toroidal pore and the barrel-stave pore differ in that in the toroidal pore the peptides always remain associated to the bilayer´s hydrophilic-hydrophobic interface, while in the barrel-stave pore the peptides cross the bilayer from one side to the other (Figure 1.22 B/D). In the toroidal pore model, the asymmetric insertion of peptide helixes exclusively into one of the membrane leaflets leads to an increase of membrane tension. When a threshold tension is reached, the bilayer structure becomes unstable, inducing lipids to fold into a highly curved pore where the membrane leaflet becomes continuous as a toroidal hole. Thus, as monolayers are in contact, they form a continuous structure with positive monolayer curvature in the perpendicular plane to the membrane and negative curvature in the plane of the membrane. The generated structure is known as a proteolipidic pore, in which the rim of the pore is formed by both lipids headgroups and protein molecules. The curvature stress could be alleviated by the localization of protein molecules at the edge of the pore and/or by peptide-generated membrane curvature (Fuertes et al,

2010b; Fuertes et al, 2011; Huang, 2000; Matsuzaki et al, 1996; Valcarcel et al, 2001; Yang et al, 2001) **(**Figure 1.23**).**

In other words, it is important to consider that membranes are non-covalent 2D assemblies kept together by the hydrophobic effect. This means that disrupting the continuity of the membrane bilayer has a high energetic cost. Therefore, it is not trivial how a protein would induce membrane opening. When membranes are under stress they are tensed, and beyond a certain threshold the planar assembly disrupts and a pore opens (Lee et al, 2004). The toroidal pore model proposes that lipids at such a pore rim bend to avoid exposure of the hydrophobic acyl chains to the aqueous environment (Ludtke et al, 1996). As a consequence, the two membrane leaflets form a continuous surface that is brought into contact by lipids at the curved pore edge. It is this high membrane curvature that is responsible for the high energy cost of maintaining the open pore conformation. The energy cost is directly proportional to the perimeter or length of the pore. For this reason, the driving force for toroidal pore closure is known as line tension (in contrast to membrane or surface tension, which is proportional to the area). To keep a toroidal pore stably open, the energy cost of the bent membrane at the pore edge needs to be reduced by stabilizing the curved structure (Karatekin et al, 2003).

In the last years, several groups including ours have gathered different lines of evidence supporting that active forms of BAX forms toroidal pores of proteolipidic nature. BAX decreases planar membrane lifetime and form pores with variable conductance states (Basanez et al, 1999). In addition, the characteristics of the pore formed by BAX are affected by modifying the physical properties of the membrane with lipids with different intrinsic monolayer curvature (Basanez et al, 2002; Terrones et al, 2004). On the other hand, a peptide derived from the helix α5 of BAX forms pores with lipid molecules in the lumen as demonstrated by X-ray diffraction (Qian et al, 2008b) (Figure 1.22B/D) and conductance experiments for this peptide (Garcia-Saez et al, 2005) and BAX proteins (Basanez et al, 1999). These data are also in line with the transbilayer lipid movement coupled with the membrane permeabilization exerted by BAX (Epand et al, 2003; Garcia-Saez et al, 2006; Terrones et al, 2004).

Moreover, BAX and BAK release high molecular-weight markers from liposomes (Bleicken et al, 2010; Kuwana et al, 2002; Schafer et al, 2009; Terrones et al, 2004; Terrones et al, 2008). In agreement with this, cryo-EM analysis of large unilamellar vesicles in presence of these proteins revealed membrane openings of heterogeneous range of sizes (25-100 nm). However, it was not possible to identify proteinaceous structures at the pore edges, in stark contrast to channel forming toxins (Tilley et al, 2005).

Additional support for the proteolipidic pore model is based on the membrane inserting helices of BAX/BAK. As mentioned before, the pore forming domain of BAX/BAK that corresponds to α5α6 helices are positively charged and too short to span the bilayer, and these features are less compatible with the barrel-stave channels, which are largely restricted to peptides of neutral

charges and oriented perpendicular to the membrane. It has also been proposed that α4-α5 may lie between the lipid headgroups, generating positive curvature and tension in the outer leaflet of that membrane leading to proteolipidic pore formation (Czabotar et al, 2013).

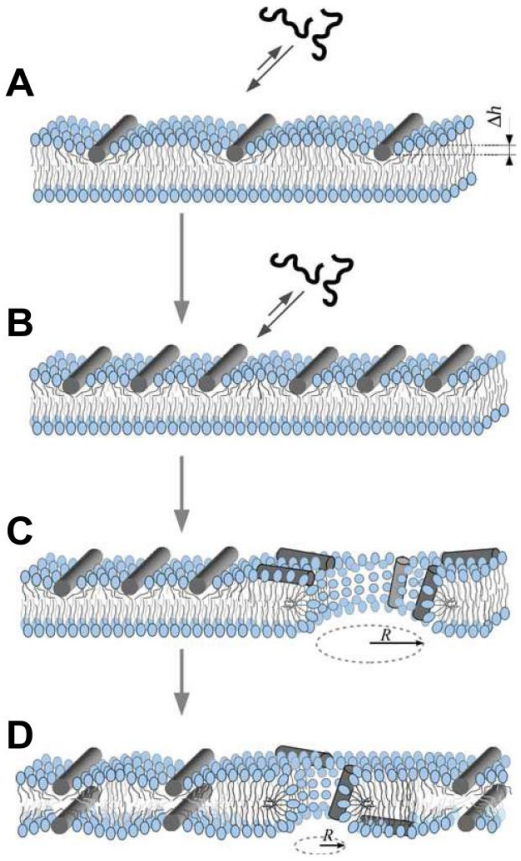

Figure 1.23 Mechanism of pore formation by cationic amphipatic peptides. (**A**) Pore-forming peptides bind to lipid bilayers coupled to folding of the peptide (in this case as an α-helix). Peptides insert in the interface among the lipid headgroups, generating changes in the physical properties of the membrane as asymmetric area stretching and membrane thinning (Δh). (**B**) Membrane perturbations increases peptide binding and it has been postulated that peptides would stabilize membrane defects and reduce the energy barrier for pore formation. (**C**) Once the pore is formed, the initial pore is large. Thus, the peptides could diffuse through the pore and insert into the internal monolayer decreasing the line tension that tends to close the pore. (**D**) Nevertheless, the peptides at the edge or near the pore reduce the line tension, until equilibrium is reached where the pore is smaller. Adapted from (Fuertes et al, 2011).

In the last years in combination with confocal techniques, additional atomic force microscopy (AFM) experiments on supported bilayers and electron microscopy of outer membrane vesicles (OMVs) and lipid nanodisks containing BAX confirmed protein enrichment at the rim of membrane pores of variable sizes where the pore wall was not completely covered by protein molecules (Kuwana et al, 2016; Salvador-Gallego et al, 2016; Xu et al, 2013) (Figure 1.24). Together, the evidence reveals an unexpected model for BAX (and probably BAK) mediated MOMP where oligomerization at the MOM induces the formation of heterogeneous toroidal pore structures that are flexible and evolve overtime leading to the release of apoptotic factors.

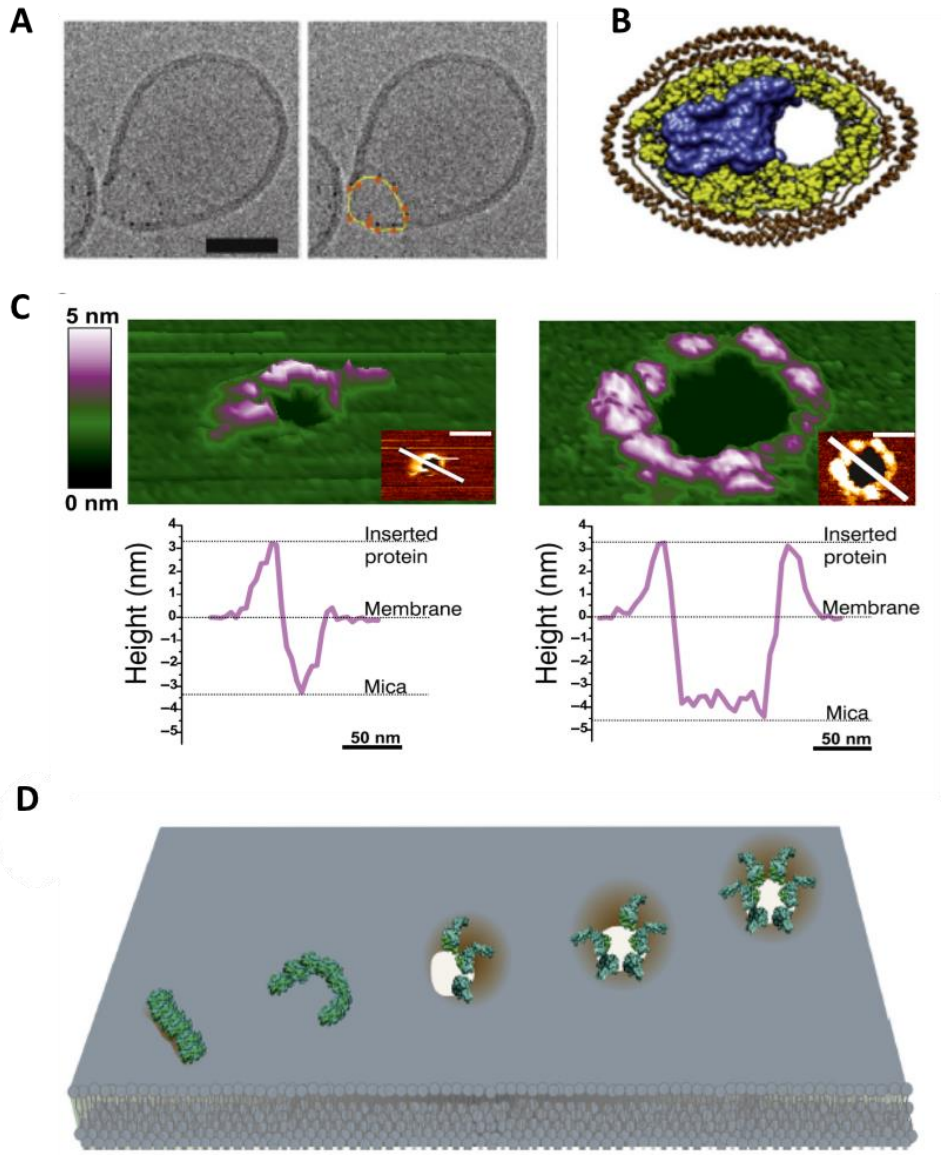

Figure 1.24 Recent evidences of the proteolipidic nature of BAX pore formation. (**A**) Cryoelectron microscopy (cryo-EM) image of gold-labelled BAX delineating a pore in the membrane of a vesicle. In the corresponding image, the pore is outlined in yellow and BAX in orange for visual purposes. Bar,40nm. Taken from (Kuwana et al, 2016) (**B**) Model of nanodisk structure (yellow) containing a single unit of BAX/BID peptide (blue surface) based on cryo-EM data. Taken from (Xu et al, 2013) (**C**) 3D AFM topography of a BAX arc (left) and ring (right). Both images reveal a circular dark hole that spans the lipid membrane (green). BAX molecules around the pore rim (magenta and white) protrude 3.97 ± 1.02 nm above the membrane plane, as confirmed by the height profiles shown below each image (corresponding to the white line in the 2D image insets). The topography of the arc structure reveals a pore only partially surrounded by BAX molecules, while lipids alone form the rest of the pore rim. Images are shown in a 42° tilted representation. Taken from(Salvador-Gallego et al, 2016). (**D**) Models for BAX (cyan) structures, including (left to right) lines, arcs, and rings, leading to pore formation in the membrane (grey). Taken from (Cosentino & Garcia-Saez, 2017).

1.9 MEMBRANE CONFORMATIONS AND FUNCTIONS OF THE ANTIAPOPTOTIC PROTEINS

According to some authors, BCL-2 type proteins are anchored to the MOM via their C-terminal domain while maintaining the overall solution structure. This conformation would easily explain inhibitory interactions of BCL2-type proteins with proapoptotic partners at the MOM level, via the same BH3-into-groove interactions described in solution-based studies (Day et al, 2005; Day et al, 2008; Hinds et al, 2007; Landeta et al, 2014; Liu et al, 2003b; Petros et al, 2000).

By contrast, Andrews DW´s group and others gathered evidence that membrane insertion of the helices α5 and α6 of BCL-2 and BCL-XL, prevented oligomerization of membrane bound BAX by hairpin-hairpin interactions (Billen et al, 2008; Dlugosz et al, 2006; Shamas-Din et al, 2013; Zhang et al, 2004). In line with these observations, biophysical studies with model membranes suggest that not only BCL-2 but also BCL-XL can insert α5α6 into the hydrophobic matrix of the lipid bilayer under certain experimental conditions (Garcia-Saez et al, 2004; Losonczi et al, 2000; Thuduppathy et al, 2006a). Regardless, it is important to point out that extensive membrane insertion of BCL-2 type proteins almost certainly eliminates the BH3-binding groove present in soluble structures of BCL-2-type proteins (Basanez & Hardwick, 2008).

Other evidence links extensive membrane insertion of antiapoptotic proteins and a phenotypic switch linked with acquisition of BAX-like pore-forming activity (Basanez et al, 2001; Clem et al, 1998; Cheng et al, 1997; Menoret et al, 2010; Michels et al, 2004). Of note, pores formed by BCL-2 type proteins appear generally smaller than pores formed by BAX and BAK (Basanez et al, 2001; Bleicken et al, 2013b; Clem et al, 1998; Etxebarria et al, 2008; Garcia-Saez et al, 2009; Ko et al, 2007; Lei et al, 2006; Peng et al, 2009; Thuduppathy et al, 2006b; Valero et al, 2012). It has been argued that this is due to the fact that BCL-2-like proteins lack the oligomerization capability of BAX-type proteins (Bleicken et al, 2013b). However, it has also been described that certain BCL-2-type proteins oligomerize under exposure to mild heat, acidic pH, or specific detergents (Denisov et al, 2007; Feng et al, 2008; Jeong et al, 2004; O'Neill et al, 2006; Zhang et al, 2004).

Moreover, in our group it has been reported that mitochondria specific lipid CL is able modulate the antiapoptotic capacity of MCL1 (Landeta et al, 2014). As the membrane content of CL is increased, MCL1 not only loses its inhibition capacity, but also is able to permeabilize model membranes. However, general aspects such as specificity, stoichiometry or the regulation of this new proapoptotic activity remains poorly understood. In this point it is worthy to mention that antiapoptotic overexpression has considered as the main cause of chemotherapeutic resistance. In this context, where the membrane plays a crucial role regulating BCL2 interactoma, membrane composition could become a key target in drug development.

1.10 INSIGHTS INTO THE OVERLOOKED BFL1

B-cell lymphoma 2-related protein A1 (BCL2A1), also known as A1 in mouse and BCL2-related gene expressed in fetal liver in humans (BFL1), is one of the least studied antiapoptotic BCL2 proteins. Although the *BFL1* gene was discovered in the early 90s (Choi et al, 1995; Lin et al, 1997; Orlofsky et al, 1991), BFL1 remains one of the least well understood BCL2 family proteins. In the following section I will describe the most relevant features attributed to BFL1, as follows: i) expression and regulation, ii) structure, iii) interaction partners, and iv) role in chemotherapeutic resistance and tumorigenesis.

BFL1 expression and regulation

In mouse, A1 is predominantly expressed in hematopoietic cells, but in humans it shows a more widespread distribution, including lung, small intestine testis and smooth muscles cells (Karsan et al, 1996b). The transcription of *BCL2A1* gene is an extensively regulated process. Indeed, A1 was found to be modulated by tumour necrosis factor (TNF)α and identified as a NF-κB target gene (Karsan et al, 1996a; Zong et al, 1999). Additional pathways such as CD40 and ERK signalling or antigen response are linked with A1 activities (Kater et al, 2004; Morgan et al, 2004). Moreover, A1 transcription can also be increased by extreme cellular oxygen levels (He et al, 2005; Kim et al, 2005). Of note, A1 exerts an antiapoptotic activity under both cellular conditions hyperoxia and low levels of ROS.

Structure

Human *BFL1* gene contains 3 exons that are differently transcribed to confer at least three different variants or isoforms of this protein. The most common mRNA of BFL1 is transcribed from exons 1 and 3, resulting in a 175 aminoacids protein. Several structures are available of human BFL1 in complex with BH3-peptides (3MQP with NOXA-BH3; 3I1H with BAK-BH3 and 2VM6 with BIM-BH3). According to these structures, BFL1 consists in a central hydrophobic α-helix (α5) and four pairs of amphipatic α-helices (Herman et al, 2008). Moreover, as in the case of other BCL2-type proteins, BFL1 possess a BH3-binding hydrophobic groove constituted by BH1, BH2 and BH3 homology domains. Of note, BFL1 apparently possess two BH3-like domains in α2 and α3 helices, although the first one lacks an strictly conserved aspartic acid residue (Herman et al, 2008; Rautureau et al, 2012; Smits et al, 2008).

The C-terminal helix of BFL1 (a9) is also atypical. This is because BFL1 present an amphipatic C-terminal helix that contributes to but is not absolutely required for BFL1 targeting to the MOM, while the rest of the BCL2-type proteins display a hydrophobic C-terminal helix that functions as transmembrane region that targets and anchors them to the MOM (Brien et al, 2009; Kucharczak et al, 2005). Moreover, unlike in other BCL2-type proteins, BFL1 α9 displays an autonomous proapoptotic activity (Valero et al, 2012). In fact, BFL1 α5 and α9 have been identified as the

minimal motifs responsible for a proapoptotic pore-forming activity of the protein (Kucharczak et al, 2005; Valero et al, 2012).

Among the additional isoforms described for BFL1, the two most important are GRS or Glasgow rearranged sequence and BFL1-Short. GRS and A1 sequences differ only at two positions (N72T and Q107H). High expression levels of GRS were also observed in hematopoietic malignancies, such as chronic myeloid leukaemia and the Burkitt lymphoma cell line Raji (Kenny et al, 1997). BFL1-Short contain all 3 exons with an early stop codon forming a 163 aa protein, with nuclear rather than cytoplasmic/mitochondrial localization but conserving its antiapoptotic nature (Ko et al, 2003).

Mouse BFL1 homolog, A1, contains two exons and four copies (A1-a, A1-b, A1-c and A1-d). The A1-a, -b and -d genes consisted of two exons, whereas the A1-c gene contained 1 bp insertion in the coding region which may result in an aberrant and truncated protein by frame-shift. With the exception of A1-c, the coding regions among A1 genes are highly conserved in both amino-acid identity and 3D structure (Hatakeyama et al, 1998; Herman et al, 2008; Smits et al, 2008).

BFL1 Interaction partners

A common feature of the BCL2-type proteins is their ability to establish BH3-into groove interactions with their proapoptotic counterparts, including BAX-type and BH3 only proteins (Czabotar et al, 2014; Moldoveanu et al, 2014). However, the specific affinities exhibited by the different family members in solution and in the membrane are still under investigation. In this regard, BFL1 has been reported to bind both BAX and BAK *in vitro* and *in cellulo*, as well as the majority of BH3-only proteins, including BID, BIM, PUMA, BIK, HRK and NOXA. Moreover, other non-BCL2 binding partners have been described for BFL1, such as the autophagy-related protein Beclin-1 and Nur77-derived BCL2-converting peptide (NuBCP-9). Interestingly, interaction with Nur77 unleashes a proapoptotic phenotype in BCL2, although whether it remains to be determined whether the same is true for the case of BFL1 (Kathania et al, 2011; Kolluri et al, 2008)(Figure 1.25).

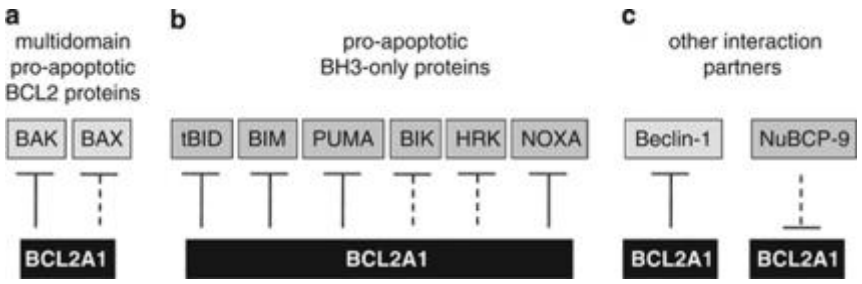

Figure 1.25 Interaction partners of BCL2A1. Binding by BCL2A1 can inhibit or neutralize pro-apoptotic multidomain BCL2 proteins (A) and BH3-only proteins (B). In addition, BCL2A1 can sequester Beclin-1 (C). Binding by NuBCP-9 may inhibit the anti-apoptotic function of BCL2A1. Taken from (Vogler, 2012).

Recently, NOXA SABH-BH3 peptide has been identified as a high-affinity ligand of BFL1 (Huhn et al, 2016). According to the authors, this new class of stapled peptides inhibitors confer a highly potent a specific BH3-like ligand that binds irreversibly to the antiapoptotic BFL1 via disulfide bonding, thereby blocking it antiapoptotic activity. Of note, BFL1 has described of probably as the one of most promiscuous prosurvival protein due to its structural plasticity, indeed, BFL1 is able to heterodimerize with several proapoptotic partners (Smits et al, 2008). In this context, having an specific BH3 peptide partner could be specially relevant in cancer therapy as they are other BH3 mimetic such as the BAD-like ABT-737 and the NOXA-like S63845 (Kotschy et al, 2016).

Mice knockout phenotype

In 2017, a prominent goal to understand the biological role of BFL1 was achieved with the generation of all-A1-isoform KO mice by the group of Marco Herold in collaboration with Andreas Villunger´s group (Berberich & Hildeman, 2017; Schenk et al, 2017; Tuzlak et al, 2017). The generation of gene-deficient mice have facilitated the comprehension of the function of many BCL2 proteins, and therefore this A1 KO mice confers an invaluable tool to address the specificities of BFL1 functions in a physiologically relevant system.

Surprisingly, the phenotype elicited by this new A1 all isoforms KO mice was similar to the wt, suggesting a functional redundancy of A1 with other antiapoptotic proteins in the control of T cell-dependent immune responses. Although different type of analysis were performed, these results are inconsistent with previous studies where mice lacking some (but not all) A1 isoforms behaved dissimilarly to the wt in apoptosis regulation under certain settings and cellular systems (Hamasaki et al, 1998; Xiang et al, 2001). Based on results obtained with the all-A1 KO cells, it has been postulated a model where BFL1 compensates the inhibition activity of MCL1 and BCL2, and immune cell survival is governed by collaboration among all the antiapoptotic members (Carrington et al, 2017).

The role of BFL1 in chemotherapeutic resistance and tumorigenesis

Because of its function in the hematopoietic system it is not surprising that overexpression of BFL1 is frequently associated with different forms of leukaemia and lymphoma (Vogler, 2012). High expression levels of BFL1 in advanced tumour stages suggests that this protein may facilitate tumour progression. BFL1 contribution to tumorigenesis was demonstrated recently in anaplastic large cell lymphoma (Piva et al, 2006) and in squamous cell carcinoma (Kathpalia et al, 2006). Finally, BFL1 plays a critical role in chemotherapeutic resistance as the central function of BFL1 is to suppress apoptosis upon toxic stimulus and consequently to prevent cell death upon chemotherapy. In this regard, an excess of BFL1 has been shown to be resistant to etoposide (Wang et al, 1999), staurosporine (Shim et al, 2000) or cisplatin (Cheng et al, 2000).

Despite extensive research effort there are still several unanswered question regarding the mode of BFL1 action, and its links to human physiology and pathology. In this thesis, we attempted to elucidate the detailed molecular mechanism by which BFL1 modulate MOM permeability.

1.11 OBJECTIVES

The BCL2 protein family modulates the point of no return in the mitochondrial pathway of apoptosis that being the perforation of the MOM, which allows release of mitochondrial apoptogenic factors into the cytosol. Despite intense research effort, exactly how BCL2 family proteins operate at the MOM level remains incompletely understood.

The general aim of this study is to advance in our knowledge of the molecular mechanisms of action of BCL2 family proteins at the membrane level. Our focus is in the prototypical proapoptotic BCL2 family member BAX, and the less well understood antiapoptotic BFL1 protein. We combined studies in simplified model systems and in living cells, mainly using quantitative biophysical techniques.

Specific Aims:

1- To gain insight into inactive and active BAX membrane conformations.
2- To elucidate the mechanism by which BFL1 inhibits apoptosis, by analysing three putative modes of action: (1) retrotranslocation of inactive BAX from the membrane into the cytosol (MODE-0), (2) heterodimerization with and neutralization of cBID at the membrane level (MODE-1), and (3) heterodimerization with and neutralization of activated BAX at the membrane level (MODE-2)
3- To understand the role of the cardiolipin as a modulator of BFL1 and BCLXL membrane activities.

CHAPTER 2:

Experimental procedures

2 Experimental procedures

This chapter gathers general information about the experimental techniques used throughout the present thesis. The application of these techniques to specific purposes will also be briefly discussed within the corresponding section of the Results chapter.

2.1 RECONSTITUTED MODEL SYSTEMS

Given the inherent complexity of the molecular network controlling commitment to MOMP, one of the major challenges is elucidating the BCL-2 family protein interactions within intact cells at molecular level. In addition, as mentioned in the Chapter 1, these interactions could take place in two different environments: the cytosol or the membrane. Taking into account the difficulty of obtaining mechanistic information of BCL-2 proteins within dying cells, in this thesis we use simplified and compositionally-defined in vitro reconstituted systems consisting of pure lipid model membranes and purified proteins or peptides. The reductionist systems used in this thesis allows studying the interaction between proteins and lipids, side-lining the complexity of the biological membranes and having the opportunity of varying the composition and properties of the membrane in a controlled manner.

2.1.1 Lipid component

Biological membranes are enclosing double layers that organize within or around the cell, defining chemically or biochemically different environments. Being a physical barrier is not their only function, because due to their dynamic nature, biomembranes actively participate in reception and transduction of different cellular signals, as well as in other essential cellular processes, including oxidative phosphorylation and endo/exocytosis.

2.1.1.1 Lipids: classification and properties

Type of lipids

Lipids are a highly varied group of amphipatic molecules compromising a polar headgroup and a hydrophobic moiety (usually acyl-chain-based). Lipids have the ability to self-assembly in complex structures as vesicles, being energetically favourable structures.

The major groups of membrane lipids are phosphoglycerides, sphingolipids, glicolipids and sterols (Figure 2.1).

Phosphoglycerolipids

Phosphoglycerolipids or phosphoglycerides are the most abundant lipids in biomembranes. Their structure contains a glycerol backbone that could be linked to one or two acyl chains by an ester bound and one phosphate group. The later based on the variability of the headgroup can be derivatized to give different phosphoglycerolipids such as phosphatidylcholine (PC), phosphatidylethanolamine (PE), phosphatidylinositol (PI), phosphatidylglycerol (PG), phosphatidylserine (PS) or phosphatidic acid (PA). Due to the nature of the headgroup, these lipids can be anionic (PI, PG, PS and PA) or zwitteronic (PC and PE) at physiological pH. One of the mostly studied phospholipid in this thesis is cardiolipin (CL) that contains three glycerol molecules with four acyl chains and two phosphate groups that confer it an anionic nature.

Sphingolipids

Instead of a glycerol backbone, sphingolipids have sphingosine, a long-chain amino alcohol. In this group we can find from simplest structures to major structures: sphingosine, shingosine-1-P, ceramide, sphingomyelin etc.

Other sphingolipids, instead of a sphingosine backbone, they contain a sphinganine; but this type of lipids is less abundant.

Glycolipids

Glycolipids are membrane components composed of lipids that are covalently bonded to monosaccharides or polysaccharides. Depending on the nature of their lipid backbone, there are two main groups: glycoglycerolipids (glycerolipid structure) and glycoshingolipids (shingolipid structure). These types of lipids are typically located in the extracellular monolayer.

Sterols

Sterols, also known as steroid alcohols, are a subgroup of the steroids, with the most familiar type of animal sterol being cholesterol. They are amphipathic lipids composed by a steroid ring and a small acyl chain. The hydrophilic part of the sterols consists in a hydroxyl group. Sterols and related compounds play essential roles in the physiology of eukaryotic organisms. For example, cholesterol forms part of the cellular membrane in animals, where it affects the cell membrane's fluidity and serves as secondary messenger in developmental signalling.

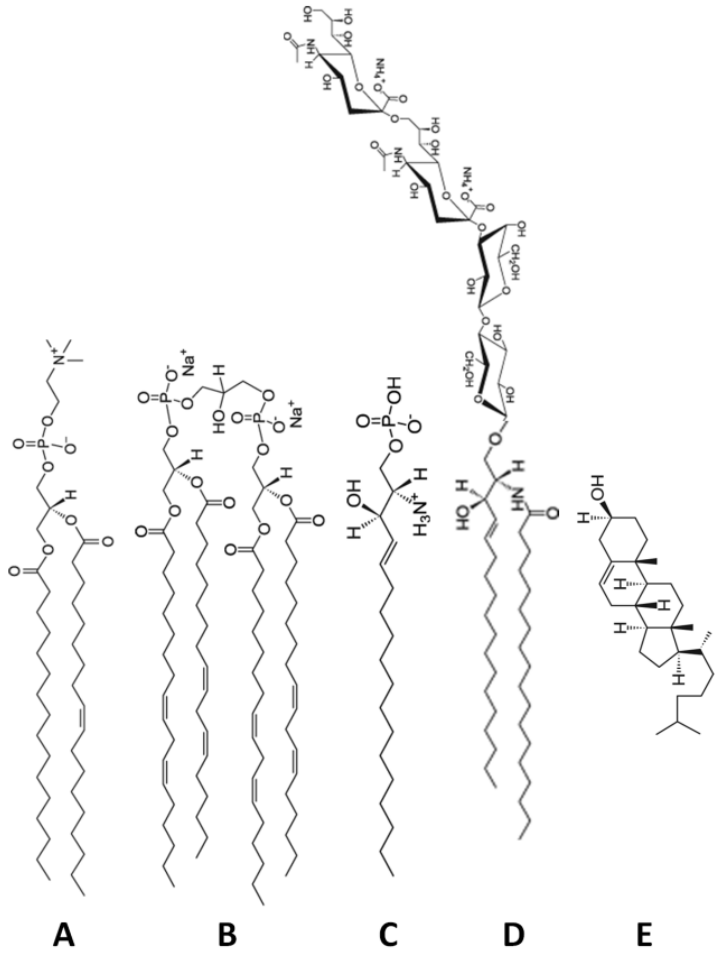

Figure 2.1. Scheme of structures of different type of lipids. Lipids are by far the chemically most diverse class of biomolecules. Beside the different headgroups, the length and saturation of the acyl chains multiply the possible combinations. Phosphoglycerolipids are represented by the predominant specie in egg PC (**A**) and cardiolipin (**B**). The sphingolipids are sphingosine-1-P (**C**) and the glycosphingolipid GD3 (**D**). And finally, the structure of cholesterol (**E**) is shown.

Lipid polymorphism

The polymorphism of lipids is due to their effective molecular shape that depends on the compatibility of the volume of polar headgroup and the size of the hydrophobic tails. Therefore, the variety of lipid structures with different morphologies is referred to lipid polymorphism. The packing parameter (P) of a lipid can be defined as:

$$P = \frac{\mathrm{V}}{\mathrm{A.l}}$$

eq. 2.1

where, *V* is the entire volume of the lipid, *A* is the area of the lipid headgroup at the lipid-water interface, and *l* is the length of the lipid. Lipids possessing a cross-sectional area of the headgroup similar to that of the acyl chain (P=1) adopt a "cylindrical" form and organize themselves into planar lipid bilayers. By contrast, lipids differing in headgroup and acyl-chain cross-sectional areas lead to positively-curved (P > 1) and negatively-curved (P < 1) non-bilayer lipid organizations. It is noteworthy that highly-curved nonbilayer lipid structures, are thought to occur in living cells at local sites of membrane fusion and fission (Mouritsen, 2011).

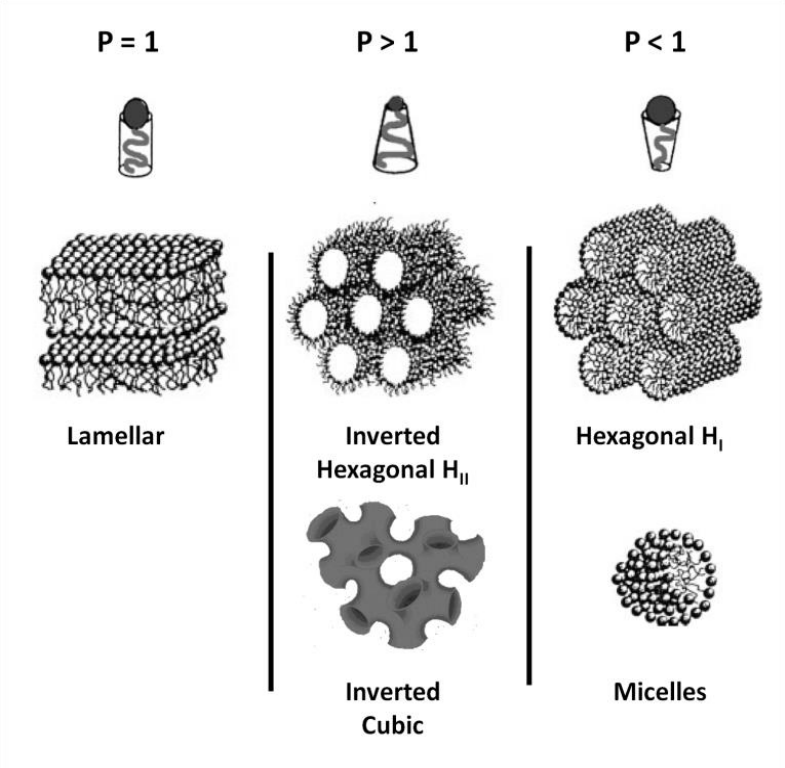

Figure 2.2 Schematic illustration of the concept of lipid polymorphism, showing the lipid geometry and the predicted morphologies adopted by lipid self-assembly. Lipids with cylindrical geometry (P=1) aggregates favouring lamellar structures. Negatively curved lipids (P>1) could assembly forming inverted hexagonal (HII) and cubic phases. Finally, lipids with positive curvature formed micelles and Hexagonal (HI) structures. (Modified from (Mouritsen, 2011).

The polymorphic behaviour of a particular lipid not only depends upon its specific chemical structure, but may also be affected by environmental parameters, such as temperature, water content, pH, salt concentration, and presence of divalent cations (Cullis & de Kruijff, 1979).

2.1.1.2 Model membrane systems

During the last decades, different model membrane systems have been developed to study the properties of pure lipids, lipid mixtures and protein-lipid interactions. According to the method of preparation and complexity, model membranes can be divided in: (a) lipid monolayers, (b) micelles, (c) lipid vesicles (liposomes) and d) supported lipid bilayers (SLB).

Lipid Monolayers

A lipid monolayer is a monomolecular film generated at the air/water interface. Due to their amphipathic character, lipids spread on top of a water surface orienting their polar headgroups in close contact with the water surface while moving their hydrophobic acyl chains towards the air. The terms "Langmuir films" and "Langmuir balance" are also used, referring to the preparation and characterization of this type of model membranes (Langmuir, 1917).

Langmuir balance measurement represents an important source for the characterization of lipid-lipid and lipid-protein interactions. The advantages of this system over other models are that lateral pressure, molecular packing and lipid composition can be precisely controlled, as well as the absence of global membrane curvature or fluctuation effects. In the present work, Langmuir balance-based approaches have been applied to the study of lipid-protein interaction (detailed procedure is shown in protocol 14).

Micelles

As previously was explained, due to the amphipatic nature of the lipids, these molecules tend to self-assembly in aqueous environments, orienting their polar headgroups and excluding their acyl chains to the solvent. In the case of micelles, the inner part of the structure is hydrophobic and is generally formed by fatty acids, detergents or lysophospholipids that have an inverted cone shape.

The Critical Micellar Concentration (CMC) is defined as the concentration of monomeric surfactants above which can self-aggregate forming micelles. Here, we use lipid concentration above the CMC to form the micelles. It becomes a very important parameter to take into account when measuring the effects of specific lipids upon incubation with other model systems or in cells, because they can induce membrane permeabilization underneath the CMC.

Liposomes

Liposomes are synthetic vesicles in where an aqueous volume is entirely enclosed by a lipid bilayer. One of the principal advantages of liposomes is the fact that they allow easy manipulation of important parameters such as curvature, lipid composition, membrane fluidity, charge density and permeability.

According to their shape and size, liposomes can be classified as follows: (a) Small Unilamellar Vesicles (SUVs), which contain a single lamella and display sizes ranging from 25-50 nm; (b) Large Unilamellar Vesicles (LUVs) have a mean diameter of 100-500 nm; (c) Multilamellar Large Vesicles (MLVs), which contain multiple lamellae, and display a wide range of sizes (100-10.000 nm) (New, 1990); and finally, Giant Unilamellar Vesicles (GUVs) may attain micrometre ranged diameters, similar size as eukaryotic cells (Figure 2.3).

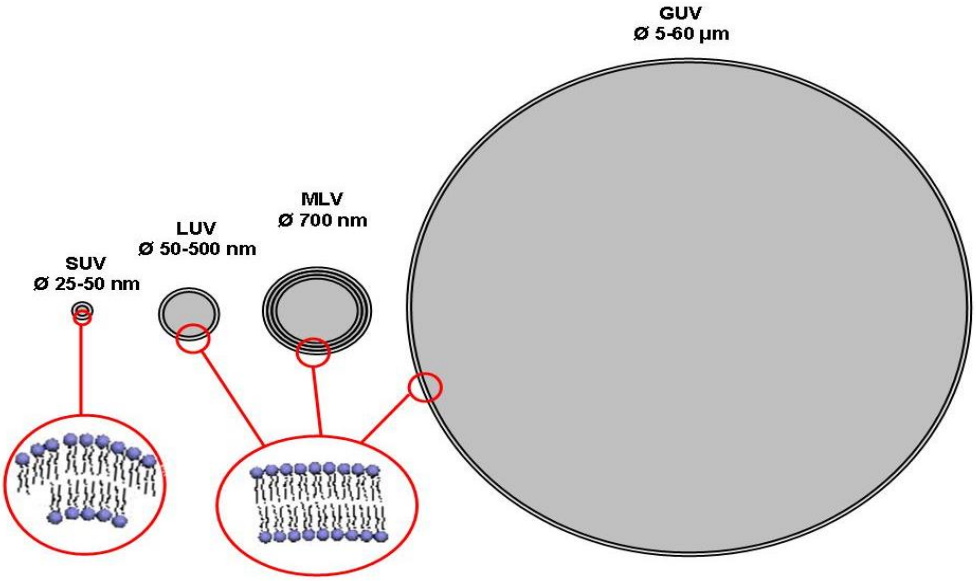

Figure 2.3 Size comparison of different type of liposomes. SUV: Small Unilamellar Vesicles. LUV: Large Unilamellar Vesicles; MLV: Multi-Lamellar; and GUV: Giant Unilamellar Vesicles. In the amplified circle the organization of the lipids within the bilayer is observed, that reflects the higher curvature in SUVs, and almost flat membranes as the size of the liposome is increased.

Due to their small diameter; SUVs present high curvature stress, which induces lipid enrichment in the external monolayer compared to the inner one (Chapman, 1984). This curvature stress makes these vesicles a good membrane model for the study of membrane fusion/fission related processes (Nieva et al, 1989), which are subjected to such stress conditions *in vivo*. In the same way, their small size is of great advantage when using in samples for optical spectroscopy since they minimize light scattering artefacts. However, as diameter increases (LUV, MLV and GUV), the curvature in certain areas of the bilayer is almost zero (Mayer et al, 1986).

Preparation of Multilamellar Vesicles (MLVs)

MLVs generation is the simplest and fastest of all liposome formation methods. So starting from the preparation of MLV, we can form different types of liposomes by simple processes as freeze and thaw cycles (FT-MLV), extrusion (LUV) or sonication (SUV).

MLVs contain between 7 and 10 concentric bilayers, each of them separated by a thin water layer. Their size is very heterogeneous, displaying an average diameter of around 700 nm but ranging from 100 to 10,000 nm. When treating vesicles with a solubilizing agent, or when looking at a protein effect upon binding to the vesicle, only the external bilayer is accessible (a 10% of the lipid concentration). A detailed protocol for multilamellar vesicle preparation used in the present work is described in Protocol 1.

Protocol 1 ***MLVs preparation***

1- Lipid stock preparation: Pure lipid stocks were usually dissolved into a chloroform/methanol (2:1 v/v) organic solution. The desired amount of lipid was pipetted from the stock in organic solution into a glass tube.
2- Evaporation of the organic solvent: The organic solvent was evaporated under a nitrogen glass flow. Then, the tube was put into a vacuum desiccator for 2 hours to completely remove the solvent.
3- Generation of MLVs: Finally, the dried lipid film was hydrated with a selected buffer and resuspended by vigorous vortexing, generating MLVs.

SUVs preparation

Generation of SUVs: Once MLVs are formed, sample is sonicated 10 sec on/10 sec off for 10 min with a tip sonicator.

Preparation of Freeze/Thaw Vesicles (FT-MLVs)

Another variation of the MLV is the Freeze and Thaw Multilamellar Vesicle (FT-MLV). In this case the preparation was carried out as described in Protocol 2.

Protocol 2 ***FT-MLV preparation***

1- Preparation of MLVs: see Protocol 1
2- FT-MLV preparation: Formed MLVs were next subjected to 10 freeze/thaw cycles, in this process concentric bilayers were reduced in number, thus vesicles had a smaller size.

Preparation of Large Unilamellar Vesicles (LUVs)

Due to the low curvature stress and homogenous lipid distribution, LUVs represent a suitable model system for most studies. LUVs are prepared by mechanical extrusion of a FT-MLVs suspension through polycarbonate porous filters of the desired size (Mayer et al, 1986). A detailed LUV preparation protocol is given below (Protocol 3).

Protocol 3 ***LUV preparation***

1- Preparation of FT-MLVs: see Protocol 2

2- Extrusion procedure: Once FT-MLVs were formed, to obtain unilamellar vesicles of a certain size, vesicles were extruded according to the method described in (Hope et al, 1985) The sample was extruded 10 times through polycarbonate filters (Nucleopore, San Diego, CA, USA) with the desired pore diameter (0.1-0.2µm) and with the help of a nitrogen gas flow of 200 psi.

3- Lipid peroxidation (optional): In order to induce lipid oxidation, LUVs (3mM) were incubated with $CuCl_2$ (20µM) at 37ºC under continuous stirring. Then, the reaction was stopped at required time (typically, 1-3h) by adding 100µM BHT and 100µM EDTA. Copper-induced oxidation was checked at 245 nm, according to (Schnitzer et al, 1998; Schnitzer et al, 2007). Next, 25µL of liposome preparation were solubilized into 750 µL absolute ethanol and measured in an Uvikon 922 spectrophotometer (Kontron instruments, Groβ-Zimmern, Germany, using quartz cuvettes with absolute ethanol in the reference cell.

SLB preparation

SLB generation: In this thesis SLB are formed based on proteoLUVs that are fused by the addition of $CaCl_2$, see a detailed explanation in protocol 18.

Preparation of Giant Unilamellar Vesicles (GUVs)

Giant unilamellar vesicles (GUVs) are a powerful membrane model due to their size (10-100 µm) which is comparable to a cell. This allows the imaging of spatially confined events at single vesicle, e.g. mechanical properties, lateral organization of bilayers or membrane/protein (even DNA) interactions (Apellaniz et al, 2010; Bernardino de la Serna et al, 2004; Bleicken et al, 2013b; Garcia-Saez et al, 2010; Garcia-Saez et al, 2007; Schon et al, 2008; Steringer et al, 2012).

The generation of giant vesicles was first described by (Reeves & Dowben, 1969), consisting of the exposure of dry lipid films to aqueous solutions, where GUVs were spontaneously generated but with very low total lipid yield and a very heterogeneous size distribution. In 1986, a new method for GUV generation was developed by (Angelova, 1986; 1992), based on the exposure of dry lipid films to an aqueous solution under an electric field, being the most generally applied

procedure in the present. This method is much faster than the previous one and higher amounts of homogeneous size vesicles can be obtained. Nevertheless, the electroformation method is strongly dependent on the lipid composition, ionic strength and pH and on the electric voltage and frequency conditions (Bagatolli, 2003). In this thesis, vesicle generation procedures have been applied to obtain giant vesicles in solution for direct microscopy measurements (see Protocol 4).

Protocol 4 ***GUV preparation***

1- Preparation of lipid mixture: Pure lipid or lipid mixture stocks diluted into a chloroform/methanol (2:1 v/v) organic solution were prepared to a final 1mM concentration. Depending on the experiment that was going to be carried out %0.05 DiI (1,1'-Dioctadecyl-3,3,3',3'-Tetramethylindo-carbocyanine Perchlorate, DiIC18, Invitrogen) or %0.2 Rho-DHPE (L-α-Phosphatidylethanolamine-N-(lissamine rhodamine B sulfonyl ammonium salt, Avanti polar lipids) was added to the lipid mixture.

2- Electroformation:
   - 6µl of the appropriate stock solution were added onto the surface of different platinum electrodes attached to specially designed Teflon chamber containing platinum-wires. Then, chamber was introduced into a high vacuum desiccator for 2 hours to remove any remaining solvent traces.
   - Next, the platinum wires were covered with 300-400µL buffer-isosmotic sucrose solution. If the transition temperature for the lipid mixture of the study was higher than RT, the chamber and the sucrose solution need to be preheated. Importantly, in order to avoid thermal evaporation, chambers need to be sealed with a glass cover.
   - The platinum electrodes were connected to a generator and the function started with a sinus wave at a voltage of 2.5V and a frequency of 10Hz during 2h, so vesicles were generated attached to the platinum wires. Then, frequency was decreased to 2Hz for 30min, and finally vesicles were gently detached from the Pt wires.

For a detailed specification on buffer, generator type or microscopy conditions in a particular assay look for Experimental procedures in the corresponding chapters.

2.1.1.3 Characterization of model membrane systems

Phospholipid concentration measurement

Accurate measurements of phospholipids are difficult to make directly, consequently the most widely used method for determination of phospholipids is the measurement of phosphate content in the sample (Bartlett, 1959; Böttcher, 1961; Fiske, 1925). Briefly, phospholipid phosphorus is first hydrolysed with perchloric acid to inorganic phosphate. Next, ammonium molybdate is added to obtain phospho-molybdic acid. The phospho-molybdic acid is then quantitatively reduced to a blue-coloured compound by ascorbic acid, and sample absorbance is measured at 812 nm.

A more detailed explanation is described in Protocol 5.

Protocol 5 ***Phospholipid concentration measurement***

1- Preparation of the samples: The phosphate calibration curve was prepared from a 1mM NaH_2PO_4 stock solution. Lipid sample was pipetted into separate tubes to be in the middle of calibration curve (approximately 50 nmol lipid phosphorous).
2- Digestion: 400µL of 70% perchloric acid ($HClO_4$) was added to each tube and let them incubate for 45min at 205°C and then cooled down to room temperature.
3- Colorimetric assay: 4mL of ammonium heptamolybdate based solution and 500µL of ascorbic acid 10% were added, while mixing the samples with a vortex. Samples were incubated for 10-15min at 100°C.
4- Absorbance measurement: Absorbance was measured at 812nm using an Ultrospec 500 pro spectrophotometer from Amersham Biosciences (Piscataway, NJ, USA).

NOTE: The mitochondrial specific lipid CL, containing two phosphate groups and need to be weighted. Moreover, cholesterol as lack in phosphate group was quantified by a commercial kit from Biosystems®.

Determination of vesicular size (Dynamic light Scattering)

Vesicle size measurements were performed using the quasi-elastic light scattering (QELS) technique, commonly known as dynamic light scattering (DLS). This technique measures the fluctuations in the intensity of the scattered light of the sample due to the Brownian motion of the particles in solution. From this data, the diffusion coefficient of the particles in the sample can be determined, and this can be related to the hydrodynamic radius (R_H) of the vesicle by the Stokes-Einstein equation (see eq.2.7).

For the measurement, we placed 50 μL of the sample, at a lipid concentration of 0.5mM, in standard acryl cuvettes. The samples were analysed in a Malvern Zeta-Sizer Nano ZS (Malvern, Instruments, UK) subjected to a He-Ne laser beam of 5mW (λ = 633 nm). The light scattered by the sample was detected with a photomultiplier placed perpendicular to the beam.

2.1.2 Protein component

In this section, it is described the methodology used in the present thesis to obtain and validate, both structurally and functionally, different recombinant BCL-2 family members and their mutants. As well as, a brief description of BAX peptides used. Importantly, proteins are with lipids, a key piece of reconstituted systems. Therefore, in order to understand their precise biological role, their accurate characterization becomes fundamental.

2.1.2.1 Site-directed mutagenesis

In vitro site-directed mutagenesis is an invaluable technique for studying protein structure and function. In this work, site directed mutagenesis has been used mainly for generating residues susceptible to be modified by fluorescent dyes.

The system used for site-direct mutagenesis (Stratagene's QuikChange® Site-Directed Mutagenesis Kit) allows site-specific mutations in virtually any double-stranded plasmid, thus eliminating the need for subcloning. In addition, no specialized vectors, unique restriction sites, or multiple transformations are required. The process consists of different steps as described in Protocol 6.

Protocol 6 ***Site-directed mutagenesis***

1- Primers design: The primers were designed containing each specific mutation, flanked by unmodified nucleotide sequence. Ideally, primers should be between 25 and 45 bases in length, with a melting temperature (Tm) of ≥78°C, and a minimum GC content of 40%. In this thesis, primer design was performed by using Primer X web page and selected candidates were synthesized by Sigma-Aldrich.

2- Plasmid preparation: Sample reactions were prepared as indicated in the User´s manual of Stratagene's QuikChange® Site-Directed Mutagenesis Kit.

1.	5µl	10× reaction buffer
	5–50ng	dsDNA template
	125ng	Oligonucleotide primer #1 (Fw)
	125ng	oligonucleotide primer #2 (Rv)
	20mM	dNTP mix
	q.s to 50µL ddH20	
2.	2.5 U	PfuTurbo DNA polymerase

Table 2.1. Concentrations required for sample preparation in a mPCR.

(next page)

3- Thermal Cycling:

Segment	Cycles	Temperature	Time
1	1	95° C	30 s
2	16	95° 55°C 72°C	30s 1 min 1 min/kb of plasmid length
3	1	4°C	

Table 2.2. Cycling Parameters for the QuikChange Site-Directed Mutagenesis Method.

4- Digestion of the Amplification Products: 1 µl of the Dpn I restriction enzyme (10 U/µl) was added to each sample reaction and incubated at 37°C for 1h to digest methylated (parental) supercoiled dsDNA.

5- Transformation of XL1-Blue Supercompetent Cells: XL1-Blue supercompetent cells, resistant to tetracycline, were thawed on ice and 50 µL aliquots for each sample were put on sample tubes. 10 µL of DpnI-treated DNA was added and the reactions were mixed and incubated on ice for 30 minutes. Transformation reactions were heated for 45 seconds at 42°C and then were placed on ice for 10 minutes. 1mL of Luria broth medium (10g tryptone, 5g yeast extract and 5g NaCl, per litre) was added and incubated for 37°C for 1 hour while shaking. Then samples were centrifuged, resuspended in a smaller volume and plated on agar plates containing the appropriate antibiotic for the plasmid vector. The transformation plates were incubated at 37°C for >16 hours. Finally, DNA plasmid was extracted by a QIAprep Spin Miniprep Kit®.

6- Sequence determination: The mutated DNA samples were sent for sequencing to determine that the mutation had been inserted and no additional changes were made in the sequence of the plasmid.

In this thesis, different variants of the recombinant proteins have been used, objects of study, some of them have been made following the procedure explained above (Table 2.2), obtained from Addgene company and some other have been developed by TopGeneTech (Quebec, Canada) company. For example, to develop BFL1 monocysteine mutants, all endogenous cysteines were removed; C4S, C19S, C55S by consecutive substitutions. Of note, we conserved C19S/C55S construct, which preserves C4 and still enables its labelling, to add the L21A and R88D single mutations. Then, using 0cys mutant as the PCR template the following monocysteine mutants were developed: Y10C, S31C, S43C, A67C, N72C, Q73C, I100C, R105C, F121C and N129C among others.

2.1.2.2 Expression and purification of proteins

Recombinant protein utilization has greatly increased in recent years. Fusion proteins are simple and convenient to work with and, for many applications, a single purification step using a commercially available affinity chromatography is generally sufficient. In the present work, Glutathione S-transferase (GST), chitin and 6 Histidine ($(His)_6$) tagged proteins have been used.

Plasmids for bacterial expression

Different plasmids were used for recombinant protein expression (Table 2.3):

- **Antiapoptotic proteins:** Plasmids for human GST-BCL-XL lacking the C-terminal 24 amino acids (BCL-XLΔC), chitin-BCL-XL version and human His_6-tag BFL1 lacking the C-terminal 26 amino acids (BFL1ΔC) have been used in this thesis. Particular features: The vector pGEX-6P-3 for expression of GST fusion proteins has a PreScission Protease target place LEVLFQ/GP. BCL-XL was kindly provided by Dr. Ana García-Sáez. His_6-tag BFL1ΔC was obtained from Addgene (Plasmid #42399, which was deposited by Nicola Burgess-Brown).
- **Proapoptotic BAX:** Plasmid for expression of human full-length BAX was kindly provided by of Dr. M Suzuki (NIH, Bethesda). The plasmid is a derivative of pTYB1 vector (New England Biolabs, Canada), in which the cDNA of human full-length BAX was subcloned into NdeI/SapI sites of the vector. The resulting plasmid, pTYB1-BAX, encodes a fusion protein of BAX and a chitin binding domain plus a self-cleavage intein at its C-terminus, which is cleaved off to obtain BAX with neither any extra amino acid nor truncation (Suzuki et al, 2000).
- **BH3 only proteins:** Plasmid for murine BID with an N-terminal His_6-tag was kindly provided by Dr. B. Antonsson.

Next, a table summarizing plasmids characteristics is built in order to collect their peculiarities, including origin, tag, resistance and growth media.

Protein insert	Plasmid	Description	Resistance	Purification media
Human BAX	pTYB1	A chitin binding domain plus a intein sealf-cleavage at the C terminal.	Amp^r	TB
Human BFL1ΔC26	pNIC28-Bsa4	A 6-histidine tag plus TEV protease cleavage at the N-terminus.	Kan^r	TB
Human BCL-xLΔC24	pGEX-6P-3	A GST-tag plus a PreScission protease cleavage site at the N-terminus.	Amp^r	LB
Human BCL-XL	pTYB2	A chitin binding domain plus a intein sealf-cleavage at the C terminal.	$Amp^r/chlo^r$	LB
Murine BID	pET23d	A 6-histidine tag plus PreScission protease cleavage at the N-terminus.	Amp^r	LB

Table 2.3. Expression plasmids, bacterial strains and antibiotic resistances used for the different proteins purification. LB (Luria Broth; 10g tryptone, 5g yeast extract and 5g NaCl, per litre). TB (Terrific Broth, 24g Yeast extract, 12g peptone, 12.5g K_2HPO_4 and 2.3g KH_2PO_4).

Protein expression and purification

Protein expression and purification is a very diverse methodology, which is very dependent on the nature of recombinant protein. In the case of BCL2 family members, full-length version of some of this protein has achieved to be purified, while others have been purified in their C-terminal lacking version which is much more soluble.

Here, protein purification protocols differ mainly according to the affinity-tag, however, a general procedure is summarized in the next scheme and protocol 7.

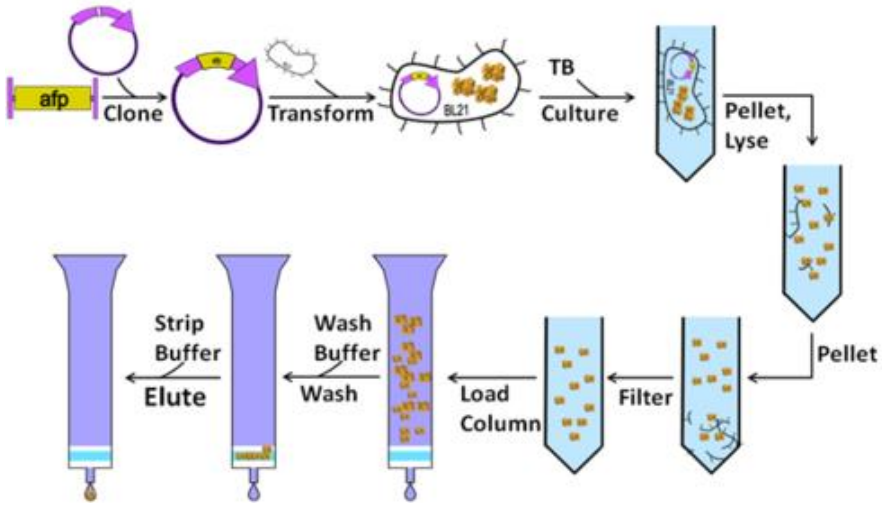

Figure 2.4. Simplified scheme of recombinant protein purification process

Protocol 7 ***Protein purification***

1- Transformation: BL21(DE3) $CaCl_2$-competent bacteria for recombinant protein expression, were transformated with ≈100ng of plasmid, as explained in protocol 6.

2- Next, a single colony of transformed bacteria was picked and placed into a flask containing 100mL of growth medium supplemented with the appropriated antibiotic (1000:1, hereafter medium*) and incubated in an orbital shaker at 37°C ON. Next, the medium was diluted 1:50 in 1L of medium* and incubated in an orbital shaker at 37°C.

3- IPTG induction and cell harvesting: Once bacterial medium reached to the appropriated confluence/O.D. $_{600nm}$: 0.8-1a.u. (for BID and BCL-XL), 1.2-1.5a.u. (for BAX) and 2-2.5a.u. (for BFL1ΔC), in order to promote protein expression, 1mM of IPTG was added, and bacteria were incubated at 18°C ON. Then, were collected by centrifugation (5,000 x *g* for 30min at 4°C) in a Beckman Coulter centrifuge using JLA-9,100 rotor and kept frozen for further purification.

(next page)

4- Cell lysis: Bacterial pellets were resuspended in bacterial lysis buffer A (see table 2.4) supplemented with freshly added lysozyme (final concentration of 1mg/ml, Sigma-Aldrich), bacterial protease inhibitors (without EDTA for His_6-tagged proteins, Roche), and 2.5µg/ml RNAse (Sigma-Aldrich). The mixture was then incubated at 4ºC in an orbital shaker for 2h to allow disruption of the bacterial cell wall. Then, samples were disrupted by using an EmulsiFlex C5 from Avestin (≥17000psi on ice), or sonicated with a tip sonicator on ice 4 x (10on/10off/10sec). Next, the suspension was centrifuged at 30,000 x *g* for 30min at 4°C in a Beckman Coulter centrifuge using JA-25.50 rotor. Finally, the pellet was discarded and the supernatant was kept on ice for further purification steps.

5- Affinity chromatography:

- Purification of His_6-tagged proteins: His_6-tagged proteins were purified by affinity chromatography using "Ni-NTA Superflow beads" (Qiagen). Beads were first washed three times with distillate water and three more times with ten bed volumes of Buffer A (Table 2.4). Then, prefiltered bacterial supernatant was incubated with washed beads for 2h in an orbital-shaker at 4°C. Next, beads were packed in a column connected to a peristaltic pump, followed by a washing step of the column with 10 bed volumes of buffer A. Then, protein was eluted by using buffer B (Buffer A with 400mM imidazole, pH8) (Table 2.4) and fractions of 0.5mL were collected for SDS-PAGE analysis and Coomassie blue staining.

  Additionally, in order to remove the 6HIS tag, protein enriched fractions were incubated with 10 µL (Stock: 10U/µL) of AcTEV protease (Invitrogen) ON at 4°C. Digested samples were incubated with 100µL of precleaned Ni-NTA beads for 2h at 4°C. Then, beads were centrifuged at 14,000rpm for 10min and supernatant, where cleavage-protein (BFL1ΔC) is, was collected.

(next page)

- Purification of GST-proteins: These GST fusion proteins were purified by affinity chromatography using "Glutathione Sepharose 4B beads" (GE Healthcare, Waukesha, WI, USA). First, beads were washed with buffer A (Table 2.4) as described earlier. Second, bacterial supernatant was mixed with washed beads and incubated for 2h in an orbital-shaker at 4°C. Then, beads were packed in a column connected to a peristaltic pump. After washing of the column with 10 bed volumes of buffer A (without Protease inhibitors), 30µL (Stock: 2000units/ml) of PreScission protease (GE Healthcare, Waukesha, WI, USA) in 5ml of buffer A were added to the column. Then, column is sealed and stored at 4°C ON for efficient protease cleavage. Finally, the cleaved protein was eluted from the column for SDS-PAGE analysis and Coomassie blue staining. Complementarily, for some experiments we eluted GST-proteins without proteolytic cleavage using 20mM of glutathione in buffer A.

- Purification of chitin-proteins: Human full-length BAX/BCLXL and its mutants were purified following procedure described in (Suzuki et al, 2000). Beads were first washed three times with ten bed volumes of buffer A (Table 2.4). The bacterial supernatant was mixed with washed beads and the mixture was incubated overnight in an orbital-rotator at 4ºC to allow binding of the protein to chitin beads. Then, beads were packed in a column connected to a peristaltic pump. Next, the column was washed with 5 bed volumes of corresponding buffer B. The column was then sealed and stored at 4ºC during 48h to allow efficient intein self-cleavage. Next, elution fractions were subjected to electrophoresis followed by Coomassie Blue staining.

5- Size exclusion chromatography (SEC): (see in the next section)

Fusion protein	Buffer A	Buffer B
His_6-tagged proteins	300mM NaCl, 20mM imidazole, 1mM $MgCl_2$, 50mMNa_2HPO_4/NaH_2PO_4. 1mM TCEP, 10% glycerol (pH 8)	Buffer A supplemented with 300mM imidazole. (pH 8)
GST fusion proteins	150mM NaCl, 50mM Tris, 1mM EDTA, 1mM TCEP, 10% glycerol (pH 7.5)	Buffer A supplemented with 20mM glutathione. (pH 7.5)
Chitin-proteins	100mM NaCl, 20mM Tris, 1mM EDTA, 1mM TCEP, 10% glycerol (pH 8)	Buffer A supplemented with 50-200mM DTT. (pH 8)

Table 2.4. Composition of purification buffers for affinity chromatography for each fusion protein.

Size exclusion chromatography (SEC)

The main application of Size Exclusion Chromatography (SEC) (also referred to as gel filtration) method is the fractionation of proteins or other molecules in solution based on their size and hydrodynamic radius. For that aim, a protein mixture is passed through a column packed with an inert porous matrix of spherical particles with determined pore sizes in an aqueous solution. Differences in the elution time of the proteins are due to different retention capacity in the pore matrix system (stationary phase). Therefore, small molecules will elute at higher volumes, whereas, larger proteins that cannot penetrate the pores will pass through the interparticle volume (mobile phase), eluting at earlier volumes. Maximum resolution can be obtained when the sample volume is 0.5% to 2% of the total volume of the column. Samples are isocratically eluted; no additional buffer is needed for the separation process, and separation can be performed within a broad pH, ionic strength and the medium accepts a variety of additives as detergents or urea.

In this thesis, SEC has been used for different objectives, in this section it has been used as the last step of the purification process, in order to obtain a homogenous and monomeric population.

Protocol 8 ***SEC***

1- Sample preparation: Fractions enriched in recombinant protein were concentrated in Centricons (Millipore) up to the 250µL-volume.
2- Gel filtration: Samples were loaded into a Superdex™ 200 HR 10/30 or Superdex 75 HR 10/300 GL size exclusion columns (Amersham Pharmacia Biotech, Uppsala, Sweden), equilibrated in KHE buffer (100mM KCl, 10mM HEPES, 1mM EDTA, pH 7.5) with 1mM TCEP and 10% glycerol. In the particular case of BFL1, the equilibration buffer was; 300mM NaCl, 20mM HEPES, with 1mM TCEP and 10% glycerol. Elution was performed at 0.3-0.5mL/min flow-rate, at 4°C and monitoring UV absorbance at 280nm.
3- Protein detection: Peak protein fractions were concentrated up to 10-200µM by ultrafiltration in 3YM Microcons, and analyzed by SDS-PAGE and Coomassie-blue staining.

2.1.2.3 Protein fluorescent labelling

For several studies such as Fluorescence Correlation Spectroscopy (section 2.2.2.3.), proteins must be labelled with fluorescent probes. For labelling, we use selected thiol-reactive dyes that can be conjugated with native cysteines present in the protein sequence or mutationally engineered for this aim. For FCS experiments, proteins were labelled with Alexa Fluor dyes that produce bright and photostable conjugates, Alexa fluor®-488-C5-maleimide and Alexa fluor®-647-C2-maleimide (Invitrogen, Carlsbad, CA). Moreover, IANBD, a thiol-specific iodoacetamide derivative of NBD, was used for studying protein:protein and protein:lipid interactions.

A general procedure for dye conjugation reaction (labelling) is described in Protocol 9.

Protocol 9 ***Protein Fluorescent labeling***

1- Sample preparation: Protein was diluted (0.2-0.5mg) in 1mL KHE at pH 7 containing 1mM of TCEP and incubated for 30min at 37°C to reduce disulfide bonds.
2- Labeling procedure: 5-10 molar excess of dye Stock (20mM IANB in DMSO or Alexa Fluor 10mM in DMSO) were incubated with the protein sample overnight at 4°C while constant stirring and protecting them from light.
3- Blocking reaction: Sample was centrifuged at 14,000rpm for 10min and the supernatant was loaded to a PD-10 Desalting column (GE Healthcare, Waukesha, WI, USA) previously equilibrated with KHE 1mM DTT. Here, conjugation reaction is blocked by DTT and labeled protein is separated from the non-conjugated free dye.
4- Determination of the degree of labeling: see section 2.1.2.5 Characterization of proteins.

2.1.2.4 Protein non-fluorescent labelling

For the topology assessment by using non-fluorescent probes, thiol-reactive PEG-Mal (Methoxil poliethileneglycol Maleimide) molecules (NANOCS) have been used. Theses probes can be conjugated with native cysteines present in the protein sequence or mutationally engineered for this purpose. Two different approaches were used to characterize the topology of different BCL2 family proteins at the membrane level.

First, the combination of monocysteine mutants with the relatively small probe 0.5kDa PEG-Mal, was used to obtain information about the implication of labelled residue (and its adjoining) in the protein membrane activities. Here, the labelling was performed as described in the protocol 9, but using 0.5kDa PEG-Mal probe instead of fluorescent dyes.

Second, a bigger thiol-reactive probe (5kDa PEG-Mal) was used to study the solvent exposure of each monocysteine residue, stablishing afterwards, the accessibility pattern and protein topology in the equilibrium. The irreversible binding of this 5kDa probe to exposed monocysteines, adds an extra weight to the protein that could be detected as a shift by SDS-PAGE. In this particular case, the protein labelling is done after its incubation with model membranes, mitochondria or semi-intact cells in the presence/absence of other BCL2 proteins. Thus, samples containing monocysteine mutants were incubated with 0.25-1mM of 5kDa PEG-Mal for 30min at variable temperature (4°C, RT and 37°C) under continuous stirring. Then, samples were blocked by adding

5mM DTT/NEM. Finally, SDS-PAGE analysis and Coomassie blue staining or Western blotting was performed as described in the protein visualization section 2.1.2.5 and protocol 10).

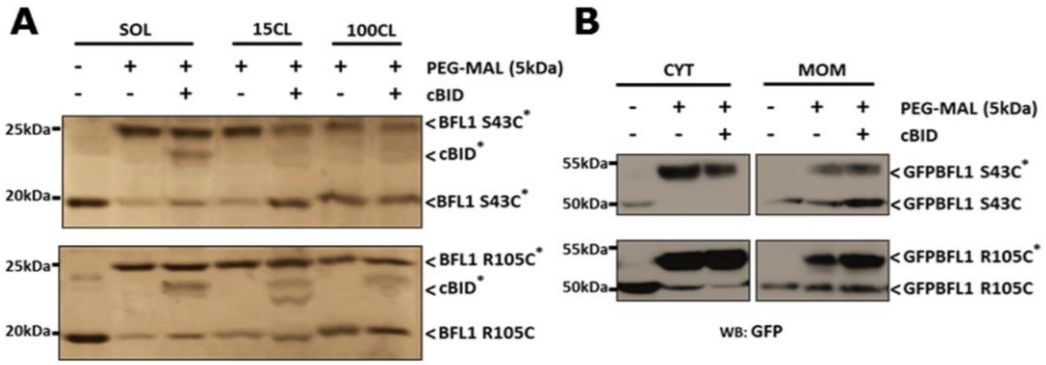

Figure 2.5. Topology assessment by using thiol-reactive PEG-Mal molecules (NANOCS). SDS-PAGE: (*Left)* coomassie blue staining. (right) Western blotting.

2.1.2.5 Characterization of proteins.

Protein concentration measurement

Protein concentration was quantified using either the Bradford protein assay (Bradford *et al.*, 1976) or absorbance measurement at 280nm. What follows is a brief description of main characteristics of each procedure:

- **Bradford:** Coomassie Brilliant Blue G-250 dye binds selectively to positively charge residues and aromatic residues, and this binding is accompanied by a shift in absorbance maximum from 465nm to 595nm. The working range of the technique is 1-1500µg/ml protein and the assay was performed using the standard test tube protocol and a set of pre-diluted bovine serum albumin (BSA) protein assay standards.
- **Absorbance at 280nm:** Proteins in solution absorb ultraviolet light with absorbance maxima at 280nm, due to the presence of amino acids with aromatic rings. Secondary, tertiary, and quaternary structure all affect absorbance, therefore factors such as pH, ionic strength, etc. can alter the absorbance spectrum. Following Lambert-Beer equation with a theoretically calculated extinction coefficient, we can estimate protein concentration.

$$A = \varepsilon c l \qquad \text{Eq. 2.1}$$

Where A is the absorbance, ε the extinction coefficient, c concentration and l cuvette length

- **Determination of the degree of labelling:** The degree of labelling can be calculated measuring the ratio of fluorescent dye and protein concentration. Fluorescent dye concentration can be measured by the absorbance value of the dye at the absorption maximum wavelength, and the protein concentration, following the methods explained above. If non-conjugated free dye is present, the degree can be overestimated, FCS measurements or MS Spectrometry can be done to confirm the results. Additionally, PEG-Mal labelling was calculated as the ratio between the intensity, assessed by Quantity One software (Fujifilm USA, Valhalla, NY), of shifted and non-shifted bands obtained from coomassie blue staining or WB.

Visualization and Detection techniques

There are a variety of methods for visualization and detection of proteins in-gel and on-membranes. In this section, several gel stains used in this thesis are described and summarized in the protocol 10.

Protocol 10 ***Protein detection***

The whole procedure can be divided in 2 steps: (1) gel electrophoresis and (2) visualization and detection.

(1) Gel electrophoresis: samples were separated according to the method of Laemmli (Laemmli, 1970). In this method, are separated mainly according to the molecular weight by denaturing sodium dodecyl sulfate polyacrylamide gel electrophoresis (SDS-PAGE) in 10-15% polyacrylamide gels, with 20 mM Tris-Cl (pH 7.9), 100 mM NaCl, 70 mM EDTA, 2% (w/v) SDS as running buffer.

(2) Visualization and detection:

1- Fluorescence: Fluorescently-labeled proteins were directly visualized in a gel using a Molecular Imager Versadoc (Bio-Rad, PA, USA). (next page)

2-Coomassie staining: Gels were stained with Coomassie solution (0.1% Coomassie R250, 10% acetic acid, 40% methanol) and then de-stained with 20% methanol, %10 glacial acetic acid. The reaction is based on the reversible electrostatic interaction of the colorant molecules with the amine groups of the protein.

3- Silver Staining: Gels were stained by using Silver Stain Plus kit (BIORAD) and then de-stained by following kit instructions.

4- Western blot (Immunoblotting): After gel electrophoresis, the procedure can be divided in three steps:

- Transference: Proteins were transferred onto nitrocellulose membrane (Protran nitrocellulose membrane; Whatman Inc, NJ, USA) by electroblotting at 12V for 45min, in a Trans-Blot SD (Bio-Rad, PA, USA) using 20mM Tris-HCl (pH 8), 100mM NaCl, 70mM EDTA, 15% MeOH as transfer buffer.
- Blocking: To prevent nonspecific interactions, the membrane was blocked with 5% non-fat dry milk in PBS (137mM NaCl, 10mM Na_2HPO_4, 10mM NaH_2PO_4 pH7) and supplemented with 0.05% Tween 20 (PBS-T). Blocking was performed in an orbital shaker at room temperature for 1 hour.
- Detection: The membrane was incubated for 1h at RT or ON at 4^{o}C in a 1:2,000 with an appropriate primary antibody diluted in %2.5 non-fat dry milk PBS-T. After 3X10 min washes in PBS-T, the membrane was incubated in a 1: 5,000 dilution with the corresponding horseradish peroxidase (HRP) conjugated secondary antibody for 1h on a shaker at room temperature. Finally, detection was carried out using the chemiluminescent ECL-Plus Western blotting reagent (Pierce, Rockford, IL, USA) and visualized on Hyperfilm™ ECL™ (PerkinElmer Life Sciences, Boston, MA, USA).

Structure studies

Circular Dichroism

Circular dichroism (CD) is a technique used for determining the secondary (Far-UV CD) or tertiary (Near-UV CD) structure of biomolecules. In addition, it is also useful to study their conformational changes and stability, either in solution or in model membrane systems, such as detergents or lipid vesicles. The relatively small amount of sample required and the simple data analysis have made this technique widely used. However, its main drawback is that, in contrast to other techniques like X-ray diffraction or nuclear magnetic resonance (NMR), the three dimensional atomic structure of the sample cannot be determined.

CD is a type of light absorption spectroscopy based on the differential absorption of the left and right circularly polarized components of linearly polarized radiation by optically active chiral molecules. The most abundant chromophores in proteins are the amide group and the side chains of aromatic amino acids, and the electronic transitions that produce upon absorption vary in wavelength and intensity, depending on their spatial localization. Thus, information about secondary and tertiary structure can be obtained. In the present work, CD has been used to study the structure of several BCL-2 family proteins either in solution to determine if purified proteins were well structured.

The Far-UV CD spectra were collected using the following parameters a 1-nm step size over 260 to 190nm wavelength range, speed 50nm/min; response 1s; bandwidth 2nm in a spectropolarimeter Jasco J-810 (Jasco Spectroscopic Co. Ltd., Hachioji City, Japan) equipped with a JASCO PTC-423S temperature control unit. Each measurement was the average of 20 scans, which was background- subtracted. All samples were allowed to equilibrate for 10min prior to CD analysis. Taking into account Lambert-Beer´s law, the degrees of ellipticity (θ) can be converted to mean residue molar ellipticity ($deg \cdot cm^2 \cdot dmol^{-1}$):

$$[\theta] = \frac{\theta}{(10.l.n.c)}$$

eq. 2.2

where θ are the degrees of ellipticity; l is the length of the pathway in cm; n, the number of peptide bounds and c the protein concentration in molar.

Finally, secondary structure content was estimated from the far-UV spectra using CDPro software (http://lamar.colostate.edu/-sreeram/CDPro/main.html) (Sreerama & Woody, 2004b). This prediction program, based on databases containing CD spectra of proteins whose structure has been solved with atomic resolution techniques such as X-ray crystallographically or NMR, is an online interface for the use of several open source algorithms (including CONTINLL, SELCON3 and CDSSTR) for analysing protein CD spectra.

As mention before, CD is also a useful technique to follow the thermal stability of a protein at a characteristic wavelength under increasing temperature. In our case, the multidomain proteins are α-helical proteins, so the signal at the 222nm is registered continuously as a function of temperature. Comparing these curves at different conditions, we analysed whether differences in the melting temperature of the protein occurred.

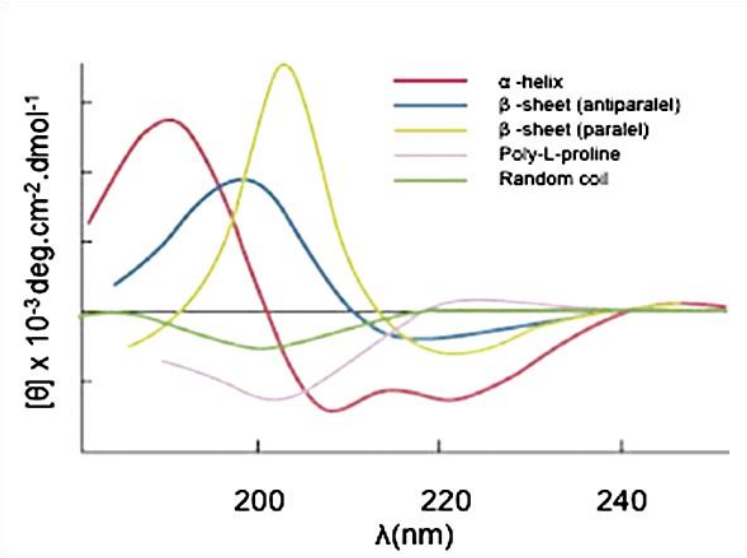

Figure 2.6 Representative circular dichroism spectra. α-helix structures present a double minimum at 222 and 208-210 nm and an intense maximum at 191-193 nm. The ratio between these intensities reflects the helicity of the peptides or proteins analysed. In contrast, β structures present a single minimum localized between 210 and 225 nm and a maximum between 190 and 200, depending on if they have a parallel or antiparallel arrangement. Finally, unordered structures, present a minimum around 200 nm and several weak bands between 220 and 230, either positive or negative**.**

To assess the thermal stability of the BCL-2 proteins studied, sample components (proteins with or without liposomes) were incubated for 1h in PBS buffer 37°C prior to the beginning of measurements. CD data was collected at 222nm wavelength every 1°C from 25°C to 90°C. The midpoint of the melting transition was estimated using the first derivative converter available in the software of the CD instrument with a window of nine data points and a 2nd degree polynomial smoothing.

Intrinsic tryptophan fluorescence spectroscopy

The intrinsic fluorescence of aromatic amino acids can be applied for studying protein stability. Changes in the intrinsic tryptophan (Trp) fluorescence of proteins often occur upon conformational changes or ligand binding. In general, the quantum yield of tryptophan fluorescence increases in intensity (sometimes accompanied with a blue shift) when tryptophan is buried to a more hydrophobic environment, and decreases when it is exposed to an aqueous medium. Thus, is sensitive to a possible conformational change, and therefore tryptophan

fluorescence can be applied for determining changes caused by cahotropic agents, membrane-interaction or ligand-binding, among others (Bakas et al, 1996; Ostolaza & Goni, 1995; Soloaga et al, 1998; Zhao & Kinnunen, 2002). A general procedure is described in Protocol 11.

Protocol 11 ***Intrinsic tryptophan fluorescence***

1- Sample preparation: First, sample components (protein, drugs, liposomes…) were incubated for 10min prior the measurement at RT while stirring in 750µL KHE.

2- Fluorescence measurement: Spectra were recorded in an 8100 Aminco-Bowman luminescence spectrometer (Spectronic Instruments, Rochester, NY, USA) between 305nm and 405nm (4nm bandpass) at a scan rate of 1 nm/s, using an excitation wavelength of 295 nm (4nm bandpass). The slit widths for excitation and emission were kept at 4nm, with the experiment conducted at RT. The contribution of the buffer or liposomes alone was subtracted as blank.

Differential scanning fluorimetry (DSF)

DSF monitors thermal unfolding of proteins in the presence of a fluorescent dye and is typically performed by using a real-time PCR instrument. The fluorescent dyes that can be used for DSF are highly fluorescent in non-polar environments, such as the hydrophobic sites in unfolded proteins, compared to aqueous solution where their fluorescence is quenched. In recent time, the use of extrinsic fluorescent dyes such as ANS, Bis-ANS, Sypro-Orange and others has increased, because of their versatility, sensitivity and suitability for high-throughput screening. (Hawe et al, 2008a; Hawe et al, 2008b; Semisotnov et al, 1991).

In a DSF experiment, the fluorescence intensity is plotted as a function of the temperature; this generates a sigmoidal curve that can be described by a two state transition. The inflection point of the transition curve (Tm) is calculated applying Boltzmann fitting.

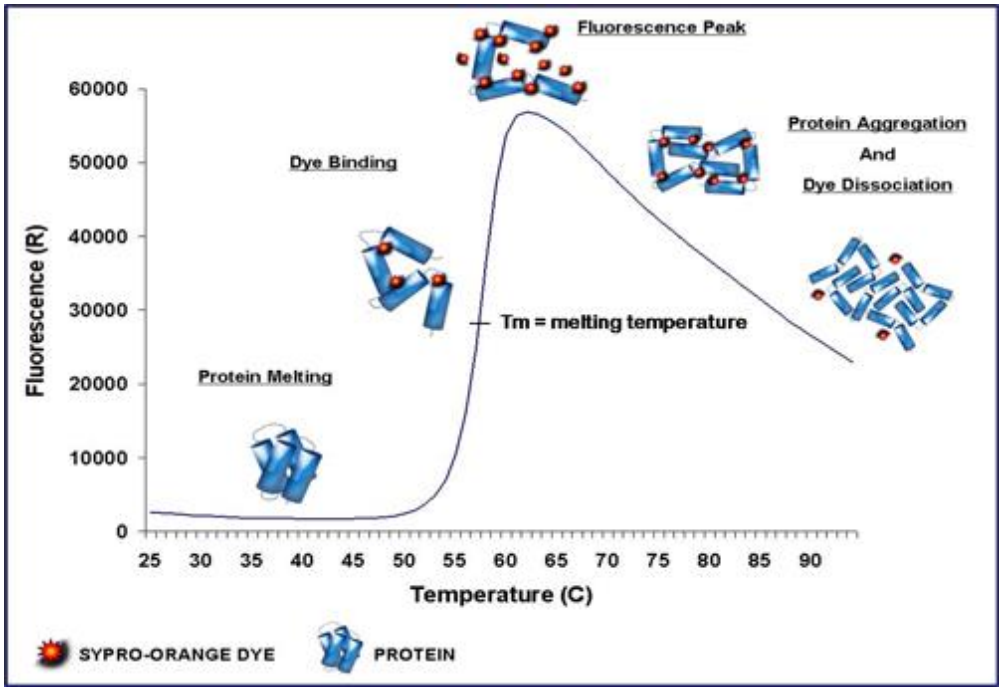

Figure 2.7. Diagram of a typical thermal shift assay

Protocol 12 **DSF/ ANS Fluorescence**

1- Sample preparation: Protein (1µM final concentration) was diluted in 1mL KHE at pH 7,4 containing 10µM of 8-Anilinonaphthalene-1-sulfonic acid (ANS).

2- Fluorescence measurement: Emission fluorescence were recorded in a FLUOROLOG HORIBA JOBIN YVON coupled with a peltier LFI 3551, at λ_{EM}=485±nm, between 60°C and 95°c (1°C/min increase), using an excitation wavelength of 350 nm (4nm bandpass).

NOTE: For these experiments is particularly important to seal the cuvette with a lid to avoid thermal evaporation.

2.1.2.6 Synthetic peptides.

The synthetic peptides used in this thesis emulate some of the alpha helixes present in the proapoptotic BAX. All synthetic peptides (>90%purity assessed by HPLC) were purchased from Biomatik (Wilmigton, DL, USA).

Name	Sequence
BAX α5 peptide	FNWGRVVALFYFASKLVLKALCT
BAX α6 peptide	VPELIRTIMGWTLDFLRERL
BAX α7-8 peptide	LGWIQDQGGWDGLLSYFG

Table 2.5 Different peptides sequences of the BAX alpha helixes.

Peptide concentration measurement

The bicinchoninic acid (BCA) assay (Smith et al, 1985) was performed using the standard test tube protocol and a set of pre-diluted bovine serum albumin (BSA) protein assay standards. This BCA method employs the reduction of Cu^{2+} to Cu^{1+} by protein in alkaline medium and this creates a purple-coloured product that absorbs at 562nm. The working range of the technique is 5 µg/ml-2 mg/ml. Importantly, unlike the Coomassie dye-binding methods, the universal peptide backbone also contributes to colour formation, helping to minimize variability caused by protein compositional differences.

2.2 METHODS RELATED TO RECONSTITUTED MODEL SYSTEMS

2.2.1 Protein-lipid interaction: membrane-association

Numerous approaches have been used to assess the interactions of proteins and lipids, those that have been used in the present thesis are described in the following sections.

2.2.1.1 Binding of proteins to liposomes

In order to have an observable effect on a membrane, the protein must first associate with it. A commonly used method to determine protein-lipid interaction is studying the binding of proteins to liposomes. The protocol used in this type of experiments involved incubation of the protein (or the combination of them) with liposomes and separation of lipid-associated from lipid-free fractions. This model membrane system is compiled in protocol 13.

Protocol 13 ***Binding of BCL2 proteins to liposomes***

1- Sample preparation: Proteins and liposomes were first incubated in KHE buffer at 37°C for 1h while shaking.
2- Sucrose gradient float-up centrifugation: Following incubation of the proteins with the liposomes at 37°C, the sample is adjusted to 1.4M sucrose using sucrose stock solution prepared in KHE and loaded at the bottom of a discontinuous sucrose gradient (medium layer of 0.8M, upper layer of 0.5M sucrose). The sample is centrifuged at 4°C for 3 hours at 500,000 x *g* in a Beckman Optima TLX Benchtop ultracentrifuge (Beckman Coulter Miami, FL, USA), using a TLA 120.2 rotor. During ultracentrifugation, due to their lower density, liposomes and liposome-bound proteins float up to the top fraction of the gradient whereas free protein remains at the bottom (a total of 4 samples).
3- Protein detection: Finally, proteins were detected by immunoblotting or by fluorescence detection and integrated densities were measured using Quantity One software (Fujifilm USA, Valhalla, NY).

2.2.1.2 Lipid Monolayers experiment

Lipid monolayer experiments are based on the measurement of the water surface tension by means of a suspended solid probe that is slightly introduced into the gas-liquid interface. The forces generated by surrounding molecules (surface active compounds as lipids or proteins) produce an excess cohesive energy called the surface free energy that can be related to the forces detected by the probe which can be further related with surface pressures (π).

Typically, lipid monolayer experiments are used in two types of experiments. In the first one, the two-dimensional lipid density can be controlled by compressing the monolayer, obtaining compression isotherms. This type of experiments allows determining phase transitions and the collapse pressure.

In the second type of experiment, the one used in this work to assess BAX α helixes capacity to penetrate in the monolayer, the area of the interface is maintained constant and the changes in surface pressure (π), due to the addition of a protein or peptide, are registered as a function of time (Brockman, 1999; Fidelio et al, 1986). By comparing the values of π under different conditions (lipid composition, the temperature, the ionic strength of the medium, etc.), one can obtain information about the parameters influencing the interaction.

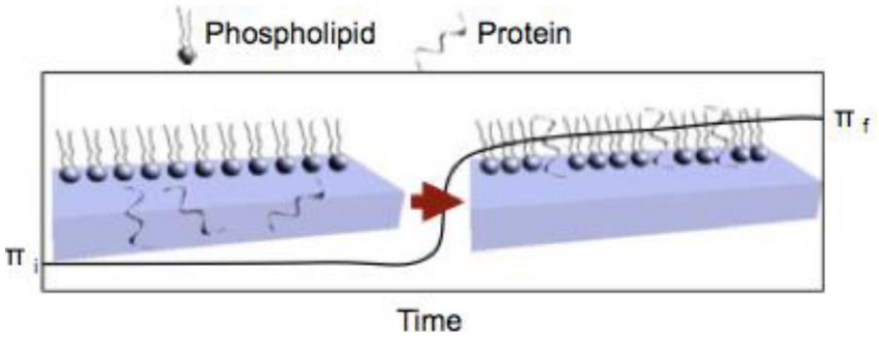

Figure 2.8. Schematic representation of the process of protein insertion into a lipid monolayer. The initial pressure of the monolayer is adjusted to the desired value (πi). The protein inserts into the monolayer increasing the surface pressure until reaching the equilibrium (πf). Δπ is then calculated using $\Delta\pi = \pi_f - \pi_i$.

A particularly useful parameter to study the monolayer-penetrating capacity of a protein is to determine its critical pressure (π_C), this is the value of π at which Δπ becomes zero or in other words, the minimum surface pressure at which the protein is no longer able to penetrate the monolayer. This parameter can be calculated by plotting the increase of pressure (Δπ) as a function of the initial surface pressure (π0), being the exclusion pressure the value when equation turns zero. It is to be stressed that cell membranes are proposed to have a surface pressure of around 30 mN/m (Janmey & Kinnunen, 2006). However, this value is controversial and can largely vary. Lipid monolayer experiments are described in Protocol 14.

Protocol 14 ***Lipid Monolayer experiments***

1- Monolayer preparation: After calibration of the Langmuir balance, a small volume of the lipid mixture (1mM in chloroform) was spread onto 1,25mL KHE buffer to form a monolayer with a given initial surface pressure (π_0).

2- Protein injection and surface pressure measurement: Once the surface pressure of the monolayer was stabilized, the protein solution was injected into the water subphase through a small hole drilled at an angle through a trough. Changes in surface pressure (Δπ) were measured as a function of time, using a Kibron μTrough S tensiometer (Helsinki, Finland).

Note: It is important to point out that proteins could also move to the water/air interphase, generating an increase of surface pressure without a lipid monolayer. Therefore, first we have to determine which minimum protein concentration can be used in which the increase of surface pressure is constant in the absence of lipid monolayer. This will determine above which initial surface pressure we can start measuring in the presence of lipid monolayer.

2.2.1.3 ^{31}P nuclear magnetic resonance (^{31}P-NMR)

NMR is based on the fact that atomic nuclei oriented by a strong magnetic field absorb radiation at characteristic frequencies that depends on the type of nucleus and the environment. The parameters that can be measured on the resulting spectral lines can be interpreted in terms of molecular structure. The neutrons and protons composing an atomic nucleus have an intrinsic quantum property of spin or angular momentum (L) and associate nuclear magnetic moment (μ). Both momentums are vectorial magnitudes. The angular momentum can be expressed as in the (eq. 2.3) where I is the spin.

$$L=[I(I+1)\hbar]^{1/2}$$

eq. 2.3

The spin of any nucleus with an odd mass number A is half-integral, e.g. ^{1}H, ^{13}C, ^{15}N, ^{19}F, ^{31}P. These nucleuses generate magnetic dipoles. On the other hand, the spin of any nucleus with and even mass number A and odd charge number Z is integral, e.g. ^{2}H, ^{14}N. These nucleuses do not represent spherical symmetry of charge; their observation is more difficult by RMN. Finally, the spin, and hence the magnetic moment, of any nucleus with both A and Z even is zero. This rule is important since the observation of resonance hinges on the existence of magnetic moment is unobservable in most abundant isotopes of biological elements.

In absence of a magnetic field the μ of the different nuclei can adopt any direction. When the nucleuses are placed in a magnetic field (B_0), however, the angular momentum tends to align in the direction of the field. Only two orientations defining two energy levels are possible for a nuclear spin ½, parallel or antiparallel to B_0.

For a transition from one energetic level to the other, an absorption or emission of a quantum of radiation (hν) is required. Resonant absorption will occur when electromagnetic radiation of the correct frequency to match this energy difference is applied. The absorption will occur when:

$$\Delta E=h\nu=\gamma B_0/2\pi$$

$$\nu_0=\gamma B_0/2\pi$$

eq. 2.4

where ν_0 is the Larmour frequency, which typically corresponds to the radio-frequency range of the electromagnetic spectrum. It is this resonant absorption that is detected in NMR.

Several aspects of membrane structure and dynamics can be studied by NMR, such as the orientation and motility of hydrocarbon chains, the environment of polar head groups, lipid flip-flop, etc. In this thesis, ^{31}P-RMN of MLV dispersions of phospholipids has been used to directly assess whether these peptides disrupt the membrane lipid bilayer structure. When lipids are

organised in a bilayer, fast axial reorientation of lipids about their long axis results in partial averaging of the chemical shift anisotropy giving rise to characteristic spectra with a low field shoulder and a high field peak (Killian, 1998). In the hexagonal phase, the phospholipids are arranged in long tubes, with their headgroups surrounding an aqueous channel, the lipids now also undergo fast reversed asymmetry. Other phase that can be adopted by lipids is the cubic phase. This consist of interwoven networks of aqueous channels where lipids undergo complete motional averaging leading to an isotropic ^{31}P-RMN signal (Killian, 1998).

The ^{31}P-NMR spectrum of MOM-like liposomes showed the high-field peak and low-field shoulder typical of a planar bilayer arrangement of membrane lipids. Therefore, changes in the intensity of this peak or the appearance of other peaks (around the chemical shift position of phospholipids experiencing isotropic motion) could be indicative of highly curved non-bilayer type lipid dispositions

Protocol 15 ***^{31}P-NMR experiments***

1- Sample preparation: Samples for ^{31}P NMR were prepared by dispersing 15 µmol of dry MOM-like lipid mixtures in 0.5 ml of KHE buffer alone or containing the peptide of interest (0.15 µmol). Multilamellar vesicle suspensions were freeze-thawed 3 times in liquid N2 to disperse the added proteins in the lipid membranes, and the liposomes were spun down in an Eppendorf centrifuge (14000 g, 15 min, 4 °C). Pellets were loaded directly into 5-mm Pyrex NMR tubes.

2- NMR measurement: High power, proton noise-decoupled 31P NMR spectra were recorded at 25 °C on a Bruker AV-500 spectrometer operating at 202.4 MHz using 5-mm broadband inverse probes with z-gradient equipment. 1024 free induction decays were averaged using a 2-s recycle delay. Spectra were processed and evaluated using TOPSPIN 1.3 (Bruker) and plotted with 80-kHz line broadening.

Of note: These experiments were carried out in the NMR service of the university of the Basque country (UPV/EHU)

2.2.1.4 COMPUTATIONAL TOOLS

Main biophysical characteristics of BAX-derived peptides were determined by MPEx (Snider et al, 2009) and Heliquest (Gautier et al, 2008). Monte Carlo (MC) simulations of the interaction of peptide molecules with MOM-like membranes were performed using the MCPep (Gofman et al, 2012a) web server. The web server´s output includes the free energy of peptide-membrane association, the energetically favourable peptide-membrane depth of penetration and tilt, and snapshots of example simulations with the centroid conformation of the largest cluster (in PDB format).

MPEx: designed for examination of membrane protein sequences using hydropathy-plot methods popularized by Kyte and Doolittle (1982). That is, it is based on sliding-window analysis that represents an amino acid sequence as a sequence of numbers representing physical or statistical properties of the amino acid sequence. The most common physical property is hydropathy, which is based upon the free energy of partitioning of amino acids between water and membrane. The whole-residue partitioning scales predict with considerable accuracy the transmembrane (TM) segments of membrane proteins of known structure as shown by (Jayasinghe et al, 2001),

Heliquest: this program calculates the physicochemical properties and amino acid composition of an alpha-helix and screens databank to identify protein segments possessing similar features. This server is also dedicated to mutating helices manually or automatically by genetic algorithm to design analogues of defined features (Gautier et al, 2008).

MCPep Server: The helical content of the peptide is calculated based on the conformations obtained from the simulations. A residue is defined to be in an α-helical region if the rotational angles of its two adjacent bonds lay within the interval typical for an α-helix (-120°±30°) (Kessel et al, 2003). The percentage of conformations where a residue is found in the helical state is calculated and presented in the output files. The rotational angles of the peptide's ends cannot be defined, and the two residues at the N-terminal and the two residues at the C-terminal are neglected.

2.2.2 Protein-protein interaction in solution and lipid environment

2.2.2.1 Oligomerization assays

According to current models, a crucial step in the activation of BAK/BAX is their oligomerization. However, this homo-oligomerization capacity that is frequently associated with apoptotic phenotype, has also been described for some antiapoptotic proteins. In this work, the oligomeric degree of the BFL1 was examined with three different approaches: gel filtration assays, cross-linking assay and by total internal reflection microscopy (TIRFm).

Gel filtration assay

In this section, size exclusion chromatography (SEC) or gel filtration have been used to determine the oligomeric state of BFL1 in the presence/absence of CL enriched model membranes. SEC can provide valuable information of membrane protein quaternary structure. Typically, the protein of interest is first extracted from the membrane using non-denaturing detergents of small micellar size (CHAPS, octylglucoside…), and then the sample is subjected to gel filtration chromatography. Based on the observation that CHAPS (but not other detergents such as octylglucoside, or TX-100) does not induce the oligomerization of many BCL2 family proteins including BFL1, we chose this detergent to extract inserted BFL1 from the liposomal membrane. The protocol is described in Protocol 16.

Protocol 16 ***Oligomerization assay by SEC***

1- Sample preparation: Samples (protein alone or in the presence of liposomes) were incubated in a final volume of 100µL in KHE at 37°C for 30 minutes while stirring. Then CHAPS was added to a final concentration of 3% and incubate the mixture at 4°C for 30 minutes.

2- Gel filtration: Samples were loaded into a Superdex™ 75 HR 10/30 size exclusion column (Amersham Pharmacia Biotech, Uppsala, Sweden), equilibrated in KHE buffer with 3% CHAPS. Elution was performed at 0.5ml/min flow-rate, at 4°C and monitored by UV absorbance at 280nm.

Crosslinking assay

For determining the oligomeric state of BFL1 (intermolecular crosslinking), a cysteine modifying agent has been used to link cysteines present in BFL1. This agent is the redox catalyst copper (II) (1,10-phenanthroline)$_3$ (CuPhe), that is formed by the mixture of 1,10-phenanthroline monohydrate (Sigma-Aldrich) and anhydrous copper(II) sulphate (Cu(II)SO4; Sigma-Aldrich). CuPhe enhances the rate air-oxidation of all sulfhydryl groups present in the cysteines at neutral pH. The crosslinking is effective only over an extremely short distance, as the disulphide bond is about 2.05 Å in length. Briefly, the procedure is detailed in Protocol 17.

Protocol 17 ***Oligomerization assay by cross-linking***

1- CuPhe complex preparation: The CuPhe stock was 30mM $CuSO_4$ and 100mM 1,10-phenanthroline in 4:1 water/ethanol.

2- Sample crosslinking: Samples (proteins in the presence or absence of liposomes) are incubated at 37° for 30 minutes in KH (KHE without EDTA), and for disulphide bond formation CuPhe stock is added and diluted 100-fold into the sample, let them incubate at 4°C for 30 minutes or some minutes at room temperature.

3- Blocking the reaction: The oxidation was blocked by adding 20mM EDTA to chelate copper and 20mM N-ethylmaleimide (NEM) to block unreacted cysteine residues.

4- Protein detection: Samples were analyzed by non-reducing SDS-PAGE gels and detected by coomassie blue staining or immunoblotting using anti-HIS antibody.

2.2.2.2 Total internal Reflection Fluorescence (TIRF)

Total internal reflection fluorescence (TIRF) microscopy (also called evanescent wave microscopy) provides a means to selectively excite fluorophores in an aqueous or cellular environment very near a solid surface (within ≤100nm) without exciting fluorescence from regions farther from the surface. Fluorescence excitation by this thin zone of electromagnetic energy (called an evanescent field) results in images with very low background fluorescence, virtually no out of focus fluorescence, and minimal exposure of cells to light at any other planes in the sample (Figure 2.9A). The unique features of TIRF have enabled numerous applications in biochemistry and cell biology, such as i) Selective visualization of cell/substrate contact regions, ii) Micromorphological structures and dynamics on living cells, iii) Long-term fluorescence movies of cells during development in culture and iv) protein oligomerization states among others (Figure 2.9B-E). (Axelrod, 2001a; Axelrod, 2001b; Subburaj et al, 2015).

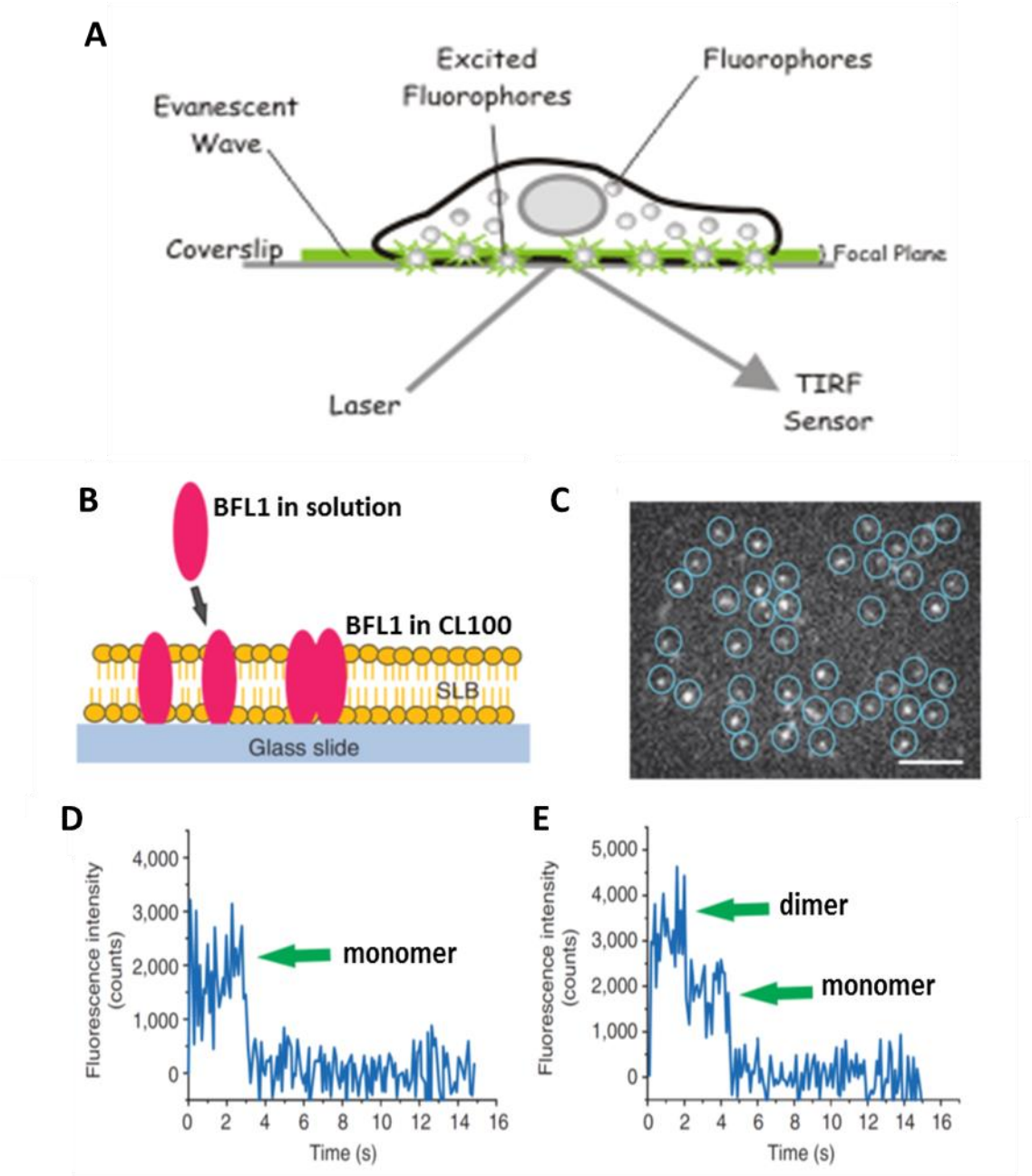

Figure 2.9. General scheme of TIRF experiment. (a) Simplified scheme of evanescent wave exciting specifically the focal plane due to laser incidence degree. **(b)** Schematic representation of the experimental setup showing a supported lipid bilayer with BFL1g bound to it. **(c)** Epifluorescence image of BFL1g molecules immobilized on a supported lipid bilayer. Scale bar, 1µm. Each particle was detected and the fluorescence intensity measured over time. Detected particles are shown in circles to help visualization. **(d,e)** Fluorescence intensity of two representative individual particles showing photobleaching steps (arrow). Adapted from (Subburaj et al, 2015).

In this thesis, the TIRF microscopy was performed in Ana Garcia-Saez ´s lab (Tubingen, Germany), under the supervision of Dr Katia Consentino. Concretely, we used this technique in order to assess homo-oligomerization degree of BFL1 in model membranes. Here combining SLB (Protocol 18) and recombinant- Alexafluor488-labelled (protocols 7 y 9) BFL1ΔC (C19S, C55S).

Protocol 18 **SLB formation**

1- LUV preparation: pure CL LUV in PBS (1mM) were formed as described in protocol 3.
2- BFL1-LUV binding and homo-oligomerization: 0.5-1.5nM of BFL1ΔC-a488 were incubated with 1mM LUV for 1h at 37º (final volume of 150µL).
3- $CaCl_2$ for membrane fusion: proteoLUVS were incubated in a precleaned-chamber* in the presence of $CaCl_2$ (3mM, 0.5µL of 1M stock) at 37º for 2 min.
4- Washing: Isosmotic PBS (300µL) was added and subsequently removed for at least 10 times, in order to remove free $CaCl_2$ and non-fused LUVs.
5- Data acquisition and analysis.

*Importantly, chambers need to be cleaned with piranha solution (3:1 mixture of concentrated sulfuric acid and hydrogen peroxide), in order to constitute homogeneous supported lipid bilayers. This cleaning procedure was specifically done to remove organic residues and to enhance the hydrophilicity of the glass surface. Slides were thoroughly rinsed with deionized water and sonicated with deionized water for 5min. Before further usage, they were dried using a clean nitrogen stream. Individual slides were glued on the upper part of the measurement chamber (Lab-Tek 155411, Nunc, original borosilicate coverglass was manually removed) using glue. Once cleaned, chambers can be stored in MQ water for as much one week.

Microscope settings and stoichiometry analysis

As experiments were developed in collaboration with Dr Katia Cosentino. Microscope settings and date analysis were based on (Subburaj et al, 2015) but optimised according to sample peculiarities exhibited by BFL1 in pure CL vesicles. In brief, samples were excited on a modified

Zeiss Axiovert 200M epifluorescence microscope at 37 ºC using a diode laser (iBeam smart 488, Toptica, Germany) via a X100, numerical aperture=1.46 Apochromat objective (Zeiss) for an illumination time till=1ms and a delay of 90 ms between frames (number of frames=500) with an intensity of 5 $kWcm^{-2}$ (measured at the sample).

As for the stoichiometry analysis, the images acquired were used for the stoichiometry analysis based on the fluorescence intensity of the particles. For this purpose, individual particles with a single photobleaching step were detected via a threshold and their fluorescence intensity was estimated by fitting with a Gaussian. The estimated values were used to build a histogram of the distribution of fluorescence intensities that was fitted a Gaussian that provided the mean intensity μ and s.d. σ of a single fluorophore. In our experimental data N_{max} is 6 and therefore we restricted our fittings up to hexamers. For determining the stoichiometry of BFL1, ≈500 individual particles were detected and analysed for each experiment. The distribution of the fluorescence intensity of all the particles was fitted with a sum of six Gaussians using obtained μ and σ values.

2.2.2.3 Fluorescence correlation spectroscopy (FCS)

The biological function of molecules depends not only on their structure, but also on their mobility and dynamic properties, which are strongly influenced by the environment. Using single molecule techniques requires no synchronization of underlying molecular kinetics, because just observing a single member of the system we can study that configuration at any given time. Thus, the main advantage of single-molecule techniques is that one can study individually the distribution of the mechanism of action of biological molecules (Haustein & Schwille, 2004). For instance, we can distinguish if changes in the measured parameter are observed only for a subpopulation in the system (Johnson et al, 2005). The low concentrations needed similar to physiological conditions, and application to equilibrium systems are additional important advantages of this system.

Fluorescence correlation spectroscopy (FCS), a single-molecule-based technique, allows inherent averaging of thousands of single-diffusion events, allowing precise estimation of diffusion coefficients and particle concentrations through the comparison of the fluctuations in fluorescence intensity of a system in equilibrium in a very small measurement volume (Schwille, 2001). At thermal equilibrium, the fluctuations in fluorescence intensity quantified by FCS could be due to the diffusion of fluorophores through the focal volume or changes in their emission properties due to chemical reactions and/or photo-dynamic processes. Consequently, not only diffusion coefficients, dye concentrations and particle sizes can be measured, conformational changes and molecular interactions can be also assessed by this technique (Bacia et al, 2006; Haustein & Schwille, 2004; Kahya, 2006).

During the last years, FCS has been successfully employed for the study of membrane dynamics and protein/lipid interactions (Betaneli & Schwille, 2013; Bleicken et al, 2017; Bleicken et al, 2013b; Garcia-Saez et al, 2009; Ries et al, 2009; Steringer et al, 2012). In this work, FCS was

used for the study of the interactions among BCL-2 family proteins, specially BFL1 interaction network, in solution and at different membrane compositions.

The FCS setup (Figure 2.10) combines a confocal microscopy system with fluorescence correlation/cross-correlation capabilities. In general, this setup consists of an inverted microscope in combination with high numerical aperture objective (f.e. 40x NA 1.2 UV-VIS-IR C-Apocromat water-immersion objective, Zeiss, Germany), several lasers for excitation (f.e. Ar-ion (488 nm), HeNe (561 nm) or HeNe lasers (633 nm)) and several detection channels with fiber-coupled avalanche photo diodes (ADPs) to achieve efficient detection. The incoming laser light is reflected by the dichroic mirror and focused by the microscope objective to a spot of approximately 0.3-0.5µm diameter. The photons emitted within the focal volume of the sample passes the dichroic filter and finally through a pinhole that is inserted into the image plane which reduces the detection volume in the z-direction, resulting in a measurement volume ranging femtoliters. For detection, APDs with single-photon sensitivity are usually used. This configuration allows high signal/noise ratio when using fluorophore concentrations from 0.1nM to 1µM. The fluorescence trace can be then correlated with a hardware or a software correlator.

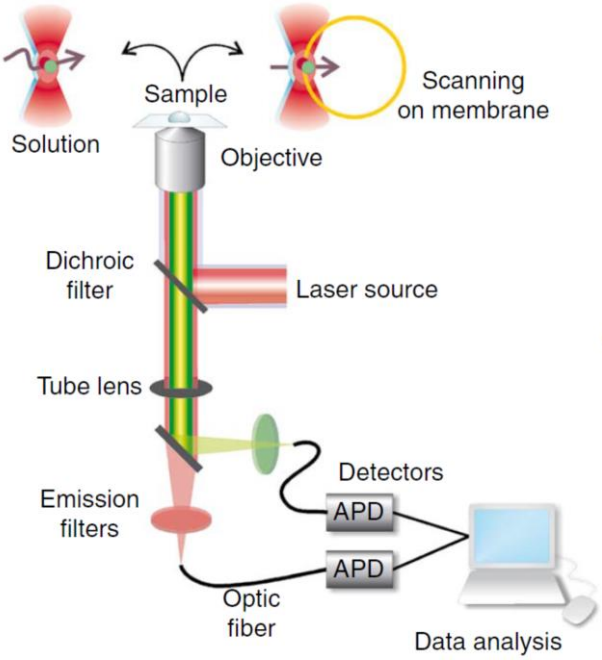

Figure 2.10 Scheme of a typical FCS setup. Optical setup is based on an inverted laser-scanning microscope. The sample is excited by a laser beam and the emitted photons are spectrally filtered and passed through a pinhole, limiting the detection volume in z-direction, and finally, the detector is an avalanche photodiode coupled to an autocorrelator. Diffusion and binding of proteins in solution are measured by FCS, using a fixed detection volume. In contrast, for the measurements in the membrane, scanning FCS is used and the focal volume is perpendicular to the plane of the membrane (Garcia-Saez et al, 2009).

In principle, the autocorrelation function, *G(τ)*, is a measure of the self-similarity of the fluorescence signal after a lag time (τ), hence, it resembles the conditional probability of finding a molecule in the focal volume at a later time, τ, given it was there at time 0 (Figure 2.11A). The characteristic decay time of the autocorrelation function is related to the time that the fluorophore spends within the focal volume, which depends on the mobility of the particle: The larger the diffusion coefficient, the faster the decay. The mathematical tool that relates the fluorescence signal with itself (auto-correlation) at different times can be calculated as:

$$G(\tau) = \frac{\langle \delta F(t) \,.\, \delta F(t + \tau) \rangle}{\langle (F(t) \rangle^2}$$

eq. 2.5

where, *G* is the autocorrelation function, *F* is the fluorescence intensity as a function of time *t*, and τ is the correlation time. The angular brackets refer to time averaging, so that δF(t)= F(t)-F(t).

To obtain the parameters of interest, the correlation curve obtained is fitted with a mathematical model based on the characteristics of the system that gives rise to the fluorescence fluctuations, like diffusion of the fluorophore and triplet state. This model also considers the size and the shape of the focal volume, the molecular brightness of the fluorophore, and its concentration as a function of position and time. For FCS experiments in solution, a function that models the 3D Brownian motion of fluorescently labelled particles is used (Table 2.6). Then, the diffusion time, τ_D, is related to the diffusion coefficient *D*:

$$\tau_D = {\omega_0^2}/{4\,D}$$

eq.2.6

The waist radius of the focus, ω_0, is calibrated by the fitting of the autocorrelation curve obtained in the same experimental conditions for a dye (f.e. free Alexa488 or Alexa647) of known diffusion coefficient.

In general, protein molecules diffusing in solution are assumed to approximate a spherical shape, using the Einstein-Stokes relationship, we could calculate the hydrodynamic radius (R) of each particle in the system, once the diffusion coefficient of each particle is estimated:

$$D = \frac{k_\beta\, T}{6\,\pi\,\eta\,R}$$

eq.2.7

where, k_β is the Boltzmann constant, *T* is temperature in degrees Kelvin, η is viscosity of solution in which particle is diffusing, and *R* is the hydrodynamic radius of the spherical particle.

In most cases, the triplet state population of the fluorophore contributed to the fluorescence fluctuations and it can be taken into account by an additional factor as Table 2.6 shows.

A powerful variation of FCS is the dual-colour fluorescence-correlation spectroscopy where two species labelled with spectrally different dyes (to avoid cross talk and thus false positives) are studied (Bacia et al, 2006; Haustein & Schwille, 2004). In this way, the two fluorophores are excited within the same focal volume using two overlapping laser beams, and photons are detected using different spectral channels with signals $F_g(t)$ and $F_r(t)$, in this case for the green and red species respectively. If two species interact they will diffuse together in the focal volume, and simultaneous fluorescence fluctuation will be recorded. The analysis of the latter in both channels yields a cross-correlation function that gives us information of the concentration of the complex:

$$G_{gr}(\tau) = \frac{\langle \delta F_g(t) \,.\, \delta F_r(t + \tau) \rangle}{\langle F_g(t) \rangle \, \langle F_r(t) \rangle}$$

eq.2.8

The degree of complex formation (%CC) can be calculated by comparing the amplitude *G(0)* of the auto- and cross-correlation curves:

$$\%CC_{gr/r} = \frac{C_{gr}}{C_{gr} + C_r} = \frac{G_{gr}\,(0)}{G_r\,(0)} \; and \; \%CC_{gr/g} = \frac{C_{gr}}{C_{gr} + C_g} = \frac{G_{gr}\,(0)}{G_g\,(0)}$$

eq.2.9

where, C_{gr}, C_r and C_g are the concentrations of the complex *gr* (the complex formed by green-labeled and red-labeled species), and the forms *g* (green specie) and *r* (red specie), respectively. Therefore, %CC can be express with respect to the amount of red particles or green particles.

For measurements in the membrane, dual color scanning FCS (SFCCS) was performed, which allows the measurement of the interaction of different species in the membrane (Figure 2.11B). In the case of GUV samples, the detection volume is repeatedly scanned perpendicularly through the equator of the membrane. In this two-focus SFCCS variant, two parallel lines are scanned through the membrane in an alternating fashion at distance *d*. This distance can be measured by repeatedly scanning over a film of dried fluorophores and measuring the distance between the bleached traces in a high-resolution LSM image. This setup eliminates the need to calibrate the detection volume. The intersections of these two lines with the membrane give rise to two intensity traces $F_1(t)$ at focus 1 and $F_2(t)$ at focus 2, from which the auto-correlation and also the spatial cross-correlation curve of the fluorescence in the two foci can be calculated:

$$G_{12}(\tau) = \frac{\langle \delta F_1(t) \,.\, \delta F_2(t + \tau) \rangle}{\langle F_1(t) \rangle \, \langle F_2(t) \rangle}$$

eq.2.10

Modelling the spatial cross correlation function to a two-dimensional diffusion of a fluorescently labelled particle in a Gaussian elliptical detection area is given in Table 2.6. Once the distance *d* is known, the concentration *C*, the diffusion coefficient *D*, and the waist of the laser focus ω_0 can be determined directly by fitting the data without any additional calibration. The photons in the two foci are not collected within the same time window, but with a delay t_d, which is usually given by the scan period, so during fitting data t_d has to be taken into account. When two spectral channels are employed, the red and the green auto and cross-correlation curves can be calculated. By globally fitting the auto-correlation curves, the spatial-cross-correlation and the cross-correlation curves, we can estimate the total concentration of green and red particles, as well as the concentration of the complex (Garcia-Saez et al, 2009).

Diffusion type	Model function
3D diffusion	$G_{3D}(\tau) = \frac{1}{N}\left(1+\frac{\tau}{\tau_D}\right)^{-1} \frac{1}{\sqrt{1+\frac{\tau}{\tau_D . S^2}}}$
3D diffusion with triplet	$G_{3D+T}(\tau) = \left[1 + T(1-T)^{-1}\exp\left(-\frac{\tau}{\tau_T}\right)\right] G_{3D}(\tau)$
2D diffusion for two foci SFCS	$G_{12}(\tau) = \frac{1}{C\pi S\omega_0^2}\left(1+\frac{4D\tau}{\omega_0^2}\right)^{-1/2}\left(1+\frac{4D\tau}{\omega_0^2 S^2}\right)^{-1/2}\exp\left(-\frac{d^2}{\omega_0^2 + 4D\tau}\right)$

Table 2.6. Model functions for fitting of FCS data. Here *G* is the autocorrelation curve, *N* is the average number of particles in the detection volume, τ is the lag time and τ_D is the diffusion time. τ_T corresponds to the triplet time, ω_O is the waist of the detection volume, *T* is the fraction of fluorophores in the triplet state within the detection volume and *S* is the structure parameter. The terms introduced to correct for 3D diffusion are also valid for two components. In the 2D diffusion model, *d* represents the distance between the two foci.

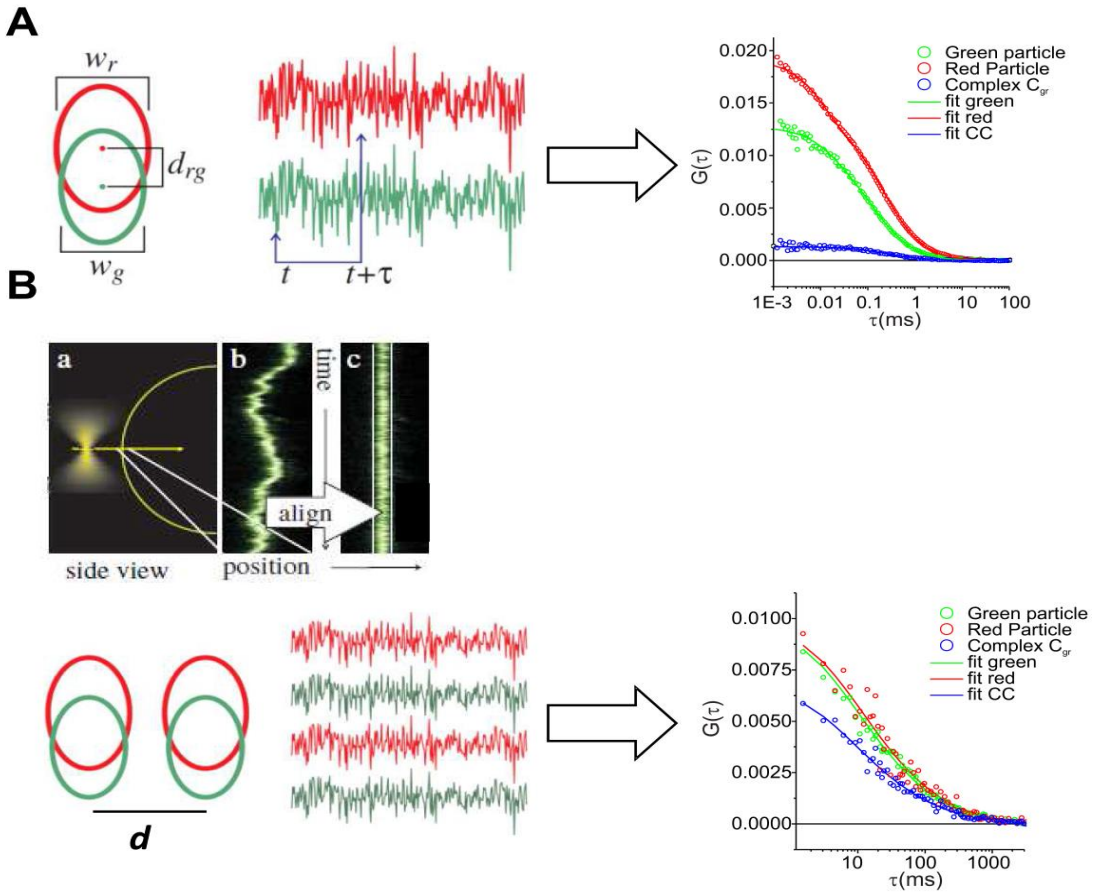

Figure 2.11 Principles of the FCS and scanning FCS. (**A**) Fluorescent molecules diffusing through the detection volume give rise to fluctuating fluorescence intensity. The auto-correlation curve (green and red squares) measures the self-similarity of these fluctuations and is used to determine the concentrations and diffusion coefficients. The cross-correlation curve (blue squares) compares the intensity fluctuations in the red and the green channels. (**B**) In scanning FCS, the detection volume is repeatedly scanned perpendicularly through a vertical membrane (**A**). The individual scans can array as pseudo-images, in which vertical axis represents the time. The fluorescence intensity observed corresponds to the membrane (**B**). The membrane fluctuations observed can be corrected for by shifting each line scan to obtain a straight line (C). The combination of dual-focus FCS with dual-color FCS results does not require calibration of the detection volume if the distance *d* is known, distance between the two detection volumes. Altogether, these data is used to calculate the auto- and cross-correlation curves of both particles and the complex at the membrane of an individual GUV (Adapted from (Ries et al, 2010)).

The FCS experiments of this work were performed in Ana Garcia-Saez´s lab (Tubingen, Germany) using a Confocor 3 module in a LSM710 microscope with a C-Apochromat 40x 1.2 water immersion objective (Zeiss, Oberkochen, Germany) at 22°C. For the FCS experiments, briefly, first of all the microscope setup should be aligned and calibrated, then data acquisition can be carried out. Depending in the FCS variant used the protocol differs (see Protocols 19 and 20).

Protocol 19 ***FCCS in solution***

1- Setup alignment and calibration: In order to obtain a proper alignment, the calibration measurement is performed by the simultaneous addition of two dyes spectrally similar to the fluorophores (Alexa-488 and Alexa-633). As follows:

   a. The excitation lasers were turned on around 30min prior to the measurement, to allow stabilization of the light source.
   b. An observation chamber containing 200µL of 50nM of dyes solution were placed in the microscope, and FCS mode was setup. In the Light Path window, the lasers were selected to a power of 0.5% (the same conditions were used in the data acquisition)
   c. The sample was focused using the Count rate window. To avoid aberration of the cover slide, the detection volume should be at least 150µm above the glass surface. In addition, the position of the correcting ring in the objective was optimized to maximize the counts per molecule in the detection volume.
   d. A calibration measurement was performed: 30s x 3 times at 0.5% laser power (the same conditions were used in the data acquisition for comparison).
   e. The data obtained for the calibration sample was fitted with a 3D diffusion for 1 component and triplet. The triplet state, diffusion time and structural parameters should be similar to those obtained in previous measurements or similar to those published. If these parameters are far from the expected values, the system is not correctly aligned, so the calibration procedure should be repeated.

2. FCCS measurement: Once the system was aligned, the measurements of the samples in solution were carried out. Proteins of study were diluted at different concentrations (typically 200nM) and were let to incubate in solution for a defined time, and FCS experiment was carried out as in the calibration procedure.
3. Fitting procedure: The fittings of the auto-correlation and cross-correlation were performed with a software written in MATLAB (Mathworks) to the models above described (2C 3D).

Protocol 20 ***SFCCS in GUV membrane***

1- Sample preparation: GUVs were electroformed (see section Preparation of GUVs, Protocol 4). Then, an 8-well observation chamber (Lab-Tek® eight-chambered No. 1.0 borosilicate cover glass from Nalge Nunc International, Rochester, NY, USA) was blocked with 10mg/mL BSA (non-fatty acid bovine serum albumin, Sigma Aldrich) to prevent attractive interactions between GUV and the glass substrate. After 1h of incubation, the observation chamber was extensively rinsed with Milli-Q water. The desired buffer with an osmolarity matching the glucose solution was added and the labelled BCL-2 proteins were added at low concentrations. Finally, an approximate volume of 80µL of electroformed GUV was transferred to the buffer with a micropipette. Of note, tip must be cut in order to widen the opening avoiding a possible GUV rupture. Sample preparation was incubated until the proteins bound to the membrane (≈2h). Of note, the membrane was not labeled with any fluorophore to avoid possible crosstalk in the measurements (more detailed procedures are described in Model membrane systems section, GUV preparation subsection).

2- SFCCS setup: The microscope was aligned as explained for FCCS in solution experiments and then the SFCCS setup of the microscope was selected (laser potency used was 0.1-0.5%, depending on the brightness of the sample).

3- SFCCS measurement: The equator plane of a GUV was selected and an image was taken. Then the membrane of interest was zoomed and the central horizontal line of the scanning square was lined perpendicular to the membrane. The Imaging setup was selected: track every line, frame size 32x times 2y, both directions, Speed 13 and with these settings the scan time was 1.68 msec. While scanning was performing the photon counter (a hardware correlator Flex 02-01D/C (http://correlator.com) was detecting the photon arrival times.

4- Data analysis: The data analysis was performed with software written in MATLAB (Mathworks). The photon stream was binned in 2 μs bins and arranged it as matrix such that every row corresponded to one-line scan. The membrane movements were corrected by calculating the maximum of a running average over several hundred-line scans and shifting it to the same column. The fitting was done by an average over all rows with a Gaussian and only the elements of each row between -2.5 σ and 2.5 σ to construct the intensity trace were added. The autocorrelation and spectral and spatial cross-correlation curves from the intensity traces were computed and excluded irregular curves resulting from instability and distortion. The resulting auto- and cross-correlation functions were fitted with a nonlinear least-squares global fitting algorithm to the analytical models described above. Finally, cross-correlation percentages (CC%) calculated from FCCS measurements were corrected for labeling degree of the proteins used in each experiment.

2.2.3 Detection of functional and structural activation in lipid environment

2.2.3.1 Fluorimetric measurements of vesicular contents release

A common experimental approach using model systems to study the bilayer perturbations generated by membrane active peptides and proteins relies on the measurement of the fluorescence changes of vesicle-encapsulated fluorescent probes (Basanez et al, 2001; Ellens et al, 1985; Ladokhin et al, 1997). Two different applications of this idea have been used throughout this thesis.

ANTS/DPX release

In this assay, the fluorescent probe ANTS (8-aminonaphtalene-1,3,6-trisulfonic acid sodium salt) and its quencher DPX (p-xylenebis(pyridinium)bromide) are co-encapsulated in the aqueous compartment of the liposomes. By entrapping both ANTS and DPX inside the vesicles, their close proximity allows DPX to quench ANTS fluorescence by collision. Upon addition of a membrane-perturbing agent, both molecules "*leak out*" and are diluted into the external medium where they hardly interact, inducing an increase of ANTS fluorescence. Thus, by monitoring ANTS fluorescence, vesicle bilayer permeabilization, can be followed in time (Figure 2.12). This approach was initially developed (Ellens et al, 1985) to measure vesicle fusion, an inverse

situation in which both molecules were entrapped into separate vesicle populations. The procedure is detailed in Protocol 21.

Protocol 21 ***Vesicular contents release***

ANTS/DPX release:

1- ANTS/DPX encapsulated LUV preparation: LUVs were prepared as explained in protocol 3 with an additional step. In this case, lipid film is hydrated with a buffer containing tfluorescent probes: 12.5mM ANTS, 45mM DPX, 20mM NaCl and 5mM Hepes, pH 7.4, 200-220mosm/Kg. After the extrusion, LUV containing the probes were separated from the unencapsulated probes by a PD-10 Desalting column (GE Healthcare, Waukesha, WI, USA) that was eluted with 5mM Hepes and 100mM NaCl (pH 7.4, 200-220mosm/Kg) and the lipid concentration is measured.

2- Sample preparation: 150μM ANTS/DPX loaded LUV (unless otherwise specified) and small amounts of proteins (nM range) are monitored along the time at different temperatures and constant stirring.

3- Fluorescence measurement: The sample is excited at 355nm (slits 4nm) and the fluorescence emission is monitored at 520nm in an 8100 Aminco-Bowman luminescence spectrometer (Spectronic Instruments, Rochester, NY, USA).

4- Calculations of the percentage of content release: The extent of marker release was quantified on a percentage basis according to the following equation:

$$\%\text{Leakage} = \frac{(F_t - F_0)}{(F_{100} - F_0)} * 100 \qquad \text{eq.2.11}$$

where F_t is the measured fluorescence of protein-treated LUV at time *t*, F_0 is the initial fluorescence of the LUV suspension before protein addition, and F_{100} is the fluorescence value after complete disruption of LUV by addition of $C_{12}E_8$ (final concentration, 0.5mM).

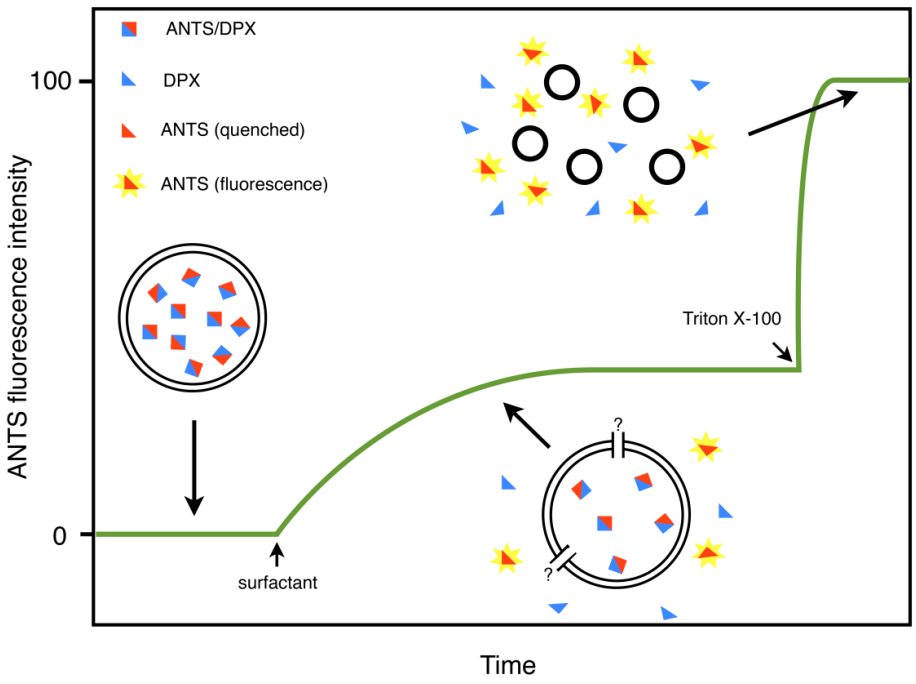

Figure 2.12 Schematic overview of the ANTS/DPX leakage assay. Upon incorporation of the surfactant into the membrane, vesicle enclosed ANTS and DPX are externalized through membrane defects, (?) in the picture. An increase on ANTS fluorescence is observed. Triton X-100 is generally added for complete vesicle solubilization into mixed vesicle lipid/surfactant/Triton X-100 micelles that gives the 100 % leakage value (i.e. maximum ANTS fluorescence). In our case, $C_{12}E_8$ detergent was used.

2.2.3.2 GUV permeabilization

Single vesicle study of the internalization of different dyes to the inside of GUVs is an invaluable tool to provide a deeper insight into the mechanism of pore formation by peptides and proteins (Apellaniz et al, 2010; Bleicken et al, 2013b; Fuertes et al, 2010a; Lee et al, 2008; Schon et al, 2008; Tamba & Yamazaki, 2009). Taking into account that biological systems are intrinsically heterogeneous, this method gives us the opportunity to study the pore forming mechanism at single vesicle level, contrary to bulk experiments in LUVs, in which the information obtained is an average of the processes of the overall population. In the present work, confocal microscopy in GUVs has been applied to the characterization of the inhibition capacity of BFL1 in MOM-like GUV and its permeabilization activity triggered in pure CL vesicles. The procedure is detailed in Protocol 22.

Protocol 22 ***GUV permeabilization assay***

1- GUV preparation: GUVs were electroformed as explained in the Protocol 4.

2- Sample preparation: An 8-well observation chamber (Lab-Tek® eight-chambered No. 1.0 borosilicate cover glass from Nalge Nunc International, Rochester, NY, USA) was filled with 700µL of a blocking solution (10mg/mL fatty acid free BSA, Sigma Aldrich) for 1h. Next, observation chamber was extensively rinsed with Milli-Q water. Then, 320µL of the desired buffer with an osmolarity matching the glucose solution was added to the chamber. In addition, BCL-2 proteins and different fluorophore permeabilization markers were added. Different combination of markers has been used during this thesis: Cyt c-A488/Allophycocyanin (APC) (300nM each) with or without free Alexa-555 (1µM). All the components were mixed gently by pipetting. Subsequently, an approximate volume of 80µL of electroformed GUV were transferred to the buffer (Note: The end of a micropipette tip is cut to widen the opening and to avoid rupture of GUV in suspension. Moreover, GUVs are mixed gently the sucrose suspension in the electroformation chamber and then GUVs should be added slowly on the top of the buffer in the observation chamber. Incubation conditions were 2h for a typical permeabilization experiments.

3- Measurements: Then observation chamber was placed on the confocal fluorescence microscopy. The measurements were performed at 25°C and the microscope used was a commercial LSM710 inverted confocal fluorescence microscope with a C-Apochromat 40x 1.2 water immersion objective (Zeiss, Oberkochen, Germany). Excitation light came from an Ar-ion (488 nm), HeNe (561 nm) or HeNe lasers (633 nm). A spectral beam guide was used to separate emitted fluorescence. Images were processed with ImageJ (http://rsbweb.nih.gov/ij/), and data analysis was as described below.

Image analysis

a) End-point permeabilization mechanism.

The study of the end point permeabilization mechanism, characterized by the final properties of the process: total extent permeabilization and the distribution of the degree of filling for the dyes at single-GUV level, giving us the information of possible size of the pore and if that mechanism is "all or none" or "graded". The analysis was done as described in (Bleicken et al, 2013b; Fuertes, 2011; Fuertes et al, 2010a).

The degree of GUV filling was calculated as:

$$\%GUV\ filling = \frac{(F_{in} - F_0)}{(F_{out} - F_0)} .100$$

eq. 2.12

where F_{in} and F_{out} are the average fluorescence intensities inside and outside a GUV, and F_0 is the background fluorescence inside the GUV at time 0 for a given dye. In image analysis the fluorescence is related to the arbitrary grey values. We arbitrarily set the threshold for a non-permeabilized GUV to <20% of dye leak-in. In these approaches several hundred (>50 for each condition) of GUVs were analysed per experiment.

b) Binding Profile

GUV permeabilization reproduces the final pore formation and content release (or incorporation in this case) elicited by the BCL2 proteins. Importantly, the amount of protein required to permeabilize GUV, and cooperativity between the labelled BCL2 proteins constitutes a very profitable information to gain insight protein:lipid and protein:protein interactions. For this purpose, we take advantage of ImageJ plugin denominated Radial Profile, which give use information of the presence of the fluorescently labelled protein in the GUV membrane. Remarkably, even if FCS or its membrane variant SFCCS is a much more sensitive technique, with this approach we obtain a quantitative information extremely rapidly. Moreover, we can combine permeabilization and membrane binding assays.

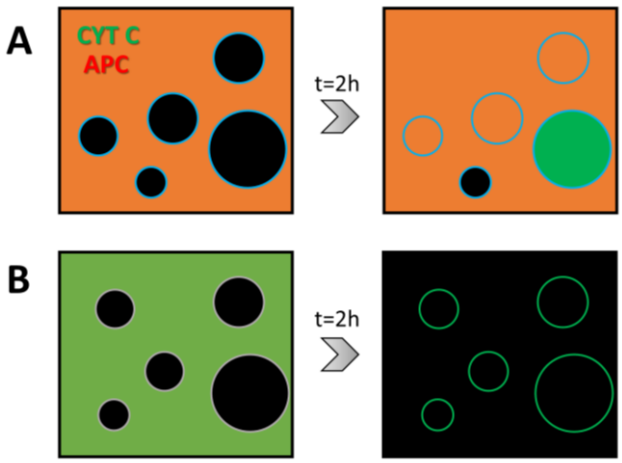

Figure 2.13. Experimental setups of the study of membrane binding and pore formation at the equilibrium. (**A**) In the study of the pores at the equilibrium, non-labelled BAX/cBID are mixed with FITC-a488/APC dyes in the presence of MOM-like GUVs and incubated 2h at RT. (**B**) Binding profile experiment. Alexa 488/647-labelled BCL2 proteins, are incubated with GUV and their membrane binding is assessed after 2h incubation.

2.2.3.3 Fluorescence spectroscopy techniques

Fluorescence spectroscopy has long been considered one of the most useful biophysical techniques available to scientists studying the structure and function of proteins. Furthermore, protein fluorescence can provide a variety of information, such as the extent of rotational motional freedom, the exposure of amino acid side chains to quenchers, and intra-molecular distances. In this thesis, NBD dye was used in order to characterize the structure adopted by pore forming BAX and BFL1 at the membrane level during their activation process.

NBD fluorescence spectroscopy

The study of the structure adopted by BCL2 membrane proteins in their biological locus has been considered as one of the outstanding task in the field. Here, we adapt to our system a method that combines fluorescently dyed monocysteine mutants in the presence of model membranes and specific fluorescent quenchers that allow us to scrutinize the controversial topology of these proteins in both healthy and apoptotic conditions. For this purpose, we first obtain several monocysteine mutants spreads along the structure of BAX and BFL1. Then, as described previously we labelled them with NBD and validate their structure and function as described in the protocol 10, 12-13 and 23 respectively. Remarkably, NBD election as a fluorescent dye was not arbitrary. This particular dye has several properties that ensures its adequacy.

First, this fluorescent dye is extremely sensitive to the polarity of the environment, small changes in pH or the electrostatic environment is detected as a shift in the maximum emission wavelength and in the fluorescence intensity. Moreover, its relatively small size is less prominent to interfere with the protein structure or function. Furthermore, it intermediate hydrophobicity enables the

study of the labelled protein in the presence of model membranes, because as it happens with other more hydrophobic dyes like acrylodan or coumarin, a very hydrophobic dye could trigger an unspecific membrane insertion.

In NBD experiments, when NBD-labelled residue moves from an aqueous milieu (i.e. the surface of a soluble protein) to a hydrophobic environment (i.e. the nonpolar interior of the membrane or a protein), its emission intensity increases while its wavelength of maximum emission shifts to the blue (Figure 2.14). In addition, since the protein is labelled with a unique NBD moiety at a single location in the protein, this approach provides a methodology to characterize the structural changes that occur at specific sites of the protein when it is associated to the membrane.

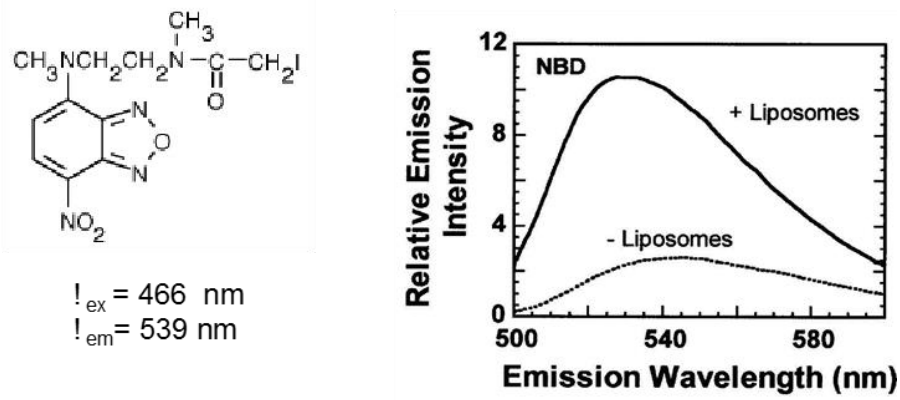

Figure 2.14: Site-specific NBD fluorescence. ***left,*** Chemical structure of IANBD. λex and λem are maximum fluorescence excitation (ex) and emission (em) wavelengths of IANBD in water. ***right,*** Changes in the fluorescence of the NBD moiety of NBD-labelled Perfringolysin O upon binding to cholesterol-containing liposomes. Taken from (Heuck et al, 2000).

Protocol 23 ***NBD Fluorescence experiments***

1. Sample components (NBD-protein or NBD-protein plus liposomes) are incubated for 10-30 min at RT/37°C prior to beginning of measurements at RT/37°C.
2. NBD spectra are recorded in an 8100 Aminco-Bowman luminescence spectrometer between 500 nm and 640 nm (5 nm bandpass) at a scan rate of 1 nm/s, using an excitation wavelength of 465 nm (4 nm bandpass). The slit widths for excitation and emission were kept at 4 nm, with the experiment conducted at 37°C in a 1cmXcm quartz cuvette under constant stirring. The contribution of the buffer or liposomes alone was subtracted as blank.

Fluorescence attenuation by doxyl-lipids

The movement of a labelled residue into a nonpolar milieu could result from: (i) its burial in the nonpolar interior of a protein; (ii) its movement into a nonpolar interface between two proteins or (iii) its exposure to the nonpolar core of the membrane. The non-polar membrane interior can be distinguished from the other two possibilities by examining the NBD quenching ability of doxylated-lipids containing nitroxide (NO) collisional quenching moieties that are restricted to locations within the nonpolar core of the bilayer.

When an excited fluorescent dye collides with some molecules and ions, its excitation energy is lost and no fluorescent photon is emitted. This phenomenon, termed collisional quenching of fluorescence, provides a direct method for determining accessibility. If the dye and quencher moiety are able to contact each other dynamically, emission intensity and lifetime will decrease. Whereas, if dye and quencher are in different compartments or locations (e.g. aqueous versus nonaqueous), the presence of the quencher in the sample will not affect/reduce dye emission. This approach has been used to demonstrate directly that specific residues within Clostridium perfringens, Perfringolysin O (PFO) toxin are exposed to and in contact with the nonpolar interior of the membrane (Heuck & Johnson, 2002; Ramachandran et al, 2002; Shepard et al, 1998) (Figure 2.15).

Liposomes used for this lipophilic quenching experiments were prepared as explained in Protocol 3, but substituting 25% mol PC for nitroxide-labelled phospholipid, 1-palmitoyl-2-stearoyl-(x-doxyl)-sn-glycero-3-phosphocholine (x-doxyl-PC, where x is equal to 5 or 12 and indicates the location of the quencher in the acyl chain of the phospholipid). Data from fluorescence quenching experiments were then normalized to the fluorescence emission from protein in LUVs lacking nitroxylated lipids. Interestingly, the combination of lipids with the quencher at different positions in the acyl chain proffers information about the depth of its membrane insertion.

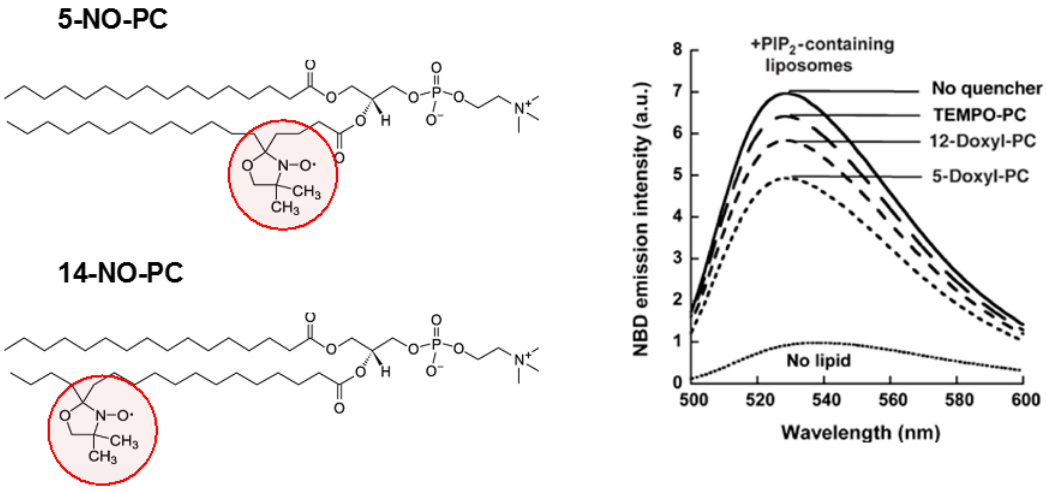

Figure 2.15: **Quenching of NBD fluorescence by nitroxide moieties located at different depths in the membrane bilayer.** ***Left***, Chemical structure of 5-doxyl-PC and 14-doxyl-PC lipids, used in this study. The nitroxide moiety is highlighted in red. Structures were taken from Avanti Polar Lipids. ***Right***, Representative emission spectra for NBD-dynamin before and after incubation with PIP2-containing liposomes (no quencher) or PIP2-containing liposomes that also contain indicated nitroxide-labeled phospholipids. Taken from (Ramachandran & Schmid, 2008).

Fluorescence attenuation by IP

In parallel, in order to obtain the complete picture, we attenuate the NBD fluorescence of those residues that are exposed to the solvent by using IP. Fluorescence quenching or attenuation by IP was obtained after addition of 200mM KI + 0.2mM Na_2SO_4. Unless otherwise stated, proteins and LUVs were incubated for 1 h before NBD fluorescence measurements. As it has done with nitroxilated lipids the fluorescence ratio between IP treated and non-treated NBD samples is plotted, obtaining this way information about the solvent exposure of the target residues.

2.3 *EX-VIVO* EXPERIMENTS

2.3.1 MITOCHONDRIA ASSAYS

2.3.1.1 Isolation of mitochondria from cultured cells

The point of no return in the mitochondrial pathway of apoptosis is MOMP, which allows the release of a variety of mitochondrial apoptogenic factors from the intermembrane space into the cytosol, such as cytochrome c or SMAC/DIABLO. Therefore, we studied the BCL2 interactoma by the capacity to bind to MOM and their ability to induce/inhibit cytochrome c release. Indeed, obtaining highly enriched mitochondria preparations is critical to evaluate the function of BCL2 proteins as these organelles are often halfway between model membranes and cells. Thus, isolated

mitochondria enable the study of recombinant BCL2 proteins in their biological locus, the MOM (Frezza et al, 2007).

Protocol 24 ***Mitochondrial isolation from cultured cells***

1. Cell harvesting: Cells from 3-4 confluent T175 flasks were collected by scrapping in 30-40ml PBS (137 mM NaCl, 2.7 mM KCl, 10 mM Na_2HPO_4, 2 mM KH_2PO_4, pH 7.4) and centrifuged during 5 min at 4°C (950xg, hereafter all the centrifugations were done at 4°C). The supernatant was discarded and the pellet resuspended in 4ml ice-cold Mitochondrial Isolation Buffer (MIB) containing 210 mM mannitol, 70 mM sucrose, 10 mM Hepes (pH 7.5), 1mM EDTA and freshly added protease inhibitors (Roche).
2. Cell homogenization: The cell suspension was after transferred to a pre-cooled 5ml glass-teflon Elvehjem potter (Sigma-Aldrich) for homogenization. In the first homogenization 20 strokes were done, then it was centrifuged for 10 min at 1500x g and the supernatant (SN1) was recovered, while the pellet was resuspended again in 2ml cold MIB. This resuspended pellet was homogenized for a second time with 20 strokes and it was then centrifuged for 10 min at 1500x g. The supernatant (SN2) was recovered and the pellet was resuspended in 1 ml cold MIB. It was again homogenized with 20 strokes and centrifuged for 10 min at 1500x g. The supernatant (SN3) was recovered and the pellet was then discarded.
3. Mitochondria isolation: Next, SN (1, 2 and 3) were collected and mitochondria were isolated by centrifugation (10 min, 7000x g). The supernatant was discarded and the pellet, which contains mitochondria, was resuspended in 200 µL cold MIB.
4. Concentration measurement: Mitochondria concentration was determined by Bradford assay, normally obtaining 200µL at ≈4-6 mg/ml.

Cytochrome-c release experiments: A classical method to assess MOMP induction by a purified protein is to examine its capacity to release cyt c from isolated mitochondria (Arnoult, 2008; Bossy-wetzel and Green, 2000). Briefly, mitochondria at a protein concentration of 1 mg/ml were incubated with the protein of interest for 30 min at 30-37°C in release buffer (RB buffer, 125 mM KCl, 10 mM Hepes-KOH (pH 7.4), 0.5 mM EGTA). Then, samples are centrifuged for 10 min at 14000x g to separate released cyt c from mitochondria-enclosed cyt c. Finally, the cyt c content

of each fraction is determined in a semi-quantitative manner by SDS-PAGE and immunoblotting using mouse BD Pharmigen (Franklin Lakes, NJ U.S.A) anti cyt c antibody clone 7H8.2C12.

2.3.2 EUKARYOTIC CELL PROCEDURES

2.3.2.1 Cell culture

Wildtype (WT) and SV40 transformed $BAX^{-/-}BAK^{-/-}$ double knockout (DKO) mouse embryonic fibroblasts (MEFs) were kindly provided by Dr. I Marzo (University of Zaragoza, Spain). WT and DKO HCT 116 cells were kindly provided by Prof. Ana García-Sáez (University of Tubingen, Germany). MEFs were grown in Dulbecco's Modified Eagle Medium and HCT116 cells in McCoy5A media (Invitrogen, U.S.A); both supplemented with 10% fetal bovine serum (Invitrogen), 1% Penicylin-Streptomicyn-Ionomycin solution (Invitrogen) in an atmosphere of 5% CO_2 at 37°C.

2.3.2.2 Plasmids for eukaryotic cell transient transfection

cDNA of human full-length BFL1 from Addgene (plasmid #36973, deposited by: Bill Sugden) was PCR-amplified with PfuTurbo Polymerase as explained in 2.1.2.1.1. In both cases, restriction sites were introduced in the forward and reverse primers respectively. Purified PCR products were digested with *KpnI* and *XhoI* (NEB) during 1 hour at 37C, subjected to gel purification and then ligated into a previously digested and dephosphorylated pCI-neo vector from Promega (WI, U.S.A) which carries the human cytomegalovirus (CMV) immediate early enhancer/promoter region to promote constitutive expression of cloned DNA inserts in mammalian cells. Several clones were checked for the presence of insert and DNA was sequenced using T7 promoter primer. Purified and digested PCR products were also ligated to a previously digested pEGFP-C3 vector. Moreover, once BFL1 was inserted GFP-BFL1 was used as a template to obtain L21A and R88D mutants. Furthermore, same protocol was used earlier in the lab to insert proapoptotic BAX and its 1-2/L-6 variant in pCi-neo vector and pEGFP-C3 vector from Promega.

2.3.2.3 Transient cell transfection

Cells were transfected using jetPRIME® (Polyplus Transfection, France) following steps described inhttp://www.polyplus-transfection.com. The detailed procedure is described in Protocol 25.

Protocol 25 ***Transient cell transfection***

The following conditions are given for a 6-well plate. For other culture formats visit the manufactures website: http:// www.polyplus-transfection.com.

1. Cell seeding: 300.000 cells per well were seeded into 2 ml growth medium 20h before the transfection.
2. Medium removal: 1-3h before transfection we substitute cells medium for one without antibiotic.
3. Mixture preparation (per well): 2 µg DNA were diluted into 200 µL jetPRIME buffer and mixed by vortexing (the mixture was incubated for 10 min at RT). Then, 4 µL jetPRIME were added, vortexed for 10 seconds and spin down briefly (the mixture was incubated for 20 min at RT).
4. DNA adding: 200 µL transfection mix per well was added, drop wise, onto the cells in serum containing medium and distributed evenly.

The plates were gently rocked back and forth and from side to side.

2.3.2.4 Cell fixation, permeabilization and immunofluorescent staining

Immunofluorescence (IF) is a powerful technique that utilizes fluorescent-labelled antibodies to detect specific target antigens. Applications include the evaluation of cells in suspension, cultured cells, tissue, beads, and microarrays for the detection of specific proteins. IF techniques can be used in both, fresh and fixed samples. In IF, antibodies are chemically conjugated to fluorescent dyes. These labelled antibodies bind to the antigen of interest, which allows for antigen detection through IF techniques such as: flow cytometry or fluorescence or confocal microscopy. Moreover, cell fixation immobilizes antigens while retaining cellular and subcellular structure and permeabilization allows for access of antibodies to all subcellular compartments. A general fixation, permeabilization and immunofluorescent staining procedure are described in protocol 26.

Protocol 26 ***Immunofluorescent staining***

1. Cell fixation and permeabilization: cells were seeded on a coverslip and depending on experiments requirements, were also transiently transfected as explained in protocol 25. Next, cells were fixed using 4% formaldehyde diluted in PBS for 20 min at RT. Then, cells were first washed with PBS and then permeabilized by the addition of cold acetone (-20°C) for 10 minutes, and washed again three times with PBS.
2. Blocking and incubation with antibodies: Coverslips containing fixed and permeabilized cells were incubated for 45min with 3% BSA in 0.1% Triton X-100 containing PBS (PBST). Then, cells were incubated with the primary antibody (1:200 in 3% BSA in PBST) in a humidified chamber for 1 h RT. The solution was then decanted and cells washed three times with PBST followed by incubation with the secondary antibody (1:400 in 3% BSA-PBST) for 1h at RT in darkness. Finally, secondary antibody was removed and cells were washed three times with PBST.
3. Mounting: Coverslips were mounted on the slides using a drop of mounting medium (Fluorsave).

2.3.2.5 Subcellular fractionation assays

Mitochondrial-share comprehends a sophisticated network that connects different cellular compartments including ER. Thus, isolated mitochondria are deficient in all these membranes that historically have been related with BCL2 function and MOMP. So that, using digitonin (a cholesterol dependent detergent) we are able to isolate cellular membranes from the cytosol. Of note, due to its differential lipid composition the integrity of plasmatic membrane which is enriched in cholesterol, is disrupted. The main aim of this assay is to isolate mitochondria and its associated membranes from cultured cells.

For this purpose, cells are first harvested and then permeabilized by resuspending them on permeabilization buffer (PB, 20 mM HEPES/KOH pH7.5, 100 mM sucrose, 2.5 mM $MgCl_2$, 100 mM KCl, 0.025% digitonin, protease inhibitor cocktail) for 10min on ice. Next, cells were centrifuged at 2,000x g, saving the supernatant (cytosol). Depending on the experiment cytosols and pellets (mitochondrial enriched membranes) are directly analysed by western blotting to assess the subcellular localization. Complementarily, the cytochrome c release of these pellet fractions can be analysed, as described in the protocol 24 for isolated mitochondria.

Moreover, this methodology also permits to assess whether the protein of interest is periferically attached or inserted in the membrane by incubating membrane fractions with sodium carbonate (pH 11.5). In brief, we incubate the membranes with 0.1 M Na_2CO_3 (pH 11.5) on ice during 20 min. Then pH was neutralized with 0.1 M HCl and incubated for further 5 min. Next, buffer A (400 mM Tris HCl, 100 mM $MgSO_4$, 10 mM $CaCl_2$ and DNAase) was added and samples were incubated for 10 min at 37°C. Finally, in order to separate the supernatant (containing soluble and peripherally inserted proteins) and the pellet (containing membrane attached proteins) were centrifuged at 13,000x g for 10 min at 4°C. Obtained fractions were then analysed by western blotting using an antibody against the protein of interest.

2.3.2.6 FRAP/FLIP experiments for retrotranslocation assessment

The proapoptotic Bcl-2 protein BAX, is predominantly found in the cytosol of nonapoptotic cells and is commonly thought to translocate to mitochondria following an apoptotic stimulus. The current model for BAX activation is that BH3 proteins bind to cytosolic BAX, initiating mitochondrial targeting and outer-membrane permeabilization. Recently, has been described that BAX is constitutively targeted to mitochondria but in nonapoptotic cells is constantly translocated back to the cytosol by BCL-XL mediated BH3 into groove recognition (Edlich et al, 2011a))(Schellenberg et al, 2013). In this thesis it has been examined whether BFL1 is able to retrotranslocate BAX from the mitochondria to the cytosol as BCL-XL does. This question could have been efficiently elucidated by the use of FRAP/FLIP.

Fluorescence recovery after photobleaching (FRAP) is particularly advantageous to directly assess the dynamic equilibrium between intracellular organelles such as cytosol and mitochondria (Edlich et al, 2011a; Schellenberg et al, 2013; Todt et al, 2015; Todt et al, 2013). In a typical FRAP experiment fluorescent molecules are irreversibly photobleached in a small area of the cell by high intensity illumination with a focused laser beam. Subsequently, diffusion of the surrounding non-bleached fluorescent molecules into the bleached area leads to recovery of fluorescence. In FRAP experiments, the images are analysed and processed to generate a kinetic plot of photobleaching by displaying the temporal fluorescence changes in the bleached region of the cell. The ideal fluorescent probe for use in photobleaching studies should be highly fluorescent (high quantum yield), but only moderately susceptible to photobleaching. This permits bleaching within realistic time frames, but limits bleaching during image acquisition. Green fluorescent protein is the most widely used fluorescent probe for cellular studies because of its stability, low cytotoxicity, because it does not bleach significantly at low light intensities, does not seem to be damaging to the cell after undergoing irreversible photobleaching, it can be readily expressed in several cell types where it is fused to a particular protein, and in many cases tagging a protein of interest with GFP has no significant influence on the function and localization of the protein under investigation (Ishikawa-Ankerhold et al, 2012; White & Stelzer, 1999).

Fluorescence Loss in Photobleaching (FLIP) is a complementary technique to FRAP, which has been used to reveal the connectivity between different compartments in the cell or the mobility of a molecule within the whole compartment (Cole et al, 1996; Ellenberg et al, 1997). FLIP experiments differ from FRAP and iFRAP (irreversible FRAP) by the repetitive bleaching of the same region in the specimen, thereby preventing recovery of fluorescence in that region. In FLIP experiments the repetitive bleaching occurs adjacent to the unbleached ROI. The loss in fluorescence in the region of interest (ROI) defines the mobile fraction of the fluorescently labelled protein. Conversely, the incomplete loss in fluorescence defines the immobile fraction of fluorescently-labelled protein that does not move into the continuously photo-bleached area. The observation that molecules do not become bleached suggests that they are isolated (immobilized) in distinct cellular compartments. FLIP experiments are very useful to demonstrate the connectivity and fluxes between different regions of the cell and thus is an ideal and direct method for studying the exchange of molecules between two compartments (e.g., compartments that are separated by lipid bilayers). The continuity of cellular structures, such as the Golgi apparatus, the endoplasmic reticulum, mitochondria etc. have all been studied using FLIP (Cole et al, 1996; Nehls et al, 2000; Phair & Misteli, 2000).

Protocol 27 ***FLIP experiments***

1. Cell transfection: BAX/BAK DKO HCT116 cells were seeded on 1µ-Slide 8 Well ibitreat (ibidi) in McCoy's 5A medium, grown for 20 hr, transfected with EGFP-BAX (± non-labelled pCi-BFL1) and EGFP-BAX 1-2/L-6 (± non-labelled pCi-BFL1) and EGFP-BFL1 (± non-labelled pCi-BAX) plasmids as explained in 2.3.2.3, and incubated for 6h-16 h at 37ºC with 5% CO_2.
2. Mitochondrial dying: cells were incubated with mitotracker-far red for 30 min prior to analysis. Then, we substituted the media for McCoy's 5A medium with 10mM HEPES and without phenol red and incubated 30 min at 37ºC with 5% CO_2.
3. Live imagining and Settings: Confocal analysis was performed on a Zeiss confocal LSM710 microscope equipped with 63X oil objective and laserlines to excite at 488, 561 or 633. A single spot with a diameter of 1,3 µm within the nucleus was repeatedly bleached with two iterations of 100% power of a 488 nm laser line (100% output). The diameter of a single ROI 0,52µm. Two images were collected after each bleach pulse, with 30 s between bleach pulses. After collecting 60 images, two separate measurements on the mitochondria were taken to analyze the fluorescence loss. Unbleached control cells were monitored for photobleaching due to image acquisition. The rate of loss in fluorescence on the mitochondria was calculated from fluorescence intensity measurements using the Zeiss LSM software. The fluorescence intensities were normalized by setting the initial fluorescence to 100% signal.

NOTE 1: In FRAP/FLIP experiments is particularly important to open the pinhole to the maximum, (11.56 airy units= 8,4µm diameter section)

NOTE 2: In order to ensure the presence of both plasmids and maximize the retrotranslocation effect, the plasmid ratio between GFP-tagged:non-labelled was 1:3). Protein expression amounts was assessed by WB.

NOTE 3: GFP-BAX 1-2/L-6 appears to be much more sensible to phototoxicity,

CHAPTER 3:

Structural details of BAX membrane conformations

3 Structural details of BAX membrane conformations

3.1 ABSTRACT

Despite intensive research effort, how the paradigmatic proapoptotic protein BAX forms lethal apoptotic pores at the mitochondrial outer membrane (MOM) remains incompletely understood. Here, biophysical tools and minimalist model systems were used to identify the specific regions in BAX driving apoptotic pore formation, and to gain more insight into underlying mechanisms. Fluorescence mapping revealed that fully active BAX adopts a BH3-in-groove dimeric conformation in MOM-like membranes, with BAX α4-α5 helices belonging to its core domain inserting deeper into the membrane lipid bilayer than BAX α6-α8 helices belonging to its latch domain. In our reconstituted systems, antiapoptotic BCLXL formed canonical heterodimeric BH3-in-groove complexes with BAX, and blocked membrane insertion of BAX core α4-α5 helices, but not BAX latch α6-α8 helices. Moreover, poly(ethylene glycol) (PEG) conjugation (PEGylation) at multiple individual sites along the BAX core, but not latch domain, potently inhibited BAX pore-forming activity. Additional combined computational and experimental evidence revealed that the BAX core α5 helix displays a bilayer-destabilizing membrane interaction mode that is absent in BAX latch α6-α8 helices. Based on this collective set of evidence, it is proposed that membrane insertion of the BAX core, but not latch domain, is critical for BAX apoptotic pore formation.

3.2 INTRODUCTION

BAX is a key proapoptotic member of the BCL2 family which kills cells by forming an atypical pore at the mitochondrial outer membrane (MOM) (Cosentino & Garcia-Saez, 2017). This apoptotic pore is essential for allowing the release of cytochrome c (cyt c) and other mitochondrial apoptogenic factors into the cytosol, and is considered the pivotal step in the mitochondrial apoptotic pathway (Czabotar et al, 2014). It is well established that BAX exists in an inactive conformation in healthy cells, and that functional BAX activation is tightly regulated by two other factions of the BCL2 family (Cosentino & Garcia-Saez, 2017; Czabotar et al, 2014). On the one hand, proapoptotic BH3-only proteins such as cBID trigger activation of BAX at the MOM through a complex set of conformational changes culminating with formation of the BAX apoptotic pore. On the other hand, antiapoptotic BCL2-type proteins, including BCL2 itself and BCLXL, principally act by sequestering proapoptotic BCL2 family partners in stable protein complexes at the MOM, thereby blocking apoptotic pore formation.

According to current knowledge, apoptotic pore formation relies in two distinct but interlinked biochemical activities of BAX: (1) homo-oligomerization, which is mainly mediated through BAX:BAX protein-protein interactions, and (2) perturbation of membrane structure, which primarily, if not solely, occurs through BAX:lipid interactions. Structural and functional studies have provided important insight into this dual activity of BAX. Early NMR studies revealed that inactive BAX forms a tight globular helical bundle fold comprising nine α-helices (Suzuki et al, 2000). One critical feature of the inactive BAX structure is the presence of an extended hydrophobic groove mainly comprising the BAX α3-α5 region that is also present in its close homologue BAK, as well as in all antiapoptotic BCL2-type molecules. Such canonical BCL2 hydrophobic grooves share the capacity to act as "receptors" for binding proapoptotic "BH3-ligand" domains, although other non-canonical protein:protein interaction modes between BCL2 family proteins have also been identified (Czabotar et al, 2014; Moldoveanu et al, 2014). Importantly, both the canonical BAX "receptor" groove and the BAX "BH3-ligand" domain (BAX α2) remain masked in the inactive BAX conformation, and together constitute the so-called BAX core domain (Czabotar et al, 2014). Another salient characteristic of the inactive BAX conformation is the presence of hidden hydrophobic residues with potential for membrane interaction and/or perturbation that are localized in multiple helices of the protein.

It is becoming clear that following binding by BH3-only activating ligands such as cBID, the BAX core domain (α2-α5) dissociates from the so-called BAX latch domain (α6-α8), as well as from the BAX N-terminal (α1) and C-terminal (α9) helices (Alsop et al, 2015; Czabotar et al, 2013). Nevertheless, the specific regions in the BAX molecule that drive apoptotic pore formation via BAX:BAX and BAX:lipid interactions remain ill defined. The X-ray crystal structure of a truncated GFP-BAX fusion construct comprising the entire BAX core domain provided strength to the view that the assembly of a BH3-in-groove BAX dimer is a key step in the molecular

pathway for BAX activation5. However, it remains unclear whether this crystallographic BAX core dimer structure faithfully represents the fully activated conformation adopted by BAX in a membrane environment. In fact, under certain apoptotic conditions, alternative BAX dimeric conformations have been described at the MOM level (Gahl et al, 2014; Zhang et al, 2016). Additionally, how dimeric BAX species grow into higher-order multimers is not well understood, since multiple different interdimer interfaces have been identified in BAX and its close homologue BAK (Aluvila et al, 2014; Bleicken et al, 2014; Dewson & Kluck, 2009; Dewson et al, 2012; Mandal et al, 2016; Sung et al, 2015; Zhang et al, 2016). Indeed, even the molecularity of BAX/BAK required to form functional apoptotic pores remains undetermined (Basanez et al, 2012; Nasu et al, 2016; Salvador-Gallego et al, 2016; Subburaj et al, 2015).

From the perspective of BAX:lipid interactions implicated in apoptotic pore formation, initial studies attributed a critical role to insertion of the BAX α5-α6 region into the MOM lipid bilayer as a transmembrane (TM) helical hairpin, akin to proteinaceous channel-like models proposed to explain the action of colicins (Youle & Strasser, 2008). Recent work, however, challenged this view by providing evidence that upon functional BAX activation, the BAX α5 and α6 helices: (i) dissociate from each other, rather than maintaining a hairpin configuration; and (ii) adopt a surface-parallel, rather than TM orientation (Czabotar et al, 2013; Westphal et al, 2014a). Based in these observations a new model emerged where the concerted shallow insertion of BAX α5 and α6 helices into the MOM elicits the formation of a proteolipidic apoptotic pore through destabilization of the MOM lipid bilayer structure. It has also been proposed that additional helices of the BAX core (α4)(Czabotar et al, 2013) and latch (α7, α8)(Bleicken et al, 2014; Westphal et al, 2014a) domains, as well as the C-terminal BAX α9 helix8 actively drive BAX proteolipidic pore formation through shallow membrane insertion and bilayer destabilization. However, despite the proteolipidic nature of the BAX apoptotic pore has been debated for more than a decade (Basanez et al, 1999; Basanez et al, 2012; Cosentino & Garcia-Saez, 2017; Czabotar et al, 2013; Kuwana et al, 2002; Lovell et al, 2008; Qian et al, 2008b; Terrones et al, 2004; Youle & Strasser, 2008), the exact membrane topology of individual BAX helices, and the extent to which membrane immersion of defined BAX regions contributes to BAX pore formation are still incompletely delineated. On top of this, the specific BAX:lipid and BAX:BAX interactions targeted by antiapoptotic proteins such as BCLXL to block BAX apoptotic pore formation are currently under investigation (Andreu-Fernandez et al, 2017; Czabotar et al, 2014; Czabotar et al, 2013; Landeta et al, 2014; Lee et al, 2016; Lovell et al, 2008; Llambi et al, 2011; Shamas-Din et al, 2013).

In this chapter, physiologically-relevant model systems and biophysical and biochemical tools are used in order to analyse the membrane topology of individual helices of BAX core and latch domains, as well as their specific contribution to BAX pore-forming activity. Concretely, fluorescence mapping studies were used to gain insight the structural details of BAX conformation in the membrane when its activated by cBID. Moreover, not only it was also studied

the regulatory effect exerted by the antiapoptotic BCLXL but also BAX:BCLXL interaction surface during the inhibition process.

3.3 MATERIALS AND METHODS.

In this section materials and methods required in this chapter are detailed briefly, a more extended explanation and specific information is described in the second chapter: general materials and methods.

Chemicals and reagents.

All lipids were purchased from Avanti Polar Lipids (Alabaster, AL, USA). N,N'-Dimethyl-N-(Iodoacetyl)-N'-(7-Nitrobenz-2-Oxa-1,3-Diazol-4-yl)Ethylenediamine (NBD), 1, 3, 6, aminonaphtalene-tri-sulfonate (ANTS) and p-xilene-bis-dipicolyinicacis (DPX) were purchased from Molecular Probes (Eugene, OR, USA). Methoxy PEG maleimide of 550 Da average molecular weight (PEG05k) was obtained from Nanocs (New York, NY, USA). Synthetic peptides (>90% purity) were purchased from Biomatik (Wilmigton, DL, USA). All other reagents were from Sigma (St. Louis, MO, USA).

Liposome preparation.

MOM-like lipid mixtures (PC/PE/PI/CL 50/35/10/15, mol/mol) were co-dissolved in chloroform/methanol (2:1), and organic solvents were removed by incubation under vacuum for 2h. Dry lipid films were resuspended in 100mM KCl, 10mM Hepes, 0.1mM EDTA (KHE buffer), except in experiments were 20 mM KCl, 10 mM Hepes pH 7.0, 0.1 mM EDTA, 12.5 mM ANTS and 45 mM DPX was used. Liposomes were then subjected to 5 freeze/thaw cycles, and subsequently extruded 10 times through two polycarbonate membranes of 0.2-µm pore size (Nucleopore, San Diego, CA) to obtain large unilamellar vesicles (LUVs).

Purification and labeling of BCL2 family proteins.

Recombinant BAX and BCLXL proteins were generated from the vector pTYB1 (New England Biolabs, Ipswich, MA), cells were lysed by passage through a French pressure cell, the intein tag was removed by DTT treatment, and the proteins were further purified as previously described in the material and method chapter and in (Subburaj et al, 2015; Suzuki et al, 2000). Caspase-8-cleaved BID (cBID) and BCLXLΔC were expressed and purified as described earlier in the material and method chapter and in (Landeta et al, 2014; Terrones et al, 2004). All proteins were >90% pure as evaluated by Coomassie-stained SDS-PAGE. Mutant DNAs were generated by PCR-based mutagenesis using the Quickchange mutagenesis kit (Stratagene, San Diego, CA, USA) or purchased at GenTech (Montreal, Canada). All constructs were verified by sequencing.

In a typical labeling reaction, NBD dissolved in DMSO or PEG05k dissolved in KHE were added to a 1 ml sample containing 0.5 mg of a monocysteine BAX variant, at a labeling reagent/BAX molar ratio of 10:1. Samples were incubated overnight at 4ºC, and subsequently eluted over a PD-10 column (GE Healthcare, Pittsburgh, PA, USA) equilibrated with KHE+1mM TCEP.

Cyt c release and BAX immunodetection assays.

BAX-/-/BAK-/-DKO mouse embryonic fibroblasts (MEFs) were harvested by scrapping, and homogenized with a glass-Teflon Potter-Elvehjem homogenizer in mitochondrial isolation buffer (210 mM mannitol, 70 mM sucrose, 10 mM Hepes (pH 7.5), 1 mM EDTA, and protease inhibitors). After removing heavy membrane fractions by two consecutive centrifugations at 700g for 10 min at 4ºC, mitochondria-enriched fractions were pelleted by centrifuging the resultant supernatant at 14000g for 10 min at 4ºC. Mitochondria (50 µg total protein) were incubated with recombinant BAX variants (100 nM) with or without cBID (10 nM) in 125 mM KCl, 5 mM KH_2PO_4, 2 mM MgCl2, 1 mM DTT, and 10 mM HEPES-KOH, pH 7.2, for 30 min at 30ºC. Samples were then centrifuged at 14000g for 10 min, and supernatant and pellet fractions were subjected to 15% SDS-PAGE and immunoblotting using anti-cyt c 7H8.2C-12 or anti-Bax 554104 monoclonal antibodies (BD-Biosciences, San Jose, CA, USA).

Steady-state fluorescence spectroscopy.

Fluorescence intensity and spectral analyses were done in an 8100 Aminco-Bowman luminescence spectrometer (Spectronic Instruments, Rochester, NY), in a thermostatically controlled 4x4-mm quartz cuvettes, at 25 °C. The folding properties of all mutants were examined by monitoring the intrinsic tryptophan (Trp) fluorescence spectra of each BAX mutant compared with the wt BAX. Trp spectra were recorded between 310 nm and 410 nm at a scan rate of 1 nm/s, using an excitation wavelength of 290 nm (slits 4nm). NBD fluorescence spectra in the presence of MOM-like LUVs (200 µM) and proteins of choice were recorded between 500 nm and 650 nm at a scan rate of 1 nm/s, using an excitation wavelength of 465 nm (slits 4nm). The fluorescence emission maximum (λ_{max}) values were determined from the first derivative of the smoothed spectra. To minimize vesicle light scattering, a 475nm cut-off filter was placed in the emission light path. In all cases, the signal from solvent blank (buffer or LUVs in buffer) was subtracted from the sample fluorescence. FQ=Dox was obtained using MOM-like LUVs containing 25 mol% Dox-lipid substituting equivalent amounts of PC. $F_{Q=I^-}$ was obtained after addition of 200 mM KI + 0.2 mM Na_2SO4, and sample fluorescence in the absence of quencher (F_0) was obtained from equivalent samples to which 200 mM KCl + 0.2 mM Na_2SO_4 was added. Release of LUV-encapsulated ANTS/DPX was monitored with λ_{ex}=350 nm, and λ_{em}=520 nm (slits, 8 nm). The extent of marker release was quantified on a percentage basis according to the equation: (F_t-F_0/F_{100}-F_0) x100 where F_t is the measured fluorescence of protein-treated LUVs at time t, F_0 is the initial fluorescence of the LUV suspension before protein addition, and F_{100} is the fluorescence value after complete disruption of LUVs by addition of $C_{12}E_8$ detergent (0.5 mM).

DSF Measurements.

Fluorescence measurements were made by using a Qiagen Rotor Gene RT-PCR instrument (Valencia, CA) and an Applied Biosystems 7500 instrument (Life Technologies, Carlsbad, CA). Solutions for the DSF measurements were prepared on the day of measurement using stock 500 μM dye solutions, 50 μM stock protein solutions, and the PBS buffer described above. The final solutions contained 4 % (by vol.) DMSO and 20 μM dye with protein concentrations of 1.0μM, 2.0 μM, and 5.0 μM. Each sample tube was loaded with 25 μL of the protein/dye mixture for analysis. Two replicates of each protein concentration were measured for each experiment. Measurements made on the Rotor Gene instrument were set up such that the samples would initially equilibrate at 25 °C and then increased up to 99 °C in steps of 0.5 °C, holding the temperature at each step between 15 s and 80 s. The base scan speed of the instrument is 3.5K/min. However, because of the hold times at each temperature step, the effective scan rate of the system is much lower. The effective scan rate is the change in temperature divided by the total time of the scan. For example, a DSF run with a temperature profile from 25 °C to 99 °C (T = 74 K) and a base scan rate of 3.5 K/min will take approximately 21.1 minutes to complete. Holding each 0.5 K interval for 30 seconds, will add an additional 74 minutes to the run, making the effective scan rate of 0.778 K/min or 47 K/hr. At each temperature step of the scan, fluorescence measurements were made for each sample, using the excitation and emission settings appropriate for the dye (4,4′-Dianilino-1,1′-binaphthyl-5,5′-disulfonic acid dipotassium salt (bis-ANS) λ_{exc} =365 λ_{em}= 485). The tfm values are calculated as the midpoint of the fluorescence transition. Before transition midpoints were determined, a baseline approximation was subtracted from the fluorescence. The baseline approximation was of the dye alone with no protein. This was done to be consistent with the generally accepted DSF model in which this temperature corresponds to the point where the protein is halfway unfolded. The 2 μM and 5 μM protein concentrations gave the most consistent results, and the data presented are the average of these two protein concentrations.

Monolayer surface pressure measurements.

Measurements were carried out with a MicroTrough-S system from Kibron (Helsinki, Finland) at 25 °C with constant stirring. The MOM-like lipid mixture, dissolved in chloroform, was gently spread over the surface and kept at a constant surface area. The desired initial surface pressure, πi, was attained by changing the amount of lipid applied to the airwater interface. After 10 min to allow for solvent evaporation, the protein was injected through a hole connected to the subphase. The change in surface pressure, Δπ, was recorded as a function of time until a stable signal was obtained. The linear plot of Δπ as a function of πi can be extrapolated to a πi of 0 to give the critical pressure, πc, which is a measure of the relative “penetration capacity” of a protein into the monolayer.

^{31}P-NMR Measurements.

Samples for ^{31}P NMR were prepared by dispersing 15 μmol of dry MOM-like lipid mixtures in 0.5 ml of KHE buffer alone or containing the peptide of interest. Multilamellar vesicle suspensions were freeze-thawed 3 times in liquid N_2 to disperse the added proteins in the lipid membranes, and the liposomes were spun down in an Eppendorf centrifuge (14,000 rpm, 15 min, 4 °C). Pellets were loaded directly into 5-mm Pyrex NMR tubes. High power, proton noise-decoupled ^{31}P NMR spectra were recorded on a Bruker AV-500 spectrometer operating at 202.4 MHz using 5-mm broadband inverse probes with z-gradient equipment. 1024 free induction decays were averaged using a 2-s recycle delay. Spectra were processed and evaluated using TOPSPIN 1.3 (Bruker) and plotted with 80-kHz line broadening.

Computer simulations.

Main biophysical characteristics of BAX-derived peptides were determined by MPEx (Snider et al, 2009) and Heliquest (Gautier et al, 2008). Monte Carlo (MC) simulations of the interaction of peptide molecules with MOM-like membranes were performed using the MCPep web server (Gofman et al, 2012a). The web server´s output includes the free energy of peptide-membrane association, the energetically favorable peptide-membrane depth of penetration and tilt, and snapshots of example simulations with the centroid conformation of the largest cluster (in PDB format).

3.4 RESULTS

3.4.1 Active-BAX membrane topology assessment

3.4.1.1 Structural and functional analysis of recombinant BAX monocysteine mutants.

Minimalist systems comprising recombinant purified proteins and model membranes have provided invaluable information about different structural and functional aspects of BCL2 family proteins (Bleicken et al, 2014; Lovell et al, 2008; Nasu et al, 2016; Salvador-Gallego et al, 2016; Subburaj et al, 2015). Here, a set of recombinant BAX monocysteine mutants located at strategic positions along the BAX α2-α8 helices was generated aiming to map the membrane topology and role in BAX apoptotic pore formation of specific regions of BAX core and latch domains. The three-dimensional NMR solution structure of inactive, monomeric BAX is shown in Figure 3.1A, with residues mutated to cysteine (Cys) highlighted as black spheres and BAX helical segments colored according to the following scheme: BAX α2, green; BAX α3, brown; BAX α4, blue; BAX α5, pink; BAX α6, orange; and BAX α7-α8, cyan.

First, the structural integrity of BAX variants was assessed by examining the net wavelength of maximum emission (λmax) for their tryptophan (Trp) residues. As shown in Figure 3.1B, the Trp λmax values for all monocysteine BAX mutants were similar to that of wild-type (wt) BAX indicating that the BAX variants preserve the global folding pattern of the native protein. The only exception was the BAXF116C variant showing a 6 nm blue-shift in Trp λmax. Considering that the F116 residue is localized at the very core of the BAX molecule (Fig. 3.1A), it is not surprising that the F116C substitution significantly perturbs the native BAX structure. Moreover, in order to confirm globular folding they were validated, at least one monocysteine mutant per α-helix, by a more sensitive fluorimetric technique, differential scanning fluorimetry (DSF), obtaining similar results Figure 3.1C.

To test whether Cys mutations affect the apoptotic function of this set of recombinant purified BAX proteins, it was measured their capacity to release mitochondrial cyt c. Similarly to wt BAX, all BAX variants displayed minimal cyt c release in the absence of cBID, whereas in the presence of cBID all BAX mutants displayed near complete cyt-c-releasing activity (Figure 3.1D). Here also the BAXF116C mutant was an exception, showing negligible cyt c release with or without cBID. Further immunoblotting analyses indicated that cBID-activated BAX variants targeted to mitochondria similarly to the native protein, albeit this assay proved less sensitive to that of cyt c release (Figure 3.1D).

Based on this collective set of results, it is concluded that all monocysteine BAX variants preserve the structural and functional integrity of the parent molecule, with the exception of BAXF116C which was not examined further.

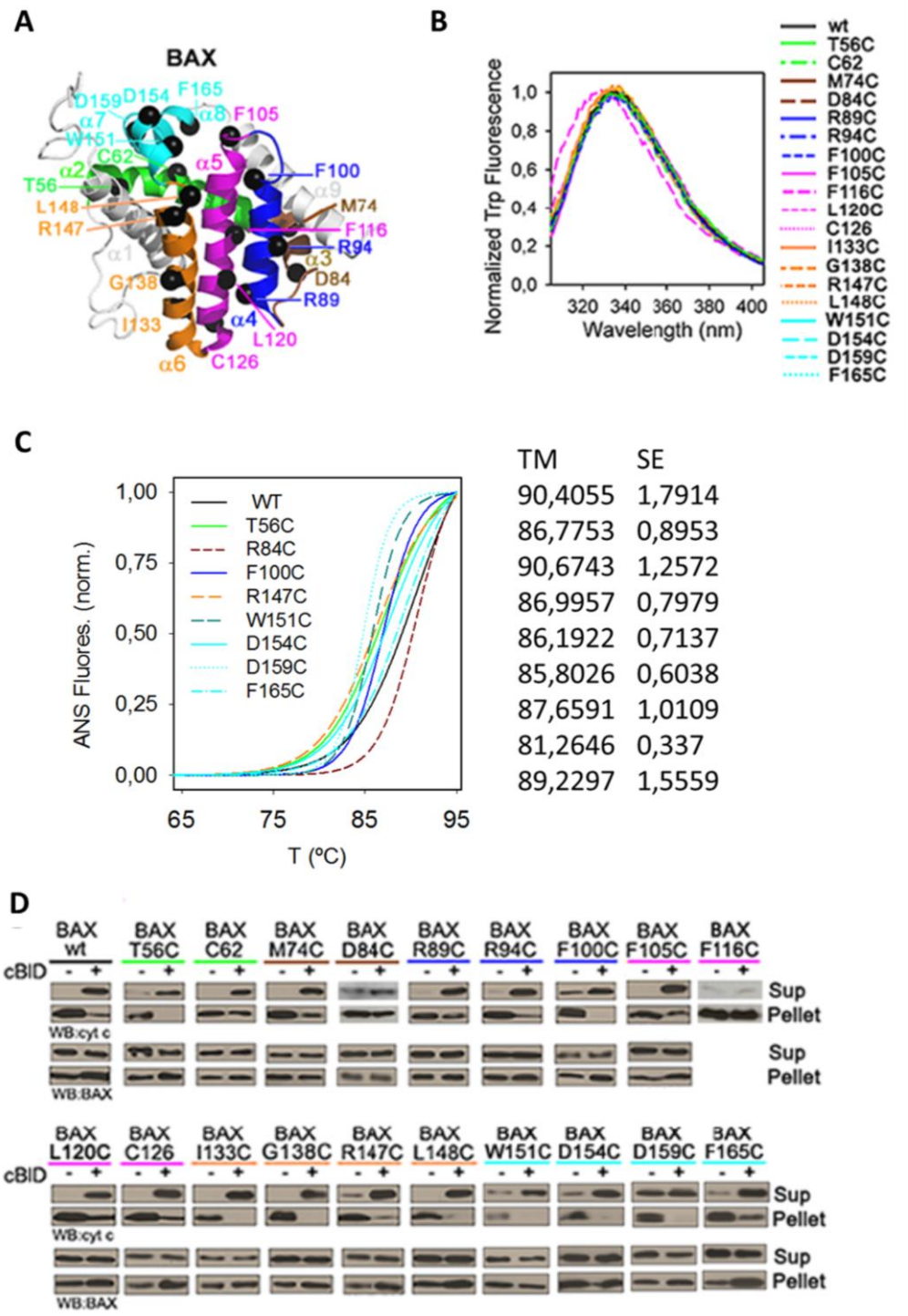

Figure 3.1. Characterization of BAX mutants. (**A**) Inactive BAX structure showing cysteine mutation sites (black spheres). (**B**) Trp fluorescence spectra of BAX proteins. (**C**) DSF fluorescence spectra of BAX proteins (**D**) Cyt-c-releasing and mitochondrial-localizing activities of BAX proteins.

3.4.1.2 Assessing the active structure of BAX at the membrane level by fluorescence mapping.

Fluorescence spectroscopy coupled to site-directed fluorescence labeling is a powerful approach to study conformations of membrane-associated proteins. In this approach, a fluorescent dye is covalently attached to the sulfhydryl group of a protein containing a single Cys residue positioned at a strategic site. NBD was chosen as the fluorescent probe in this study because it is a relatively small and uncharged dye, and its spectral properties are dramatically different in aqueous and nonaqueous environments (Alder et al, 2008; Lovell et al, 2008; Saksena et al, 2009). For example, when NBD moves from a polar environment (i.e. the hydrophilic surface of a protein) to a nonpolar environment (i.e. the hydrophobic interior of the membrane or a protein), its fluorescence emission intensity (F) increases while its λmax shifts to the blue.

Typical emission scans for selected NBD-labelled BAX mutants in the presence of MOM-like liposomes with or without cBID treatment are shown in Figure 3.2A (continuous and dotted lines, respectively). Upon treatment with cBID, most mutants exhibited notable increases in F and blue-shifts in λmax indicating transfer of NBD probes to more hydrophobic environments (Figure 3.2A, arrows). Quantitative assessment of the magnitude of NBD-BAX spectral changes induced by cBID suggests that the different sites in membrane-active BAX can be grouped in the following three broad categories (Figure 3.2B): (1) sites which go through prominent changes in F (filled bars) and are placed in hydrophobic microenvironments as assessed by their low λmax values (empty bars); i.e., R89 and F100 in BAX α4, and F105, L120, and C126 in BAX α5; (2) sites which undergo small to negligible changes in F and localize to hydrophilic microenvironments according to their high λmax values; i.e., M74 and D84 in BAX α3, G138 in BAX α6, D154 in BAX α7, and D159 in BAX α8; and (3) sites which experience rather similar changes in F ranging from moderate to notable and localize to microenvironments of middle polarity judging by their intermediate λmax values; i.e., T56 and C62 in BAX α2, R94 in BAX α4, I133, R147, and L148 in BAX α6, W151 in BAX α7, and F165C in BAX α8.

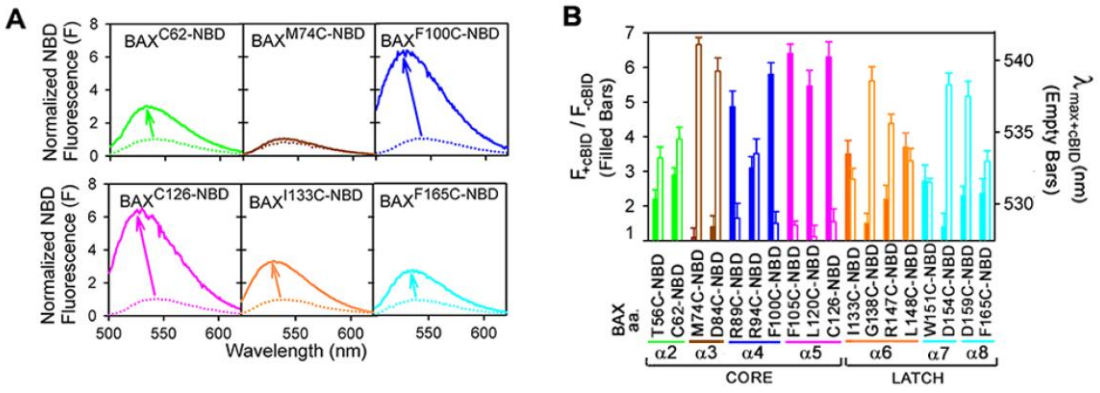

Figure 3.2 Fluorescence mapping of membrane active BAX topology. (**A**) Emission spectra of NBD-BAX variants (200 nM) with (continuous lines) or without (dotted lines) cBID (50 nM). (**B**) Filled bars: NBD intensity ratios for cBID-activated to inactive NBD-BAX variants. Empty bars: NBD λmax for cBID-activated NBD-BAX variants. Data are mean ± S.E.M. (n ≥3).

Although the spectroscopic approach described above provides valuable information, alone it does not allow distinguishing whether an NBD probe shifts to a nonpolar environment by becoming exposed to the hydrophobic interior or the interface of the lipid bilayer, or by moving into a hydrophobic site within a proteinaceous structure. To further evaluate the membrane topography of each NBD probe in active BAX variants, a series of collisional quenching experiments were performed. First, the lipophilic quenching agents 1-palmitoyl-2-stearoyl-5-doxyl-sn-glycero-3-phosphocholine (Dox5) and 1-palmitoyl-2-stearoyl-14-doxyl-sn-glycero-3-phosphocholine (Dox14) were used, two phospholipid derivatives with a NO group localized within the bilayer hydrophobic phase, close to the glycerol backbone and the bilayer midplane, respectively (Kyrychenko & Ladokhin, 2013).

The left Panel in Figure 3.3 is a histogram showing the extent of quenching by doxylated lipids for the set of monocysteine BAX mutants incubated with MOM-like liposomes and cBID. As can be seen, NBD probes attached to R89, F100, F105, L120, and C126 sites in cBID-activated BAX were substantially quenched by both Dox5 and Dox14, with the former lipid eliciting stronger quenching than the latter one. Thus, in active BAX, this set of residues localized in the BAX core α4-α5 region are placed within the hydrocarbon phase of the lipid bilayer but without reaching the bilayer midplane. By contrast, NBD attached to other sites in the BAX core domain (T56, C62, M74, D84, and R94) and a group of sites localized in the BAX latch domain (G138, R147, D154, D159) showed minimal quenching by either Dox5 or Dox14 indicating these residues do not penetrate into the hydrocarbon phase of the lipid bilayer when BAX acquires its active conformation. Lastly, a set of sites localized in the BAX latch domain (I133, L148, W151, and F165) displayed moderate quenching by Dox5 and negligible quenching by Dox14, suggesting these residues are peripherally attached to the membrane surface in cBID-activated BAX.

Next, the Dox5 quenching results for sites in the BAX core domain were mapped into the BH3-in-groove BAX dimer crystal structure (Czabotar et al, 2013) (Figure 3.3, Right). It is readily apparent that NBD sites showing strong quenching by Dox5 localize to the “bottom” part of the dimeric BAX core crystal structure expected to provide a lipophilic surface in the molecule (red spheres)(Czabotar et al, 2013), while NBD sites showing weak quenching by Dox5 are distributed along regions of the dimeric BAX core crystal structure expected not to interact with membrane lipids (black spheres). Thus, Dox5 quenching results obtained with cBID-activated BAX in MOM-like LUV fit nicely into this crystallographic BAX core dimer structure. On the other hand, mapping the Dox5 quenching results obtained for sites in the BAX latch domain into structural models for BAX α6, α7 and α8 helices reveals a potential lipophilic surface along one face of each of these three helices.

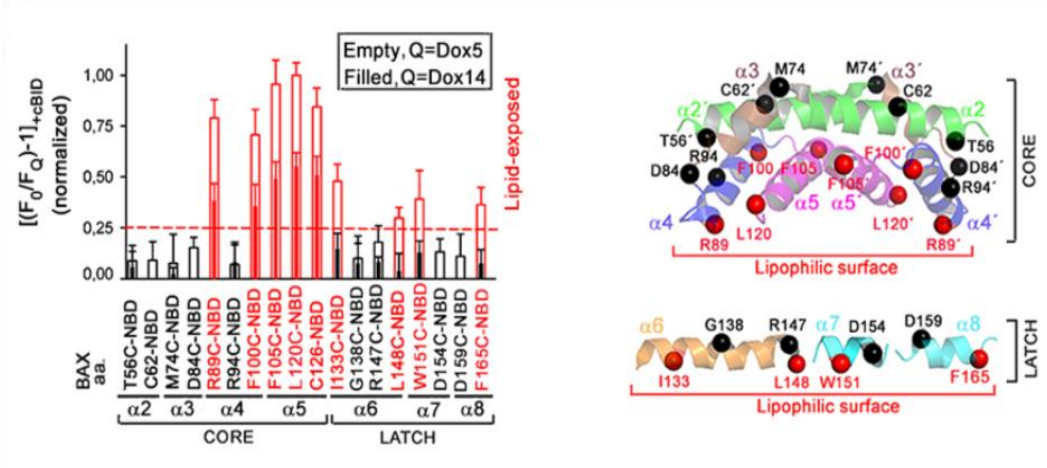

Figure 3.3. Left: Dox-quenching ratios for cBID-activated NBD-BAX variants. **Right:** BAX structures depicting Dox5-exposed (red spheres) and -unexposed (black spheres) residues. Data are mean ± S.E.M. (n ≥3).

Next, it was examined the same cBID-activated NBD-BAX mutants for quenching by the hydrophilic quencher I^- (Figure 3.4, Left). NBD attached to sites R89, F100, F105, L120, and C126 in BAX α4-α5 displayed modest to minimal quenching by I^-, consistent with the notion that these residues of the BAX core domain are buried within the membrane interior in cBID-activated BAX (Figure 3.3). On the other hand, NBD attached to multiple sites in BAX α3 (D74, M84) and BAX α6-α8 (G138, R147, L148, D154, D159, F165) showed substantial quenching by I^- supporting that all these residues of the BAX core and latch domains are at least partially solvent-exposed when BAX acquires its active conformation. The exceptions were I133 and W151 residues in the latch domain which showed more modest quenching by I^-. Lastly, NBD attached to sites T56 and C62 in BAX α2, and R94 in BAX α4 displayed weak quenching by I^-, which combined with their low quenching by Dox5 and Dox14 (Figure 3.3, Left) indicates that these three residues belonging to the BAX core domain are buried within a proteinaceous structure in active BAX.

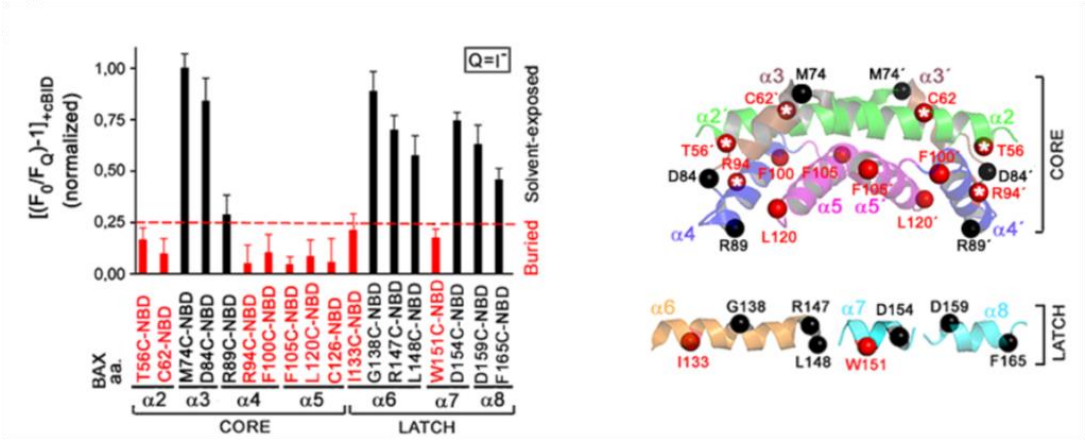

Figure 3.4 Left: I^--quenching ratios for cBID-activated NBD-BAX variants. **Right:** BAX structures depicting solvent-exposed (black spheres) and -unexposed (red spheres) residues. Data are mean ± S.E.M. (n ≥3).

Mapping I- quenching results for sites in the BAX core domain into the BH3-in-groove BAX dimer crystal structure also revealed a general agreement between experimental results and the distribution of BAX residues according to this structural model, as follows (Figure 3.4, Right). First, all residues in the BAX α4-α5 region expected to be hidden within the lipophilic surface at the "bottom" part of the dimeric BAX core structure scored as "buried" by the I^- quenching approach. Of note, R89 in the putative lipophilic surface of BAX α4 scored as "solvent-exposed", yet this residue displayed relative small quenching levels by I^- (Figure 3.4, Left). Second, residues M74 and D84 in BAX α3 that strongly scored as "solvent-exposed" by the I^- quenching method localize to surface-exposed regions in the dimeric BAX core crystal structure. Third, residues T56 and C62 in BAX α2 and R94 in BAX α4 scoring as "buried" by the I^- quenching approach localize to the protein:protein interface between the two BAX monomers in the dimeric BAX core crystal structure (red spheres with white stars). On the other hand, the mapping of I- quenching results for sites in the BAX latch domain into structural models for BAX α6, α7 and α8 helices, together with the data shown in Figure 3.4, supports the notion that the entire latch region of the activated BAX molecule adopts a peripheral disposition at the membrane displaying a lipophilic surface along one face of its component helices.

Overall, fluorescence mapping of active BAX topology in MOM-like membranes indicates that the BAX core domain adopts a BH3-in-groove dimeric structure presenting a lipophilic surface in the BAX α3-α4 region, while the BAX latch domain provides another lipophilic surface along one side of its constituent α6-α8 helices. In addition, the combined results also reveal that the BAX core α4-α5 helices penetrate deeper into the membrane hydrocarbon core than the BAX latch α6-α8 helices, but without adopting a TM orientation.

3.4.1.3 **BCLXL blocks membrane insertion of BAX core, not latch domain.**

Next, it was also analysed the effect of antiapoptotic BCLXL on NBD-BAX fluorescence changes elicited by cBID. Of note, for these experiments the $cBID^{M97A}$ mutant was used which displays negligible binding to BCLXL but preserves intact BAX activation capacity (Lee et al, 2016). Importantly, it is also considered the ongoing debate on whether antiapoptotic proteins neutralize BAX exclusively through canonical BH3-in-groove heterodimeric interactions, or also via additional non-canonical protein-protein binding interactions (Andreu-Fernandez et al, 2017; Basanez et al, 2012; Czabotar et al, 2014; Czabotar et al, 2013; Landeta et al, 2014; Lee et al, 2016; Llambi et al, 2011; Shamas-Din et al, 2013). In the former case, BCLXL is expected to exert its inhibitory action only before the BAX BH3-in-groove dimerization process has taken place, while in the latter scenario BCLXL is predicted to remain at least partially active even after BAX has become previously dimerized. When BCLXL was added before $cBID^{M97A}$ had activated BAX, the antiapoptotic protein prominently inhibited the NBD fluorescence increase observed at most sites in the BAX core, but not latch domain (Figure 3.5A, filled Bars). On the other hand,

when BCLXL was added after cBID^{M97A} had activated BAX, insignificant changes were observed in the NBD fluorescence of all BAX variants examined (Figure 3.5A, empty bars).

To directly test whether BCLXL differentially inhibits membrane insertion of BAX core and latch helices, the effect of BCLXLΔC on Dox5-mediated quenching of NBD-BAX variants was assessed. Indeed, BCLXLΔC markedly inhibited the quenching elicited by Dox5 in multiple NBD-BAX variants localized at the BAX core domain (BAX$^{R89C\text{-}NBD}$, BAX$^{F100C\text{-}NBD}$, BAX$^{L120C\text{-}NBD}$, and BAX$^{C126\text{-}NBD}$), but not the BAX latch domain (BAX$^{I133C\text{-}NBD}$, BAX$^{L148C\text{-}NBD}$, BAX$^{W151C\text{-}NBD}$, and BAX$^{F165C\text{-}NBD}$) (Figure 3.5B).

To try to further discriminate between canonical and non-canonical mechanisms of BCLXL-mediated BAX inhibition, the BCLXLΔC^{R139D} and BCLXLΔC^{L17A} variants were expected to disrupt the canonical and the BCL2-like non-canonical BCLXL:BAX binding interfaces, respectively (Figure 3.5C)(Barclay et al, 2015; Czabotar et al, 2013). Interestingly, the canonical BCLXLΔC^{R139D} mutant completely lost the ability of native BCLXLΔC to inhibit cBID-mediated BAX activation as determined by measurements of mitochondrial cyt c release (Figure 3.5D), vesicular ANTS/DPX release (Figure 3.5E), and NBD-BAX fluorescence changes (Figure 3.5F). In contrast, the BCL2-like non-canonical BCLXLΔC^{L17A} mutant preserved all these inhibitory activities displayed by the parent protein (Figure 3.5D-F).

Thus, can be concluded that antiapoptotic BCLXL inhibits both BAX core membrane insertion and BAX apoptotic pore formation via heterodimeric BH3-in-groove interactions.

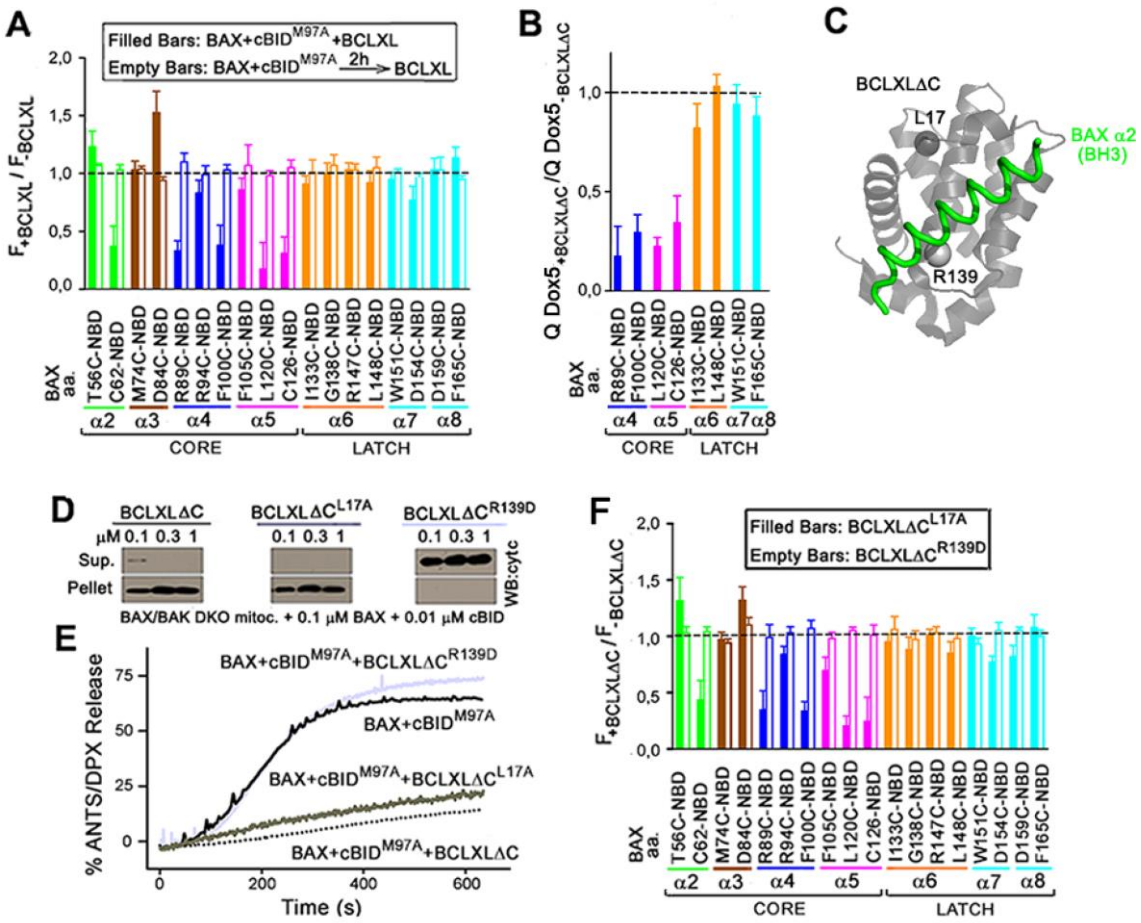

Figure 3.5 Mode of BCLXL inhibition. (**A**) Intensity ratios of NBD-BAX variants treated with cBID^{M97A} and BCLXL (500 nM) (F_{+BCLXL}) to those without BCLXL (F_{-BCLXL}). BCLXL was added together with BAX+cBID^{M97A} (filled bars) or afterwards (empty bars). (**B**) Dox5-quenching ratios for NBD-BAX variants treated with cBID^{M97A} and BCLXLΔC (5000 nM, $QDox5_{+BCLXL\Delta C}$) to those without BCLXLΔC ($QDox5_{-BCLXL}$). (**C**) Representation of BCLXLΔC:BAX BH3 complex highlighting canonical/non-canonical surfaces. (**D**) Cyt c release by BAX, cBID^{M97A}, and BCLXLΔC proteins. (**E**) ANTS/DPX release by BAX (200 nM), cBID^{M97A} (50nM), and BCLXLΔC proteins (5000 nM). (**F**) As in Panel A. Data are mean ± S.E.M. (n ≥2).

3.4.1.4 PEGylation of multiple sites at the BAX core, but not latch domain, blocks BAX apoptotic pore formation.

Next, in order to analyse the specific contribution of individual BAX core and latch residues to BAX apoptotic pore formation using a site-specific BAX PEGylation approach was used (Dozier & Distefano, 2015). To this aim, the modification of the different BAX monocysteine mutants with the small hydrophilic reagent methoxy PEG maleimide of 550 Da (PEG05k) was performed to yield a set of mono-PEGylated BAXPEG05k variants, and then compared the membrane-permeabilizing activity of each BAX mutant with or without site-specific PEGylation.

The rationale behind this experimental approach is that conjugation of a hydrophilic PEG05k molecule at a specific site in BAX should obstruct the localization of that particular BAX residue to the hydrophobic interior of the membrane or a BAX oligomerization interface, thereby potentially inhibiting BAX-induced membrane permeabilization.

Notable differences were observed in the permeabilization of MOM-like LUV elicited by cBID-activated BAX depending on the site of BAX PEGylation (Figures 3.6A, B). At the BAX core domain, PEGylation of all sites in BAX α2 and the BAX α4-α5 region potently inhibited BAX-induced liposome permeabilization, whereas PEGylation of BAX α3 sites had a more modest impact on BAX permeabilizing activity. Site-specific PEGylation at the BAX latch domain had a generally weaker effect on BAX permeabilizing activity.

The relative impact of site-specific BAX PEGylation on BAX-induced membrane permeabilization was mapped into BAX structural models (Fig. 3.6C, Right). This representation, together with those shown in Figure 3.2-3.4, illustrates that (i) the BAX sites where PEGylation strongly inhibits BAX-induced membrane permeabilization basically comprise BAX residues at the core domain implicated in BAX:BAX BH3-in-groove interaction (C62, R94) and BAX α4-α5 membrane insertion (R89, F100, F105, L120, C126); whereas (ii) the BAX sites where PEGylation weakly inhibits BAX-induced permeabilization essentially represent BAX residues localized at the solvent-exposed, non-interacting BAX core α3 helix (M74, D84), or at the peripherally membrane-attached BAX latch α6-α8 domain (I133, G138, R147, L148, W151, D159, F165).

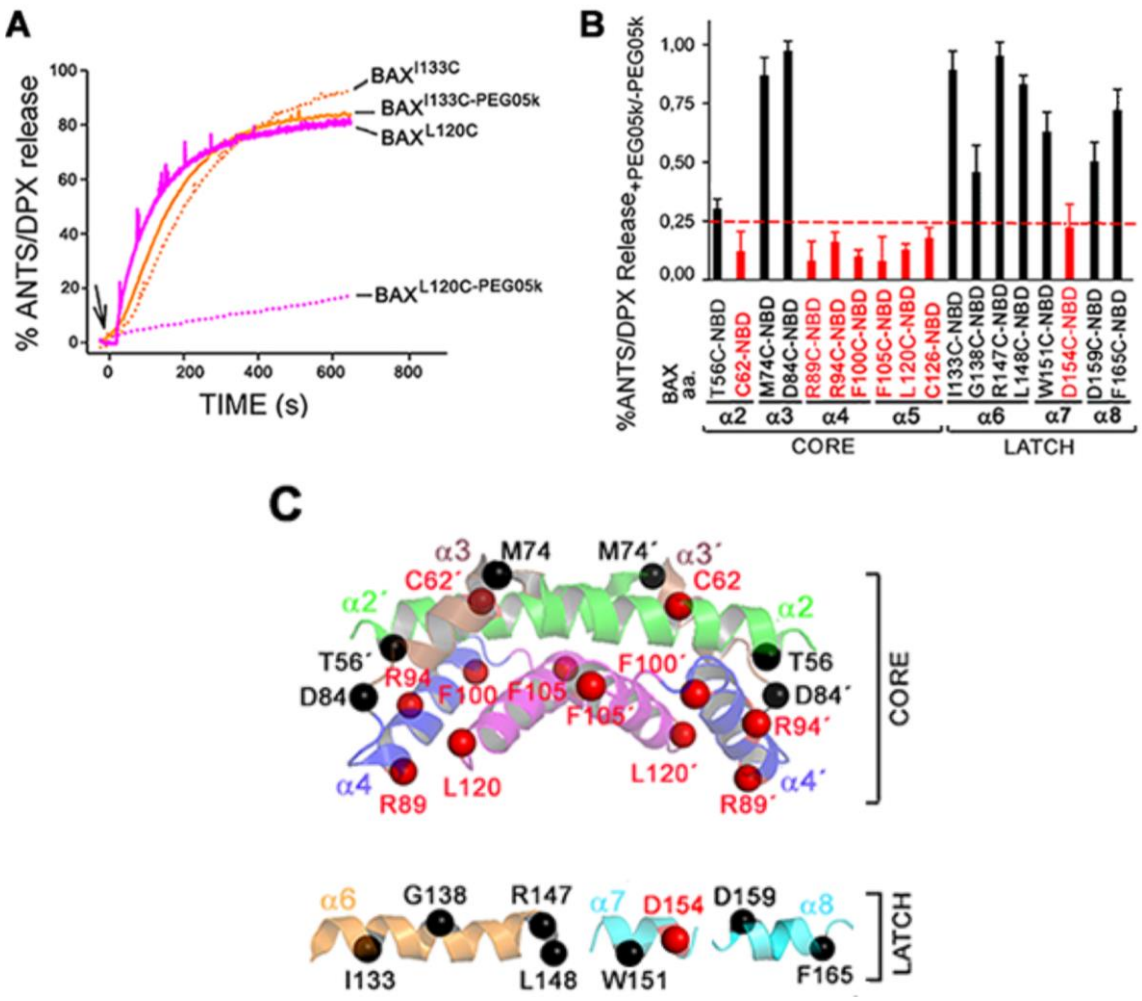

Figure 3.6: Contribution of BAX core and latch domains to membrane permeabilization. (**A**) ANTS/DPX release by cBID-activated BAX variants conjugated/unconjugated with PEG05k. (**B**) Ratios of ANTS/DPX release by BAX variants conjugated with PEG05k to BAX unconjugated with PEG05k. (**C**) BAX structures depicting residues strongly (red spheres) or weakly (black spheres) inhibiting BAX pore formation. Data are mean ± S.E.M. (n ≥3).

3.4.1.5 BAX core α5 peptide displays membrane activities that are absent in BAX latch α6 and α7-α8 peptides.

As an additional approach to try to determine the role of BAX core and latch helices in BAX apoptotic pore formation, they were examined different membrane activities of synthetic peptides representing BAX α5, α6, and α7- α8 regions. First, it was determined the main biophysical properties of BAX α5, α6, and α7- α8 regions using MPEx and Heliquest (Gautier et al, 2008; Snider et al, 2009). The BAX core α5 region showed higher mean hydrophobicity (<H>), lower mean hydrophobic moment (anphipaticity, <μH>), and more positive net charge (z) than the BAX latch α6 and α7-α8 regions (Figure 3.7A).

Next, the capacity of BAX-derived peptides to penetrate into MOM-like lipid monolayers was assessed (Figure 3.7B). For BAX α5 and BAX α6 peptides, the change in lipid monolayer surface pressure (Δp) upon peptide addition decreased linearly as a function of increasing initial surface pressure (π_0), giving critical surface pressure (π_c) values of 34.8 mN/m and 25.6 mN/m, respectively. Considering that typical π_c values for lipid bilayer membranes are in the range of 25-30 mN/m(Marsh, 1996), these data suggest that the BAX α5 peptide displays a superior capacity to penetrate into the MOM lipid bilayer compared to the BAX α6 peptide. In parallel, the membrane-permeabilizing ability of BAX-derived peptides was analysed. As shown in Figure 3.7C, the BAX α5 peptide induced ANTS/DPX release from MOM-like LUV in a dose-dependent manner, while the BAX α6 and BAX α7-α8 peptides were much less active in this experimental system.

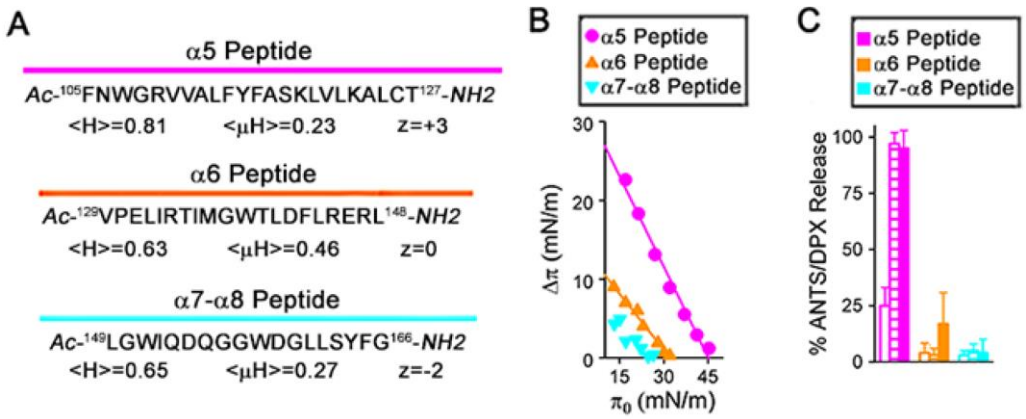

Figure 3.7 Membrane activities of BAX-derived peptides (1). (**A**) Biophysical characteristics of BAX-derived peptides. (**B**) Monolayer insertion of BAX-derived peptides. (**C**) ANTS/DPX release by BAX-derived peptides (0.1 μM, 1 μM, and 5 μM). Data are mean ± S.E.M. (n ≥2).

Similarly, the BAX α5 peptide induced a dose-dependent depletion of cyt c in BAX/BAK DKO mitochondria, whereas the BAX α6 and BAX α7-α8 peptides virtually did not release any mitochondrial cyt c at any concentration tested (Figure 3.8A). ^{31}P-NMR studies were also conducted to directly assess whether these peptides disrupt the membrane lipid bilayer structure. The ^{31}P-NMR spectrum of MOM-like liposomes showed the high-field peak and low-field shoulder typical of a planar bilayer arrangement of membrane lipids (Figure 3.8B). Addition of the BAX α5 peptide to MOM-like liposomes led to a profound change in the shape of the 31P-NMR spectrum: the bilayer-type signal markedly decreased while a prominent peak appeared around the chemical shift position of phospholipids experiencing isotropic motion, which is typical for highly curved non-bilayer type lipid dispositions. By contrast, the BAX α6 and BAX α7-α8 peptides did not significantly alter the ^{31}P-NMR spectrum of MOM-like liposomes.

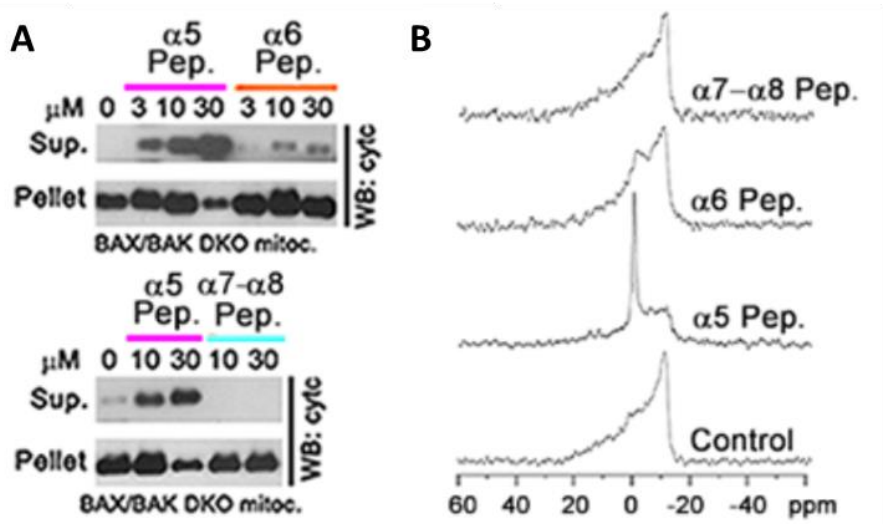

Figure 3.8 Membrane activities of BAX-derived peptides (2). (**A**) Cyt c release by BAX-derived peptides. (**B**) Effect of BAX-derived peptides on lipid bilayer structure. Data are mean ± S.E.M. (n ≥2).

Collectively, these results strongly suggest that the BAX core α5 helix displays an intrinsic capacity to insert into the MOM lipid matrix, destabilize the MOM lipid bilayer structure, and breach the MOM permeability barrier, while the BAX latch α6-α8 helices lack such membrane activities.

3.4.1.6 Computational simulations reveal dissimilar membrane interaction modes for the BAX core α5 helix, the BAX latch α6-α8 helices, and the BAX C-terminal α9 helix.

Finally, coarse-grained Monte Carlo (MC) simulations of peptides in association with MOM-like lipid bilayer membranes using the MCPep web server was perfomed (Gofman et al, 2012a). Although this computational model captures only certain characteristics of the complex peptide-lipid system, it allows obtaining quantitative information of thermodynamic parameters reflecting the mode of peptide-membrane interaction; in particular, the peptide´s membrane-association free energy (ΔG_{total}), favored membrane orientation (Tilt), and preferred membrane penetration depth (Z_{center}). Moreover, the MC simulation model has been previously tested for a variety of peptide and protein fragments in membrane environments, and reproduced available empirical data and results obtained with explicit molecular dynamics simulations with reasonable success (Gofman et al, 2012a; Gofman et al, 2012b; Gofman et al, 2010).

As a control, they were first examined three experimentally well-studied case examples in this computational system (Figure 3.9A): (1) the prototypical TM domain of glycophorin A (Harrington & Ben-Tal, 2009); (2) the N-terminal H0 helix of endophilin A1 localizing at the level of the phospholipid phosphate groups (Gallop et al, 2006); and (3) melittin, a potent pore-forming and bilayer-destabilizing cytolitic peptide that localizes at the upper region of the

hydrocarbon phase of the lipid bilayer (Lee et al, 2013). Indeed, for each one of these example cases analysed, the MCPep simulation successfully reproduced the expected peptide-membrane interaction mode (Figure 3.9A, and Table 3.1).

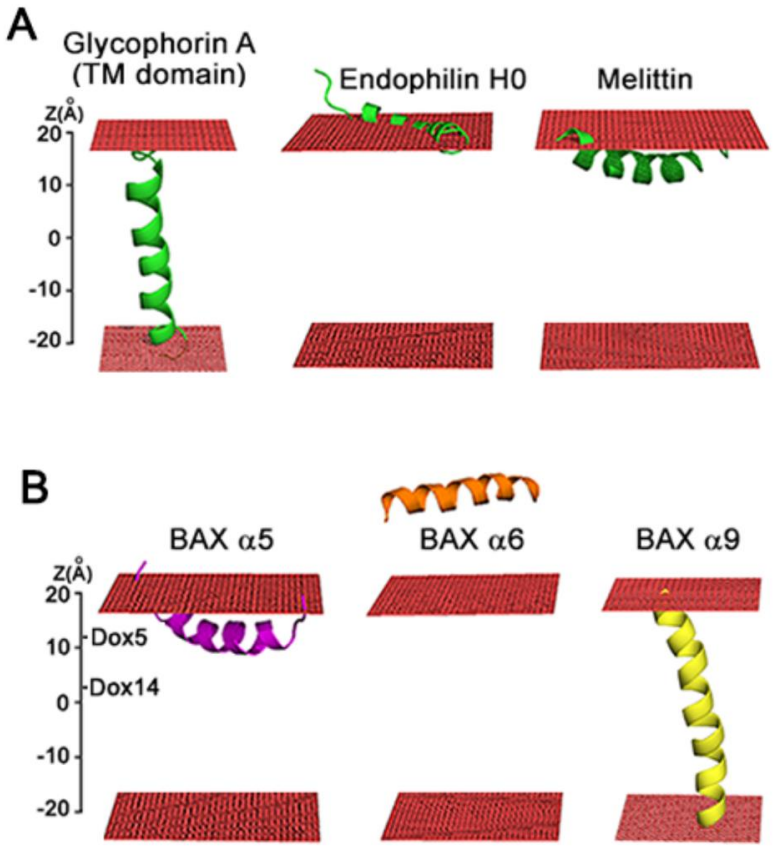

Figure 3.9. Peptide-membrane association modes assessed by MC simulations. (**A**) Example peptides; (**B**) BAX-derived peptides. Red rectangles represent phospholipid headgroups.

Peptide/Quality	ΔG_{total} (kT)	Z_{center} (Å)	Tilt (degrees)
Glycophorin A (TM)	-40.8±0.3	2.8±0.4	21.3±0.7
Endophilin H0	-7.7±0.1	22.4±0.7	68.3±0.6
Melittin	-22.9±0.2	18.5±0.3	79.4±0.5
BAX α5	-26.1±0.3	18.1±0.1	78.9±0.3
BAX α6	-3.7±0.4	36.2±0.7	58.0±0.4
BAX α7-α8	-0.8±0.5	45.3±0.6	53.8±0.4
BAX α9	-17.7±0.1	0.8±0.1	11.5±0.4

Table 3.1: Thermodynamic characteristics of interaction between different peptides and MOM-like membranes.

All values are reported as means ± standard error. ΔG_{total}, the total free energy of peptide-membrane association; Zcenter, the average distance of the peptide´s centre of mass to the membrane midplane; Tilt, the angle between the N´-to-C´ vector of the peptide´s helical core and the membrane normal.

Then, it was examined the membrane-interaction modes of BAX α5, α6, α7-α8, and α9 peptides by MCPep (Figure 3.9B, and Table 3.1). Remarkably, the BAX core α5 peptide displayed a membrane-interaction mode very similar to that of the melittin peptide, by localizing into the sub-surface region of the membrane with a membrane-association free energy of -26.1 kT, its geometrical center at an average distance of 18.1 Å from the membrane midplane, and its principal axis nearly parallel to the membrane surface. By contrast, the BAX latch α6 and α7-α8 peptides interacted very weakly with the membrane (ΔG_{total} < 5kT), and for the most part, remained in the aqueous phase (Z > 30 Å). Lastly, the most energetically favored disposition for the BAX C-terminal α9 peptide was the TM orientation.

Thus, the dissimilar membrane interaction modes of the BAX core α5 peptide and the BAX latch α6 and α7-α8 peptides disclosed by MCPep simulations concur with experimental results showing that the former peptide, but not the latter ones, possesses intrinsic membrane-inserting, pore-forming and bilayer-destabilizing activities (Figures 3.7 and 3.8). MCPep computational results also qualitatively agree with fluorescence mapping studies showing that membrane active BAX inserts the core α5 helix deeper into the lipid bilayer than the latch α6-α8 helices (Figure 3.2-3.4).

3.4.2 Assessing inactive BAX membrane structure in model membranes and in situ in the MOM

Recent information indicates that functional activation of BAX/BAK at the MOM level requires interaction with mitochondrial membrane lipids in addition to selected BH3-only proteins (Hollville & Martin, 2012; Zhang & Saghatelian, 2013). Therefore, as the conformational rearrangements that many BCL2 family proteins apparently undertake to become functionally active occur in a lipid bilayer environment, the interaction with mitochondrial membrane lipids, especially the CL, has been gaining attention. In fact, a growing body of evidence indicates that the BCL2-regulated MOM permeabilization pathway is a lipid-assisted process, but exactly how specific mitochondrial lipids impact on BCL2 family proteins is poorly understood (Crimi & Esposti, 2011; Osman et al, 2011).

Previous studies in our lab (Dr Ane Landajuela´s thesis) using site-specific fluorescence labelling and fluorescence spectroscopy of NBD-BAX monocysteine mutants revealed that inactive BAX does not breach the membrane permeability barrier and peripherally interacts with CL-containing liposomes. Nevertheless, this peripheral membrane interaction induces localized structural

changes in BAX through a previously unidentified surface of the molecule, most prominently including C-terminal BAX α7-α9 helices and flanking regions. Those model membrane studies also detected exposure of N-terminal residues of BAX, akin to the conformational changes observed during early stages of the BAX activation process. Interestingly, functional regions potentially implicated in BAX intramembranous oligomerization (BH3 domain, canonical BH3-binding groove, and α6 helix), or membrane perforation (central α5 helix) remained basically unaltered upon BAX membrane association.

As a continuation of those studies, here we used the same set of monocysteine BAX mutants and SCAM (Single Cysteine Accesibility Methodology) to assess conformation of BAX in MOM-like model membranes and in isolated $BAX^{-/-}/BAK^{-/-}$ DKO mitochondria. Of note, our SCAM analysis enables the study of membrane BAX structural details in a label-free environment, avoiding possible NBD induced artifacts or aberrations. In this structural characterization protocol, it was analysed the cysteine accessibility to PEG-Mal5kDa, a 5kDa molecule that binds both specifically and irreversibly to exposed cysteines adding to the bounded molecule an extra weight. This modification is detected as a shift in the BAX band by SDS-PAGE, combined with coomassie blue staining for the studies in liposomes or an anti-BAX western blotting when we analyse the topology in the mitochondria. The effects exerted by membrane binding/insertion on the set of 27 monocysteine BAX mutants is shown in Figure 3.10 and summarized in Figure 3.11. Moreover, Figure 3.10 also includes the structural location and the theoretical exposure of each individual residue.

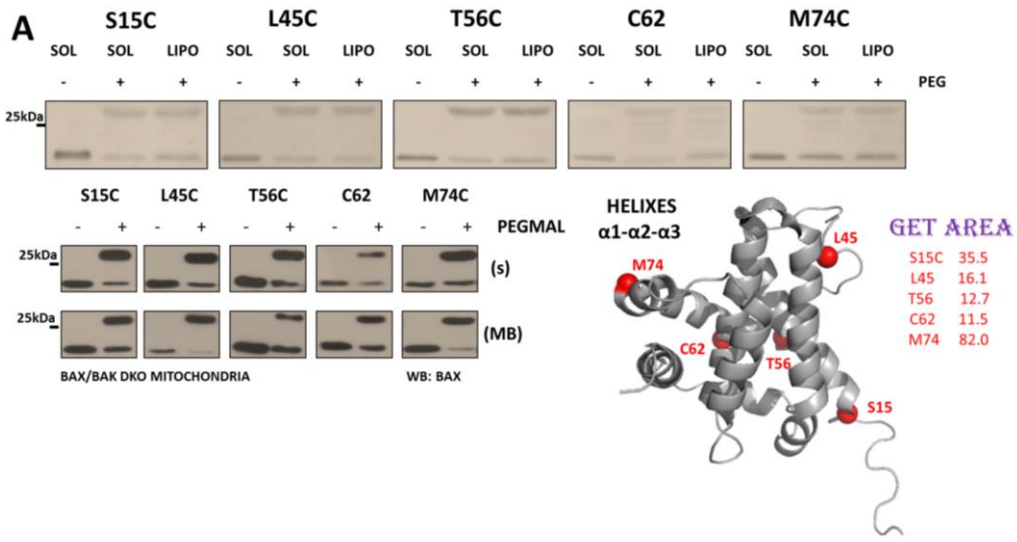

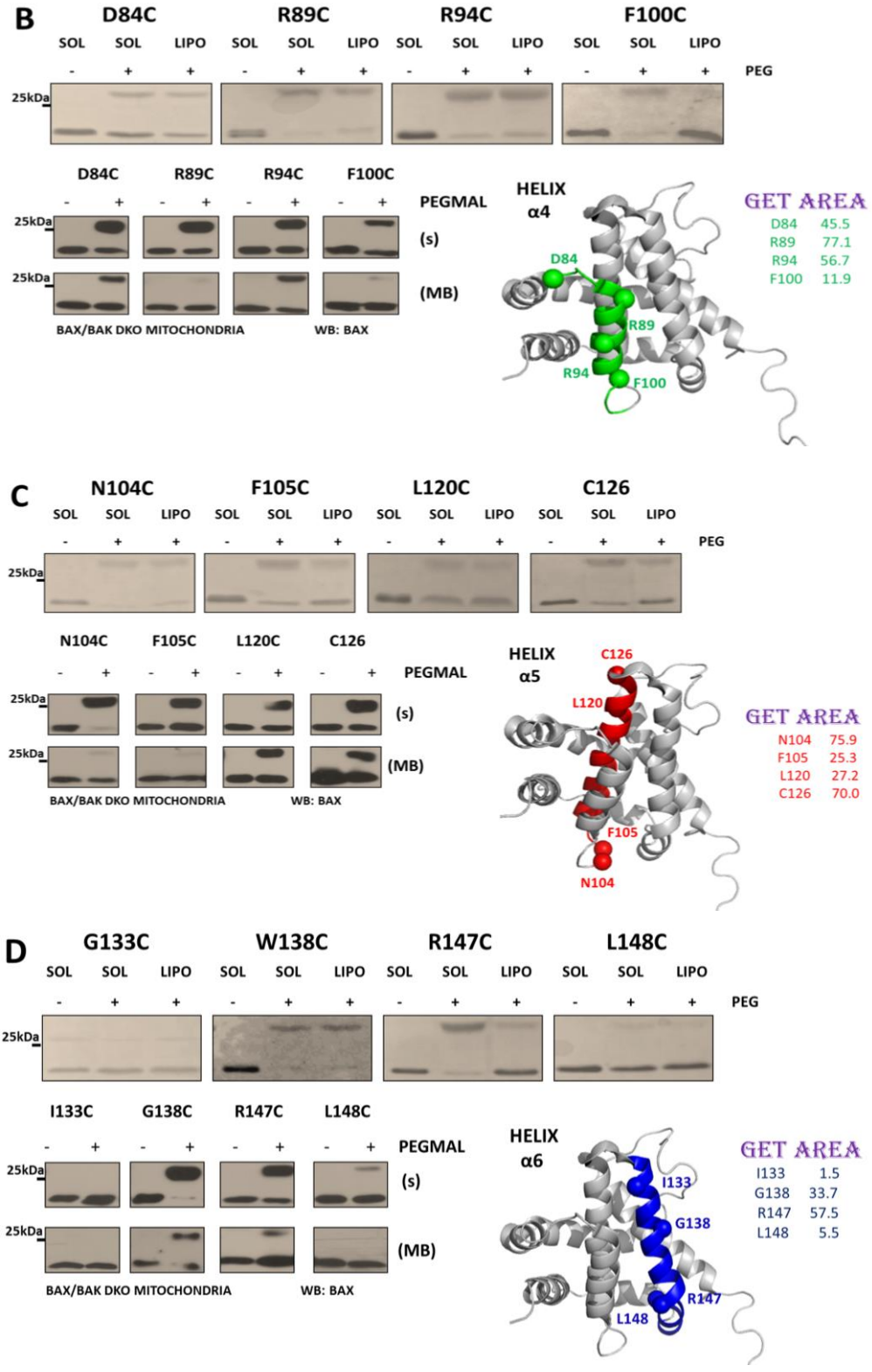
B
D84C
R89C
R94C
F100C
SOL SOL LIPO SOL SOL LIPO SOL SOL LIPO SOL SOL LIPO
- + + - + + - + + - + + PEG
25kDa
D84C R89C R94C F100C
- + - + - + - + PEGMAL
25kDa (s)
25kDa (MB)
BAX/BAK DKO MITOCHONDRIA
WB: BAX
HELIX α4
D84
R89
R94
F100
GET AREA
D84 45.5
R89 77.1
R94 56.7
F100 11.9
C
N104C
F105C
L120C
C126
SOL SOL LIPO SOL SOL LIPO SOL SOL LIPO SOL SOL LIPO
- + + - + + - + + - + + PEG
25kDa
N104C F105C L120C C126
- + - + - + - + PEGMAL
25kDa (s)
25kDa (MB)
BAX/BAK DKO MITOCHONDRIA
WB: BAX
HELIX α5
C126
L120
F105
N104
GET AREA
N104 75.9
F105 25.3
L120 27.2
C126 70.0
D
G133C
W138C
R147C
L148C
SOL SOL LIPO SOL SOL LIPO SOL SOL LIPO SOL SOL LIPO
- + + - + + - + + - + + PEG
25kDa
I133C G138C R147C L148C
- + - + - + - + PEGMAL
25kDa (s)
25kDa (MB)
BAX/BAK DKO MITOCHONDRIA
WB: BAX
HELIX α6
I133
G138
R147
L148
GET AREA
I133 1.5
G138 33.7
R147 57.5
L148 5.5

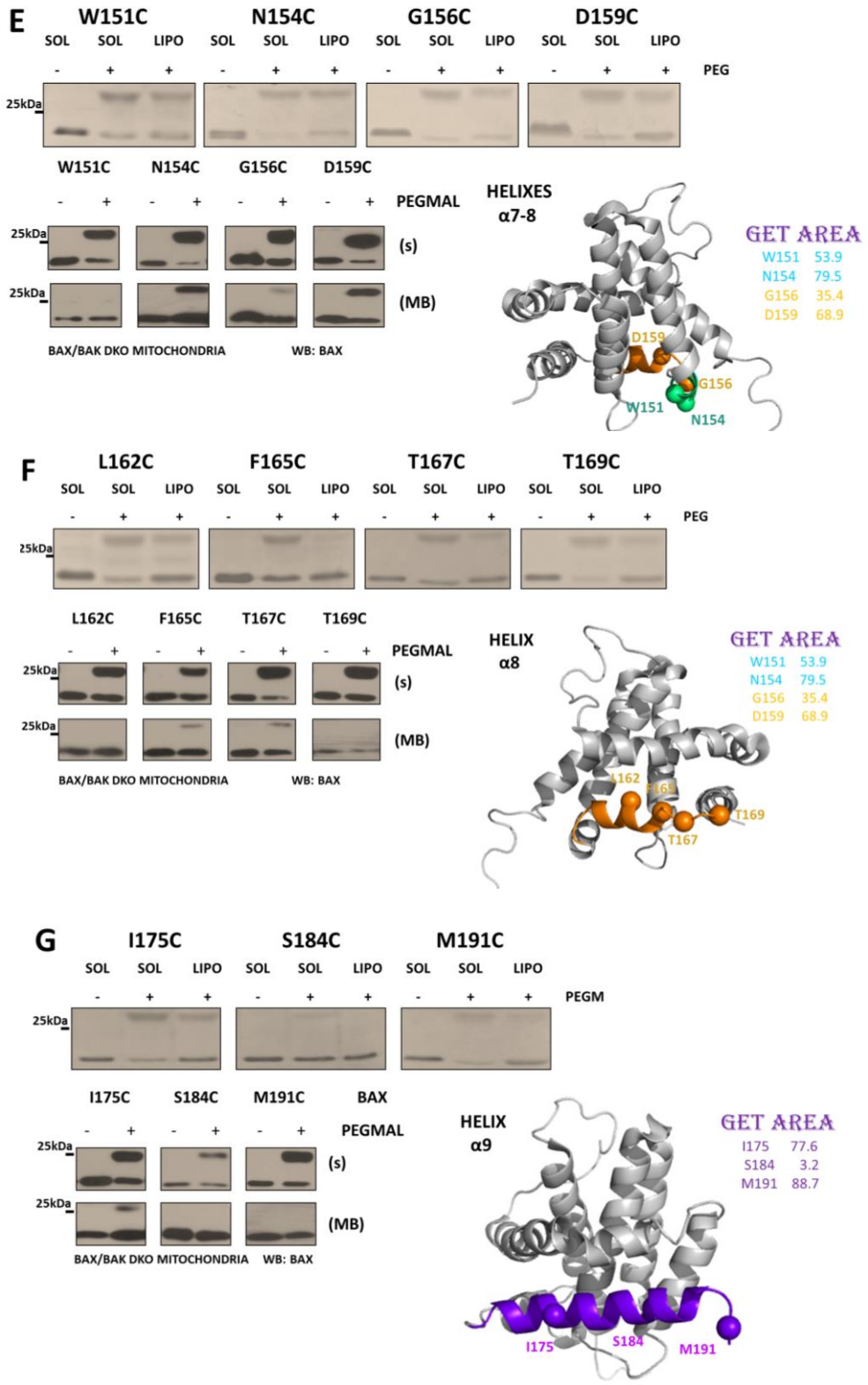

Figure 3.10 SCAM analysis of BAX conformation in different environments. (A-H) Right, Structural model generated in PyMol depicting individual amino acid residues along BAX structure substituted by cysteines (PDB=1F16). **Top-left:** SCAM analysis of BAX with or without Mito-like LUVs; **Bottom-left,** SCAM analysis of BAX with or without isolated mitochondria.

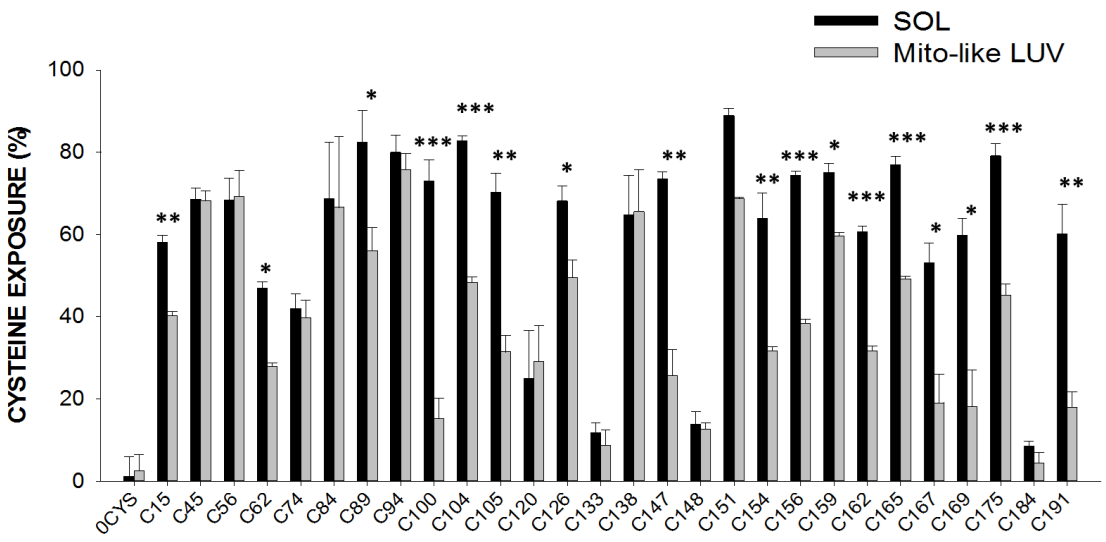

Figure 3.11 Quantitative SCAM analysis of BAX conformations. The ratio between label/non-label BAX monocysteine mutants in the presence (grey bars) absence (black bars) of model membranes. (n=3, S.D.). *, ** and ***: p= <0.001, <0.025 and <0.05 respectively.

As shown in Figures 3.10 and 3.11, the exposure pattern obtained for BAX in solution is basically consistent with BAX solution NMR structure. However, SCAM analyses indicated that upon interaction with MOM-like LUVs of isolated mitochondria BAX undergoes localized conformational changes that are basically consistent with previous results generated in our lab using NBD-BAX mutants and fluorescence spectroscopy, where BAX interacts with the membrane via its C-terminal α7-α9 helixes and flanking regions. Moreover, specific residues surrounding the canonical groove that have been implicated in BAX dimerization and retrotranslocation. Concretely, canonical C62 (in the α2/BH3 domain) and R89 (in α4) experiment a decrease in the exposure in Mito-like LUVs and in isolated mitochondria. One possible interpretation of SCAM results is that the MOM lipid bilayer contributes to release BAX α9 from the canonical groove (Figure 3.12). It is also compatible with the view that interaction with the MOM facilitates BAX dimerization by increasing the accessibility of BAX BH3 domain and BAX canonical groove.

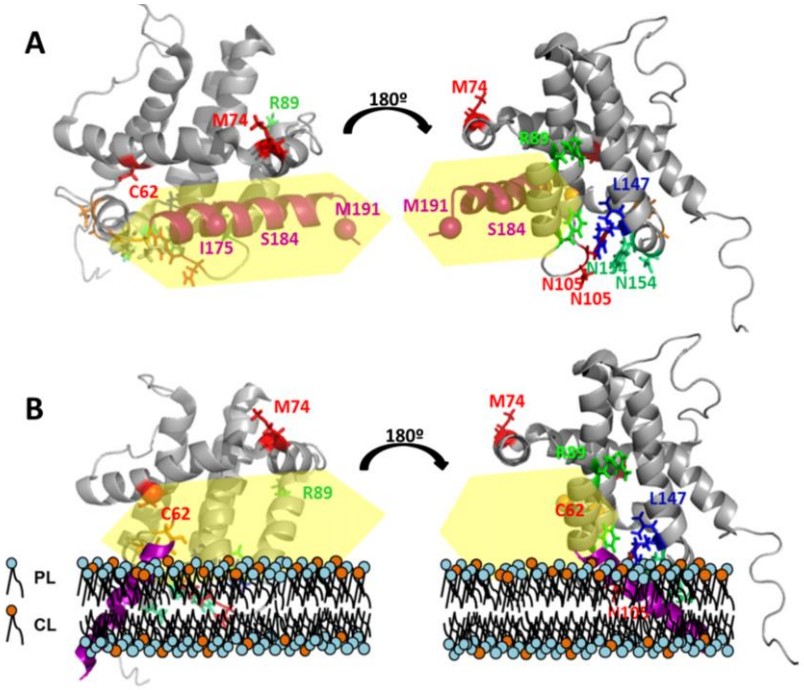

Figure 3.12. Schematic representation of BAX topology according to SCAM results (A) in solution and **(B)** in Mito-like and MOM. CL= Cardiolipin PL: Phospholipid.

Complementarily, BAX membrane topology was analysed in membranes lacking mitochondrial specific lipid CL. In coherence with previous studies in our lab, BAX maintains its solution folding in the presence of this specific membranes (Figure 3.13). Thus, mitochondrial membrane lipids, specially the CL, could modulate BCL2 proteins membrane topology, and possibly their interaction network.

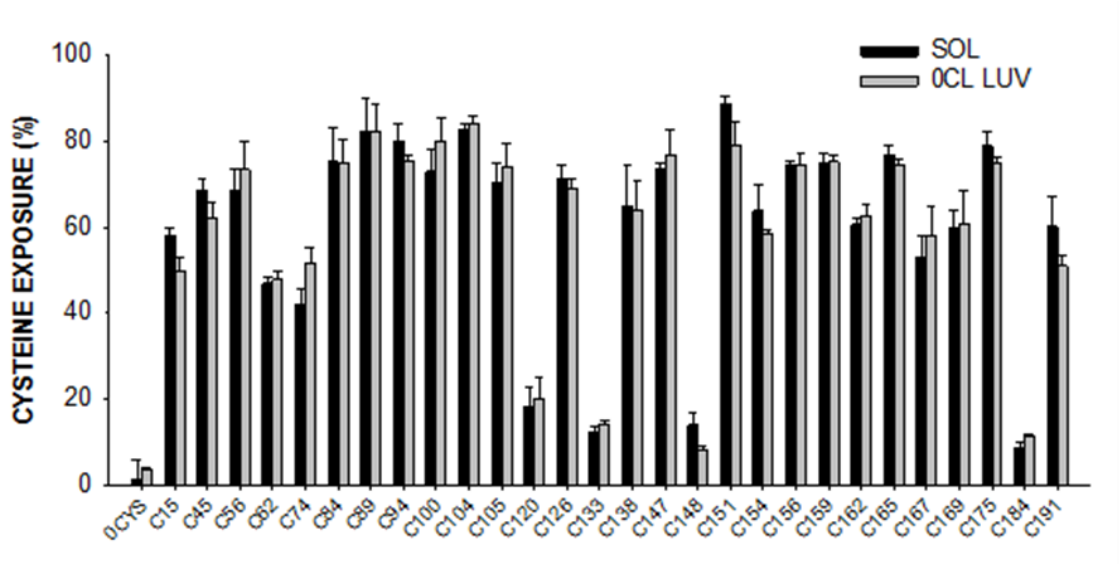

Figure 3.13 Analysis of BAX interaction with CL-lacking LUV assessed by SCAM. The ratio between label/non-label BAX monocysteine mutants in the presence (grey bars) absence (black bars) of model membranes.

Altogether. this set of results, combined with the findings that BAX bound to CL-containing liposomes or MOM remains monomeric, does not breach the membrane permeability barrier, leads us to propose that the membrane-associated form of BAX described in this study represents an early conformational state of the protein along the pathway of its functional activation. We name this configuration the "lipid-primed" conformation of BAX.

3.5 DISCUSSION

How BCL2 family proteins modulate apoptosis through MOM permeability changes has been intensively studied during the last two decades (Basanez et al, 2012; Cosentino & Garcia-Saez, 2017; Czabotar et al, 2014; Czabotar et al, 2013; Youle & Strasser, 2008). However, a comprehensive view of this fundamental process regulating cell fate is still lacking. In this chapter, using a variety of biophysical and biochemical techniques applied to minimalist in vitro reconstituted systems, it is provided new insight into how BAX and BCLXL regulate the formation of mitochondrial apoptotic pores through specific protein:protein and protein:lipid interactions.

This work adds significantly to a growing number of studies indicating that the BAX BH3-into-groove dimerization process plays a fundamental role in BAX-elicited apoptotic pore formation (Bleicken et al, 2014; Czabotar et al, 2013; Sung et al, 2015; Zhang et al, 2016). Not only it is shown that the BAX BH3-in-groove dimeric conformation persists in the fully active conformation of BAX rather than merely being and intermediate in the molecular pathway for BAX activation (Figure 3.2-3.4); this site-specific BAX PEGylation analyses also revealed that PEGylation of multiple individual BAX core residues implicated in BAX BH3-in-groove dimerization effectively block the BAX pore-forming activity (Figure 3.6). By contrast, these studies do not support the so-called BAXα2α3α4 dimeric structure for fully active BAX, although it cannot be discarded that BAX may transiently adopt this alternative dimeric structure at early stages of its functional activation pathway (Zhang et al, 2016). Concerning high-order BAX multimers, our site-directed fluorescence BAX mapping and PEGylation studies are consistent with the view that BAX BH3-in-groove dimers can grow into higher-order BAX multimeric species with optimal membrane-permeabilizing activity through multiple BAX interdimer interfaces (Aluvila et al, 2014; Bleicken et al, 2014; Dewson & Kluck, 2009; Dewson et al, 2012; Mandal et al, 2016; Sung et al, 2015; Zhang et al, 2016). In this scenario, the lower stability of such BAX interdimer interfaces would preclude their detection by the steady-state fluorescence analyses used here, while PEGylation of a single BAX interdimer interface would not be sufficient to efficiently block BAX multimerization and pore formation.

Another ongoing debate in the BCL2 research field pertains to the precise mechanisms through which antiapoptotic BCL2-type proteins inhibit BAX activation and action (Czabotar et al, 2014;

Landeta et al, 2014; Llambi et al, 2011; Moldoveanu et al, 2014; Shamas-Din et al, 2013). According to canonical models, antiapoptotic proteins neutralize proapoptotic partners via heterodimeric BH3-in-groove complexes that in principle, should be formed before BAX BH3-in-groove homodimers had been assembled. On the other hand, non-canonical models postulate that antiapoptotic proteins can use binding interfaces other than their canonical groove to form inactive complexes with BAX-type proteins, conceptually even after the building-up of BAX BH3-in-groove homodimers had occurred. In this regard, our combined results showing the differential effects exerted by the sequential addition of BCLXL on BAX topology, the inhibition of BAX α5 membrane insertion by BCLXL, as well as the opposite effects of canonical and non-canonical BCLXLΔC mutants on BAX membrane activities (Figure 3.5), support the notion that BCLXL principally acts by sequestering the BAX BH3 domain into its canonical groove thereby blocking BAX BH3-in-groove homodimerization. Nevertheless, these results do not exclude that the recently described non-canonical BCLXL α9:BAX α9 surface contributes to form neutralizing BCLXL:BAX complexes (Andreu-Fernandez et al, 2017).

Another important finding is that BAX apoptotic pore formation is driven by lipid interactions established by BAX α4-α5 helices, but not BAX α6-α8 helices, despite both the core and latch domains of BAX associate with the membrane lipid bilayer when the protein acquires its active conformation. Empirical and computational data indicate that the primary origin of this dissimilar behavior of BAX core and latch helices is their differential membrane penetration degrees: BAX α4-α5 localize to the upper region of the hydrocarbon core of the lipid bilayer, whereas BAX α6-α8 localize to a more superficial region of the membrane interface. This is in line with current knowledge on the membrane penetration-depth of pore-forming helical peptides such as melittin, which in that way produce the optimal surface tension and curvature stress within the membrane required to destabilize its lipid bilayer structure and open a proteolipidic pore therein (Kozlov et al, 2014; Lee et al, 2013; Zemel et al, 2008). It appears reasonable to propose that other specific features of the BAX BH3-in-groove structure, such as its dimeric and curved nature, may also contribute to BAX-mediated destabilization of the membrane lipid bilayer structure. The finding that BCLXL selectively inhibits membrane insertion of BAX α4-α5 helices, but not BAX α6-α8 helices, further supports that interaction of the BAX core domain with membrane lipids drives BAX apoptotic pore formation, while the BAX latch domain merely plays a passive role in this process.

These results prompt to reconsider certain assumptions made in recent models proposed to explain proteolipidic pore formation by BAX-type proteins. Specifically, in the so-called “clamp model” the insertion of the BAX latch α6-α8 region into the MOM lipid bilayer was considered a key determinant for BAX proteolipidic pore formation (Bleicken et al, 2014). However, in that study the degree of membrane insertion of BAX α6-α8 helices and the contribution of the BAX latch region to BAX pore-forming activity were not explicitly examined. Similarly, the so-called “in-plane” model postulated that shallow membrane insertion of multiple BAX helices, including

those of the latch domain, drives BAX proteolipidic pore formation (Westphal et al, 2014a). However, in the latter study, the topological analyses of the BAX latch domain were limited to the BAX α6 helix, and BAX α6 membrane topology was assessed using a biochemical technique with lower spatial resolution than the one used here. Nevertheless, our results are not necessarily incompatible with the proposal of the "in-plane" model stating that the BAX latch domain plays an active role in BAX apoptotic pore expansion by sliding into the lumen of a nascent BAX proteolipidic pore in such a manner that decreases its line tension (Westphal et al, 2014a). The intrinsic curvature of the dimeric BAX core domain may also contribute to enrichment of BAX molecules at the pore edge (Kuwana et al, 2016), thereby reducing pore line tension as proposed in the "clamp" model (Bleicken et al, 2014; Subburaj et al, 2015).

Finally, it was further characterized the inactive monomeric BAX membrane conformation, in both model membranes and in isolated mitochondria. This "lipid-primed" conformation of BAX displays some similarities, but also notable differences, with available high-resolution structures of BAX in lipid-free environments, which have been linked to early stages of the BAX activation process (Czabotar et al, 2013; Walensky & Gavathiotis, 2011) (Figures 3.10-3.12 and 1.7 respectively).

The most noticeable similarity is the "unlatching" of BAX C-terminal helices revealed by X-Ray crystal structures of domain-swapped BAX dimers (Czabotar et al, 2013). As regards to the "unlatched" BAX structure described by Czabotar et al., considering the diminishment of PEG5kDa exposure are much more prominent in multiple residues localized within or at the vicinity of BAX α7α8α9, together with the fact that α8 is a short amphipatic helix preceded by two glycines with potential for high conformational flexibility, it appears reasonable to propose that upon membrane binding at least the entire BAXα8 is detached from the core of the molecule and translocates to the membrane surface. In support of this possibility, according to previous studies of our lab (Dr Ane Landajuela´s thesis) with NBD-BAX and doxylated lipid, the F165 residue which is originally oriented towards the protein interior in soluble BAX, penetrates into the bilayer interior in the lipid-primed conformation of BAX.

On the other hand, based on the modest or negligible changes observed for residues 133 and 138 when BAX binds to membranes, it appears much less likely that BAXα6 is detached from the core of the molecule in the "lipid-primed" conformation of BAX. This is contrasting to the "unlatched" BAX structure found in membrane-free environments, where the three helices α6, α7 and α8 are completely dislodged from the rest of the molecule (Czabotar et al, 2013). Finally, the "lipid-primed" BAX conformation described here is clearly incompatible with the "BH3-in-groove" symmetric BAX dimer structure reported by Czabotar et al., since several residues directly implicated in BAX dimerization (T56 and R94) according to this X-ray structure do not undergo significant changes. Moreover, SCAM analysis suggest that in the "lipid-primed" conformation (i) the overall integrity of BAX canonical BH3-binding groove is retained, and (ii)

the orientation of the BAX molecule with respect to the membrane is optimal for allowing insertion of proapoptotic BH3 domains into BAX canonical groove.

In conclusion, this study provides novel structural and mechanistic information on structural details of BAX membrane topology and how BCLXL and lipids modulate the topology and the formation of lethal mitochondrial pores. These experimental approaches that can precisely monitor the structure and function of specific regions of BAX at the membrane level which may impact on the development of therapeutics that target this protein, and could potentially be used with other BCL2 family members as well.

CHAPTER 4:

BFL1 modulates apoptosis at the membrane level through a bifunctional and multimodal mechanism

4 BFL1 modulates apoptosis at the membrane level through a bifunctional and multimodal mechanism

4.1 ABSTRACT

BFL1 is a poorly understood apoptosis-regulatory BCL2 family protein that acts at the mitochondrial outer membrane (MOM) level through a complex protein:protein and protein:lipid interaction network. In this chapter, was carried out a comprehensive analysis on the mode of BFL1 action based on quantitative studies performed in both cellular and minimalist model systems, and taking into account the role of the MOM environment. On the one hand, it is shown that in membranes with nonapoptotic lipid compositions BFL1 displays three distinct antiapoptotic modes, all of which are based on canonical heterodimerizing interactions between BFL1 and its proapoptotic BCL2 family binding partners. On the other hand, these studies revealed that apoptotic-like membranes obstruct the three antiapoptotic activities of BFL1 and unleash a prodeath activity that is based on noncanonical homooligomerization and pore formation of the protein. Moreover, they were also identified mechanistic similarities and dissimilarities between BFL1 and BCLXL, the paradigmatic antiapoptotic BCL2 family protein. Based on these findings can be proposed that BFL1 modulates apoptosis through a bifunctional and multimodal mechanism of action that is susceptible to regulation by the MOM lipid composition.

4.2 INTRODUCTION

Apoptotic programmed cell death plays an essential role in many human cell physiological processes and pathologies. During apoptosis, cellular stress signals converge in the mitochondria to induce mitochondrial outer membrane permeabilization (MOMP) (Czabotar et al, 2014). MOMP typically represents the point of no return in the mitochondrial apoptotic pathway and it is mainly regulated by BCL2 family proteins. Members of this protein family are typically divided in three groups based on their general impact in cell viability and the presence of up to four conserved BCL2 homology (BH) motifs: (i) BCL2-type apoptosis repressors, which contain all four BH motifs and primarily function by inhibiting MOMP (BCL2, BCLXL, BFL1, and others); (ii) BAX-type apoptosis effectors, which contain BH1-BH3 motifs and directly elicit the MOMP once they are activated (BAX, BAK and perhaps BOK); and (iii) BH3-only apoptosis activators (BID, BIM, NOXA, and others), which instigate the function of BAX-type effectors (Chen et al, 2005; Letai et al, 2002). Despite the relevance of the above classification, many unanswered questions exist concerning the molecular mechanisms by which BCL2 family proteins exert their biological function. Chief among them is to elucidate the exact pattern of interactions comprising the BCL2 interactome and their precise structural nature (Basanez et al, 2012; Czabotar et al, 2014; Delbridge et al, 2016)(Basanez et al, 2012; Czabotar et al, 2014; Delbridge et al, 2016)(Basanez et al, 2012; Czabotar et al, 2014; Delbridge et al, 2016)(Basanez et al, 2012; Czabotar et al, 2014; Delbridge et al, 2016)(Basanez et al, 2012; Czabotar et al, 2014; Delbridge et al, 2016)(Basanez et al, 2012; Czabotar et al, 2014; Delbridge et al, 2016)(Basanez et al, 2012; Czabotar et al, 2014; Delbridge et al, 2016)(Basanez et al, 2012; Czabotar et al, 2014; Delbridge et al, 2016)(Basanez et al, 2012; Czabotar et al, 2014; Delbridge et al, 2016)(Basanez et al, 2012; Czabotar et al, 2014; Delbridge et al, 2016)(Basanez et al, 2012; Czabotar et al, 2014; Delbridge et al, 2016), particularly taking into account the mitochondrial outer membrane (MOM) environment. This is important in view of the high complexity and diversity of protein:protein interactions involving BCL2 family members, and also considering that during apoptosis most, if not all, BCL2 family proteins are targeted to the MOM via a C-terminal Tail-Anchor (TA) motif (Lindsay et al, 2011).

From a structural viewpoint, it is remarkable that despite their opposing biological functions, antiapoptotic and proapoptotic multidomain BCL2 family members share the same globular folding solution, characterized by eight amphipatic helices surrounding a central hydrophobic helix (Muchmore et al, 1996; Suzuki et al, 2000). Moreover, all multidomain BCL2 family proteins display an elongated hydrophobic groove mostly comprising BH1 and BH2 motifs that serves as a receptor-site for binding BH3 motifs of ligand partners. Solution-based structural and biochemical studies revealed that this canonical BH3:groove interaction mechanism relies in

engagement of several hydrophobic residues of the BH3 ligand into corresponding hydrophobic binding pockets on the receptor groove, together with formation of a salt bridge between strictly conserved Asp and Arg residues at the BH3 ligand and BH1 receptor sites, respectively (Czabotar et al, 2013; Moldoveanu et al, 2013). However, since the canonical BH3:groove interface has been principally characterized in membrane-free environments, it may not represent the main or exclusive protein:protein interaction surface through which BCL2 family proteins modulate the apoptotic process once they are localized in the MOM. Consistent with this notion, in recent years an increasing number of non-canonical interaction surfaces have been identified in a variety of BCL2 family proteins (Andreu-Fernandez et al, 2017; Barclay et al, 2015; Gavathiotis et al, 2008). Two prominent examples are the BH4 and TA motifs of BCL2 and BCLXL which can mediate heterodimeric interactions with BAX implicated in apoptosis repression. However, it remains to be clarified whether non-canonical interactions universally contribute to apoptosis inhibition by BCL2-type proteins.

In fact, despite intense research effort, a consensus view is still missing on how BCL2-type proteins inhibit apoptosis via protein:protein interactions. Early models proposed that BCL2 and its close homologues repress apoptosis by forming stable neutralizing heterodimers either with proapoptotic BAX-type effectors (direct model), or with BH3-only activators (indirect model)(Korsmeyer et al, 1993). Subsequent models shifted towards a bimodal interaction mode of action where antiapoptotic proteins stably sequester the two classes of proapoptotic molecules, rather than only one of them (Chen et al, 2015; Leber et al, 2007; Llambi et al, 2011). At the same time, these bimodal models differed regarding specific features of the BCL2 interaction network.

For example, the embedded-together model emphasized that the MOM environment is critical to expose otherwise hidden non-canonical surfaces in BCL2-type repressors that are generally required for their interaction with and neutralization of BAX-type effectors and BH3-only activators. The unified model ascribed less prominent roles to the MOM and to non-canonical interactions in the BCL2 interactome, and further proposed that BCL2-type repressors invariably bind BAX-type effectors strongly than BH3-only activators. The interconnected hierarchical model gave no particular importance to the MOM and to non-canonical interactions, and postulated that in the course of the apoptotic process, repressors always sequester activators before and with higher affinity than effectors. In addition, recent studies uncovered a distinct antiapoptotic mode of action for BCLXL which is not appropriately integrated in any of the bimodal interaction models described above(Edlich et al, 2011b; Schellenberg et al, 2013; Todt et al, 2015; Todt et al, 2013). Here, even under nonapoptotic conditions, BCLXL keeps BAX inactive using a retrotranslocation activity mediated through canonical and non-canonical BCLXL:BAX interactions of transient nature. Importantly, it remains to be clarified whether or not the BAX retrotranslocation activity recently discovered for BCLXL constitutes a general

antiapoptotic mode of action for all BCL2-type proteins. On top of this, another long-standing and often overlooked issue in the BCL2 research field is the capacity of every antiapoptotic protein examined to date to promote –rather than inhibit- apoptosis under defined conditions, although the exact mechanisms and molecular interactions underlying the proapoptotic functions of BCL2-type proteins are incompletely understood (Basanez et al, 2012; Basanez et al, 2001; Cheng et al, 1997).

BFL1 is one of the least extensively studied BCL2-type proteins. It is accepted that BFL1 plays a key role in preventing apoptosis under specific physiological settings and that BFL1 represents a promising target for therapeutic intervention against selected types of human cancer, akin to BCL2 and BCLXL. In fact, BFL1 is a recognized contributing factor for chemoresistance to diverse anticancer agents, including navitoclax recently approved by the FDA. However, the molecular mode of action of BFL1 is much less well understood than those of BCL2 and BCLXL. In this chapter, a thorough analysis of the mechanism of BFL1 action at the molecular level is performed, using a multidisciplinary analysis based on quantitative biophysical techniques applied to cellular and minimalist model systems, and paying special attention to the potential role of the membrane environment in the pattern and nature of BFL1 protein:protein interactions.

These studies revealed that BFL1 displays three distinct antiapoptotic modes in the presence of a membrane environment, all of which are exclusively elicited through canonical heterodimerizing interactions between BFL1 and its proapoptotic partners. Additionally, it is described a novel proapoptotic mode of action of BFL1 unleashed by the mitochondrial lipid cardiolipin (CL) and mediated by non-canonical homooligomerization and membrane poration activities of the protein. Here, common and distinguishing features between the molecular mechanisms of action of BFL1 and BCLXL were also identified. Based on these collective findings, it is proposed a new bifunctional and multimodal model for apoptosis regulation by BCL2-type proteins.

4.3 MATERIALS AND METHODS

In this section materials and methods required in this chapter are detailed briefly, a more extended explanation and specific information is described in the second chapter: general materials and methods.

Chemicals and reagents.

Phosphatidylcholine (PC), Phospatidylethanolamine (PE), Phosphatidylinositol (PI), 18:1 DGS-NTA (Ni) and Heart-Cardiolipin (CL) were from Avanti Polar Lipids (Alabaster, AL, USA). DiD,

DIO and Hoechst 33342 (Invitrogen). Alexa Fluor 488 C5 Maleimide and Alexa Fluor 647 C2 Maleimide were from (Thermofisher). 1, 3, 6, aminonaphtalene-tri-sulfonate (ANTS) and p-xilene-bis-dipicolyinicacis (DPX) were purchased from Molecular Probes (Eugene, OR, USA). All other reagents were from Sigma (St. Louis, MO, USA).

Retrotranslocation assays: FLIP measurements and plasmids.

FLIP experiments were done based on (Edlich et al, 2011a) and as explained in the general materials and methods chapter. First, BAX/BAK DKO HCT116 cells were seeded on 1µ-Slide 8 Well ibitreat (ibidi) in McCoy's 5A medium, grown for 20 hr, transfected, and incubated for 6h-16h at 37ºC with 5% CO_2. Confocal analysis was performed on a Zeiss confocal LSM710 microscope equipped with 63X oil objective and laserlines to excitate at 488, 561 or 633. For GFP-BAX translocation assay, the cells were incubated with mitotracker-far red for 30 min prior to analysis. Then, we substituted the media for McCoy's 5A medium with 10mM HEPES and without phenol red and incubated 30 min at 37ºC with 5% CO_2. Then, a single spot with a diameter of 1,3 µm within the nucleus was repeatedly bleached with two iterations of 100% power of a 488 nm laser line (100% output). The diameter of a single ROI was 0,52µm. Two images were collected after each bleach pulse, with 30 s between bleach pulses. After collecting 60 images, two separate measurements on the mitochondria were taken to analyse the fluorescence loss. Unbleached control cells were monitored for photobleaching due to image acquisition. The rate of loss in fluorescence on the mitochondria was calculated from fluorescence intensity measurements using the Zeiss LSM software. The fluorescence intensities were normalized by setting the initial fluorescence to 100% signal. Plots are shown as normalized fluorescence over time. GFP-BFL1 plasmid was generated by PCR-based sequence amplification and posterior insertion in pEGFP-C3 (from EGFP-BAK, a generous gift from Richard Youle (Addgene plasmid # 32564), whereas plasmids of non-labelled BAX and cBID were inserted in pCi-neo-myc vectors. Furthermore, GFP-BAX WT and GFP-BAX-1-2/L-6 plasmids were provided thankfully by N. Brady and F. Edlich, respectively. Finally, we thank Dr. Frank Essmann and Prof. Klaus Schulze-Osthoff for providing the $Bax^{-/-}Bak^{-/-}$ DKO HCT116 cells.

Purification and labelling of recombinant BCL2 family proteins.

Mutant DNAs were generated by PCR-based mutagenesis using the Quickchange mutagenesis kit (Stratagene, San Diego, CA, USA), purchased at Addgene and GenTech (Montreal, Canada). All constructs were verified by sequencing. Full-length human BAX and cBID and their variants BAX C62S, C126S, E6C, cBID C30S and BFL1ΔC and its variants for fluorescent labelling were purified as described in the general material and method chapter and in (Bleicken et al, 2013a; Landeta et al, 2015; Landeta et al, 2011). cBID and BCLXLΔC (BCLXL lacking the C-terminal 24 aminoacids) were expressed and purified as described earlier in the general materials and

methods chapter and (Terrones et al, 2004; Terrones et al, 2008). All protein preparations were >95% pure as assessed by SDS-PAGE and Coomassie staining. In a typical protein labelling reaction, $AlexaFluor_{488}$/$AlexaFluor_{647}$ dissolved in DMSO were added to a 1 ml sample containing ≈25μM of BCL2 protein at a labelling reagent/BCL2 protein molar ratio of 10:1, samples were incubated overnight at 4 ºC, and subsequently eluted over a PD-10 column pre-equilibrated with 100 mM KCl, 10 mM Hepes, pH 7.4 1 mM EDTA (KHE buffer).

Circular dichroism.

The CD spectra were collected using the following parameters a 1-nm step size over 260 to 200nm wavelength range, speed 50nm/min; response 1s; bandwidth 2nm in a spectropolarimeter Jasco J-810 (Jasco Spectroscopic Co. Ltd., Hachioji City, Japan) equipped with a JASCO PTC-423S temperature control unit. Each measurement was the average of 20 scans, which was background-subtracted. All samples were allowed to equilibrate for 10min prior to CD analysis. Secondary structure content was estimated from the far-UV spectra using CDPro software (http://lamar.colostate.edu/-sreeram/CDPro/main.html) (Sreerama & Woody, 2004a; Sreerama & Woody, 2004b). To assess the thermal stability of the BCL2 proteins studied, CD data was collected at 222nm wavelength every 1°C from 25°C to 90°C. The midpoint of the melting transition was estimated using the first derivative converter available in the software of the CD instrument with a window of nine data points and a 2nd degree polynomial smoothing. Protein concentration in all case was 3μM in PBS buffer.

TIRF experiments. Supported lipid bilayers formation and data acquisition.

LUVs were incubated with 0.5nM of BFL1ΔCg, BFL1ΔCg L21A and BFL1ΔCg R88D to be in the single-molecule regime, for 1h at room temperature. After the indicated incubation time, BFL1ΔCg-containing proteoliposomes were used to create SLBs on piranha-cleaned glass slides (0.13–0.16-mm thickness, Menzel) (for details see (Subburaj et al, 2015)) without any lipid dilution and the SLBs were immediately imaged. SLB were analysed using a modified Zeiss Axiovert 200M epifluorescence microscope using a 488 laser (Ichrome MLE-LFA multi laser, Toptica) equipped with a α Plan-Fluor 100x/1.46 oil objective (Zeiss), a Laser-TIRF 3 Imaging System (Zeiss) and a EM-CCD camera (iXon 897, Andor). Samples were illuminated for 35 ms with a delay time between frames of 25 ms (number of frames 1000) with an intensity of ~ 0.1 kW/cm2.

Stoichiometry analysis. The images acquired were used for the stoichiometry analysis based on the fluorescence intensity of the particles using an in-house algorithms implemented in Python (Python Software Foundation, https://www.python.org/). Bright spots were automatically

detected using an implementation of the Difference of Gaussians method (http://scikit-image.org/docs/dev/api/skimage.feature.html) and thresholding. Selected particles were defined by a region of interest (ROI) of a defined pixel size (2x2) and fitted to two-dimensional (2D) Gaussians. Background subtraction was performed by defining a ROI around the particle´s ROI having a larger pixel size (3x3). Localized particles were discarded based on the distance and on the width of the 2D Gaussian, to avoid overlapping ROIs or multiple particles in the same ROI. This algorithm provided the brightness value for each spot. Stoichiometry counting was performed using the brightness analysis method as previously described (Subburaj et al, 2015). Briefly, the obtained brightness values were plotted as a probability density function or as a Gaussian distribution. Monomeric BFL1ΔCg particles were obtained by spreading BFL1ΔCg particles directly on a cleaned glass coverslip and selected by photobleaching analysis (Ulbrich & Isacoff, 2007) after smoothing of the signal with a median filter. For this purpose, individual particles with a single photobleaching step were detected via a threshold and their fluorescence intensity was estimated by fitting with a Gaussian. By convolution, the monomer brightness distribution was used to calculate the brightness distributions for higher oligomers. Finally, the overall brightness distribution was fitted by a linear combination of the N-mer contributions. The area under each curve was used to calculate the percentage of occurrence of each species, which was further corrected by taking into account that not all BFL1ΔCg molecules in a particle are labelled due to partial labelling. Correction for partial labelling efficiency was performed as previously described (Subburaj et al, 2015). Only proteins having > 60% labelling efficiency were considered for experiments and data collection. The graphs with the distribution of species correspond to the average values obtained from the different experiments, and the error bars correspond to the averaged errors in the individual experiments, as they were larger than the S.D.

GUV preparation.

GUV-type vesicles were prepared as described previously in the general materials and methods chapter and in (Bleicken et al, 2013a). Briefly, around 4 µl of the lipid mixture stock (1 mM) in chloroform was spread on the platinum wires of the electroformation chamber. After solvent evaporation, the wires were immersed in 200 mM sucrose buffer, and electric pulses of 10 Hz were provided for 2 h, followed by 2-Hz pulses for 30 min. Due to lower GUV stability relative to LUV/SUV-type liposomes, we used GUV with the following lipid compositions: PC60/PE30/PI10/CL0 (0% CL), PC35/PE30/PI10/CL25 (mol/mol) (25%CL), and CL (100% CL).

GUV permeabilization and size determination experiments.

BCL2 family proteins and Rho-4-kDa dextran/APC were mixed in LabTec chambers (NUNC) with 1,2-diphytanoyl-sn-glycero-3-phosphoethanolamine-N-(7-nitro-2-1,3-benzoxadiazol-4-yl)-

labelled GUV to a final volume of 400 µl (KHE buffer). After 2 h of incubation at room temperature, images collected with a confocal fluorescence microscope (see microscope specifications below). The percentage of fluorescent probes internalization to the lumen of GUV was measured with ImageJ software as described previously (Bleicken et al, 2013a; Landeta et al, 2015) .Size determination was performed manually by using the measurement tool in the ImageJ.

GUV Confocal Microscopy Analysis.

Microscopy observations of protein recruitment to GUV, FCCS and two-focus SFCCS measurements in GUV were prepared as described previously (Landeta et al, 2015). In brief, for the observation of protein binding to GUV membrane fluorescently labelled proteins and liposomes were incubated together for 2 h at 22/37/43 °C. Fluorescence images were processed with ImageJ software using the plug-in "Radial profile," where the protein bound to the GUV membrane was normalized to the values obtained in solution. FCCS measurements were performed at 22 °C using a ConfoCor3 module with attenuated excitation light from argon ion (488 nm) and helium-neon lasers (633 nm). Proteins were incubated in the observation chamber for 20 min before carrying out FCCS measurements.

To obtain auto- and cross-correlation curves, raw fluorescence fluctuation data were fitted to a three-dimensional diffusion model with homemade software. For two-focus SFCCS measurements in GUV, the measurement time was 300 s, and the bin time was 2 µs. The autocorrelation and spectral and spatial cross-correlation curves were computed from the intensity traces, and irregular curves resulting from instability and distortion were excluded from the analysis. We fitted the auto- and cross-correlation functions with a nonlinear least-squares global fitting algorithm (2Dimensions 2Focus 2Color). As a result of the analysis of FCCS data, surface concentrations of single colour particles (Cr and Cg) and two-colour particles (CCrg) as well as their diffusion coefficients were determined. FCCS results were also corrected for fluorescence cross-talk and for protein labelling degrees (BFL1ΔCg WT, L21A and R88D 70-73-68% respectively, BFL1ΔCr 65-70-70% respectively, BAXr 60% and cBIDr 60%). Complex % values were calculated with respect to the amount of the green particles (CCrg X 100/Cg), being the percentage value between CCrg two-colour particles (the green and red complexed molecules) and the total green particles (the free and the complexed ones). The theoretical maximum of the %CC was calculated relative to the labelling efficiencies as described in (Bleicken et al, 2017; Ries et al, 2010).

Liposome preparation.

MOM-like lipid mixtures were co-dissolved in chloroform/methanol (2:1), and organic solvents were removed by incubation under vacuum for 2h. Dry lipid films were resuspended in 100 mM KCl, 10 mM Hepes, pH 7.4 1 mM EDTA (KHE buffer), except in experiments were 20 mM KCl, 10 mM Hepes pH 7.0, 1 mM EDTA, 12.5 mM ANTS and 45 mM DPX was used. Liposomes were then subjected to 10 freeze/thaw cycles, and subsequently extruded 10 times through two polycarbonate membranes of 0.2-µm pore size (Nucleopore, San Diego, CA) to obtain large unilamellar vesicles (LUVs).

Lipid peroxidation assay.

LUV of PC/PE/PI and PC/PE/PI/CL (3mM lipid mixture in EDTA-free ANTS/DPX buffer) were incubated at 37ºC after addition of $CuCl_2$ (20µM) at zero time. Copper-induced oxidation was monitored at 245nm according to (Klein, 1970; Pinchuk et al, 1998; Schnitzer et al, 1998; Schnitzer et al, 2007) in a Uvikon 922 spectrophotometer (Kontron instruments, Groβ-Zimmen, Germany), using quartz cuvettes with absolute ethanol in reference cell.

Steady-state fluorescence spectroscopy.

Fluorescence intensity and spectral analyses were done in an 8100 Aminco-Bowman luminescence spectrometer (Spectronic Instruments, Rochester, NY), in thermostatically controlled 4x4-mm quartz cuvettes, at 25 °C. Trp spectra were recorded between 305 nm and 405 nm at a scan rate of 1 nm/s, using an excitation wavelength of 295 nm (slits 4 nm). Release of LUV-encapsulated ANTS/DPX was monitored with λ_{ex}=350 nm, and λ_{em}=520 nm (slits, 8 nm). The extent of marker release was quantified on a percentage basis, 10 min after cBID addition, according to the equation: $(F_t\text{-}F_0/F_{100}\text{-}F_0)$ x100, where F_t is the measured fluorescence of protein-treated LUVs at time t, F_0 is the initial fluorescence of the LUV suspension before protein addition, and F_{100} is the fluorescence value after complete disruption of LUVs by addition of $C_{12}E_8$ detergent (0.5 mM). Unless otherwise stated, BAX, cBID, BFL1, concentrations were 150 nM. Lipid concentration was 150 µM.

Size exclusion chromatography.

BCL2 proteins (5µM) were incubated at 37ºC for 1h under continuous stirring in solution and in the presence pure CL LUV (500µM lipid in KHE). Then, liposomes were solubilized with 3% CHAPS final concentration for 30min at RT, and loaded in a pre-equilibrated (buffer B with 3% CHAPS) Superdex75.

Cyt c release assay in isolated mitochondria.

$BAX^{-/-}/BAK^{-/-}$DKO human colon tumour (HCT) 116 cells were harvested by scrapping, and homogenized with a glass-Teflon Potter-Elvehjem homogenizer in mitochondrial isolation buffer (210 mM mannitol, 70 mM sucrose, 10 mM Hepes (pH 7.5), 1 mM EDTA, and protease inhibitors). After removing heavy membrane fractions by two consecutive centrifugations at 700 *g* for 10 min at 4 ºC, mitochondria-enriched fractions were pelleted by centrifuging the resultant supernatant at 14000 *g* for 10 min at 4 ºC. Mitochondria (50 µg total protein) were incubated with recombinant BAX (100 nM) with or without cBID (10 nM) in release buffer (125 mM KCl, 5 mM KH_2PO_4, 2 mM $MgCl_2$, 1 mM DTT, and 10 mM HEPES-KOH, pH 7,4), for 30 min at 30 ºC. Samples were then centrifuged at 14000 *g* for 10 min, and supernatant and pellet fractions were subjected to SDS-PAGE and immunoblotting analysis using anti-cyt *c* 7H8.2C-12 (BD-Biosciences, San Jose, CA, USA)

Cyt c release assay in semi-intact cells.

Transfected BAX/BAK DKO HCT116 cells ($\approx 10^6$) were harvested by scrapping and resuspended in permeabilization buffer consisting of 120 mM KCl, 10 mM NaCl, 1 mM KH2PO4, 20mM HEPES-Tris (pH 7.4) supplemented with 0.025% w/v digitonin. Then, digitonized cells were were pelleted by centrifuging the resultant supernatant at 14000 *g* for 10 min at 4 ºC. Semi intact cells were incubated with recombinant BAX variants (100 nM) with or without cBID (50 nM) in release buffer for 30 min at 30 ºC. Samples were then centrifuged at 14000 *g* for 10 min, and supernatant and pellet fractions were subjected to SDS-PAGE and immunoblotting analysis using anti-cyt *c* 7H8.2C-12 (BD-Biosciences, San Jose, CA, USA), and anti-GFP ChIP grade ab290.

GFP-BCL2 proteins localization, cyt c release by immunoblotting and nucleus morphology analysis.

$BAX^{-/-}/BAK^{-/-}$ DKO and WT HCT 116 cells growing into a coverslip were transiently transfected with jetPRIME for 16h, thereafter, if necessary, were treated with 1µM rotenone/staurosporine (0, 4, 8 and 16h). Then, cells were incubated with Mitotracker (Red CMX Ros, invitrogen) 200nM at 37oC for 30min and washed twice with PBS before fixation with 3,8% paraformaldehyde. Next, coverslips were immunoblotted with a primary anti-cyt antibody (life technologies) and a secondary fluorescent anti-mouse 633 (life technologies) and finally nucleus, were dyed with Hoechst 33342 (Invitrogen). Samples were visualized in an inverted confocal microscope (TE2000 U, Nikon, Melville, NY) equipped for epifluorescence and with a Nikon D-eclipse C1si confocal spectral detector, using an X60, 1.45 numerical aperture, oil immersion objective. Images were processed by FiJi.

Apoptotic nuclei characterization in living cells.

$BAX^{-/-}/BAK^{-/-}$DKO HCT 116 cells were growth and transfected as describe above, and then cells were treated with the toxicant (rotenone or staurosporine 1µM for 6h at 37ºC with 5% CO2). Next, we substituted the media for a prewarmed media containing 1µM Hoechst 33342 and 3µM propidium iodide (Sigma) for 30 min. Subsequently, cells membrane integrity (PI containing cells) and nucleus morphology of transfected cells were analyse by using Leica DMI3000 and processed using Fiji.

4.4 RESULTS

4.4.1 BFL1 retrotranslocates BAX from mitochondria and mitochondria-like liposomes under nonapoptotic conditions through canonical, rather than non-canonical, interactions.

BCLXL has been shown to maintain BAX inactive in healthy cells by continuously retrotranslocating BAX from the mitochondria into the cytosol. Thus, it was first analysed whether BFL1 shares with BCLXL this mode of action. GFP-BAX was ectopically expressed in BAX/BAK DKO HCT116 cells in the presence or absence of BFL1, and GFP-BAX retrotranslocation was analysed under nonapoptotic conditions using Fluorescence Loss In Photobleaching (FLIP) (Figure 4.1A)(Edlich et al, 2011a). To this aim, it was repeatedly bleached a region in the nucleus of a transfected cell (Figure 4.1B, white square), and the decay of GFP fluorescence in the targeted cell was followed by assigning regions of interest in the cytoplasm (Figure 4.1B, green circle) and on the mitochondria (Figure 4.1B, red and blue circles). GFP-BAX readily crosses the nuclear envelope, and cytosolic GFP-BAX fluorescence of the targeted cell was rapidly bleached by FLIP, whereas the neighboring reference cell fluorescence (black circle) remained stable. After reducing the cytosolic GFP-BAX signal, the mitochondrial GFP-BAX pool was readily apparent (Figure 4.1C, arrow). Consistent with previous reports, the decay of mitochondrial GFP-BAX fluorescence by FLIP occurred in a time frame of about 10 minutes following a first-order kinetic at a rate that is markedly slower than that of cytosolic GFP-BAX (Figures 4.1D and 4.1E). Importantly, BFL1 overexpression increased the FLIP rate of mitochondrial GFP-BAX without affecting the FLIP rate of cytosolic GFP-BAX (Figure 4.1D and 4.1E).

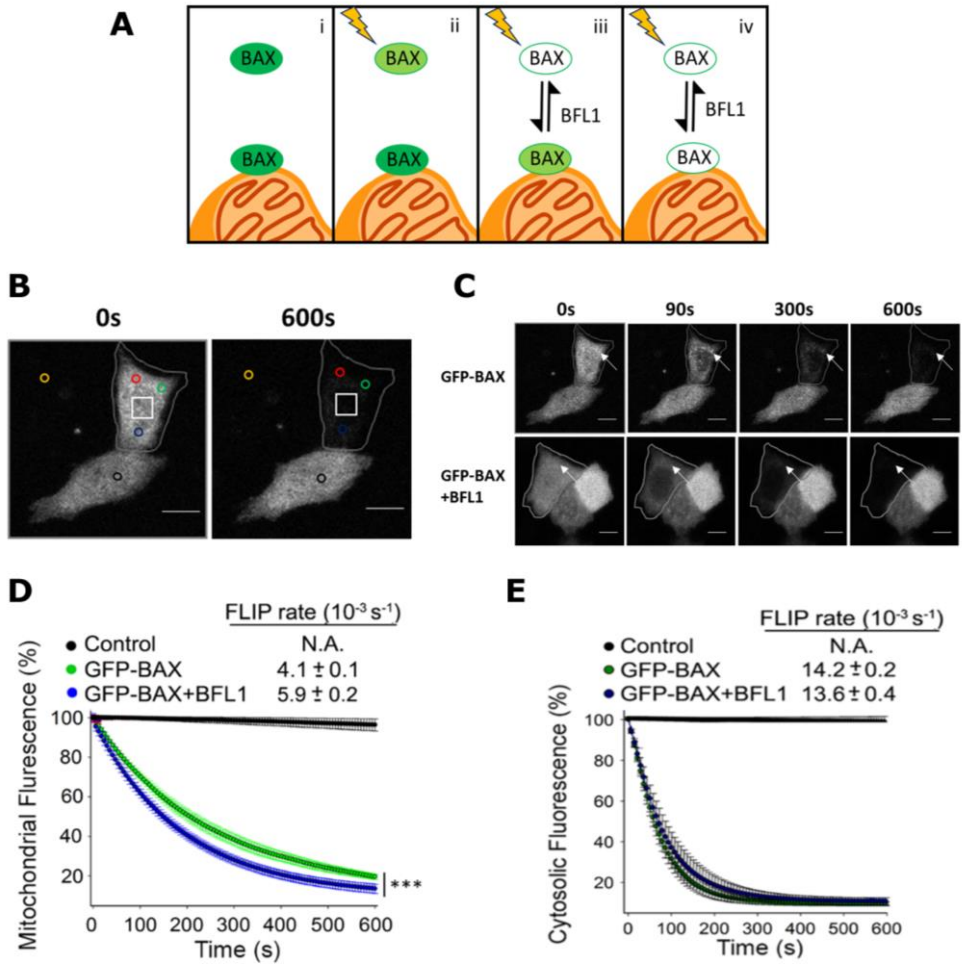

Figure 4.1. BFL1 retrotranslocates BAX from mitochondria. (A), Pictorial scheme of experimental design: (i) Before bleaching, GFP-BAX was localized in mitochondria and cytosol; (ii) FLIP bleaches cytosolic GFP-BAX; (iii) bleached GFP-BAX molecules translocate to the mitochondria while fluorescent GFP-BAX retrotranslocates into the cytoplasm; (iv) After continued FLIP, all GFP-BAX molecules are bleached. (**B)**, GFP-BAX fluorescence monitorization in a typical FLIP experiment. Region marked as a white square was bleached 20 times at 488nm. GFP-BAX fluorescence variations on the mitochondria are detected in two areas (red circle and green circle, respectively), and changes in the cytosolic fluorescence (blue circle). Black circles indicate adjacent cells fluorescence, which serves as a control for cell-specific bleaching. Scale bars, 10µm. (**C-D)**, **Mitochondrial GFP-BAX fluorescence was monitored during fluorescence loss in photobleaching (FLIP) assay. (C)**, representative images showing time-dependent FLIP of GFP-BAX in the absence (top) and presence (bottom) of overexpressed BFL1. Arrows denote mitochondria. Scale bars, 10µm (***D),*** Average FLIP kinetics for multiple cells expressing only GFP-BAX (green line) and in the presence of BFL1 (blue line). (**E)**, Average FLIP cytosolic kinetics for multiple cells expressing only GFP-BAX (green and black line) and in the presence of BFL1 (blue and black line). n>20 ROI for each condition of 3 independent experiments. Control represents GFP-BAX fluorescence in a neighbor cell. ***, *p*= <0.001. *Error bars*, S.D.

GFP-BFL1 also showed a dynamic localization between mitochondrial and cytosolic compartments in nonapoptotic HCT116 BAX/BAK DKO cells, and BAX overexpression increased the FLIP rate of mitochondrial, but not cytosolic, GFP-BFL1 (Figure 4.2A). These results strongly suggest that in intact nonapoptotic HCT116 BAX/BAK DKO cells BAX and BFL1 co-retrotranslocate together from the mitochondria into the cytosol, analogous to previous results obtained with BAX and BCLXL. Nevertheless, comparing these results with prior data it became apparent that BFL1 and BCLXL do not behave in an identical manner, since: (i) BFL1 overexpression accelerates mitochondrial GFP-BAX retrotranslocation to a lower extent (44%) than BCLXL overexpression (83%), and (ii) GFP-BFL1 retrotranslocates from mitochondria with a higher FLIP rate (4.6 ± 0.2 X $10^{-3}s^{-1}$) than GFP-BCLXL (1.4 ± 0.1 X $10^{-3}s^{-1}$). Next, it was also examined the performance of a BAX variant which is predictably unable to heterodimerize with BFL1 through canonical BH3:groove and non-canonical BH4:BH4 interactions due to intramolecular tethering (GFP-BAX 1-2/L-6). The GFP-BAX 1-2/L-6 mutant displayed a very low mitochondrial retrotranslocation rate that did not detectably change upon BFL1 overexpression (Figure 4.2B).

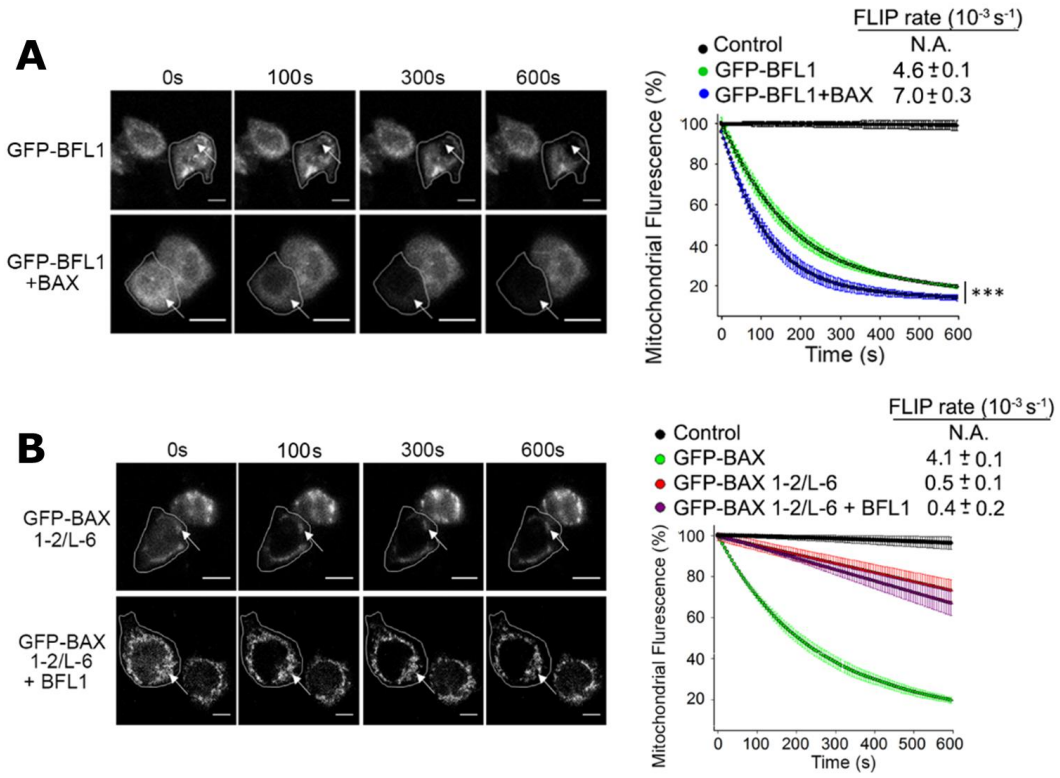

Figure 4.2 BFL1 and BAX are in a codependent dynamic equilibrium between cytosol and the membrane. (A), Mitochondrial GFP-BFL1 fluorescence was monitored during fluorescence loss in photobleaching (FLIP) assay. ***Left***, Representative images showing time-dependent FLIP of GFP-BFL1 in the absence (top) and presence (bottom) of overexpressed BAX. Arrows denote mitochondria. Scale

bars, 10µm ***Right,*** Average FLIP kinetics for multiple cells expressing only GFP-BFL1 (green line) and in the presence of BAX (blue line). >20 ROI for each condition of 3 independent experiments. Control represents GFP-BFL1 fluorescence in a neighbor cell. ***, *p*= <0.001. *Error bars*, S.D. (**B-Left),** Representative images showing time-dependent FLIP of GFP-BAX 1-2/L6 in the absence (top) and presence (bottom) of overexpressed BFL1. Arrows denote mitochondria. Scale bars, 10µm (**B-Right),** Average FLIP kinetics for multiple cells expressing only GFP-BAX 1-2/L6 (redline) and in the presence of BFL1 (purple line). >20 ROI for each condition of 3 independent experiments. Control represents GFP-BAX 1-2/L6 fluorescence in a neighbor cell.

Then, it was examined whether the BFL1-mediated BAX retrotranslocation process observed in intact healthy cells can also be reproduced in minimalist systems (Bleicken et al, 2013a; Bleicken et al, 2013b; Landeta et al, 2015; Lovell et al, 2008). To this aim, BFL1ΔC26 lacking its TA motif (termed BFL1ΔC hereafter) was used because this construct can be obtained in a highly purified and homogeneous form, and also since a number of cellular studies showed that BFL1ΔC preserves the antiapoptotic function of BFL1 (Brien et al, 2009; Kucharczak et al, 2005). Unfortunately, FLIP methodology cannot be applied in this experimental system because the inter-GUV areas could not be bleached efficiently. Thus, as in a recent study with BCLXL and BAX (Bleicken et al, 2017), the extent of binding of fluorescently-labelled BCL2 family proteins is quantitatively analysed to individual GUVs using confocal fluorescence microscopy. First, BFL1ΔC and BAX variants respectively were produced and subsequently labeled with Alexa 488 and Alexa 647 fluorophores (termed BFL1ΔCg and BAXr hereafter), and it was confirmed that these proteins retain the basic structural and functional properties of their native unlabeled counterparts (Figure 4.3) (Bleicken et al, 2016).

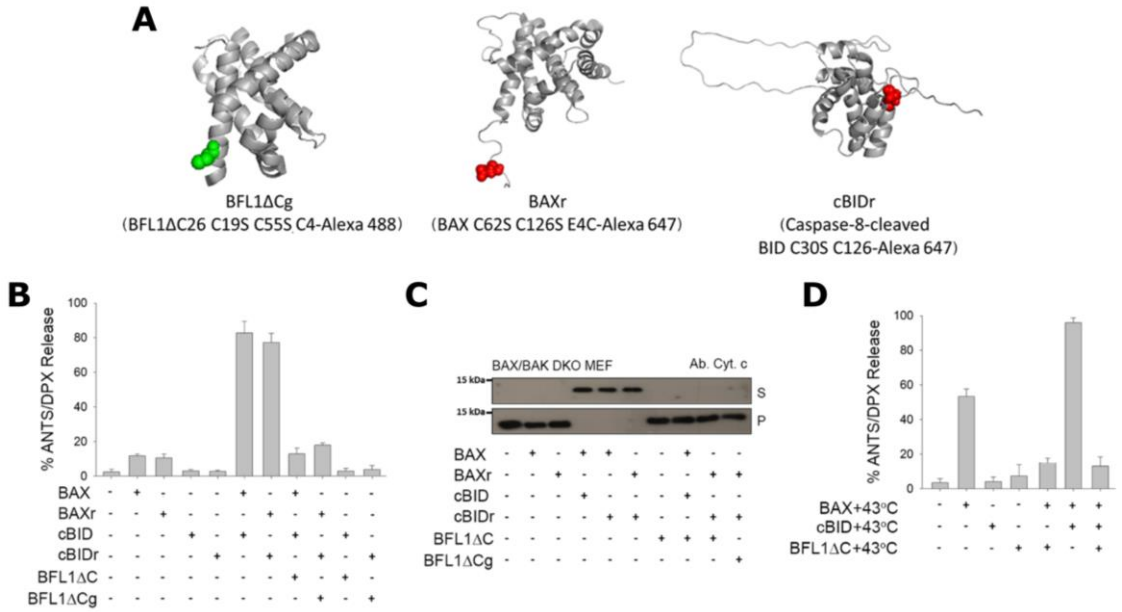

Figure 4.3 BFL1ΔCg, BAXr, and cBIDr maintain structural and functional properties of native unlabeled counterparts. (A), Three-dimensional structures of BFL1ΔC26 (PDB code 2VM6), BAX (PDB code 1F16), and BID (PDB code 1DDB) displaying as *colored spheres* the monocysteine residue where the Alexa-fluorophore is conjugated to generate BFL1ΔCg, BAXr, and cBIDr variants used in this study. (**B**), Percentage of ANTS/DPX permeabilized LUV in the presence or absence of the indicated BCL2 proteins (cBID$_{(R)}$=150nM, BAX$_{(R)}$=150nM and BFL1ΔC$_{(G)}$=450nM) at room temperature. Mean values ± S.D. (*error bars*) correspond to 3 independent experiments. (**C),** Effect of BCL2 proteins on the release of cytochrome *c* from mitochondria isolated BAX$^{-/-}$/BAK$^{-/-}$ DKO HCT116 (BAX/BAK double knock out human colon carcinoma cells). **(D),** Percentage of ANTS/DPX permeabilized LUV as explained in (**B)** section but at 43ºC.

Next it was proceeded to the incubation of fluorescently-labelled proteins, alone or combined, with Mito-like GUVs containing different amounts of CL for 2h, and the increase of fluorescence intensity at the rim of the GUV membrane was visualized and quantified for multiple individual vesicles. As shown in Figure 4.4A-B, BFL1ΔCg and BAXr, alone or in combination, did not significantly bind to GUVs devoid of CL (0% CL GUVs). However, BAXr but not BFL1ΔCg, appreciably bound to GUVs containing CL levels that are typically found in mitochondrial contact sites (CS) under nonapoptotic conditions (25% CL). Importantly, co-incubation with BFL1ΔCg reduced by more than 70% the mean level of BAXr binding to 25% CL GUVs. By contrast, BFL1ΔCg and BAXr, each one alone, bound extensively to 100% CL GUVs emulating CL microdomains described in apoptotic cells, and co-incubation with BFL1ΔCg did not significantly reduce BAXr binding to this type of GUVs. These results suggest that BFL1 lacking its TA motif can retrotranslocate BAX from Mito-like GUVs under healthy-, but not apoptotic-like, conditions.

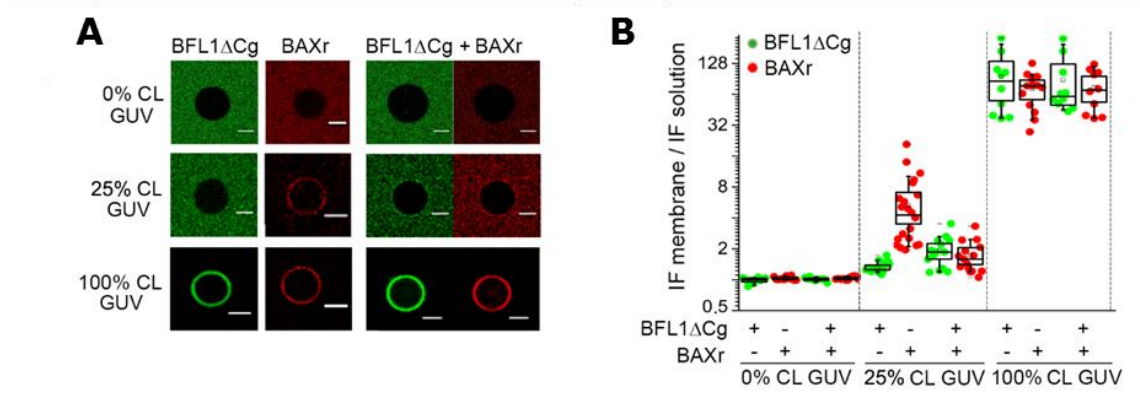

Figure 4.4. BFL1ΔCg/BAXr binding profile in GUVs. Alexa$_{488}$-labelled BFL1ΔC (BFL1ΔCg) and Alexa$_{647}$-labelled BAX (BAXr) were incubated at 37ºC with GUV containing different amounts of CL followed by analysis of protein localization by confocal fluorescence microscopy. **(A),** Representative GUV images. (**B),** The ratio of maximum normalized integrated intensity values in membrane (*IF membrane*) and solution (*IF solution*) fluorescence obtained from radial profiles was measured for BFL1ΔCg (100 nM) and BAXr (100 nM) in GUVs of the indicated lipid compositions:

55PC/30PE/10PI/0CL mol/mol (0CL), 35PC/30PE/10PI/25CL mol/mol (25CL), and (100CL). In this box chart and raw data (*dots*) representation, the *box* represents the 96% confidence interval; *inside* the *box*, the media and median are represented by the *small square* and the *line*, respectively; and the errors correspond to 80% of the data. For each condition, at least 10 GUV were analysed from 3 independent experiments.

In order to further confirm this possibility additional experiments were performed. To this aim, BAXr was incubated first with 25% CL GUVs for 2 hours in the absence or presence of two well-established BAX-activating proapoptotic factors (cBID and mild heat, Figure 4.3B-D), followed by subsequent incubation of these mixtures with unlabeled BFL1ΔC for 2 more hours, and quantitative determination of the degree of BAXr binding to the liposomal membrane using confocal fluorescence microscopy. BFL1ΔC diminished the amount of BAXr bound to the GUVs in the absence of BAX activators, but not in their presence (Figure 4.5C). Next, it was examined the implication of canonical and BH4-mediated non-canonical BFL1ΔC:BAX interactions in the BAX retrotranslocation process reconstituted *in vitro* under healthy-like conditions.

To this aim, the behavior of two single-residue BFL1ΔC mutants was analysed: (i) BFL1ΔC R88D, showing a charge reversal in the strictly conserved Arg residue of the BH1 motif that is critical to establish canonical BH3:groove interactions, and (ii) BFL1ΔC L21A, affecting a Leu residue localized in the BH4 motif of BCL2, BCLXL, and BFL1, and whose equivalent Leu-Ala mutation in BCL2 blocks the interaction between the BH4 motif of BCL2 and BAX and diminishes the antiapoptotic function of BCL2 (Barclay et al, 2015) (Figure 4.5D). Preliminary studies showed that the two BFL1ΔC point mutants preserve the structural folding of the native protein (Figure 4.5A). Importantly, the non-canonical BFL1ΔC L21A mutant completely retained the ability of BFL1ΔC to inhibit the release of cytochrome c induced by BAX from isolated HCT116 BAX/BAK DKO mitochondria, whereas the canonical BFL1ΔC R88D variant completely lost this capacity (Figure 4.5B-left). Moreover, ectopically expressed BFL1 L21A, but not BFL1 R88D, behaved as BFL1 inhibiting the cytochrome c release elicited by BAX in semi-intact HCT116 BAX/BAK DKO cells (Figure 4.5B-right). Similarly, BFL1ΔC L21A acted as its native counterpart inhibiting the BAX retrotranslocation process reconstituted *in vitro*, while BFL1ΔC R88D totally lost this capacity (Figure 4.5C). Prompted by these observations, the effect of a BCLXL construct lacking its TA motif in our minimalist system (BCLXLΔC24, termed BCLXLΔC hereafter) was examined in this CS-like membranes. Unlike BFL1ΔC, BCLXLΔC did not reduce the level of BAXr binding to 25% CL GUVs under healthy-like conditions. This is in accordance with previous reports showing that BCLXL requires non-canonical interactions mediated by its TA motif to retrotranslocate mitochondrial BAX in nonapoptotic cells (Andreu-Fernandez et al, 2017; Bleicken et al, 2017; Todt et al, 2013).

To summarize, this set of experiments demonstrated that in healthy cells BFL1 retrotranslocates BAX from the mitochondria to the cytosol in a similar, but not identical, manner to BCLXL. BFL1-mediated BAX retrotranslocation can be reconstituted in a minimalist system under healthy-, but not apoptotic-like like conditions, and this process requires canonical, rather than non-canonical, interactions between BFL1 and BAX.

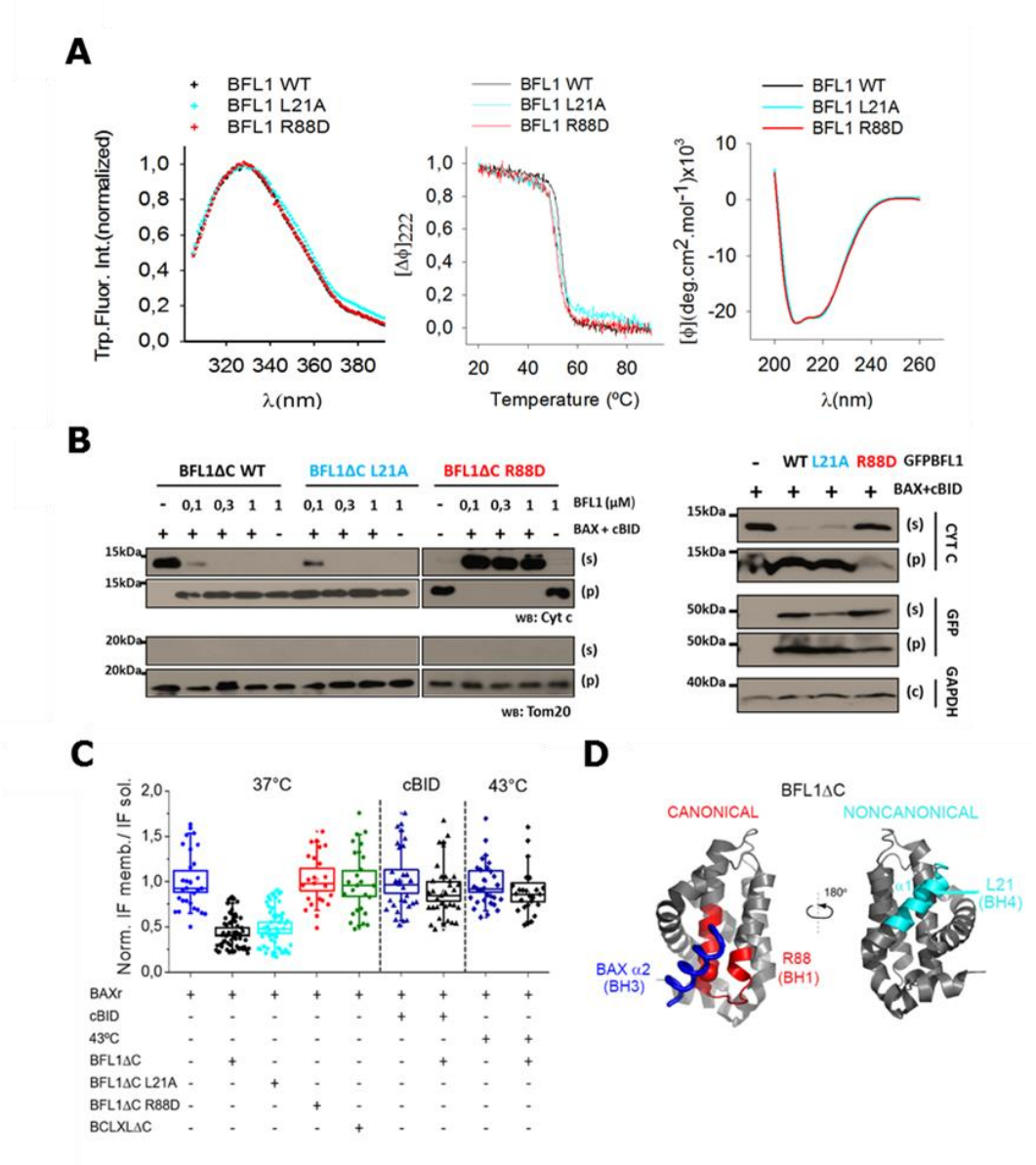

Figure 4.5. BAX retrotranslocation can be recapitulated *in vitro* with recombinant BFL1ΔC and model membranes. Structural and functional characterization of BFL1ΔC canonical/non-canonical mutants. (**A-left)**, Representative Trp fluorescence spectra of BFL1ΔC WT and mutants, (**middle**) thermal denaturation assay and **(right**) circular dichroism spectra**.** (**B)**, Assessment of cyt c release inhibition by BFL1ΔC mutants (**left**) and GFP-BFL1 mutants (**right**) in isolated mitochondria of BAX/BAK DKO HCT116 cells respectively. Protein concentration were cBID (50nM) and BAX (100nM). **(C),** In vitro

reconstitution of BAXr membrane retrotranslocation. BAXr (150 nM) was incubated with CS-like GUV at 37 ºC (-/+ cBID, 20nM) and 43 ºC for 2h. Then, samples are incubated 2h at RT (25ºC) in the presence/absence of 450nM of BFL1ΔC WT, L21A and R88D and BCLXLΔC. Finally, binding profile was measured and represented as explained above. **(D),** Structural representation of BFL1ΔC (PDB:2vm6) in grey, depicting specific residues mutated, L21 (located in the BH4, colored cyan) and R88 (located in the canonical groove, colored in red). BAX BH3 domain is illustrated in dark blue.

4.4.2 FCCS experiments reveal that BFL1ΔC forms canonical heterodimers or non-canonical homodimers in mitochondria-like membranes depending on CL levels

To obtain quantitative information on the capacity of BFL1 to form stable complexes in solution and in mitochondria-like membranes are used point and scanning FCCS, respectively. FCCS is a technique with single molecule sensitivity that measures fluctuations in fluorescence intensity over time of individual particles labeled with spectrally different dyes as they diffuse through the detection volume of a confocal microscope. The resulting fluorescence intensity traces are temporally auto-correlated and cross-correlated to generate auto-correlation (AC) and cross-correlation (CC) curves, respectively. The amplitudes of AC curves (red and green lines in Figure 4.6A) are inversely proportional to the total concentrations of fluorophores, while the amplitudes of the CC curves (blue lines in Figure 4.6A) are directly proportional to the fraction of molecules forming complexes. The percentage of complex formation (% CC) is estimated by referring the amount of complex to the total concentration of protein (Figures 4.6B-E).

In line with previous work, FCCS experiments were performed using physiological protein concentrations and after incubating the mixtures for 2h to ensure equilibrium conditions. Based on background CC levels obtained with free and membrane-bound dyes, mean CC values above 2% and 9% indicated protein complex formation in solution and at the GUV membrane, respectively [(Figure 4.7) and (Bleicken et al, 2017; Ries et al, 2010)]. For the BFL1ΔCg/cBIDr pair, in solution, CC curves with positive amplitudes and CC levels in the 4-11% range were obtained (Figure 4.6A Left, and Figure 4.6B). By contrast, insignificant CC was obtained for the BFL1ΔCg/BAXr pair under the same experimental conditions (Figure 4.6A, Left, and Figure 4.6D). Thus, these data indicate that in solution BFL1ΔC displays some capacity to form hetero-complexes with cBID, but not with BAX.

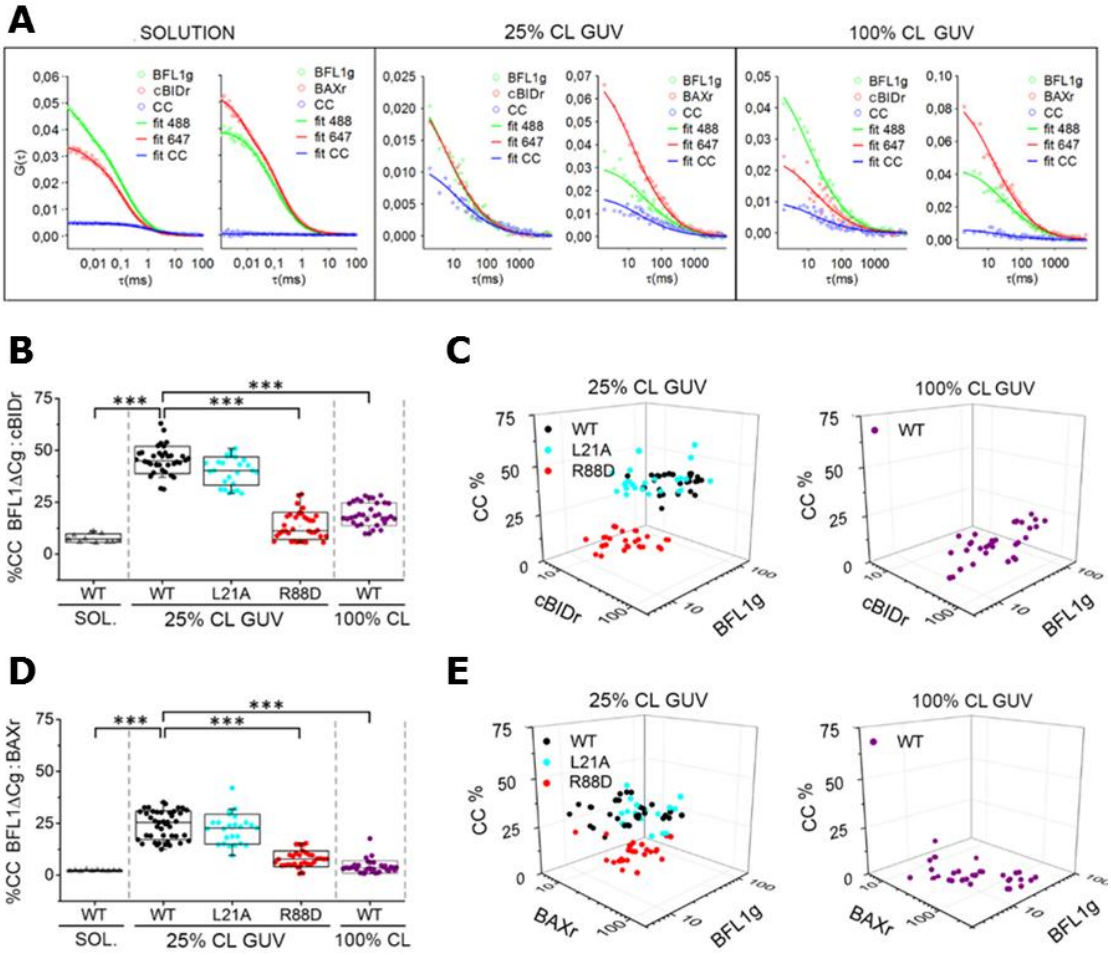

Figure 4.6. FCCS analysis of BFL1ΔCg:BAXr and BFL1ΔCg:cBIDr heterodimerization in solution and in CL-containing membranes. (A-C), FCCS analysis of BFL1ΔCg:BAXr and BFL1ΔCg:cBIDr complex formation in solution, and CS-like liposomes (35PC/30PE/10PI/25CL mol/mol (CL25) GUV and CL100 GUV. (**A)**, Dots represent raw data; straight lines, fitted autocorrelation curves (green and red), and cross-correlation curves (blue). **B and D**, quantification of canonical and non-canonical BFL1 mutations in BFL1:cBID (**B**) and BFL1:BAX (**D**) complex formation in solution and in GUVs. **C and E**, percentages of BFL1:cBID (**C**) and BFL1:BAX (**E**) complex formation were represented on a *3D plot* as a function of individual protein concentrations (molecules/μm^2). Protein concentrations for FCS in solution were 200 nM of each protein. In SFCCS experiments; BFL1g (50 nM), BAXr (50 nM) and $Alexa_{647}$-labelled cBID (cBIDr, 20 nM) in CS-like GUV and 20nM of each protein in 100CL GUV. Data correspond to 5–6 independent experiments, with more than 30GUV analysed for each condition. ***, p= <0.001. *Error bars*, S.D. Box chart and raw data (*dots*) representation as described in Figure 4.4. In **B and D**, red lines indicate the minimum (dashed lines) and the maximum (dotted lines) %CC considering dimer formation and the degree of labelling.

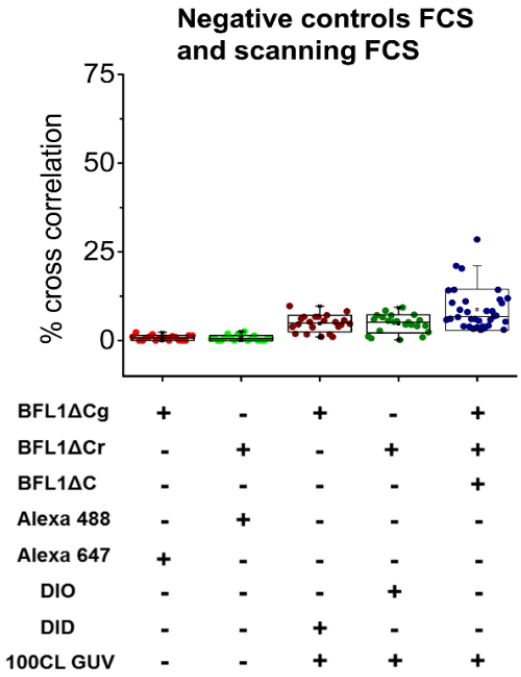

Figure 4.7 Negative controls for FCS and SFCCS analysis of BFL1ΔCg:BFL1ΔCr complex formation. As FCS negative controls we measured the %CC between BFL1ΔCg (200nM) and Alexa647 and BFL1ΔCr (200nM) and alexa488 in solution. SFCCS controls were %CC between BFL1ΔCg (20nM) and DID, BFL1r (20nM) and DIO, and BFL1ΔCg(20nM):BFL1ΔCr(20nM): BFL1ΔC(60nM) in 100CL GUV. Box chart and raw data representation of complex formation, further experimental details were described in Fig 4.4.

For membrane experiments, a unique advantage of scanning FCCS is that only the contributions of membrane-bound proteins to the fluorescence signal are considered in the data analysis, because the FCCS signal is acquired by a linear scanning across the membrane plane of the GUV. Thus, scanning FCCS allows quantifying the ability of BFL1ΔC to form stable protein complexes at the membrane level, without interference of membrane-to-solution retrotranslocation processes. In experiments with 25% CL GUV, they could not be performed scanning FCCS studies using BFL1ΔCg/BAXr because the levels of protein bound were very low under these experimental conditions (Figure 4.4). So that, in this section the interactions between BFL1ΔCg and cBIDr and between BFL1ΔCg and heat activated BAX (43º) are examined, because these protein combinations showed proper capacity for binding to 25% CL GUV. Here, CC curves with positive amplitudes were obtained for both BFL1ΔCg/cBIDr and BFL1ΔCg/activated-BAXr mixtures in 25% CL GUVs (Figure 4.6A, middle). CC levels were notably higher for BFL1ΔCg/cBIDr than for BFL1ΔCg/activated-BAXr. Thus, in 25% CL membranes, BFL1ΔC forms stronger hetero-complexes with the BAX activator cBID than with activated BAX itself. Moreover, in 25% CL GUVs, at all protein concentrations measured, the BFL1ΔCg/cBIDr pair

displayed % CC values close to the maximum level expected for heterodimeric complexes (Bleicken et al, 2017; Ries et al, 2010) (Figures 4.6B-E). Of note, CC levels for BFL1ΔCg/cBIDr were much lower in solution than in 25% CL GUVs indicating that hetero-interactions between BFL1ΔC and proapoptotic partners are enhanced in this type of membranes.

Next, the contribution of canonical and non-canonical interactions between BFL1ΔC and proapoptotic partners in the formation of stable hetero-complexes was analysed in 25% CL GUVs. While the non-canonical BFL1ΔCg L21A mutant interacted with both cBIDr and activated-BAXr in a manner indistinguishable from that of BFL1ΔCg, the canonical BFL1ΔCg R88D mutant virtually lost all the capacity of the native protein to form complexes with either cBIDr or activated-BAXr (Figures 4.6B-E). Thus, at the membrane level, BFL1 forms stable hetero-complexes with both cBID and activated BAX via canonical BH3:groove interactions, without requiring BH4- or TA-mediated non-canonical interactions. Then, it was also analysed BFL1ΔC hetero-interactions in apoptotic-like 100% CL GUVs. The BFL1ΔCg/cBIDr pair showed CC curves with small positive amplitudes and low but significant CC levels, whereas the BFL1ΔCg/BAXr pair showed CC curves and CC percentages that were indistinguishable from background (Figure 4.6A Right, Figures 4.6B-E). This occurred despite the fact that all proteins efficiently bound to 100% CL GUVs (Figure 4.4 and 4.8).

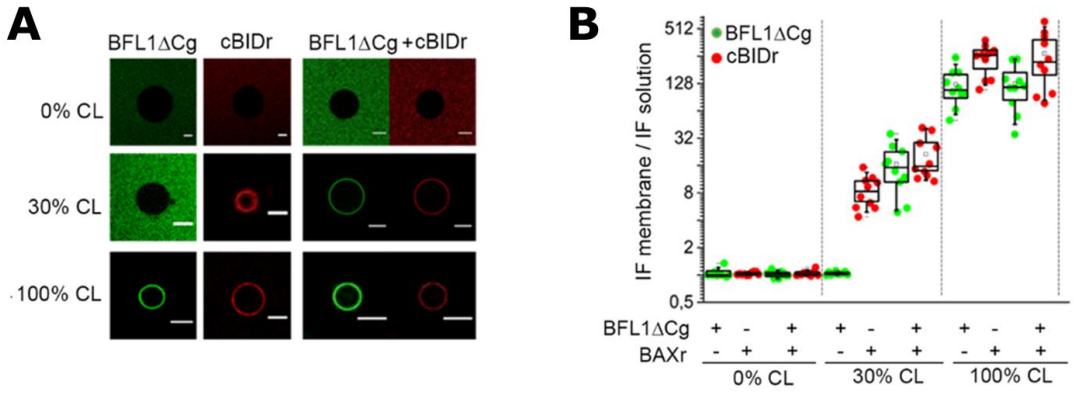

Figure 4.8 cBIDr promotes BFL1ΔCg binding to the membrane. BFL1ΔCg and cBIDr were incubated with GUV containing different amounts of CL followed by analysis of protein localization by confocal fluorescence microscopy. (**A),** Representative GUV images. (***B),*** The ratio of maximum normalized integrated intensity values in membrane (*IF memb*.) and solution (*IFsol*.) fluorescence obtained from radial profiles was measured for BFL1ΔCg (100 nM) and cBIDr (30 nM) in GUVs. Vesicles compositions and box chart and raw data representation as described in Figure 4.4.

Next, FCCS was used in order to assess the capacity of BFL1ΔC to form homo-complexes in solution and membrane environments. Of note, appropriate scanning FCCS experiments could not be performed in 25% CL GUVs due to the low level of BFL1ΔC binding to these vesicles

(Figure 4.4). FCCS analyses revealed that BFL1ΔCg and BFL1ΔCr form homo-complexes in 100% CL GUVs, but not in solution nor in the presence of an excess of non labelled BFL1ΔC (Figure 4.9A-B and 4.8). CC levels for the BFL1ΔCg/BFL1ΔCr pair were similar at all protein concentrations measured and were not distant from maximum values expected for BFL1ΔC homodimeric complexes based on (Bleicken et al, 2017; Ries et al, 2010). BFL1ΔC R88D behaved as BFL1ΔC forming homo-complexes in 100% CL GUVs (Figure 4.9A-B), which is in stark contrast to the dramatic loss in hetero-complex formation observed for this mutant in 25% CL GUVs (Figures 4.6B-E). Furthermore, the non-canonical BFL1ΔC L21A mutant partially lost the capacity of BFL1ΔC to form homo-complexes in 100% CL GUVs (Figure 4.9A), unlike the equivalent abilities shown by this mutant and the native protein to form hetero-complexes in 25% CL GUVs.

To further examine the quaternary structure of BFL1 homo-complexes in different environments Total Internal Reflection (TIRF) and size-exclusion chromatography (SEC) were used. TIRF experiments with single-molecule sensitivity revealed that in 0% CL membranes the majority of BFL1ΔC exists as a monomeric species, while in 100% CL membranes BFL1ΔC predominantly adopts a dimeric conformation (Figure 4.9C). Consistent with scanning FCCS results, the canonical BFL1ΔC R88D mutant homodimerized as efficiently as BFL1ΔC, while the non-canonical BFL1ΔC L21A variant only retained the homodimerization capacity of its native counterpart in part. SEC analyses showed that in the absence of membranes BFL1ΔC elutes as a monomeric protein (Figure 4.9D, discontinuous black line), whereas in the presence of 100% CL liposomes the protein elutes as larger particles (Figure 4.9D, continuous black line) that may correspond to mixed micelles containing CL and dimeric BFL1ΔC or to BFL1ΔC complexes of higher stoichiometry. As observed in FCCS and TIRF studies, the canonical, but not the non-canonical BFL1ΔC mutant, reproduced the behavior displayed by BFL1ΔC in the SEC assay (Figure 4.9D). Additional SEC experiments showed that unlike BFL1ΔC, BCLXLΔC fully retains its monomeric nature in the presence of 100% CL liposomes, while BAX mostly elutes in the void volume of the column (Figure 4.9D).

To summarize, based on these collective set of results can be conclude that (i) in solution and in mitochondrial-like membranes, BFL1ΔC generally forms stronger hetero-complexes with cBID than with activated BAX; (ii) membranes with a healthy-like mitochondrial lipid composition (25% CL) enhance formation of stable hetero-complexes between BFL1ΔC and proapoptotic partners through a canonical BH3:groove interaction mechanism; and (iii) apoptotic-like 100% CL membranes promote formation of non-canonical BFL1ΔC homo-complexes, a feature that is not shared by BCLXLΔC.

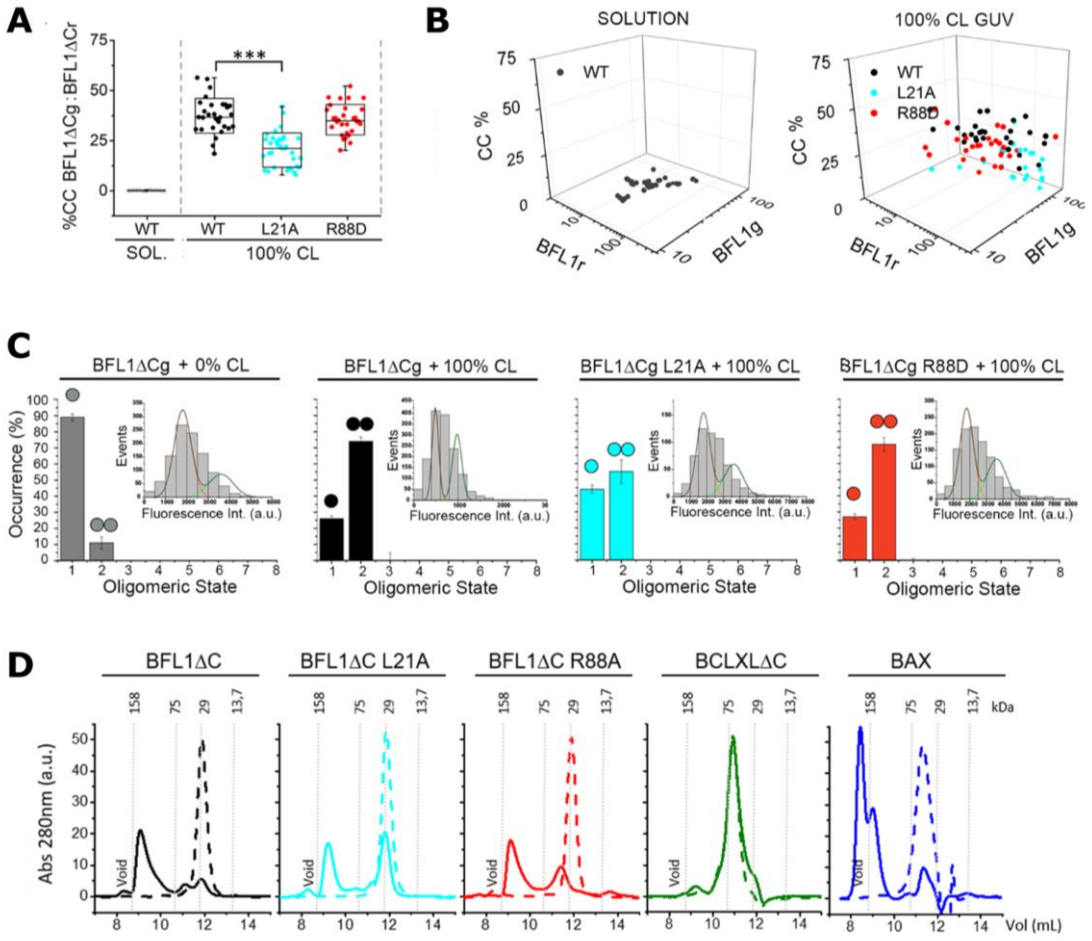

Figure 4.9 BFL1ΔC forms non-canonical homo-oligomers in pure CL liposomes. (A), Homo-oligomerization (BFL1ΔCg:BFL1ΔCr complex formation) of BFL1ΔC WT and its canonical and non-canonical mutants in solution, and pure CL GUV (100CL) analysed by FCCS and SFCCS. ***Left,*** Box chart and raw data representation and ***right,*** *3D plot* as a function of individual protein concentrations (molecules/μm^2). Other experimental details as described in Figure 4.4 and Figure 4.6B/D. Red lines indicate the minimum (dashed lines) and the maximum (dotted line) %CC considering dimer formation and the degree of labelling. (**B),** Analysis of BFL1ΔC quaternary structure by Total Internal Reflection (TIRF) in (0CL) and pure CL (100CL) supported lipid bilayers (SLB). BFL1ΔCg analysis with 0CL SLB also included 1% DGS-NTA(Ni) lipids. Representation of the percentages of the quaternary structures of BFL1ΔCg or its canonical and non-canonical mutants in pure CL SLB (100CL). Monomers and dimers were calculated from the averaged distributions of species from 3 different experiments, after correction for partial labelling. The error bars correspond to the average error for each species. **Inset plot,** fluorescence intensity distribution of BFL1ΔCg or its variants particles bound to SLB. Approximately 1000 particles were analysed. The resulting histograms were fitted with a linear combination of two Gaussians to estimate the occurrence of particles containing one (orange) and two (green) labelled molecules. The cumulative fit is shown in black. The area of the fitted Gaussians is proportional to the fraction of each species. **(C),** Quaternary structure study of BFL1ΔC and its variant by size-exclusion chromatography (SEC) in solution and in pure CL GUV (100CL). Proteins were incubated in the absence (dashed lines) or in the presence of 100CL LUVs (solid lines) followed by 3%CHAPS addition, and Superdex-75 chromatography. Analysed proteins were BFL1ΔC (black lines), BFL1ΔC L21A (cyan lines), BFL1ΔC R88D (red lines), BCLXLΔC (dark green lines) and BAX (dark blue lines). Protein

standards were: ribonuclease A (13.7 kDa), Carbonic anhydrase (29 kDa), Conalbumin (75 kDa) and Aldolase (158 kDa).

4.4.3 BFL1ΔC adopts different conformations in CL-containing membranes and in pure CL membranes

To test whether membrane CL levels affect specifically to BFL1 conformation, NBD-based fluorescence mapping strategy was used. To this aim, a set of monocysteine BFL1ΔC variants spread along the whole protein structure were produced and tested that maintain structural and functional properties of the native protein (Figure 4.10). Next, BFL1ΔC monocysteine mutants were site-specifically labelled with NBD, an environmentally sensitive fluorescent dye, followed by analysis of NBD fluorescence properties in the monocysteine BFL1ΔC variants and combining them with lipids containing doxyl groups as explained in the previous chapter, we were able to stablish BFL1 membrane topology at different lipid compositions.

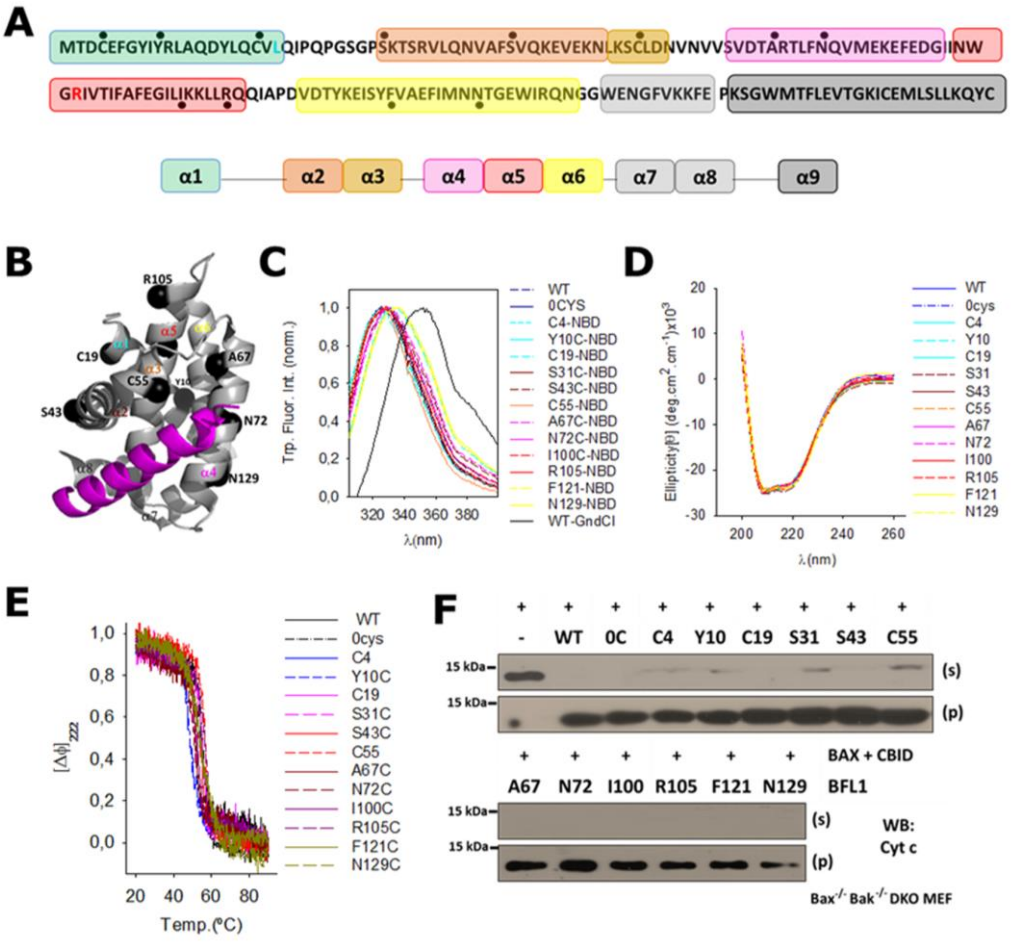

Figure 4.10. Structural and functional characterization of NBD-labelled monocysteine BFL1ΔC mutants. (**A)**, Primary structure of BFL1 indicating specific residues mutated to Cys for subsequent labelling with the environmentally sensitive NBD fluorophore (black circles). (**B)**, Structural representation of BFL1ΔC26 (2vm6) depicting specific residues mutated to Cys for subsequent labelling with NBD (black spheres). (**C)**, Representative Trp fluorescence spectra of NBD-labelled monocysteine BFL1 mutants. (**D)**, Secondary structure assessment of BFL1ΔC monocysteine mutants by circular dichroism. E, Thermal denaturation assay for the set of BFL1 monocysteine mutants. **(F)**, Assessment of cyt c release inhibition by BFL1ΔC mutants in BAX/BAK DKO MEF isolated mitochondria. Protein concentration: cBID (50nM) and BAX 100nM, and 1μM of each monocysteine BFL1ΔC mutant.

As shown in Figure 4.11A-B, all monocysteine BFL1ΔC mutants underwent minimal changes in NBD fluorescence in the presence of CL-containing LUVs. Co-addition of BAX together with CL-containing LUVs did not produce further spectral changes in any NBD-labelled monocysteine BFL1 mutant. However, co-addition of cBID together with CL-containing LUVs produced a prominent increase in the fluorescence intensity of BFL1ΔC S43C-NBD, accompanied by a ∼4 nm blue-shift in the λmax(em) of this variant (Figure 4.11A). Of note, the S43 residue is localized at the BH3-binding-groove of BFL1 supporting the notion that cBID and BFL1 form canonical BH3-in-groove complexes, which apparently maintain the global BFL1 solution fold. Moreover, NBD-quenching experiments with doxylated lipids showed insignificant effects for all BFL1 variants, including residues in the hydrophobic core (α5-α6), in the absence or presence of cBID or BAX, strongly suggesting, in contraposition to reported for other BCL2-type antiapoptotic proteins, that cBID:BFL1 complex formation does not lead to BFL1 membrane insertion (Billen et al, 2008; Dlugosz et al, 2006; Lovell et al, 2008; Shamas-Din et al, 2013; Zhang et al, 2004).

Next, the behaviour of the same set of NBD labelled monocysteine BFL1ΔC mutants was analysed in the presence of pure CL LUVs, with or without proapoptotic proteins (Figure 4.11B). Remarkably, all BFL1ΔC monocysteine mutants underwent substantial changes in NBD fluorescence in the presence of pure CL LUVs alone, and co-addition of cBID or BAX did not produce further changes in the NBD fluorescence intensity of any BFL1ΔC mutant examined (Figure 4.11B-left). Furthermore, in the presence of pure CL LUVs all NBD-labelled BFL1ΔC mutants displayed substantial quenching by doxylated lipids, suggesting that multiple BFL1 regions insert into the membrane lipid bilayer under these conditions (Figure 4.11B, right).

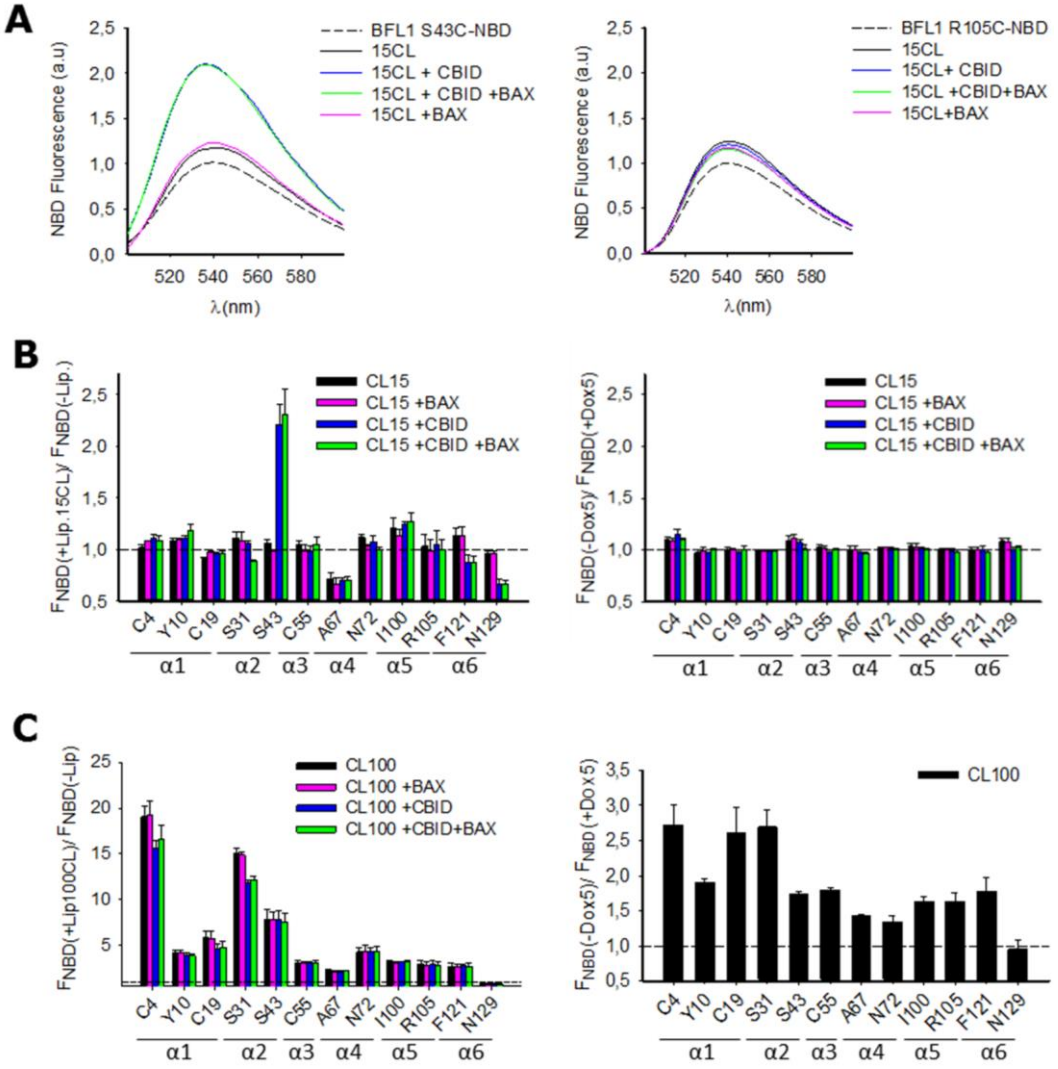

Figure 4.11. **Analysis of BFL1 membrane topology by NBD fluorescence mapping.** (**A**), Representative NBD fluorescence emission spectra of indicated monocysteine BFL1 mutants incubated with or without MOM-like LUV (15CL) and proapoptotic proteins. In all cases, NBD fluorescence was normalized to the peak intensity of the NBD spectrum in buffer alone. Protein/lipid concentrations: 150nM of each BCL2 protein and 150μM lipid. **B, C Left**, Average NBD fluorescence intensity ratios(+LUV/-LUV) of monocysteine BFL1 mutants incubated with MOM-like (45PC/30PE/10PI/15CL, termed CL15) (**B**) and CL100 (**C**) LUVs. **Right,** Dox5-quenching of NBD-BFL1 mutants in MOM-like (B) and 100 CL (C) LUVs. n= 3-4 independent experiments. Error bars, S.D.

Complementarily, BFL1 membrane topology was studied by the Single Cysteine Accessibility Method (SCAM). Here, BFL1ΔC monocysteine mutants were treated with PEG-5kDa, and PEGylated proteins were identified by SDS-PAGE analysis of protein migration patterns. SCAM

analysis of PEG-5kDa exposure of all monocysteine residues, confirmed that BFL1 maintains its global structure in CL-containing, but not in pure CL LUVs (Figure 4.12)

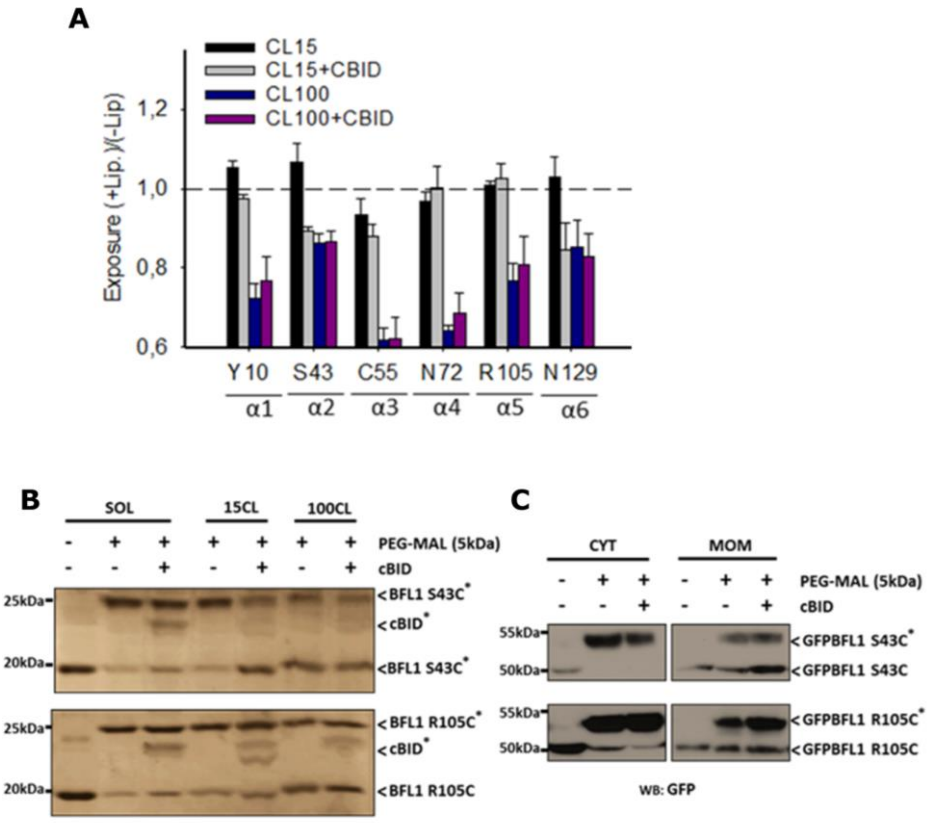

Figure 4.12. Analysis of BFL1 membrane topology by single cysteine accessibility method (SCAM) (I). (**A**) Average 5kDaPEGMAL-exposure pattern of monocysteine BFL1ΔC mutants under above-mentioned conditions (CL15 or CL100 /SOL). (**B**), Representative coomassie blue stain of CYS exposure pattern of S43C and R105C monocysteine mutants of BFL1ΔC assessed by using 5kDaPEGMAL in the presence/absence of proapoptotic cBID, in solution, CL15 and CL100 liposomes. *PEG-mal labelled BFL1 monocysteine mutant (n=3). All LUV experiments 150μM lipid and 150nM of each protein. (**C**), Representative CYS exposure pattern of GFP-BFL1 S43C and R105C BFL1 FL at the MOM of digitonized BAX/BAK DKO MEF cells assessed by anti-GFP WB (n=3).

Further SCAM experiments were performed with selected GFP-BFL1ΔC mutants (S43C, canonical-groove and R105C, hydrophobic core) expressed in BAK/BAX DKO MEFs. Both mutants showed a similar behaviour at the mitochondria level and with CL-containing liposomes (Figure 4.12C-D).

To summarize, BFL1 membrane topology analyses showed that BFL1 interacts with cBID in CL-containing LUVs through canonical BH3-in-groove interactions that maintain the global solution fold of the protein. By contrast, in pure CL LUVs, BFL1 undergoes a massive structural

rearrangement with extensive membrane insertion of the protein, thereby disrupting its BH3-binding groove and abolishing its capacity to interact with proapoptotic partners

4.4.4 BFL1ΔC forms non-canonical proteolipidic pores in pure CL membranes

Next, it was examined the impact of BFL1ΔC on membrane permeability. In a first set of assays, spectrofluorimetry and LUVs encapsulating the small-sized dye/quencher ANTS/DPX (m.w. <1kDa) were used as a model membrane system. As shown in Figure 4.13A, the impact of BFL1ΔC on liposome membrane permeability correlated well with the capacity of BFL1 to form hetero- and homo-complexes (Figs 4.6 and 4.9). Thus, in 25% CL LUVs, BFL1ΔC inhibited the ANTS/DPX release elicited by cBID-activated BAX, and this inhibitory function on membrane permeabilization was also observed with the non-canonical BFL1ΔC L21A mutant, while it was totally lost in the case of the canonical BFL1ΔC R88D mutant. By contrast, BFL1ΔC itself elicited the release of ANTS/DPX from pure CL LUVs, and this autonomous membrane-permeabilizing function of BFL1ΔC was efficiently reproduced by the canonical BFL1ΔC R88D mutant, but not by the non-canonical BFL1ΔC L21A (Fig 4.13B).

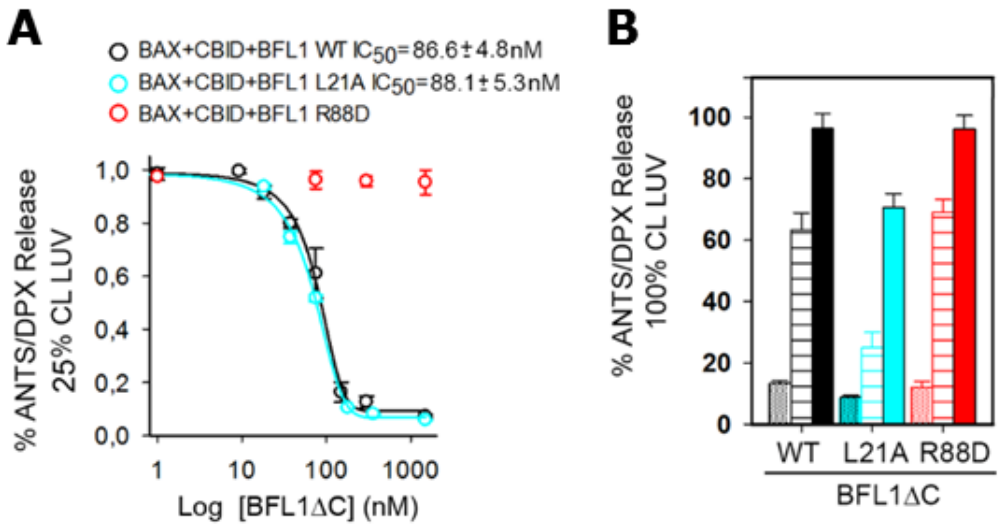

Figure 4.13. BFL1ΔC displays opposing effects on membrane permeability depending on CL (I). (A), Dose-dependence of extents of vesicular contents release (ANTS/DPX release) inhibition elicited by BFL1ΔC WT and its canonical/non-canonical mutants in 35PC/30PE/10PI/25CL mol/mol (25CL) LUV. (n = 3) *Error bars*, S.D. **(B)**, ANTS/DPX release elicited by BFL1ΔC WT (black) and its canonical(red)/non-canonical (cyan) mutants in pure CL LUV (100CL). Protein concentration: Dotted bars

(60nM), Dashed bars (120nM) and filled bars (180nM). **C,** Representative images of 100CL GUV after the incubation with BCL2 proteins in the presence of 4kDa dextrans and the fluorescent protein allophycocyanin (APC, 104kDa). Scale bars, 10µm. **D,** Percentage of permeabilized GUV measured by filling of externally added FITC-4-kDa dextran and APC (104kDa). ***E,*** GUV size normalized to the control n>50 of 3 independent experiments. ***, *p*= <0.001. *Error bars*, S.D. Box chart and raw data (*dots*) representation as described in Figure 4.4.

Next, was explored the size of the membrane perturbation created by BFL1ΔC in pure CL membranes. Here, it was simultaneously analysed the internalization of FITC-4KDa and APC-104kDa into pure CL GUVs by confocal fluorescence microscopy. In pure CL GUVs, BFL1ΔC elicited more extensive internalization of FITC-4 kDa than APC-104 kDa, while BAX produced similarly extensive internalization of both fluorescent markers, and cBID and the antiapoptotic BCLXLΔC did not allow internalization of any of them. Consistent with spectrofluorimetry results obtained in LUVs, the canonical BFL1ΔC R88D mutant permeabilized pure CL GUVs similarly to BFL1ΔC, while the non-canonical BFL1ΔC L21A variant showed diminished active (Fig. 4.14A and B).

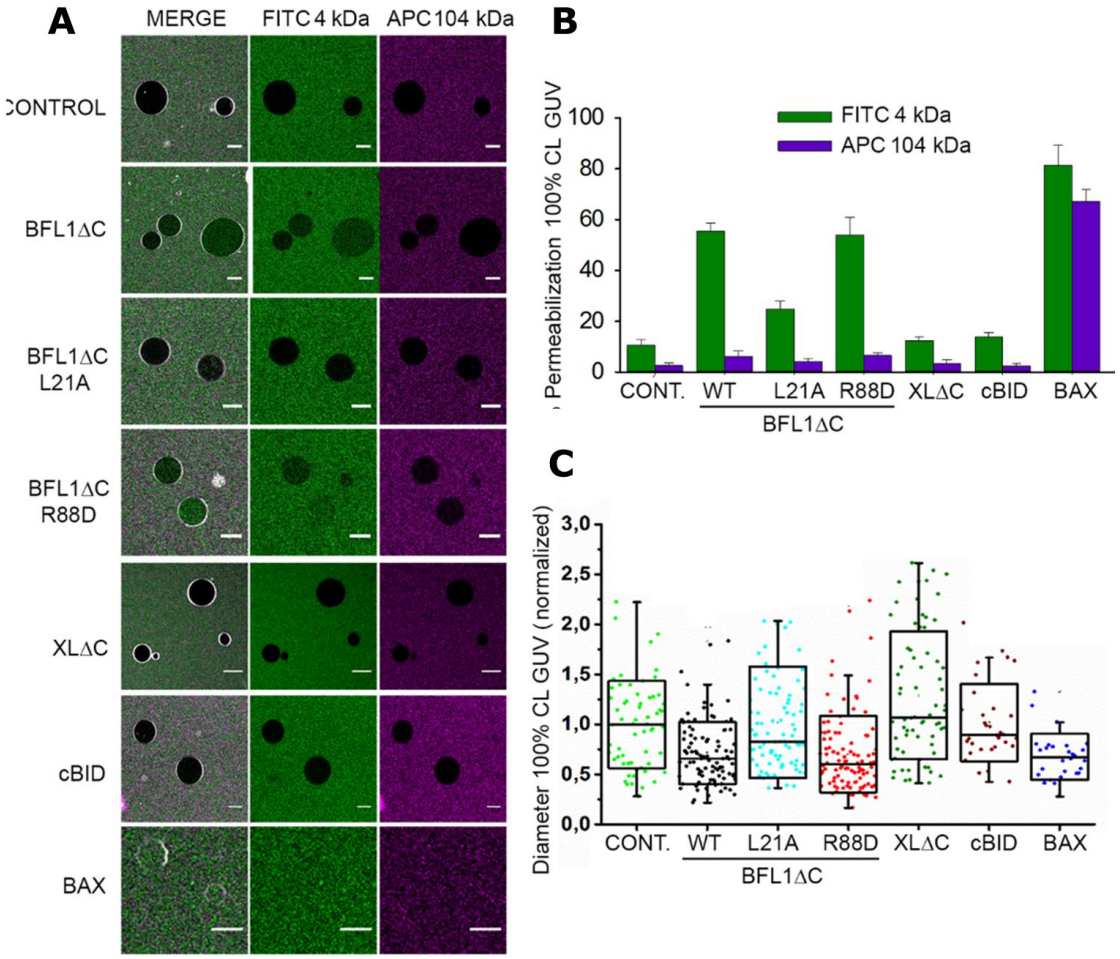

Figure 4.14. BFL1ΔC displays opposing effects on membrane permeability depending on CL (II). (**A),** Representative images of 100CL GUV after the incubation with BCL2 proteins in the presence of 4kDa dextrans and the fluorescent protein allophycocyanin (APC, 104kDa). Scale bars, 10μm. **(B),** Percentage of permeabilized GUV measured by filling of externally added FITC-4-kDa dextran and APC (104kDa). ***(C),*** GUV size normalized to the control n>50 of 3 independent experiments. ***, *p*= <0.001. *Error bars*, S.D. Box chart and raw data (*dots*) representation as described in Figure 4.4.

Accumulating evidence indicates that BAX-type proteins permeabilize membranes by forming proteolipidic pores (Salvador-Gallego et al, 2016; Terrones et al, 2004). BAX-induced proteolipidic pore formation in CL-containing GUVs has been linked to a reduction of GUV diameter that can be inhibited by BCLXL (Bleicken et al, 2016). Consistent with this, it was observed that heat-activated BAX significantly permeabilize (Figure 4.15A) and reduced the diameter of CL-containing GUVs (Figure 4.15B). This process was inhibited by BFL1ΔC and its non-canonical L21A variant, but not by its canonical R88D variant (Figure 4.15A-B). In stark contrast, BFL1ΔC and its canonical R88D variant, but not its non-canonical L21A variant, reduced the diameter of pure CL GUVs (Figure 4.14C). Complementarily, taking into account that oxidized CL (CLox) accumulates in apoptotic cells it was also examined the impact of CLox in BFL1ΔC pore-forming activity. Indeed, substitution of CL by CLox exacerbated ANTS/DPX release from LUVs by BFL1ΔC (Figure 4.15C). BFL1ΔC canonical R88D variant, but not BFL1ΔC non-canonical L21A mutant, preserved BFL1ΔC´s pore-forming activity in CLox LUVs.

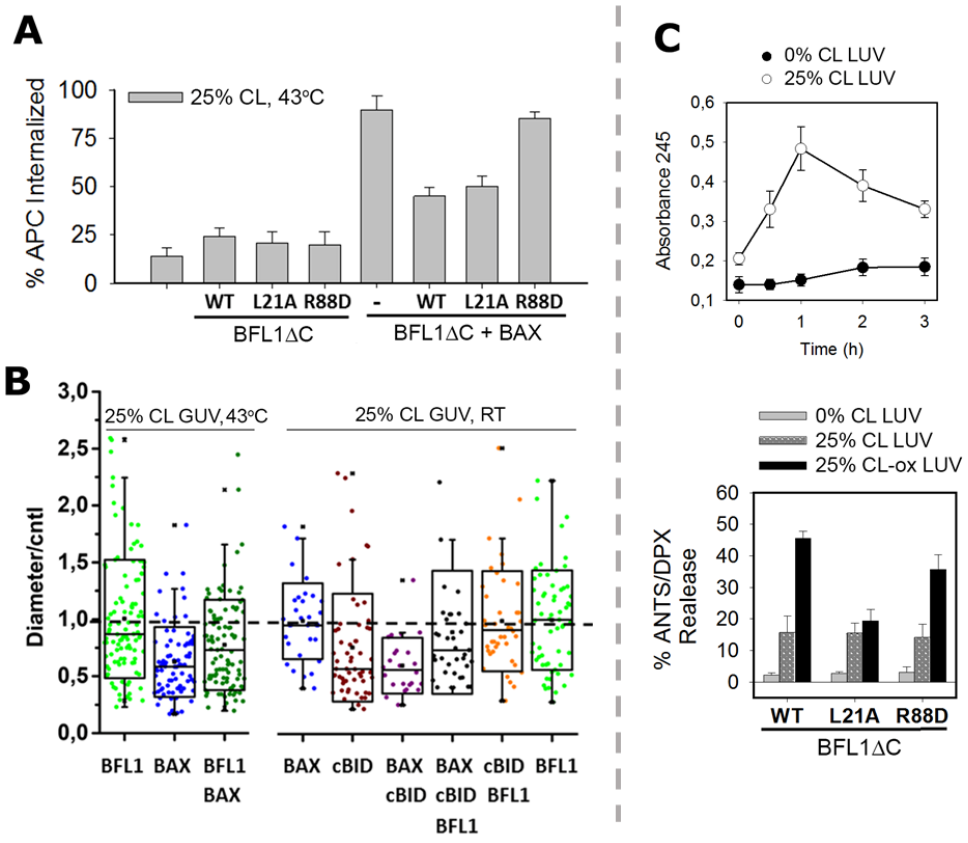

Figure 4.15. Effects of BFL1ΔC variants in heat-activated BAX in CS-like GUV. (A), Percentage of APC (104kDa) internalization upon the incubation of BCL2 protein(s) in CS-like GUV at 43ºC. **(B),** BFL1ΔC inhibits both membrane remodeling activities elicited by its proapoptotic counterparts in 25CL GUV. Box chart and raw data representation of GUV size normalized to the control upon the incubation of BCL2 protein(s) in CS-like GUV at two different temperatures (RT and 43ºC). Other experimental details were described in Figure 4.4. (**C**), Oxidized-CL increases the proapoptotic activity of BFL1ΔC. ***Left***, Kinetics of copper-induced oxidation of 60PC/30PE/10PI (0CL) and 35PC/30PE/10PI/30CL (25CL) LUV. ***Right,*** Extents of ANTS/DPX release elicited by BFL1ΔC WT and its canonical/non-canonical mutants in 0CL LUV (gray bars), 25CL (dotted bars), and oxidized-25CL (black bars). Protein/lipid ratio was (1:300).

Based on this set of results, can be concluded that BFL1ΔC oligomerizes via non-canonical interactions to form proteolipidic pores in pure CL and CLox-containing membranes.

4.4.5 BFL1, but not BCLXL, promotes BAX/BAK-independent apoptosis when stimulated by CL-externalizing drugs.

Prompted by the results obtained in minimalistic *in vitro* reconstituted systems, we decided to examine whether BFL1 oligomerizes and/or increases membrane permeability in a more physiological environment. To this purpose, GFP-BFL1- and GFP-BCLXL-transfected HCT116 cells were treated with the apoptosis-inducing agent rotenone at a suboptimal dose that induces mitochondrial CL externalization and oxidation, followed by immunofluorescence analyses of cytochrome c release and GFP-BFL1/GFP-BCLXL visualization(Jiang et al, 2008; Kagan et al, 2004; Kagan et al, 2005). As shown in Figure 4.16A, sub-optimal rotenone treatment produced cyt c release and clustering in cells expressing GFP-BFL1, but not GFP-BCLXL.

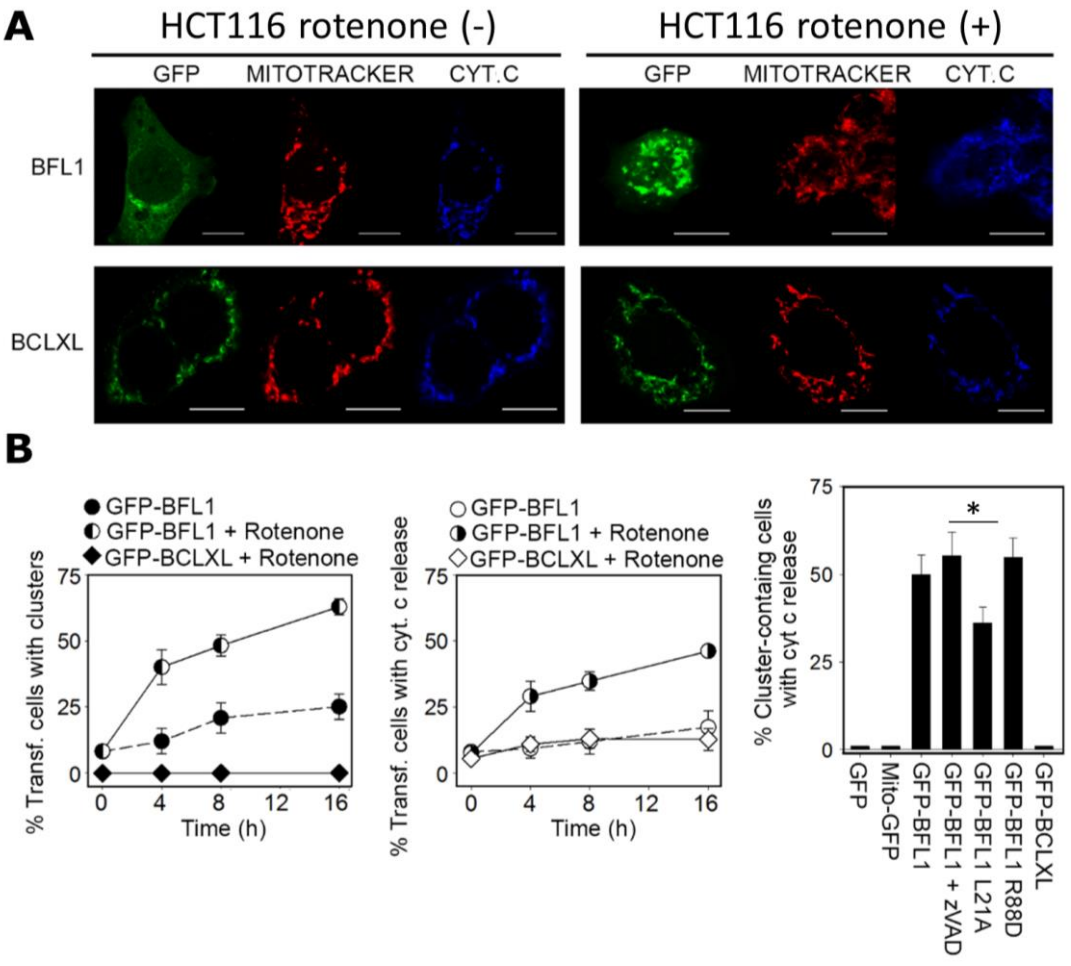

Figure 4.16. Rotenone-mediated CL oxidation induces BFL1 clustering and mitochondrial cyt c release in HCT 116 cells. (A), Representative images of GFP-BFL1 and GFP-BCLXL cellular distribution (in green), cyt c localization (in blue) and mitotracker intensity (red) in the presence/absence

of rotenone (1µM,4h) in HCT 116 cells. Scale bars, 10µm. (**B)**, Kinetics of apoptotic cluster formation (***left***) and MOMP (cyt c release) (***middle)*** in transfected cells at different times. *Error bars*, S.D. ***Right***, quantification of the percentage of cyt c release in cluster presenting transfected cells. and *, p= <0.05. *Error bars*, S.D.

Suboptimal rotenone treatment did not produce cytochrome c release or clustering in HCT 116 cells transfected with GFP or Mito-GFP (Figure 4.16B-right and 4.17). zVAD did not reduce rotenone-induced cytochrome release or BFL1 clustering, indicating both processes are caspase-independent (Figure 4.16B-right). In coherence with previous results, in cells transfected with the non-canonical GFP-BFL1 L21A mutant, but not the canonical GFP-BFL1 R88D variant, cytochrome c release and GFP-BFL1 clustering were partially reduced (Figure 4.16B-right).

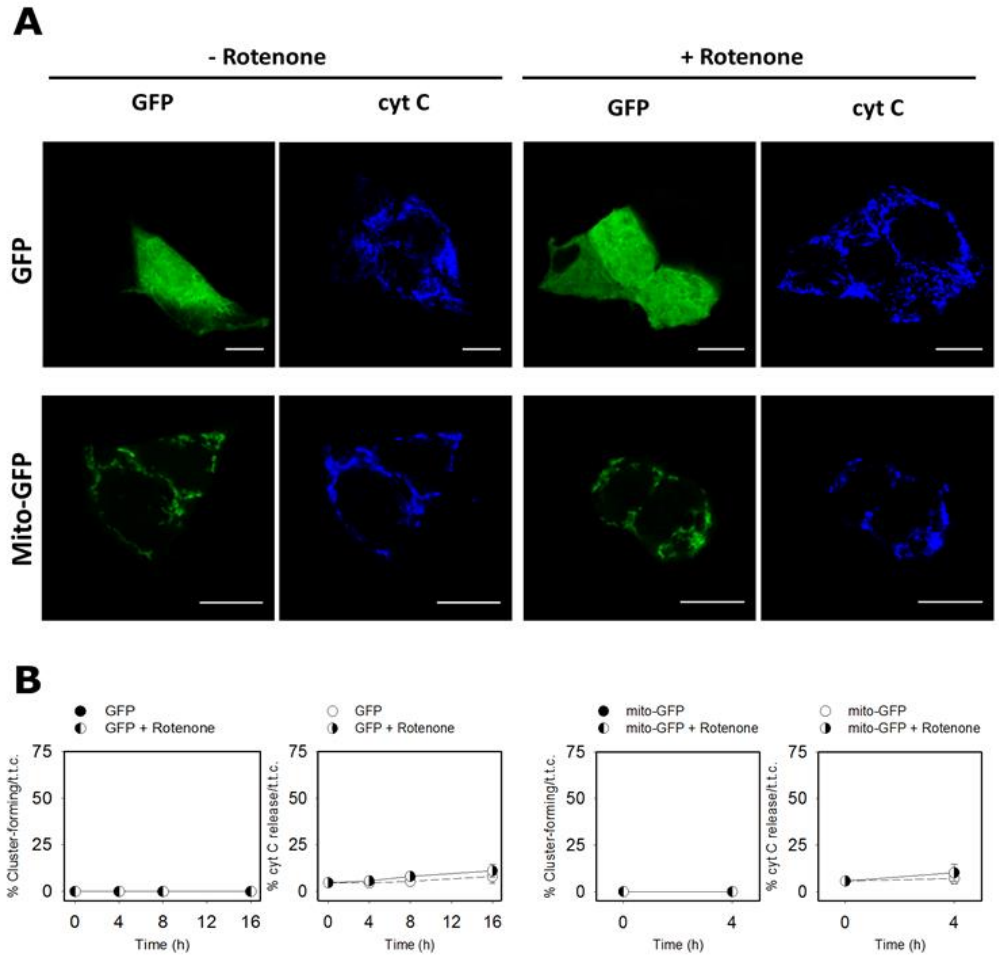

Figure 4.17. Rotenone-mediated CL oxidation does not induce any GFP or Mito-GFP clustering nor mitochondrial cyt c release in HCT 116 cells. (A), Representative images of GFP and Mito-GFP cellular distribution (in green) and cyt c localization (in blue) in the presence/absence of rotenone (1µM,4h) in HCT 116 cells. Scale bars, 10µm. (**B)**, Kinetics of cluster formation and MOMP (cyt c release) for GFP (***left)*** and for Mito-GFP (***right)*** in the presence/absence of rotenone (1µM,4h) in transfected cells at different times. *Error bars*, S.D.

Next, various apoptotic features were examined in rotenone- and staurosporine-treated BAX/BAK DKO HCT166 cells with or without ectopic expression of GFP-BAX, GFP-BFL1 and GFP-BCLXL. As shown in Figure 4.18A-B, rotenone and staurosporine treatment induced clustering, cytochrome c release, and pyknotic nuclei in GFP-BAX and GFP-BFL1 expressing cells, but not in GFP-BCLXL expressing cells. GFP-BAX had more pronounced effect than GFP-BFL1.

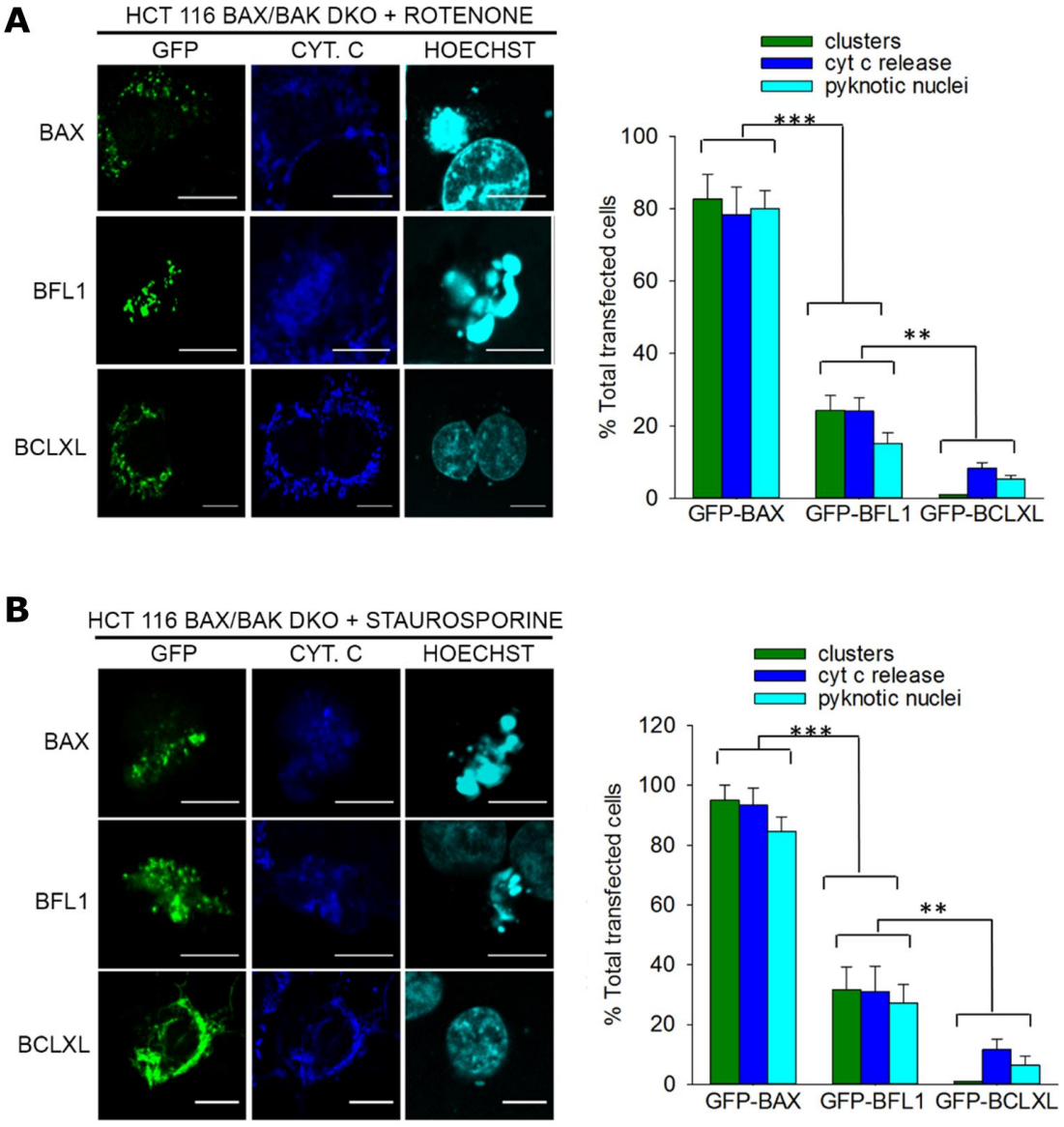

Figure 4.18. Rotenone- and staurosporine-mediated CL oxidation induces BFL1 clustering, mitochondrial cyt c release and apoptotic nuclei formation in BAX/BAK DKO HCT 116 cells. A and B, *Left*, Representative images of GFP-BAX, GFP-BFL1 and GFP-BCLXL cellular distribution (green), cyt c localization (in dark blue) and nuclear morphology (cyan) in the presence of rotenone (1μM,6h) (**A**)

or staurosporine (1µM,6h) (**B**) in BAX/BAK DKO HCT 116 cells. Scale bars, 10µm. *Right*, Quantification of cluster- (green bars), MOMP- (dark blue bars) and apoptotic nuclei- (cyan bars) presenting cells of total transfected cells in the presence of rotenone (1µM,6h) (**A**) or staurosporine (1µM, 6h) (**B**) in BAX/BAK DKO HCT 116 cells.

Of note, the levels of cytochrome c release and BFL1 clustering were lower in rotenone-treated BAX/BAK DKO HCT 166 relative to rotenone-treated normal HCT 166 cells, despite GFP-BFL1 was equally expressed in wt and BAX/BAK DK HCT116 cells (Figure 4.19A-B). The relative clustering levels of GFP-BFL1 and its canonical and non-canonical mutants were maintained in rotenone-treated BAX/BAK DKO HCT 166 cells (Figure 4.19-C).

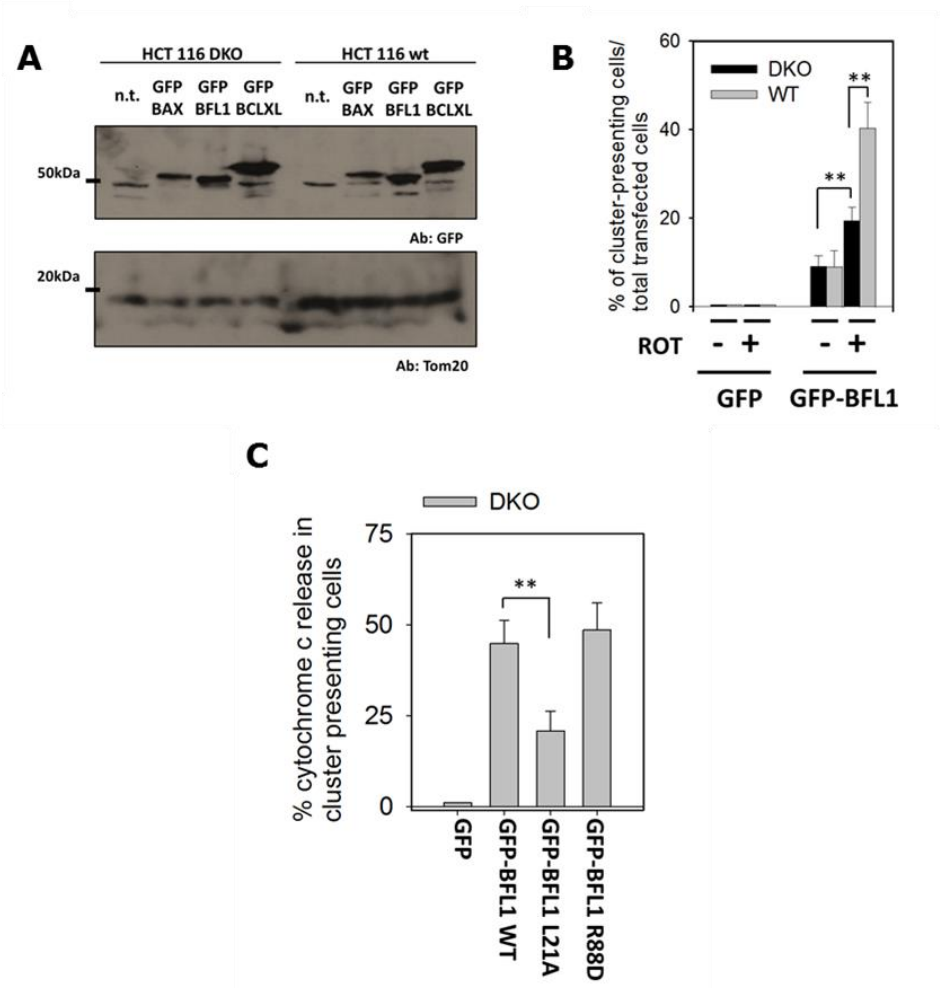

Figure 4.19. (A), GFP-BAX, GFP BFL1 and GFP-BCLXL expression levels in BAX/BAK DKO HCT116 and HCT 116 WT cells assessed by western blotting anti-GFP**.** Loading control was determined by anti-TOM antibody. (**B),** Comparison of total cluster formation of GFP and GFP-BFL1 in both cells lines (-/+) 1µM rotenone treatment for 4h. (**C),** quantification of the percentage of cyt c release in cluster presenting transfected cells after rotenone treatment (1µM, 6h). **, *p*= <0.025. *Error bars*, S.D.

Based on this collective data, it is proposed that rotenone and staurosporine treatment unleashes a lethal clustering and MOMP activity of BFL1 that is not mediated via canonical BH3:groove interaction mechanism, and which is not present in the antiapoptotic BCLXL (Figure 4.20).

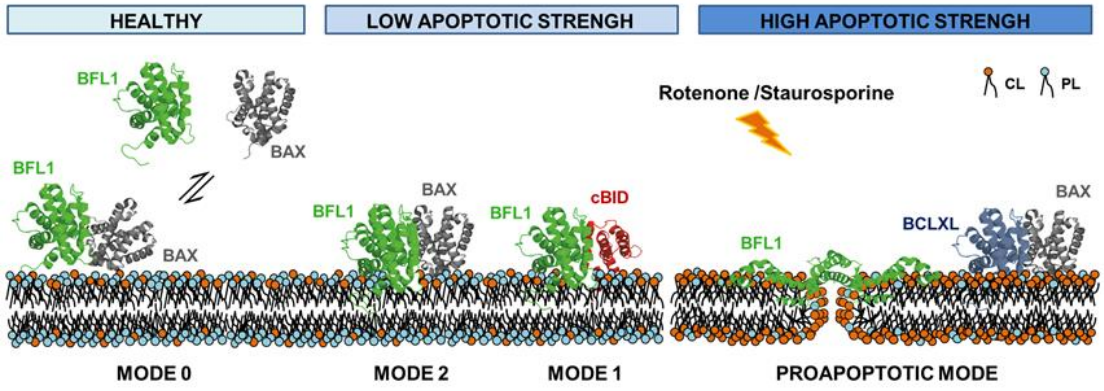

Figure 4.20. Schematic representation of all three inhibition modes carried out by BFL1 upon a canonical BH3-into groove interactions: MODE 0 at healthy conditions (**left**), MODEs 1 and 2 at low apoptotic conditions (**middle**) and ProDeath MODE of BFL1 but not BCLXL at high apoptotic pressure conditions (**right**).

4.5 DISCUSSION

BFL1 has recently emerged as an important factor for oncogenesis and chemoresistance. However, our current mechanistic knowledge for BFL1 is much more limited than for BCL2 and BCLXL (Fan et al, 2010; Haq et al, 2013; Mahadevan et al, 2005; Moldoveanu et al, 2014; Placzek et al, 2010; Westphal et al, 2014b) (Huhn et al, 2016; Schenk et al, 2017; Tuzlak et al, 2017). In this chapter, it was performed a multidisciplinary approach applied to a variety of *in vitro* and *in celullo* systems to gain new insight into the modes of action of BFL1, particularly in the membrane environment. These results support the view that BFL1 possesses three antiapoptotic modes described before for BCLXL that are mediated via canonical BH3:groove interactions, as well as a BAX-like proapoptotic mode mediated by non-canonical interactions that can be unleashed by cardiolipin.

On the one hand, different lines of evidence indicating that BFL1 can inhibit apoptosis via three distinct mechanisms are provided. First, it is shown that BFL1 shares with BCLXL (Edlich et al, 2011a), the capacity to accelerate BAX shuttling from the mitochondria into the cytosol, designated as MODE 0 or retrotranslocation inhibitory mechanism. A mutant of BAX that is

unable to expose its BH3 domain (Edlich et al, 2011a) only displayed slow retrotranslocation rates. Thus, BFL1 may exert this retrotranslocation function through canonical BH3-in-groove interactions with BAX. Importantly, this phenomenon can be recapitulated using recombinant BAX and BFL1ΔC proteins and CS-like liposomes under healthy-, but not apoptotic-like conditions. Moreover, several evidences were provided to assert that the TA motif of BFL1 is not required to retrotranslocate BAX from the membrane, which is unlike the situation found for BCLXL. However, these results do not exclude the possibility that the TA domain of BFL1 participates in BAX retrotranslocation *in cellulo*.

Using minimalist systems and SFCCS, was also successfully reproduced the formation of stable BFL1ΔC:cBID (active BID) and BFL1ΔC:BAX (heat-activated BAX) complexes corresponding to MODE 1 and MODE 2 inhibitory mechanisms, respectively. In this context, these data clearly support the notion that BCL2-type (BCLXL, BFL1) proteins inhibit apoptosis, while maintaining the global solution fold via canonical BH3 into groove, neutralizing BH3-only and BAX-type proteins, rather than only one of these two classes of proapoptotic molecules. Of note, the existence of membrane-associated complexes between BFL1 and activated BAX has not been conclusively shown before. It is also noteworthy that protein-titration and protein-mutagenesis studies performed with this minimalist systems indicate that BFL1ΔC:cBID complexes display higher affinities than BFL1ΔC:BAX complexes while both interactions are based on canonical BH3-in-groove interactions. This is in concordance with previous results (Bleicken et al, 2017; Landeta et al, 2014) but in apparent contradiction with previous work proposing that all mitochondria-associated BCL2-type proteins display higher affinities for BAX-type proteins than for BH3-only proteins since non-canonical interaction surfaces hold tighter the former but not the latter proapoptotic proteins to their antiapoptotic counterparts (Llambi et al, 2011). Although the possibility that BFL1 interactions taking place at the mitochondria may differ from those captured in our minimalist systems cannot be excluded. It should be mentioned here that the main conclusions of that study were based on results obtained with BCLXL, BCL2, and MCL1, while BFL1 was left largely unexplored.

Importantly, it was also shown by SFCCS that BFL1ΔC loses the capacity to form hetero-complexes with BAX and cBID in membranes containing pure CL, while it gains the ability to homo-oligomerize under these conditions. The homooligomerization of BFL1ΔC in liposomes seems to be driven, at least in part, by a non-canonical interaction surface involving the BFL1ΔC BH4 motif, rather than the canonical BH3:groove interaction. This notion was further supported by using TIRF and SEC analyses, where BFL1ΔC and the canonical mutant R88D, but not the non-canonical L21A mutant, dimerized in pure CL membranes. Of note, some evidence indicates that in addition to canonical interactions, non-canonical interactions can participate in the BCL2 interaction network (Andreu-Fernandez et al, 2017; Barclay et al, 2015; Gavathiotis et al, 2008).

Moreover, BFL1 is quite peculiar as it is one of the few BCL2 proteins lacking a conserved BH3 domain.

A remarkable and often overlooked property of BCL2-type proteins is their capacity to switch from an antiapoptotic to a proapoptotic phenotype (Basanez et al, 2001; Landeta et al, 2014; Megyesi et al, 2016). Here, it was observed that pure CL or oxidized CL unleash a non-canonical pore forming activity in BFL1 that presents similarities and dissimilarities with that of BAX. On the one hand, as observed with BAX, the BFL1 pore is associated with homo-complex formation (Figure 4.9), sallow membrane insertion (Figure 4.11) and membrane remodeling (Figure 4.14). On the other hand, BFL1 forms complexes and pores of smaller sizes than BAX in liposomal membranes. In addition, the basis for BFL1 homodimerization is not the canonical BH3-in-groove interactions, which is unlike the case of BAX. Importantly, it is also given the physiological relevance of the findings in minimalist systems. Specifically, it is shown that exposure/oxidation of mitochondrial CL by rotenone and staurosporine triggers non-canonical BFL1 clusterization, cytochrome c release and pyknotic nuclei formation, independent of BAX and BAK. Despite the exact relationship between BFL1 clusterization and cytochrome c release remains to be determined, it is noteworthy that BAX and BAK also form clusters during apoptosis which purportedly act as the crucial effectors of MOMP.

Thus, taking all this information into account, can be proposed that CL or CLox accumulated at the mitochondria under apoptotic conditions triggers a phenotypic switch in BFL1. Consequently, BFL1 shifts from an antiapoptotic molecule capable to neutralize activated BAX and cBID at the MOM through three different canonical heterodimerizing interactions (MODE 0, 1 and 2), to a proapoptotic factor which homo-oligomerizes via non-canonical interactions (ProDeath MODE) to form proteolipidic pores at the MOM that breach its permeability barrier. Despite not being as potent as BAX-induced cell death, this mechanism could be important in a high apoptotic pressure scenario, where BFL1 helps the cell to die with its buried proapoptotic activity. Alternative mechanisms such as calpain cleavage or alternative splicing may also unleash the pore-forming capacity of BFL1 triggering its conversion into a proapoptotic factor (Valero et al, 2012). Further studies are warranted to assess whether the BFL1 phenotypic switch unveiled here can be triggered by other apoptosis-related lipids, as well as to determine whether this ProDeath -mode of action is specific for BFL1 or can be extended to other BCL2-type proteins. Finally, the potential therapeutic use of the findings described in this study should not be dismissed.

CHAPTER 5:

General Discussion and Final Conclusions

5 General discussion, relevance and final conclusions

Tissue homeostasis is defined as the equilibrium between cell death and proliferation, thus, its dysregulation could end in pathological situations, such as cancer or neurodegenerative diseases. Apoptosis or cell suicide is a kind of programmed cell death, considered as the main regulator of this cellular balance. Apoptosis can occur through two main pathways: the "extrinsic" or death receptor pathway and the most frequent "intrinsic" or mitochondrial pathway (Czabotar et al, 2014). Concerning the mitochondrial pathway, BCL-2 family proteins are the main modulators of apoptosis which primarily act by regulating the breaching of the mitochondrial outer membrane (MOM) permeability barrier via an apoptotic pore that allows for the release of multiple apoptogenic mitochondrial factors into the cytosol (Westphal et al, 2014b).

During the last decades, crucial advances have been made in our mechanistic and structural understanding of BCL-2 family proteins. We now know that different BCL-2 family members can be classified in three main groups, based on apoptosis-related functional and structural criteria (Czabotar et al, 2014; Gimenez-Cassina & Danial, 2015; Westphal et al, 2014a): (1) BAX-type proapoptotic proteins, which once activated, directly form the mitochondrial apoptotic pore; (2) BH3-only proapoptotic proteins, which trigger functional activation of BAX-type proteins; and (3) BCL-2-type antiapoptotic proteins, which inhibit proapoptotic partners and the mitochondrial apoptotic pore. Importantly, under certain conditions, this subgroup could exhibit a bifunctional phenotype that could contribute to breach permeability barrier (Basanez et al, 2012; Basanez et al, 2001; Cheng et al, 1997; Landeta et al, 2014). We also know that many BCL-2 family proteins are amphitropic proteins that shuttle between a cytosolic conformation and a membrane-associated conformation depending on the physiological status of the cell (Edlich et al, 2011a; Lindsay et al, 2011; Schellenberg et al, 2013; Todt et al, 2015; Todt et al, 2013). Moreover, BCL-2 family proteins can also perform functions unrelated to mitochondrial apoptotic pore regulation in healthy cells (Doghman-Bouguerra & Lalli, 2017).

High-resolution X-Ray crystallography and solution NMR studies revealed that all BAX-type and BCL-2-type proteins share a common helical globular fold (Czabotar et al, 2013; Herman et al, 2008; Moldoveanu et al, 2013; Muchmore et al, 1996). A remarkable feature of these solution-based protein structures is the presence of a hydrophobic groove in BCL-2-type and BAX-type proteins, that can act in a receptor-like manner to engage BH3 domains of binding partners. Complementarily, other non-canonical surfaces have been proposed to participate in BCL2 interactoma (Andreu-Fernandez et al, 2017; Barclay et al, 2015; Gavathiotis et al, 2008). Largely based on this structural information as well as in binding studies in lipid-free environments, a number of models have been put forward to explain how different BCL-2 family proteins regulate MOM permeabilization via protein:protein interactions (Chen et al, 2015; Korsmeyer et al, 1993; Llambi et al, 2011). More recently, the importance of the MOM and its lipid composition in the mode of action of several BCL-2 family members has also been recognized (Cosentino & Garcia-

Saez, 2017; Leber et al, 2007; Subburaj et al, 2015). However, most of these models do not appropriately integrate the fact that BAX and BCLXL constantly shuttle on and off the mitochondria, nor the capacity of BCL2-type proteins to reverse their antiapoptotic phenotype under certain physiological conditions.

Understanding the structural changes driving BAX-type proteins from an apoptosis-inactive conformation to a fully activated structure responsible for MOMP has been considered the "holy grail" of the apoptosis research (Youle & Strasser, 2008). These events, are usually encompassed in the following subsections: 1) Early activation steps (N-terminal and BH3 exposure), 2) Membrane insertion, 3) Oligomerization and 4) Pore formation. Moreover, in the last years, several groups have reported that the formation of BAX supramolecular assemblies, in the form of semi-arcs, rings and clusters are directly linked with apoptotic phenotype, being fundamental to form a pore, enabling the release of mitochondrial content (Grosse et al, 2016; Nechushtan et al, 2001; Salvador-Gallego et al, 2016; Uren et al, 2017). However, two main aspects of BAX activation process remain obscure: i) the exact topology that BAX adopts in the membrane and ii) the minimal BAX subunits required to permeabilize the MOM.

In addition, as BCL2 family proteins play their biological role in the membrane, the lipid component is gaining attention. Concretely, the mitochondrial specific lipid CL, has been hailed as one of the key regulators of apoptosis. Indeed, CL content, distribution and redox state are reported to be fundamental for BAX-type proteins activities in model membranes and *in vivo* (Jiang et al, 2008; Kagan et al, 2004; Kagan et al, 2005). Moreover, during apoptosis selective ROS-mediated CL peroxidation is required for mitochondrial cyt c release (Osman et al, 2011). Furthermore, CL clusters can stabilize highly curved regions such as and those CL-formed lipid domains could act as signalling platforms for BCL2 proteins (Garofalo et al, 2005; Garofalo et al, 2003; Malorni et al, 2007; Sorice et al, 2009). However, not all the studies ascribe fundamental role to CL in BCL2 protein family function, and the exact function of the CL and other mitochondrial lipids in the activation of BCL2 family proteins remains ill defined.

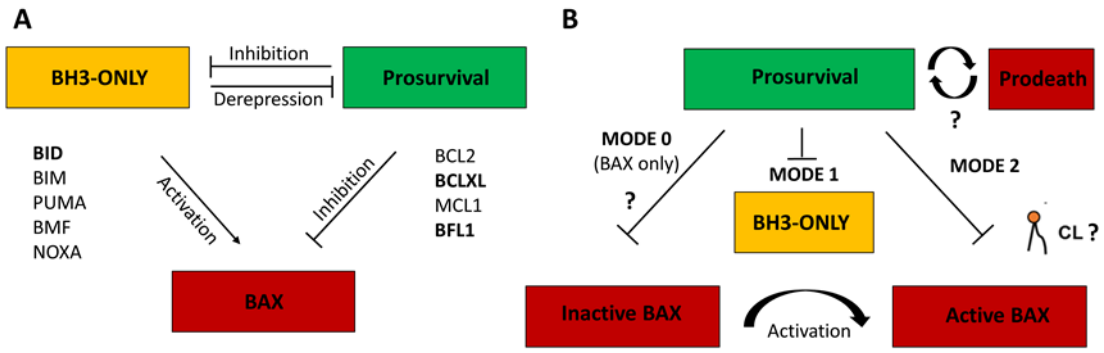

Figure 5.1 Schematic representation of the BCL2 family interaction network. (**A**) The BCL2 family can be divided into three classes: the proapoptotic BAX-type proteins, the proapoptotic BH3-only proteins and the prosurvival proteins. The prosurvival proteins inhibit the activity of the proapoptotic members of

BCL2 family. The BH3-only proteins activate BAX and BAK either directly (activation) or indirectly (derepression). The BAX-type proteins breach MOM permeability barrier. (**B**) Inhibition by prosurvival proteins may occur via three MODEs. During MODE 0, prosurvival proteins bind to peripheral BAX at the mitochondria and retro-translocate it to the cytosol. During MODE1 inhibition the antiapoptotic proteins sequester BH3-only proteins to stop them to activate BAX. During MODE 2 the antiapoptotic proteins form a complex with activated BAX to prevent MOMP.

The main aim of this Thesis is to advance in our understanding of the molecular mechanisms of action of BCL2 family proteins at the membrane level. Our focus is in the proapoptotic BCL2 family member BAX, and in the antiapoptotic BFL1.

In order to fulfil the general objective, the following specific aims were proposed:

Specific Aims:

1- To gain insight into inactive and active BAX membrane conformations.
2- To elucidate the mechanism by which BFL1 inhibits apoptosis, by analysing three putative modes of action: (1) retrotranslocation of inactive BAX from the membrane into the cytosol (MODE-0), (2) heterodimerization with and neutralization of cBID at the membrane level (MODE-1), and (3) heterodimerization with and neutralization of activated BAX at the membrane level (MODE-2)
3- To understand the role of the cardiolipin as a modulator of BFL1 and BCLXL membrane activities.

In this Thesis, several quantitative biophysical techniques were applied on model membranes and cellular systems. The inherent complexity of the apoptotic process makes very challenging to obtain detailed information about the mechanism of action of specific members of BCL2 family proteins in the native cellular context. Fortunately, several groups, including ours, have reported that is possible to mimic the basic mechanisms of action of this family of proteins, *in vitro* using model membranes and recombinant purified proteins. Of note, in this Thesis *in cellulo* experiments were combined with the *in vitro* studies to gain more insight into BAX and BFL1 modes of action.

In the first part of my Thesis, the study of both active and inactive membrane topologies of BAX was carried out by using a multidisciplinary approach and recombinant proteins. Fluorescence mapping revealed that fully active BAX adopts a BH3-in-groove dimeric conformation in MOM-like membranes, with BAX α4-α5 helices belonging to its core domain inserting deeper into the membrane lipid bilayer than BAX α6-α8 helices belonging to its latch domain. Moreover, in our reconstituted systems, antiapoptotic BCLXL formed canonical heterodimeric BH3-in-groove complexes with BAX, and blocked membrane insertion of BAX core α4-α5 helices, but not BAX latch α6-α8 helices. Furthermore, poly(ethylene glycol) (PEG) conjugation (PEGylation) at

multiple individual sites along the BAX core, but not latch domain, potently inhibited BAX pore-forming activity. Additional combined computational and experimental evidence revealed that the BAX core α5 helix displays a bilayer-destabilizing membrane interaction mode that is absent in BAX latch α6-α8 helices.

Then, it was characterized the inactive BAX membrane conformation (in the absence of apoptotic stimulus) using SCAM (Single Cysteine Accessibility Methodology). Specifically, the exposure pattern of more than twenty monocysteine mutant was analysed in solution and upon membrane interaction from isolated mitochondria and model membranes. According to PEGylation exposure pattern, inactive-BAX adopts a globular folding in the membrane, leading its C-terminal BAX α7-α9 helixes. Moreover, additional changes were observed in residues within the BAX BH3 domain and canonical groove, suggesting that interactions with the MOM lipid bilayer alone favour partial rearrangement of these two regions of the protein. Such localized BAX structural reorganization may explain the different affinities described for BCL2 interactoma in solution and in the membrane.

Overall, we propose that in the absence of apoptotic stimulus, BAX preserves its overall globular folding but experiences localized changes at the C-terminal, canonical groove and BH3 regions, leading to what we term the "lipid-primed" monomeric BAX conformation. By contrast, when BAX becomes fully activated by cBID, the protein undergoes extensive conformational changes implicating multiple different regions necessary for BAX oligomerization and extensive membrane insertion. Importantly, we also showed that membrane interactions of the BAX core (α4-α5), but not latch domain (α6-α8), is critical for BAX apoptotic pore formation.

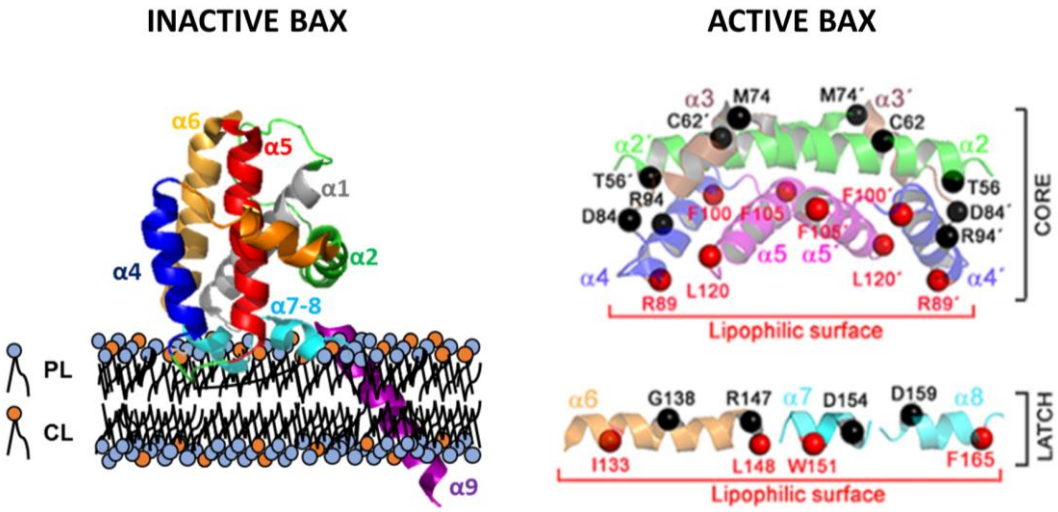

Figure 5.2. Schematic representation of inactive BAX (left) and activated BAX (right) membrane topology. The α-helixes are represented as follows: α1 (grey), α2 (green), α3 (dark-orange), α4 (dark-blue), α5 (red), α6 (light-orange), α7-α8 (cyan) and α9 (purple). CL: cardiolipin and PL: phospholipid.

As a continuation of these studies, in the second part of my Thesis the modes of inhibition of BFL1 were analysed in a lipid membrane context. Using FLIP, it was shown that BFL1 is able to retrotranslocate inactive-BAX from the membrane and applying SFCCS, I demonstrated that BFL1 forms high affinity complexes with cBID and less prominently with BAX in contact site (CS) like membranes (25CL), via a canonical BH3-into-groove interaction. In stark contrast, in solution or in pure CL (100CL) vesicles BFL1 dramatically diminished its capacity to heterodimerize with its proapoptotic counterparts.

Then, SFCCS and TIRF studies indicated that BFL1 homodimerizes in membranes containing high CL concentration. The homooligomerization of BFL1 is driven by a non-canonical interaction surface, apparently involving the N-terminal (BH4 domain) of the protein. Of note, despite the canonical BH3:groove interaction represents the dominating interaction for heteromeric and homomeric complex formation involving BCL2 family proteins, non-canonical interactions between different BCL2 family proteins have also been identified (Andreu-Fernandez et al, 2017; Barclay et al, 2015).

Next, in order to provide more structural and mechanistic details, the previously described methodology for BAX was adapted for BFL1. Thus, a fluorescence mapping of several BFL1 monocysteine mutants was performed in the presence or absence of proapoptotic partners and in membranes containing different lipid composition. In CS-like membranes BFL1 preserves the solution globular folding and inhibition capacity, but in pure CL vesicles, BFL1 undergoes a profound reorganization leading to BFL1 shallow membrane insertion. Further experiments confirm that CL-mediated groove disruption and membrane insertion of BFL1 unearths the pore forming activity of BFL1. Importantly, the antiapoptotic BCLXL in the presence of pure vesicles of this mitochondrial specific lipid, is not able to form a pore, suggesting that this process is very dependent on the nature of the "antiapoptotic" protein.

Taking all this into account, we propose that BFL1 exhibits a multimode antiapoptotic mechanism, and that BFL1 reverses its functional phenotype shifting into a proapoptotic mode at high apoptotic pressure reflected by high membrane CL content.

Finally, in the last part of my Thesis, I studied the proapoptotic phenotype of BFL1 using model membranes and in a cellular system. In the former system, I showed that BFL1 perforates CL-rich membranes and also reduces the average liposome size consistent with a BAX-type proteolipidic BFl1 pore. However, combining GUV and recombinant proteins with fluorescently labelled probes I showed that the BFL1 forms pores of smaller size than BAX. Then, I analysed the effect of CL-externalizing drugs such as rotenone and staurosporine in the behaviour of BFL1. Despite not being as potent as BAX, BFL1 wt formed clusters, induced MOMP, and elicited apoptotic nuclei in $BAX^{-/-}/BAK^{-/-}$ DKO HCT 116 cells. All these activities were substantially reduced in the non-canonical BFL1 mutant, and were completely absent in BCLXL.

This mechanism could be operative in a high apoptotic pressure scenario, where BFL1 may accelerate the apoptotic cell death process through its pore-forming activity linked to MOMP. Since overexpression of BFL1 can contribute to chemotherapeutic resistance of certain cancer cells, the reversion of BFL1 proapoptotic phenotype could be helpful in the fight against specific types of cancer.

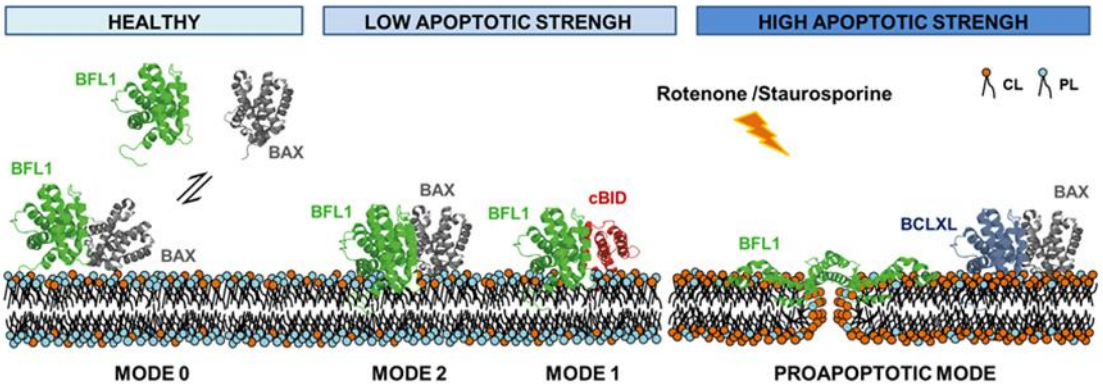

Figure 5.3 Schematic representation of all three mode of inhibition of BFL1 plus its CL-mediated proapoptotic phenotype. BFL1 (green), BAX (grey), cBID (red) and BCLXL (blue). CL: cardiolipin and PL: phospholipid.

The specific conclusions of this Thesis are:

- Inactive BAX is peripherally associated to MOM and MOM-like membranes, producing localized structural changes particularly in the C-terminal region, and leading to the "Lipid-Primed" conformation of BAX.

- Active BAX homodimerizes in the membrane by a BH3-into groove mechanism promoting membrane tension and pore formation by inserting its core, but not latch domain.
- We succeed to recapitulate all three inhibitions modes described for BCL2 antiapoptotic proteins for BFL1, in different physiologically-relevant systems. Moreover, using site-specific point mutations we conclude that BFL1 interacts with its proapoptotic counterparts mainly, if not solely, via a BH3-into-groove canonical mechanism.

- Membrane CL content modulates BFL1 heterodimerization with both BAX and cBID, as well as BFL1´s non-canonical homodimerization and pore forming activity. In concordance, CL-externalizing drugs, such as rotenone and staurosporine, promote a BFL1 specific, BAX/BAK independent, apoptotic activity in mammalian cells.

CHAPTER 6:

Resumen de la Tesis y conclusiones finales

6 Resumen de la Tesis y conclusiones finales

La homeostasis de tejidos es considerado como el equilibrio entre la muerte y proliferación celular, y es por ello que su desregulación a menudo está asociada a diversas situaciones patológicas, tales como enfermedades neurodegenerativas o el cáncer. Este equilibrio, se encuentra regulado principalmente por un mecanismo denominado apoptosis o suicidio celular. Este tipo de muerte celular programada es activado mediante dos rutas co-dependientes: (i) la ruta extrínseca donde median los receptores de muerte y la ruta intrínseca o mitocondrial la cual constituye la forma más común de muerte celular por apoptosis (Czabotar et al, 2014). En cuanto a la ruta mitocondrial, la familia de proteínas BCL2 se erige como pieza clave en la regulación de esta vía, principalmente, a nivel de la permeabilización de la membrana externa mitocondrial (MEM). Este proceso, es considerado como el punto de no retorno de la vía, en el cual se forma un poro en la MEM que permite la liberación de material ocluido en la mitocondria al citosol y una vez allí este desencadena la muerte celular por apoptosis (Westphal et al, 2014b).

En las últimas décadas, se han realizado avances de notoria importancia en el conocimiento sobre los mecanismos de acción de la familia de proteínas BCL2 (Czabotar et al, 2014; Westphal et al, 2014b). Actualmente las BCL2 se clasifican en tres subgrupos basándose criterios funcionales y estructurales (Gimenez-Cassina & Danial, 2015): (i) proteínas proapoptóticas multidominio o tipo BAX, las cuales una vez activadas, forman un poro en la membrana mitocondrial externa, (ii) las proapoptótica de único dominio BH3 o BH3-only, las cuales activan a las tipo BAX y (iii) las antiapoptóticas o tipo BCL2, las cuales inhiben a ambos tipos de proapoptóticas y por consiguiente la formación del poro apoptótico. Sin embargo, han sido descritas ciertas condiciones fisiológicas donde este último subgrupo sufre una reversión total de su fenotipo antiapoptótico y adquiere una actividad formadora de poro o proapoptótica (Basanez et al, 2012; Basanez et al, 2001; Cheng et al, 1997; Landeta et al, 2014). Además, se sabe que la localización celular de las proteínas de esta familia es de importancia capital para su actividad. Interesantemente, muchas de las proteínas de la familia son anfitrópicas (localización dual, citosólica y membranal) la cual varía en función de las condiciones celulares y el estímulo apoptótico (Edlich et al, 2011b; Lindsay et al, 2011; Schellenberg et al, 2013; Todt et al, 2015; Todt et al, 2013). Por otra parte, cabe la pena destacar que la familia de proteínas BCL2 posee múltiples y muy diversas funciones en la célula no relacionadas con la muerte celular programada o apoptosis (Doghman-Bouguerra & Lalli, 2017).

Estudios de resolución atómica, tales como la cristalografía rayos X y la resonancia magnética nuclear, han puesto de manifiesto que las proteínas tipo BCL2 o antiapoptóticas y las tipo BAX o proapoptóticas multidominio, poseen una estructura globular similar a pesar de presentar funciones contrapuestas (Czabotar et al, 2013; Herman et al, 2008; Moldoveanu et al, 2013; Muchmore et al, 1996). Atendiendo a las estructuras resueltas, esta familia de proteínas se caracteriza por poseer una estructura globular compuesta por una α-hélice hidrofóbica central

rodeada por varios pares de hélices anfipáticas. Además, tanto las proteínas multidominio, antiapoptóticas como las proapoptóticas, poseen un bolsillo hidrofóbico el cual actúa como receptor para el dominio BH3 (dominio universal de la familia) que actúa como ligando, conformando una interacción canónica comúnmente denominada como BH3 en el groove. De manera complementaria, durante los últimos años se han sugerido numerosas superficies de interacción alternativas o no-canónicas (Andreu-Fernandez et al, 2017; Barclay et al, 2015; Bleicken et al, 2017), lo cual agrega un grado extra de complejidad a las interacciones entre los miembros de la familia BCL2. La información estructural recopilada a lo largo de más de una década ha permitido el desarrollo de numerosas teorías sobre los modos de interacción proteína: proteína entre los miembros de la familia (Chen et al, 2015; Korsmeyer et al, 1993; Llambi et al, 2011). Sin embargo, estas proteínas realizan su función biológica en la membrana y es por tanto para la comprensión de su interactoma, su estudio a nivel de membrana se antoja indispensable. Recientemente, el componente lipídico y la membrana han cobrado importancia, por lo que su papel regulador en las interacciones entre los diferentes miembros de la familia está siendo objeto de estudio intensivo (Cosentino & Garcia-Saez, 2017; Leber et al, 2007; Subburaj et al, 2015).

Sin embargo, a pesar de tener diversos modelos de interacción, estos no han sido capaces de integrar: (i) el mecanismo de inhibición conocido como retrotranslocación o MODO 0 de inhibición, por el cual las proteínas antiapoptóticas son capaces translocar desde la MEM al citosol a las proteinas tipo BAX y (ii) la reversión del fenotipo antiapoptótico de las proteínas tipo BCL2.

En este contexto, el entendimiento de los cambios estructurales mediante los cuales la proteína BAX, pasa de una estructura globular inactiva, a una estructura activa en membrana responsable de la permeabilización de la MEM, se ha considerado como el santo grial en la investigación de las BCL2 (Youle & Strasser, 2008). La activación de la proteína proapoptótica BAX se asocia a 1) cambio en su segmento N-terminal y dominio BH3, 2) inserción en membrana, 3) oligomerización y 4) formación del poro apoptótico. Recientemente, varios grupos han demostrado que la formación de estructuras supramoleculares de las proteínas tipo BAX en forma de semi-arcos, anillos y clúster están relacionadas con el fenotipo apoptótico, siendo estas estructuras fundamentales para la liberación del citocromo c mitocondrial ocluido en este orgánulo (Grosse et al, 2016; Nechushtan et al, 2001; Salvador-Gallego et al, 2016; Uren et al, 2017). Sin embargo, dos importantes aspectos del proceso de activación se encuentran vagamente descritos: (i) la disposición estructural exacta que la proteína BAX adopta en membrana y (ii) la cantidad mínima de subunidades de BAX necesarias para la formación del poro.

Como se mencionaba anteriormente, puesto que la membrana conforma el locus biológico de estas proteinas, el estudio del componente lipídico y de la propia membrana se encuentra actualmente en boga. Concretamente, el lípido especifico de la mitocondria, cardiolipina (CL), se ha erigido como uno de los moduladores claves de la apoptosis. Tanto es así, que el contenido, la

distribución y el estado redox de este lípido han sido contenido de estudio en las actividades de membrana de las proteínas tipo BAX encargadas de la formación de poro apoptótico (Jiang et al, 2008; Kagan et al, 2004; Kagan et al, 2005). Ademas, diversos grupos han descrito que durante la apoptosis, la peroxidación de la CL mediada por la formación de ROS, es necesaria para la liberación del citocromo c de las crestas mitocondriales, y por ende en la consecución del fenotipo apoptótico (Osman et al, 2011). También, las peculiaridades físico-químicas de este lípido, le permiten la formación de clúster capaces estabilizar zonas de mucha curvatura, las cuales han sido descritas como potenciales plataformas de interacción de las BCL2 (Garofalo et al, 2005; Garofalo et al, 2003; Malorni et al, 2007; Sorice et al, 2009). Sin embargo, a pesar de su importancia, la función exacta de la CL en particular y de los lípidos en general, en las actividades de membrana de las BCL2, se encuentra vagamente descrita.

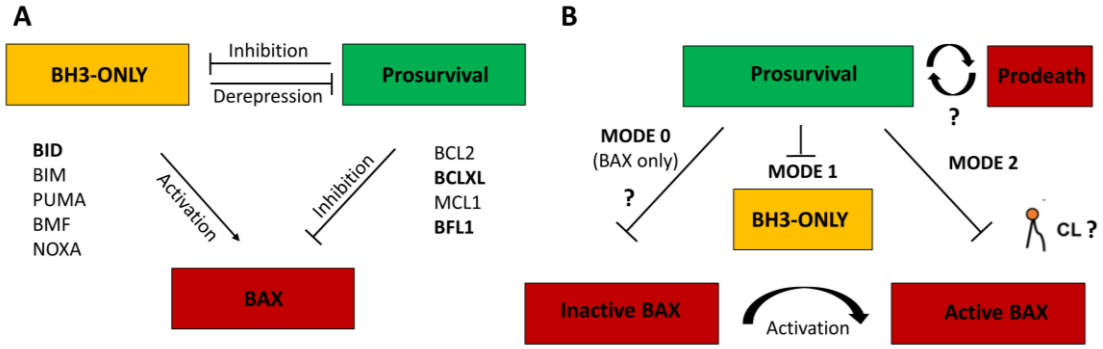

Figura R.1. Representación esquemática de la red de interacciones de la familia de proteínas BCL2. (**A**) La familia de proteínas BCL2 puede ser dividida en tres subclases: las proapoptóticas multidominio o tipo BAX, las proapoptóticas tipo BH3 solo y las antiapoptóticas o tipo BCL2. Las antiapoptóticas inhiben la actividad de ambos subgrupos de proteínas proapoptóticas. Las tipo BH3-solo activan a las tipo BAX directamente o indirectamente, mediante el desplazamiento de la antiapoptótica unida. (**B**) Las proteínas antiapoptóticas inhiben mediante tres modos de actuación. En el MODO 0, las proteínas antiapoptóticas se unen a las tipo BAX unidas periféricamente a la membrana y la retrotranslocan desde la MEM hasta el citosol. En el MODO 1, las antiapoptóticas se unen a las BH3 solo en membrana, inhibiendo por tanto la activación de estas a las tipo BAX. En el MODO 2 las antiapoptóticas forman complejo con las tipo BAX activas para así prevenir la permeabilización de la MEM.

El objetivo de esta Tesis Doctoral ha sido avanzar en la comprensión de los mecanismos de acción de la familia de proteínas BCL2, así como de los factores reguladores que modulan su actividad durante la apoptosis. Concretamente, nos centramos en dos miembros de la familia: la proapoptótica multidominio prototípica BAX, y la poco estudiada proteína antiapoptótica BFL1. Para la consecución de estos objetivos, se han realizado estudios a nivel de membrana tanto en sistemas modelo como en células, mediante diversas técnicas biofísicas cuantitativas.

A fin de materializar el objetivo general, se plantearon los siguientes objetivos específicos:

1. Caracterizar la conformación en membrana de BAX tanto en su forma activa como inactiva.
2. Dilucidar el modo de acción de BFL1, centrándonos en los tres modos de inhibición descritos para las proteínas tipo BCL2 (1) retrotranslocación de las proteínas tipo BAX (MODO-0), (2) heterodimerización con las proteinas BH3 solo (MODO-1) y (3) formando un complejo de membrana con una BAX activa.
3. Establecer el rol de la cardiolipina como modulador de las actividades de membrana de las proteínas BFL1 y BCLXL.

Dada la complejidad inherente al proceso apoptótico, resulta intrincado obtener información detallada acerca del modo de acción de miembros específicos de la familia BCL2 utilizando sistemas celulares completos. Afortunadamente, diversos grupos, incluyendo el nuestro, han comprobado que es posible reproducir los mecanismos básicos de acción de los diferentes subgrupos de la familia BCL2 *in vitro*. En esta Tesis, se han realizado estudios mecanísticos sobre las BCL2 y sus factores reguladores utilizando diversos sistemas reconstituidos compuestos por proteínas recombinantes purificadas y membranas modelo. Sin embargo, a fin de otorgar una mayor fisiologicidad a los resultados *in vitro*, gran parte de estos estudios se complementaron con ensayos celulares, validando y robusteciendo nuestras conclusiones.

En la primera parte de la Tesis, se estudió la topología de la proteína BAX a nivel de membrana en presencia y ausencia de activadores de la misma, utilizando para ello proteína recombinante, sistemas modelo que mimetizan las condiciones mitocondriales y mitocondrias aisladas. Mediante el uso de diversos mutantes monocisteína cuidadosamente seleccionados a lo largo de la estructura de la proteína, conjugados con la sonda sensible a la polaridad del ambiente, y analizando de la fluorescencia de estos residuos, concluimos que BAX completamente activa adopta en membrana una conformación dimérica tipo "BH3-intro groove". Además de confirmar que BAX activo adopta una conformación donde el dominio BH3 de un monómero de BAX se introduce en el groove de otro monómero, se ha demostrado que lo hace insertando su dominio "core" (hélices α4-α5), pero no su dominio "latch" (hélices α6-α8) en membranas modelo que imitan a la MEM.

También, en nuestro sistema reconstituido hemos podido comprobar que la proteína antiapoptótica BCLXL forma heterodímeros con BAX mediante la interacción canónica "BH3-intro groove" y que impide la inserción del dominio core responsable de la formación del poro. Ademas, utilizando estos mismos mutantes de monocisteína y conjugándolos con el compuesto polyethilene glycol (PEG, 0.5kDa) se ha podido constatar que la unión de este compuesto a los residuos del dominio core, pero no del dominio latch, capaban la actividad formadora de poro de la proteína BAX. Estudios complementarios de computación y evidencias empíricas utilizando

péptidos de diversas hélices de la proteína, confirmaron que la hélice α5 del dominio core, pero no la α6 perteneciente al dominio latch, era capaz de desestabilizar la membrana.

A fin de caracterizar el proceso de la activación de la proteína BAX, se estudió su conformación a nivel de membrana en su estado inicial inactivo o en ausencia de activador. En este caso se continuó con la conjugación del PEG-5kDa a múltiples mutantes de monocisteína, esta vez *in situ* en la propia membrana mitocondrial de células deficientes para BAX. Concretamente, analizamos el grado de exposición al PEG de las cisteínas de los diversos mutantes, estableciendo un patrón de exposición en solución y en membrana. De esta manera, concluimos que BAX inactivo, no es capaz de liberar citocromo c, adopta una estructura globular similar a la que tiene en solución, pero apoyando su C-terminal α7-α9. Este patrón muestra también, pequeños cambios en residuos cercanos al bolsillo hidrofóbico que permite la dimerización con el resto de miembros de la familia. Significativamente, estos pequeños cambios en el receptor canónico universal de las BCL2, podrían explicar las diferentes afinidades mostradas por lo miembros de la familia BCL2 en solución y en membrana.

Considerando todo referente a la topología de BAX en membrana, concluimos que en ausencia de estímulo apoptótico BAX adopta una estructura globular apoyando su C-terminal en la membrana, conformación a la cual hemos denominado "lipid primed", ya que el lípido parece favorecer la exposición del bolsillo hidrofóbico que actuará como receptor en el proceso apoptótico. Sin embargo, una vez activada, BAX adopta una configuración BH3 into groove donde la inserción del dominio core, pero no del dominio latch, se antoja indispensable para la formación del poro apoptótico.

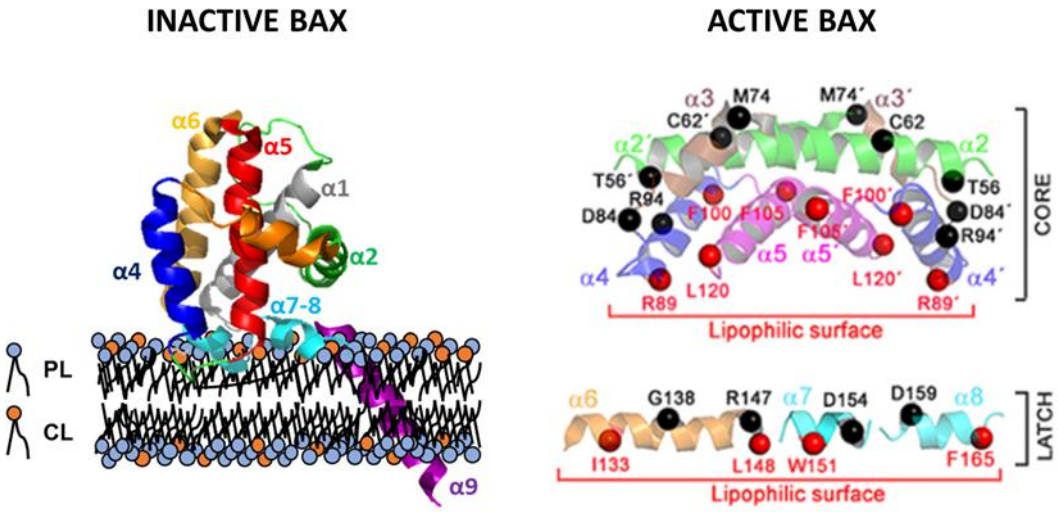

Figure R.2. Representación esquemática de la topología a nivel de membrana de BAX inactive (izq.) y active (dcha.). Las hélices α están representadas como sigue: α1 (gris), α2 (verde), α3 (naranja oscuro), α4 (azul oscuro), α5 (rojo), α6 (naranja claro), α7-α8 (cian) and α9 (morado). CL: cardiolipina and PL: fosfolípido.

Como continuación de estos estos estudios, en la segunda parte de la tesis analizamos los modos de inhibición de BFL1 en el contexto de la membrana. Mediante el uso de FLIP (fluorescencce loss in photobleaching), se mostró como BFL1 es capaz de retrotranslocar a BAX desde la membrana hasta el citosol. Utilizando SFCCS (scanning fluorescene cross correlation spectroscopy), se demostró que BFL1 forma complejos de alta afinidad vía canónica o BH3-into-groove, con la proteína BH3-solo cBID y en menor medida con BAX en membranas de composición que imita a las zonas de contacto que encontramos en las mitocondrias.

Por el contrario en membranas con alto contenido en cardiolipina, las cuales imitan los microdominios de este lípido descritos en condiciones apoptóticas, BFL1 no solo pierde la capacidad de formar heterodímeros con los miembros proapoptóticos, sino que también es capaz de homodimerizar vía una superficie no descrita previamente situada en el dominio BH4 de la proteína. Además, estudios de TIRFm (Total internal reflection fluorescence microscopy) y de tamizado molecular confirmaron que BFL1 es capad de dimerizar vía una superficie no canónica. Esta capacidad de homodimerización de BFL1, no se promueve ni en solución ni en membranas con una composición lipídica característica de condiciones celulares no apoptóticas.

Resumiendo, la capacidad inhibitoria de BFL1 es vía canónica, donde el BH3 de las proteínas proapoptóticas se introduce en el bolsillo hidrofóbico de BFL1. Sin embargo, en membranas apoptóticas enriquecidas en CL, BFL1 forma homodímeros mediante una interacción no canónica que implica su dominio BH4 (α1-α2). Este hallazgo, aunque inesperado, puede explicarse estructuralmente ya que BFL1 es una de las pocas proteinas de la familia BCL2 que no posee un dominio BH3 canónico, lo cual en principio explicaría que el homodímero formado por BFL1 no implicase a este dominio, hecho que confirmamos mediante el uso de mutantes específicos y las técnicas anteriormente descritas.

Intentando aportar detalles tanto estructurales como mecanísticos, adaptamos para BFL1 la metodología aplicada en la resolución de la topología a nivel de membrana de BAX. Por tanto, realizamos un mapeo de fluorescencia de diversos mutantes de monocisteína conjugados con NBD, en presencia/ausencia de los miembros proapoptóticos en membranas de diferentes composiciones lipídicas. A través de los datos obtenidos de los espectros de los diferentes mutantes de monocisteína, podemos concluir que en membranas de bajo contenido en CL, BFL1 adopta una conformación globular que mantiene su bolsillo hidrofóbico y por ende su capacidad de interaccionar con los miembros proapoptóticos. Sin embargo, en membranas de CL, BFL1 se reorganiza totalmente, perdiendo su estructura globular e insertando periféricamente la totalidad de sus alpha-hélices en la membrana. Seguidamente, comprobamos que esta reorganización e inserción de contenido proteico en la membrana, generaba una tensión en la misma capaz de formar un poro. Merece la pena destacar el diferente comportamiento que exhibe la proteína antiapoptótica BCLXL, ya que ésta en presencia de membranas de CL, no es capaz de perturbar

la membrana ni formar un poro, por lo que el efecto que ejerce la CL sobre BFL1 parece ser especifico del tipo de proteína antiapoptótica.

Teniendo en cuenta todo lo arriba mencionado, concluimos que BFL1 posee un mecanismo de acción multimodal (Modos 0, 1 y 2) y bifuncional (fenotipo antiapoptótico y proapoptótico) regulado por la cantidad de CL en la membrana.

En el tercer periodo de la tesis doctoral, se trató de caracterizar la naturaleza del poro formado por BFL1, tanto en membranas modelo como en sistemas celulares con mayor fisiologicidad. Primeramente, en sistemas *in vitro* observamos que BFL1 no solo formaba un poro en la membrana, sino que también parecía reducir el diámetro de las vesículas, lo cual sugeriría que la naturaleza del poro formado por BFL1 en liposomas de CL es proteolipídica (Bleicken et al, 2016). También, analizando la permeabilización en GUV (giant unilamellar vesicles), pudimos concretar que a diferencia de lo que sucede con BAX, BFL1 forma un poro de pequeño tamaño. Posteriormente, analizamos el efecto de dos drogas externalizadoras de CL como son la rotenona y la estaurosporina sobre la actividad BFL1. En coherencia con resultados previos, la externalización de CL en células de mamífero, estimula un fenotipo proapoptótico en BFL1, menos predominantemente en el mutante no-canónico y totalmente ausente en el caso de BCLXL, el cual es capaz de formar un poro en la MEM independientemente de BAX y BAK.

A pesar de que la reversión fenotípica de BFL1, ésta no induce una muerte celular tan marcada como la proteína proapoptótica BAX. Por lo que se plantea un escenario donde debido a pronunciados estímulos apoptóticos que conllevan la externalización de CL, BFL1 es capaz de promover/facilitar la muerte celular por apoptosis. En este punto cabe mencionar que la sobreexpresión de las proteínas antiapoptóticas es la principal causa de resistencia a la quimioterapia, por lo que su reversión fenotípica plantea una alternativa valiosa en la lucha contra el cáncer.

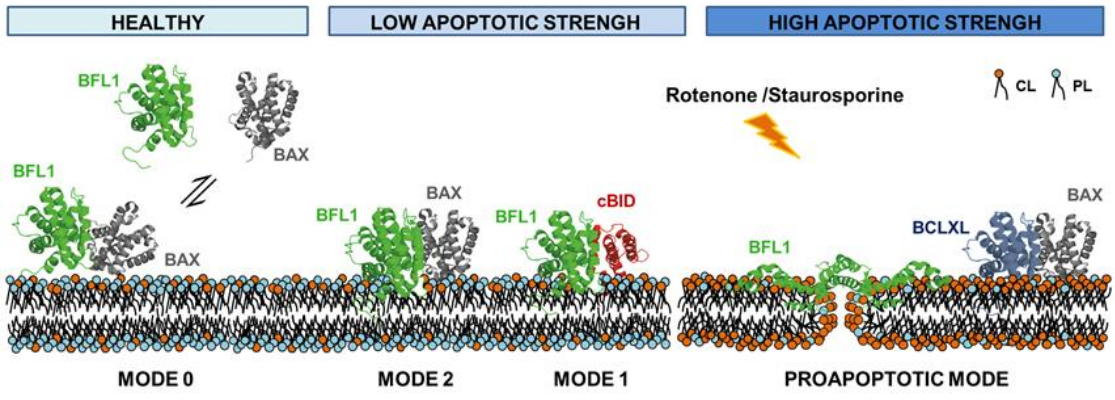

Figura R.3. Representación esquemática de los tres modos de inhibición de BFL1 y el fenotipo apoptótico mediado por CL. BFL1 (verde), BAX (gris), cBID (rojo) and BCLXL (azul). CL: cardiolipina and PL: fosfolípido.

Las conclusiones específicas de la Tesis son:

- La proteína BAX inactiva se encuentra periféricamente asociada a la MEM y a membranas que imitan su composición lipídica, produciendo cambios estructurales localizados predominantemente en el C-terminal, en una configuración denominada como “Lipid-Primed”.

- La proteína BAX activa homodimeriza en le membrana vía la interacción canonical BH3-into-groove, insertando su dominio core pero no su dominio latch, produciendo una tensión en la membrana y formando un poro.

- Se han logrado recapitular los tres mecanismos de inhibición descritos en las proteinas tipo BCL2 para BFL1, en diferentes sistemas fisiológicamente relevantes. Además, mediante el uso de mutantes puntuales concluimos que BFL1 interacciona con los miembros proapoptóticos es predominantemente, sino únicamente, mediante una interacción canónica tipo BH3-into-groove.

- El contenido de CL de la membrana modula la heterodimerización de BFL1 con tanto BAX como con cBID, además de una actividad intrínseca de BFL1 para su homooligomerization no-canónica y formadora de poro. En concordancia, las drogas externalizadoras de CL, rotenona y estaurosporina, promueven en células de mamífero esta actividad específica de BFL1 para formar un poro en la MEM de manera independiente de BAX y BAK.

Publications

1- **BAK dimers conform the minimum molecules required for the apoptotic pore formation.**
Valero JG*, **Flores-Romero H***, Landeta O, García-Porras M and Basañez G
(in preparation)

2- **BFL1 modulates apoptosis at the membrane level through a bifunctional and multimodal mechanism.**
Flores-Romero H, Ugarte-Uribe B, Cosentino K, Landeta O, García-Porras M, Ana Garcia-Sáez AJ, and Basañez G.
EMBO J (submitted)

3- **Membrane insertion of the BAX core, but not latch domain, drives apoptotic pore formation.**
Flores-Romero H, García-Porras M and Basañez G
Sci. Reports (accepted 31/10/2017)

4- **Lipid-dependent bimodal MCL1 membrane activity.**
Landeta O*, Valero JG*, **Flores-Romero H**, Bustillo-Zabalbeitia I, Landajuela A, Garcia-Porras M, Terrones O, Basañez G.
ACS Chem Biol. 2014 Dec 19;9(12):2852-63.

CHAPTER 7:

References

7 References

Adams JM, Cory S (2007) The Bcl-2 apoptotic switch in cancer development and therapy. *Oncogene* **26:** 1324-1337

Alavian KN, Li H, Collis L, Bonanni L, Zeng L, Sacchetti S, Lazrove E, Nabili P, Flaherty B, Graham M, Chen Y, Messerli SM, Mariggio MA, Rahner C, McNay E, Shore GC, Smith PJ, Hardwick JM, Jonas EA (2011) Bcl-xL regulates metabolic efficiency of neurons through interaction with the mitochondrial F1FO ATP synthase. *Nature cell biology* **13:** 1224-1233

Alder NN, Jensen RE, Johnson AE (2008) Fluorescence mapping of mitochondrial TIM23 complex reveals a water-facing, substrate-interacting helix surface. *Cell* **134:** 439-450

Alsop AE, Fennell SC, Bartolo RC, Tan IK, Dewson G, Kluck RM (2015) Dissociation of Bak alpha1 helix from the core and latch domains is required for apoptosis. *Nature communications* **6:** 6841

Aluvila S, Mandal T, Hustedt E, Fajer P, Choe JY, Oh KJ (2014) Organization of the mitochondrial apoptotic BAK pore: oligomerization of the BAK homodimers. *The Journal of biological chemistry* **289:** 2537-2551

Anderluh G, Lakey JH (2008) Disparate proteins use similar architectures to damage membranes. *Trends in biochemical sciences* **33:** 482-490

Andreu-Fernandez V, Sancho M, Genoves A, Lucendo E, Todt F, Lauterwasser J, Funk K, Jahreis G, Perez-Paya E, Mingarro I, Edlich F, Orzaez M (2017) Bax transmembrane domain interacts with prosurvival Bcl-2 proteins in biological membranes. *Proceedings of the National Academy of Sciences of the United States of America* **114:** 310-315

Angelova MI, Dimitrov, D.S. (1986) Liposome electroformation. *Faraday Discuss Chem Soc* **81:** 303-311

Angelova MI, Soleau, S., Meleard, P., Faucon, J.F., Bothorel, P. (1992) Preparation of giant vesicles by external AC electric fields. Kinetics and applications. *Prog Colloid Polym Sci* **89:** 127-131

Annis MG, Soucie EL, Dlugosz PJ, Cruz-Aguado JA, Penn LZ, Leber B, Andrews DW (2005) Bax forms multispanning monomers that oligomerize to permeabilize membranes during apoptosis. *The EMBO journal* **24:** 2096-2103

Antonsson B, Montessuit S, Sanchez B, Martinou JC (2001) Bax is present as a high molecular weight oligomer/complex in the mitochondrial membrane of apoptotic cells. *The Journal of biological chemistry* **276:** 11615-11623

Aouacheria A, Baghdiguian S, Lamb HM, Huska JD, Pineda FJ, Hardwick JM (2017) Connecting mitochondrial dynamics and life-or-death events via Bcl-2 family proteins. *Neurochemistry international* **109:** 141-161

Aouacheria A, Combet C, Tompa P, Hardwick JM (2015) Redefining the BH3 Death Domain as a 'Short Linear Motif'. *Trends in biochemical sciences* **40:** 736-748

Aouacheria A, Rech de Laval V, Combet C, Hardwick JM (2013) Evolution of Bcl-2 homology motifs: homology versus homoplasy. *Trends in cell biology* **23:** 103-111

Apellaniz B, Nieva JL, Schwille P, Garcia-Saez AJ (2010) All-or-none versus graded: single-vesicle analysis reveals lipid composition effects on membrane permeabilization. *Biophysical journal* **99:** 3619-3628

Ardail D, Lerme F, Louisot P (1991) Involvement of contact sites in phosphatidylserine import into liver mitochondria. *The Journal of biological chemistry* **266:** 7978-7981

Ardail D, Privat JP, Egret-Charlier M, Levrat C, Lerme F, Louisot P (1990) Mitochondrial contact sites. Lipid composition and dynamics. *The Journal of biological chemistry* **265:** 18797-18802

Arnoult D, Parone P, Martinou JC, Antonsson B, Estaquier J, Ameisen JC (2002) Mitochondrial release of apoptosis-inducing factor occurs downstream of cytochrome c release in response to several proapoptotic stimuli. *The Journal of cell biology* **159:** 923-929

Axelrod D (2001a) Selective imaging of surface fluorescence with very high aperture microscope objectives. *Journal of biomedical optics* **6:** 6-13

Axelrod D (2001b) Total internal reflection fluorescence microscopy in cell biology. *Traffic* **2:** 764-774

Bacia K, Kim SA, Schwille P (2006) Fluorescence cross-correlation spectroscopy in living cells. *Nature methods* **3:** 83-89

Bagatolli LA (2003) Thermotropic behavior of lipid mixtures studied at the level of single vesicles: giant unilamellar vesicles and two-photon excitation fluorescence microscopy. *Methods in enzymology* **367:** 233-253

Baggetto LG, Clottes E, Vial C (1992) Low mitochondrial proton leak due to high membrane cholesterol content and cytosolic creatine kinase as two features of the deviant bioenergetics of Ehrlich and AS30-D tumor cells. *Cancer research* **52:** 4935-4941

Baines CP, Kaiser RA, Purcell NH, Blair NS, Osinska H, Hambleton MA, Brunskill EW, Sayen MR, Gottlieb RA, Dorn GW, Robbins J, Molkentin JD (2005) Loss of cyclophilin D reveals a critical role for mitochondrial permeability transition in cell death. *Nature* **434:** 658-662

Baines CP, Kaiser RA, Sheiko T, Craigen WJ, Molkentin JD (2007) Voltage-dependent anion channels are dispensable for mitochondrial-dependent cell death. *Nature cell biology* **9:** 550-555

Bakas L, Ostolaza H, Vaz WL, Goni FM (1996) Reversible adsorption and nonreversible insertion of Escherichia coli alpha-hemolysin into lipid bilayers. *Biophysical journal* **71:** 1869-1876

Bakhshi A, Jensen JP, Goldman P, Wright JJ, McBride OW, Epstein AL, Korsmeyer SJ (1985) Cloning the chromosomal breakpoint of t(14;18) human lymphomas: clustering around JH on chromosome 14 and near a transcriptional unit on 18. *Cell* **41:** 899-906

Barclay LA, Wales TE, Garner TP, Wachter F, Lee S, Guerra RM, Stewart ML, Braun CR, Bird GH, Gavathiotis E, Engen JR, Walensky LD (2015) Inhibition of Pro-apoptotic BAX by a noncanonical interaction mechanism. *Molecular cell* **57:** 873-886

Bartlett GR (1959) Colorimetric assay methods for free and phosphorylated glyceric acids. *The Journal of biological chemistry* **234:** 469-471

Basanez G, Hardwick JM (2008) Unravelling the bcl-2 apoptosis code with a simple model system. *PLoS biology* **6:** e154

Basanez G, Nechushtan A, Drozhinin O, Chanturiya A, Choe E, Tutt S, Wood KA, Hsu Y, Zimmerberg J, Youle RJ (1999) Bax, but not Bcl-xL, decreases the lifetime of planar phospholipid bilayer membranes at subnanomolar concentrations. *Proceedings of the National Academy of Sciences of the United States of America* **96:** 5492-5497

Basanez G, Sharpe JC, Galanis J, Brandt TB, Hardwick JM, Zimmerberg J (2002) Bax-type apoptotic proteins porate pure lipid bilayers through a mechanism sensitive to intrinsic monolayer curvature. *The Journal of biological chemistry* **277:** 49360-49365

Basanez G, Soane L, Hardwick JM (2012) A new view of the lethal apoptotic pore. *PLoS biology* **10:** e1001399

Basanez G, Zhang J, Chau BN, Maksaev GI, Frolov VA, Brandt TA, Burch J, Hardwick JM, Zimmerberg J (2001) Pro-apoptotic cleavage products of Bcl-xL form cytochrome c-conducting pores in pure lipid membranes. *The Journal of biological chemistry* **276:** 31083-31091

Baulies A, Montero J, Matias N, Insausti N, Terrones O, Basanez G, Vallejo C, Conde de La Rosa L, Martinez L, Robles D, Morales A, Abian J, Carrascal M, Machida K, Kumar DBU, Tsukamoto H, Kaplowitz N, Garcia-Ruiz C, Fernandez-Checa JC (2017) The 2-oxoglutarate carrier promotes liver cancer by sustaining mitochondrial GSH despite cholesterol loading. *Redox biology* **14:** 164-177

Berberich I, Hildeman DA (2017) The Bcl2a1 gene cluster finally knocked out: first clues to understanding the enigmatic role of the Bcl-2 protein A1. *Cell death and differentiation* **24:** 572-574

Bernardino de la Serna J, Perez-Gil J, Simonsen AC, Bagatolli LA (2004) Cholesterol rules: direct observation of the coexistence of two fluid phases in native pulmonary surfactant membranes at physiological temperatures. *The Journal of biological chemistry* **279:** 40715-40722

Betaneli V, Schwille P (2013) Fluorescence correlation spectroscopy to examine protein-lipid interactions in membranes. *Methods in molecular biology* **974:** 253-278

Beverly LJ, Howell LA, Hernandez-Corbacho M, Casson L, Chipuk JE, Siskind LJ (2013) BAK activation is necessary and sufficient to drive ceramide synthase-dependent ceramide accumulation following inhibition of BCL2-like proteins. *The Biochemical journal* **452:** 111-119

Bevers EM, Williamson PL (2010) Phospholipid scramblase: an update. *FEBS letters* **584:** 2724-2730

Billen LP, Kokoski CL, Lovell JF, Leber B, Andrews DW (2008) Bcl-XL inhibits membrane permeabilization by competing with Bax. *PLoS biology* **6:** e147

Birbes H, El Bawab S, Hannun YA, Obeid LM (2001) Selective hydrolysis of a mitochondrial pool of sphingomyelin induces apoptosis. *FASEB journal : official publication of the Federation of American Societies for Experimental Biology* **15:** 2669-2679

Birbes H, Luberto C, Hsu YT, El Bawab S, Hannun YA, Obeid LM (2005) A mitochondrial pool of sphingomyelin is involved in TNFalpha-induced Bax translocation to mitochondria. *The Biochemical journal* **386:** 445-451

Bleicken S, Classen M, Padmavathi PV, Ishikawa T, Zeth K, Steinhoff HJ, Bordignon E (2010) Molecular details of Bax activation, oligomerization, and membrane insertion. *The Journal of biological chemistry* **285:** 6636-6647

Bleicken S, Hantusch A, Das KK, Frickey T, Garcia-Saez AJ (2017) Quantitative interactome of a membrane Bcl-2 network identifies a hierarchy of complexes for apoptosis regulation. *Nature communications* **8:** 73

Bleicken S, Hofhaus G, Ugarte-Uribe B, Schroder R, Garcia-Saez AJ (2016) cBid, Bax and Bcl-xL exhibit opposite membrane remodeling activities. *Cell death & disease* **7:** e2121

Bleicken S, Jeschke G, Stegmueller C, Salvador-Gallego R, Garcia-Saez AJ, Bordignon E (2014) Structural model of active Bax at the membrane. *Molecular cell* **56:** 496-505

Bleicken S, Landeta O, Landajuela A, Basanez G, Garcia-Saez AJ (2013a) Proapoptotic Bax and Bak proteins form stable protein-permeable pores of tunable size. *The Journal of biological chemistry* **288:** 33241-33252

Bleicken S, Wagner C, Garcia-Saez AJ (2013b) Mechanistic differences in the membrane activity of Bax and Bcl-xL correlate with their opposing roles in apoptosis. *Biophysical journal* **104:** 421-431

Bogner C, Leber B, Andrews DW (2010) Apoptosis: embedded in membranes. *Current opinion in cell biology* **22:** 845-851

Boldogh IR, Pon LA (2006) Interactions of mitochondria with the actin cytoskeleton. *Biochimica et biophysica acta* **1763:** 450-462

Böttcher CJF, van Gent, C.M. (1961) A rapid and sensitive sub-micro phosphorus determination. *Anal Chim Acta* **24:** 203-204

Breckenridge DG, Germain M, Mathai JP, Nguyen M, Shore GC (2003) Regulation of apoptosis by endoplasmic reticulum pathways. *Oncogene* **22:** 8608-8618

Brien G, Debaud AL, Robert X, Oliver L, Trescol-Biemont MC, Cauquil N, Geneste O, Aghajari N, Vallette FM, Haser R, Bonnefoy-Berard N (2009) C-terminal residues regulate localization and function of the antiapoptotic protein Bfl-1. *The Journal of biological chemistry* **284:** 30257-30263

Brockman H (1999) Lipid monolayers: why use half a membrane to characterize protein-membrane interactions? *Current opinion in structural biology* **9:** 438-443

Canals D, Hannun YA (2013) Novel chemotherapeutic drugs in sphingolipid cancer research. *Handbook of experimental pharmacology***:** 211-238

Cartron PF, Arokium H, Oliver L, Meflah K, Manon S, Vallette FM (2005) Distinct domains control the addressing and the insertion of Bax into mitochondria. *The Journal of biological chemistry* **280:** 10587-10598

Certo M, Del Gaizo Moore V, Nishino M, Wei G, Korsmeyer S, Armstrong SA, Letai A (2006) Mitochondria primed by death signals determine cellular addiction to antiapoptotic BCL-2 family members. *Cancer cell* **9:** 351-365

Claypool SM, Koehler CM (2012) The complexity of cardiolipin in health and disease. *Trends in biochemical sciences* **37:** 32-41

Claypool SM, Oktay Y, Boontheung P, Loo JA, Koehler CM (2008) Cardiolipin defines the interactome of the major ADP/ATP carrier protein of the mitochondrial inner membrane. *The Journal of cell biology* **182:** 937-950

Clem RJ, Cheng EH, Karp CL, Kirsch DG, Ueno K, Takahashi A, Kastan MB, Griffin DE, Earnshaw WC, Veliuona MA, Hardwick JM (1998) Modulation of cell death by Bcl-XL through caspase interaction. *Proceedings of the National Academy of Sciences of the United States of America* **95:** 554-559

Cole NB, Smith CL, Sciaky N, Terasaki M, Edidin M, Lippincott-Schwartz J (1996) Diffusional mobility of Golgi proteins in membranes of living cells. *Science* **273:** 797-801

Colell A, Garcia-Ruiz C, Lluis JM, Coll O, Mari M, Fernandez-Checa JC (2003) Cholesterol impairs the adenine nucleotide translocator-mediated mitochondrial permeability transition through altered membrane fluidity. *The Journal of biological chemistry* **278:** 33928-33935

Colombini M (2010) Ceramide channels and their role in mitochondria-mediated apoptosis. *Biochimica et biophysica acta* **1797:** 1239-1244

Cosentino K, Garcia-Saez AJ (2017) Bax and Bak Pores: Are We Closing the Circle? *Trends in cell biology* **27:** 266-275

Crain RC, Clark RW, Harvey BE (1983) Role of lipid transfer proteins in the abnormal lipid content of Morris hepatoma mitochondria and microsomes. *Cancer research* **43:** 3197-3202

Cremesti A, Paris F, Grassme H, Holler N, Tschopp J, Fuks Z, Gulbins E, Kolesnick R (2001) Ceramide enables fas to cap and kill. *The Journal of biological chemistry* **276:** 23954-23961

Crimi M, Esposti MD (2011) Apoptosis-induced changes in mitochondrial lipids. *Biochimica et biophysica acta* **1813:** 551-557

Cullis PR, de Kruijff B (1979) Lipid polymorphism and the functional roles of lipids in biological membranes. *Biochimica et biophysica acta* **559:** 399-420

Czabotar PE, Lee EF, Thompson GV, Wardak AZ, Fairlie WD, Colman PM (2011) Mutation to Bax beyond the BH3 domain disrupts interactions with pro-survival proteins and promotes apoptosis. *The Journal of biological chemistry* **286:** 7123-7131

Czabotar PE, Lessene G, Strasser A, Adams JM (2014) Control of apoptosis by the BCL-2 protein family: implications for physiology and therapy. *Nature reviews Molecular cell biology* **15:** 49-63

Czabotar PE, Westphal D, Dewson G, Ma S, Hockings C, Fairlie WD, Lee EF, Yao S, Robin AY, Smith BJ, Huang DC, Kluck RM, Adams JM, Colman PM (2013) Bax crystal structures reveal how BH3 domains activate Bax and nucleate its oligomerization to induce apoptosis. *Cell* **152:** 519-531

Chapman D (1984) Physicochemical properties of phospholipids and lipid-water systems. *CRC Press, Boca Ratón*

Chauhan D, Hideshima T, Rosen S, Reed JC, Kharbanda S, Anderson KC (2001) Apaf-1/cytochrome c-independent and Smac-dependent induction of apoptosis in multiple myeloma (MM) cells. *The Journal of biological chemistry* **276:** 24453-24456

Chen HC, Kanai M, Inoue-Yamauchi A, Tu HC, Huang Y, Ren D, Kim H, Takeda S, Reyna DE, Chan PM, Ganesan YT, Liao CP, Gavathiotis E, Hsieh JJ, Cheng EH (2015) An interconnected hierarchical model of cell death regulation by the BCL-2 family. *Nature cell biology* **17:** 1270-1281

Chen L, Willis SN, Wei A, Smith BJ, Fletcher JI, Hinds MG, Colman PM, Day CL, Adams JM, Huang DC (2005) Differential targeting of prosurvival Bcl-2 proteins by their BH3-only ligands allows complementary apoptotic function. *Molecular cell* **17:** 393-403

Cheng EH, Kirsch DG, Clem RJ, Ravi R, Kastan MB, Bedi A, Ueno K, Hardwick JM (1997) Conversion of Bcl-2 to a Bax-like death effector by caspases. *Science* **278:** 1966-1968

Cheng EH, Levine B, Boise LH, Thompson CB, Hardwick JM (1996) Bax-independent inhibition of apoptosis by Bcl-XL. *Nature* **379:** 554-556

Cheng EH, Wei MC, Weiler S, Flavell RA, Mak TW, Lindsten T, Korsmeyer SJ (2001) BCL-2, BCL-X(L) sequester BH3 domain-only molecules preventing BAX- and BAK-mediated mitochondrial apoptosis. *Molecular cell* **8:** 705-711

Cheng Q, Lee HH, Li Y, Parks TP, Cheng G (2000) Upregulation of Bcl-x and Bfl-1 as a potential mechanism of chemoresistance, which can be overcome by NF-kappaB inhibition. *Oncogene* **19:** 4936-4940

Chipuk JE, McStay GP, Bharti A, Kuwana T, Clarke CJ, Siskind LJ, Obeid LM, Green DR (2012) Sphingolipid metabolism cooperates with BAK and BAX to promote the mitochondrial pathway of apoptosis. *Cell* **148:** 988-1000

Chipuk JE, Moldoveanu T, Llambi F, Parsons MJ, Green DR (2010) The BCL-2 family reunion. *Molecular cell* **37:** 299-310

Choi SS, Park IC, Yun JW, Sung YC, Hong SI, Shin HS (1995) A novel Bcl-2 related gene, Bfl-1, is overexpressed in stomach cancer and preferentially expressed in bone marrow. *Oncogene* **11:** 1693-1698

Chou JJ, Li H, Salvesen GS, Yuan J, Wagner G (1999) Solution structure of BID, an intracellular amplifier of apoptotic signaling. *Cell* **96:** 615-624

Christofferson DE, Yuan J (2010) Necroptosis as an alternative form of programmed cell death. *Current opinion in cell biology* **22:** 263-268

Dai H, Smith A, Meng XW, Schneider PA, Pang YP, Kaufmann SH (2011) Transient binding of an activator BH3 domain to the Bak BH3-binding groove initiates Bak oligomerization. *The Journal of cell biology* **194:** 39-48

Datta SR, Ranger AM, Lin MZ, Sturgill JF, Ma YC, Cowan CW, Dikkes P, Korsmeyer SJ, Greenberg ME (2002) Survival factor-mediated BAD phosphorylation raises the mitochondrial threshold for apoptosis. *Developmental cell* **3:** 631-643

Daugas E, Susin SA, Zamzami N, Ferri KF, Irinopoulou T, Larochette N, Prevost MC, Leber B, Andrews D, Penninger J, Kroemer G (2000) Mitochondrio-nuclear translocation of AIF in apoptosis and necrosis. *FASEB journal : official publication of the Federation of American Societies for Experimental Biology* **14:** 729-739

Daum G (1985) Lipids of mitochondria. *Biochimica et biophysica acta* **822:** 1-42

Day CL, Chen L, Richardson SJ, Harrison PJ, Huang DC, Hinds MG (2005) Solution structure of prosurvival Mcl-1 and characterization of its binding by proapoptotic BH3-only ligands. *The Journal of biological chemistry* **280:** 4738-4744

Day CL, Smits C, Fan FC, Lee EF, Fairlie WD, Hinds MG (2008) Structure of the BH3 domains from the p53-inducible BH3-only proteins Noxa and Puma in complex with Mcl-1. *Journal of molecular biology* **380:** 958-971

Dejean LM, Martinez-Caballero S, Guo L, Hughes C, Teijido O, Ducret T, Ichas F, Korsmeyer SJ, Antonsson B, Jonas EA, Kinnally KW (2005) Oligomeric Bax is a component of the putative cytochrome c release channel MAC, mitochondrial apoptosis-induced channel. *Molecular biology of the cell* **16:** 2424-2432

Dejean LM, Ryu SY, Martinez-Caballero S, Teijido O, Peixoto PM, Kinnally KW (2010) MAC and Bcl-2 family proteins conspire in a deadly plot. *Biochimica et biophysica acta* **1797:** 1231-1238

Delbridge AR, Grabow S, Strasser A, Vaux DL (2016) Thirty years of BCL-2: translating cell death discoveries into novel cancer therapies. *Nature reviews Cancer* **16:** 99-109

Denisov AY, Sprules T, Fraser J, Kozlov G, Gehring K (2007) Heat-induced dimerization of BCL-xL through alpha-helix swapping. *Biochemistry* **46:** 734-740

Dewson G, Kluck RM (2009) Mechanisms by which Bak and Bax permeabilise mitochondria during apoptosis. *Journal of cell science* **122:** 2801-2808

Dewson G, Kratina T, Czabotar P, Day CL, Adams JM, Kluck RM (2009) Bak activation for apoptosis involves oligomerization of dimers via their alpha6 helices. *Molecular cell* **36:** 696-703

Dewson G, Kratina T, Sim HW, Puthalakath H, Adams JM, Colman PM, Kluck RM (2008) To trigger apoptosis, Bak exposes its BH3 domain and homodimerizes via BH3:groove interactions. *Molecular cell* **30:** 369-380

Dewson G, Ma S, Frederick P, Hockings C, Tan I, Kratina T, Kluck RM (2012) Bax dimerizes via a symmetric BH3:groove interface during apoptosis. *Cell death and differentiation* **19:** 661-670

Diaz F, Moraes CT (2008) Mitochondrial biogenesis and turnover. *Cell calcium* **44:** 24-35

Dlugosz PJ, Billen LP, Annis MG, Zhu W, Zhang Z, Lin J, Leber B, Andrews DW (2006) Bcl-2 changes conformation to inhibit Bax oligomerization. *The EMBO journal* **25:** 2287-2296

Doghman-Bouguerra M, Lalli E (2017) The ER-mitochondria couple: In life and death from steroidogenesis to tumorigenesis. *Molecular and cellular endocrinology* **441:** 176-184

Dorn GW, 2nd (2013) Molecular mechanisms that differentiate apoptosis from programmed necrosis. *Toxicologic pathology* **41:** 227-234

Dorn GW, 2nd, Maack C (2013) SR and mitochondria: calcium cross-talk between kissing cousins. *Journal of molecular and cellular cardiology* **55:** 42-49

Dozier JK, Distefano MD (2015) Site-Specific PEGylation of Therapeutic Proteins. *International journal of molecular sciences* **16:** 25831-25864

Duchen MR (2000) Mitochondria and calcium: from cell signalling to cell death. *The Journal of physiology* **529 Pt 1:** 57-68

Duchen MR (2004) Mitochondria in health and disease: perspectives on a new mitochondrial biology. *Molecular aspects of medicine* **25:** 365-451

Duchen MR, Verkhratsky A, Muallem S (2008) Mitochondria and calcium in health and disease. *Cell calcium* **44:** 1-5

Dutta S, Gulla S, Chen TS, Fire E, Grant RA, Keating AE (2010) Determinants of BH3 binding specificity for Mcl-1 versus Bcl-xL. *Journal of molecular biology* **398:** 747-762

Edlich F, Banerjee S, Suzuki M, Cleland MM, Arnoult D, Wang C, Neutzner A, Tjandra N, Youle RJ (2011a) Bcl-x(L) retrotranslocates Bax from the mitochondria into the cytosol. *Cell* **145:** 104-116

Edlich F, Banerjee S, Suzuki M, Cleland MM, Arnoult D, Wang CX, Neutzner A, Tjandra N, Youle RJ (2011b) Bcl-x(L) Retrotranslocates Bax from the Mitochondria into the Cytosol. *Cell* **145:** 104-116

Edwards AL, Gavathiotis E, LaBelle JL, Braun CR, Opoku-Nsiah KA, Bird GH, Walensky LD (2013) Multimodal interaction with BCL-2 family proteins underlies the proapoptotic activity of PUMA BH3. *Chemistry & biology* **20:** 888-902

Ellenberg J, Siggia ED, Moreira JE, Smith CL, Presley JF, Worman HJ, Lippincott-Schwartz J (1997) Nuclear membrane dynamics and reassembly in living cells: targeting of an inner nuclear membrane protein in interphase and mitosis. *The Journal of cell biology* **138:** 1193-1206

Ellens H, Bentz J, Szoka FC (1985) H+- and Ca2+-induced fusion and destabilization of liposomes. *Biochemistry* **24:** 3099-3106

Elliott MR, Ravichandran KS (2010) Clearance of apoptotic cells: implications in health and disease. *The Journal of cell biology* **189:** 1059-1070

Epand RF, Martinou JC, Montessuit S, Epand RM (2003) Transbilayer lipid diffusion promoted by Bax: implications for apoptosis. *Biochemistry* **42:** 14576-14582

Epand RF, Schlattner U, Wallimann T, Lacombe ML, Epand RM (2007) Novel lipid transfer property of two mitochondrial proteins that bridge the inner and outer membranes. *Biophysical journal* **92:** 126-137

Eskes R, Desagher S, Antonsson B, Martinou JC (2000) Bid induces the oligomerization and insertion of Bax into the outer mitochondrial membrane. *Molecular and cellular biology* **20:** 929-935

Esposti MD, Cristea IM, Gaskell SJ, Nakao Y, Dive C (2003) Proapoptotic Bid binds to monolysocardiolipin, a new molecular connection between mitochondrial membranes and cell death. *Cell death and differentiation* **10:** 1300-1309

Esposti MD, Erler JT, Hickman JA, Dive C (2001) Bid, a widely expressed proapoptotic protein of the Bcl-2 family, displays lipid transfer activity. *Molecular and cellular biology* **21:** 7268-7276

Etxebarria A, Landeta O, Antonsson B, Basanez G (2008) Regulation of antiapoptotic MCL-1 function by gossypol: mechanistic insights from in vitro reconstituted systems. *Biochemical pharmacology* **76:** 1563-1576

Etxebarria A, Terrones O, Yamaguchi H, Landajuela A, Landeta O, Antonsson B, Wang HG, Basanez G (2009) Endophilin B1/Bif-1 stimulates BAX activation independently from its capacity to produce large scale membrane morphological rearrangements. *The Journal of biological chemistry* **284:** 4200-4212

Fan G, Simmons MJ, Ge S, Dutta-Simmons J, Kucharczak J, Ron Y, Weissmann D, Chen CC, Mukherjee C, White E, Gelinas C (2010) Defective ubiquitin-mediated degradation of antiapoptotic Bfl-1 predisposes to lymphoma. *Blood* **115:** 3559-3569

Fannjiang Y, Kim CH, Huganir RL, Zou S, Lindsten T, Thompson CB, Mito T, Traystman RJ, Larsen T, Griffin DE, Mandir AS, Dawson TM, Dike S, Sappington AL, Kerr DA, Jonas EA, Kaczmarek LK, Hardwick JM (2003) BAK alters neuronal excitability and can switch from anti- to pro-death function during postnatal development. *Developmental cell* **4:** 575-585

Feng Y, Lin Z, Shen X, Chen K, Jiang H, Liu D (2008) Bcl-xL forms two distinct homodimers at non-ionic detergents: implications in the dimerization of Bcl-2 family proteins. *Journal of biochemistry* **143:** 243-252

Fidelio GD, Austen BM, Chapman D, Lucy JA (1986) Properties of signal-sequence peptides at an air-water interface. *The Biochemical journal* **238:** 301-304

Fiske CH, SubbaRow, Y. (1925) The colorimetric determination of phosphorus. *The Journal of biological chemistry* **66:** 375-400

Fleischer S, Rouser G, Fleischer B, Casu A, Kritchevsky G (1967) Lipid composition of mitochondria from bovine heart, liver, and kidney. *Journal of lipid research* **8:** 170-180

Fletcher JI, Meusburger S, Hawkins CJ, Riglar DT, Lee EF, Fairlie WD, Huang DC, Adams JM (2008) Apoptosis is triggered when prosurvival Bcl-2 proteins cannot restrain Bax. *Proceedings of the National Academy of Sciences of the United States of America* **105:** 18081-18087

Frezza C, Cipolat S, Martins de Brito O, Micaroni M, Beznoussenko GV, Rudka T, Bartoli D, Polishuck RS, Danial NN, De Strooper B, Scorrano L (2006) OPA1 controls apoptotic cristae remodeling independently from mitochondrial fusion. *Cell* **126:** 177-189

Frezza C, Cipolat S, Scorrano L (2007) Measuring mitochondrial shape changes and their consequences on mitochondrial involvement during apoptosis. *Methods in molecular biology* **372:** 405-420

Fuertes G (2011) Baxα5 at lipid membranes: structure, assembly and pore formation., Ph.D thesis, Universitat de València,

Fuertes G, Garcia-Saez AJ, Esteban-Martin S, Gimenez D, Sanchez-Munoz OL, Schwille P, Salgado J (2010a) Pores formed by Baxalpha5 relax to a smaller size and keep at equilibrium. *Biophysical journal* **99:** 2917-2925

Fuertes G, Gimenez D, Esteban-Martin S, Garcia-Saez A, Sanchez O, Salgado J (2010b) Role of membrane lipids for the activity of pore forming peptides and proteins. *Advances in experimental medicine and biology* **677:** 31-55

Fuertes G, Gimenez D, Esteban-Martin S, Sanchez-Munoz OL, Salgado J (2011) A lipocentric view of peptide-induced pores. *European biophysics journal : EBJ* **40:** 399-415

Fulda S, Meyer E, Debatin KM (2002) Inhibition of TRAIL-induced apoptosis by Bcl-2 overexpression. *Oncogene* **21:** 2283-2294

Gahl RF, Tekle E, Tjandra N (2014) Single color FRET based measurements of conformational changes of proteins resulting from translocation inside cells. *Methods* **66:** 180-187

Gallop JL, Jao CC, Kent HM, Butler PJ, Evans PR, Langen R, McMahon HT (2006) Mechanism of endophilin N-BAR domain-mediated membrane curvature. *The EMBO journal* **25:** 2898-2910

Galluzzi L, Kroemer G (2008) Necroptosis: a specialized pathway of programmed necrosis. *Cell* **135:** 1161-1163

Ganesan V, Perera MN, Colombini D, Datskovskiy D, Chadha K, Colombini M (2010) Ceramide and activated Bax act synergistically to permeabilize the mitochondrial outer membrane. *Apoptosis : an international journal on programmed cell death* **15:** 553-562

Gangoiti P, Camacho L, Arana L, Ouro A, Granado MH, Brizuela L, Casas J, Fabrias G, Abad JL, Delgado A, Gomez-Munoz A (2010) Control of metabolism and signaling of simple bioactive sphingolipids: Implications in disease. *Progress in lipid research* **49:** 316-334

Garcia-Ruiz C, Mari M, Colell A, Morales A, Caballero F, Montero J, Terrones O, Basanez G, Fernandez-Checa JC (2009) Mitochondrial cholesterol in health and disease. *Histology and histopathology* **24:** 117-132

Garcia-Saez AJ, Carrer DC, Schwille P (2010) Fluorescence correlation spectroscopy for the study of membrane dynamics and organization in giant unilamellar vesicles. *Methods in molecular biology* **606:** 493-508

Garcia-Saez AJ, Coraiola M, Dalla Serra M, Mingarro I, Menestrina G, Salgado J (2005) Peptides derived from apoptotic Bax and Bid reproduce the poration activity of the parent full-length proteins. *Biophysical journal* **88:** 3976-3990

Garcia-Saez AJ, Coraiola M, Serra MD, Mingarro I, Muller P, Salgado J (2006) Peptides corresponding to helices 5 and 6 of Bax can independently form large lipid pores. *The FEBS journal* **273:** 971-981

Garcia-Saez AJ, Chiantia S, Schwille P (2007) Effect of line tension on the lateral organization of lipid membranes. *The Journal of biological chemistry* **282:** 33537-33544

Garcia-Saez AJ, Mingarro I, Perez-Paya E, Salgado J (2004) Membrane-insertion fragments of Bcl-xL, Bax, and Bid. *Biochemistry* **43:** 10930-10943

Garcia-Saez AJ, Ries J, Orzaez M, Perez-Paya E, Schwille P (2009) Membrane promotes tBID interaction with BCL(XL). *Nature structural & molecular biology* **16:** 1178-1185

Garofalo T, Giammarioli AM, Misasi R, Tinari A, Manganelli V, Gambardella L, Pavan A, Malorni W, Sorice M (2005) Lipid microdomains contribute to apoptosis-associated modifications of mitochondria in T cells. *Cell death and differentiation* **12:** 1378-1389

Garofalo T, Misasi R, Mattei V, Giammarioli AM, Malorni W, Pontieri GM, Pavan A, Sorice M (2003) Association of the death-inducing signaling complex with microdomains after triggering through CD95/Fas. Evidence for caspase-8-ganglioside interaction in T cells. *The Journal of biological chemistry* **278:** 8309-8315

Garrido C, Galluzzi L, Brunet M, Puig PE, Didelot C, Kroemer G (2006) Mechanisms of cytochrome c release from mitochondria. *Cell death and differentiation* **13:** 1423-1433

Gautier R, Douguet D, Antonny B, Drin G (2008) HELIQUEST: a web server to screen sequences with specific alpha-helical properties. *Bioinformatics* **24:** 2101-2102

Gavathiotis E, Reyna DE, Davis ML, Bird GH, Walensky LD (2010) BH3-triggered structural reorganization drives the activation of proapoptotic BAX. *Molecular cell* **40:** 481-492

Gavathiotis E, Suzuki M, Davis ML, Pitter K, Bird GH, Katz SG, Tu HC, Kim H, Cheng EH, Tjandra N, Walensky LD (2008) BAX activation is initiated at a novel interaction site. *Nature* **455:** 1076-1081

Gebert N, Joshi AS, Kutik S, Becker T, McKenzie M, Guan XL, Mooga VP, Stroud DA, Kulkarni G, Wenk MR, Rehling P, Meisinger C, Ryan MT, Wiedemann N, Greenberg ML, Pfanner N (2009) Mitochondrial cardiolipin involved in outer-membrane protein biogenesis: implications for Barth syndrome. *Current biology : CB* **19:** 2133-2139

George NM, Evans JJ, Luo X (2007) A three-helix homo-oligomerization domain containing BH3 and BH1 is responsible for the apoptotic activity of Bax. *Genes & development* **21:** 1937-1948

George NM, Targy N, Evans JJ, Zhang L, Luo X (2010) Bax contains two functional mitochondrial targeting sequences and translocates to mitochondria in a conformational change- and homo-oligomerization-driven process. *The Journal of biological chemistry* **285:** 1384-1392

Gillies LA, Du H, Peters B, Knudson CM, Newmeyer DD, Kuwana T (2015) Visual and functional demonstration of growing Bax-induced pores in mitochondrial outer membranes. *Molecular biology of the cell* **26:** 339-349

Gimenez-Cassina A, Danial NN (2015) Regulation of mitochondrial nutrient and energy metabolism by BCL-2 family proteins. *Trends in endocrinology and metabolism: TEM* **26:** 165-175

Giorgi C, De Stefani D, Bononi A, Rizzuto R, Pinton P (2009) Structural and functional link between the mitochondrial network and the endoplasmic reticulum. *The international journal of biochemistry & cell biology* **41:** 1817-1827

Giorgio V, von Stockum S, Antoniel M, Fabbro A, Fogolari F, Forte M, Glick GD, Petronilli V, Zoratti M, Szabo I, Lippe G, Bernardi P (2013) Dimers of mitochondrial ATP synthase form the permeability transition pore. *Proceedings of the National Academy of Sciences of the United States of America* **110:** 5887-5892

Gofman Y, Haliloglu T, Ben-Tal N (2012a) Monte Carlo simulations of peptide-membrane interactions with the MCPep web server. *Nucleic acids research* **40:** W358-363

Gofman Y, Haliloglu T, Ben-Tal N (2012b) The Transmembrane Helix Tilt May Be Determined by the Balance between Precession Entropy and Lipid Perturbation. *Journal of chemical theory and computation* **8:** 2896-2904

Gofman Y, Linser S, Rzeszutek A, Shental-Bechor D, Funari SS, Ben-Tal N, Willumeit R (2010) Interaction of an antimicrobial peptide with membranes: experiments and simulations with NKCS. *The journal of physical chemistry B* **114:** 4230-4237

Gomez-Munoz A (2006) Ceramide 1-phosphate/ceramide, a switch between life and death. *Biochimica et biophysica acta* **1758:** 2049-2056

Gonzalvez F, Gottlieb E (2007) Cardiolipin: setting the beat of apoptosis. *Apoptosis : an international journal on programmed cell death* **12:** 877-885

Gonzalvez F, Pariselli F, Dupaigne P, Budihardjo I, Lutter M, Antonsson B, Diolez P, Manon S, Martinou JC, Goubern M, Wang X, Bernard S, Petit PX (2005) tBid interaction with cardiolipin primarily orchestrates mitochondrial dysfunctions and subsequently activates Bax and Bak. *Cell death and differentiation* **12:** 614-626

Gonzalvez F, Pariselli F, Jalmar O, Dupaigne P, Sureau F, Dellinger M, Hendrickson EA, Bernard S, Petit PX (2010) Mechanistic issues of the interaction of the hairpin-forming domain of tBid with mitochondrial cardiolipin. *PloS one* **5:** e9342

Gonzalvez F, Schug ZT, Houtkooper RH, MacKenzie ED, Brooks DG, Wanders RJ, Petit PX, Vaz FM, Gottlieb E (2008) Cardiolipin provides an essential activating platform for caspase-8 on mitochondria. *The Journal of cell biology* **183:** 681-696

Goonesinghe A, Mundy ES, Smith M, Khosravi-Far R, Martinou JC, Esposti MD (2005) Pro-apoptotic Bid induces membrane perturbation by inserting selected lysolipids into the bilayer. *The Biochemical journal* **387:** 109-118

Graham JM, Green C (1970) The properties of mitochondria enriched in vitro with cholesterol. *European journal of biochemistry* **12:** 58-66

Green DR (2005) Apoptotic pathways: ten minutes to dead. *Cell* **121:** 671-674

Green DR, Kroemer G (2004) The pathophysiology of mitochondrial cell death. *Science* **305:** 626-629

Griffiths GJ, Corfe BM, Savory P, Leech S, Esposti MD, Hickman JA, Dive C (2001) Cellular damage signals promote sequential changes at the N-terminus and BH-1 domain of the pro-apoptotic protein Bak. *Oncogene* **20:** 7668-7676

Griffiths GJ, Dubrez L, Morgan CP, Jones NA, Whitehouse J, Corfe BM, Dive C, Hickman JA (1999) Cell damage-induced conformational changes of the pro-apoptotic protein Bak in vivo precede the onset of apoptosis. *The Journal of cell biology* **144:** 903-914

Grijalba MT, Vercesi AE, Schreier S (1999) Ca2+-induced increased lipid packing and domain formation in submitochondrial particles. A possible early step in the mechanism of Ca2+-stimulated generation of reactive oxygen species by the respiratory chain. *Biochemistry* **38:** 13279-13287

Gross A, Yin XM, Wang K, Wei MC, Jockel J, Milliman C, Erdjument-Bromage H, Tempst P, Korsmeyer SJ (1999) Caspase cleaved BID targets mitochondria and is required for cytochrome c release, while BCL-XL prevents this release but not tumor necrosis factor-R1/Fas death. *The Journal of biological chemistry* **274:** 1156-1163

Grosse L, Wurm CA, Bruser C, Neumann D, Jans DC, Jakobs S (2016) Bax assembles into large ring-like structures remodeling the mitochondrial outer membrane in apoptosis. *The EMBO journal* **35:** 402-413

Hamasaki A, Sendo F, Nakayama K, Ishida N, Negishi I, Nakayama K, Hatakeyama S (1998) Accelerated neutrophil apoptosis in mice lacking A1-a, a subtype of the bcl-2-related A1 gene. *The Journal of experimental medicine* **188:** 1985-1992

Hanahan D, Weinberg RA (2011) Hallmarks of cancer: the next generation. *Cell* **144:** 646-674

Haq R, Yokoyama S, Hawryluk EB, Jonsson GB, Frederick DT, McHenry K, Porter D, Tran TN, Love KT, Langer R, Anderson DG, Garraway LA, Duncan LM, Morton DL, Hoon DS, Wargo JA, Song JS, Fisher DE (2013) BCL2A1 is a lineage-specific antiapoptotic melanoma oncogene that confers resistance to BRAF inhibition. *Proceedings of the National Academy of Sciences of the United States of America* **110:** 4321-4326

Hardwick JM, Chen YB, Jonas EA (2012) Multipolar functions of BCL-2 proteins link energetics to apoptosis. *Trends in cell biology* **22:** 318-328

Harner M, Korner C, Walther D, Mokranjac D, Kaesmacher J, Welsch U, Griffith J, Mann M, Reggiori F, Neupert W (2011) The mitochondrial contact site complex, a determinant of mitochondrial architecture. *The EMBO journal* **30:** 4356-4370

Harrington SE, Ben-Tal N (2009) Structural determinants of transmembrane helical proteins. *Structure* **17:** 1092-1103

Hatakeyama S, Hamasaki A, Negishi I, Loh DY, Sendo F, Nakayama K, Nakayama K (1998) Multiple gene duplication and expression of mouse bcl-2-related genes, A1. *International immunology* **10:** 631-637

Hausmann G, O'Reilly LA, van Driel R, Beaumont JG, Strasser A, Adams JM, Huang DC (2000) Pro-apoptotic apoptosis protease-activating factor 1 (Apaf-1) has a cytoplasmic localization distinct from Bcl-2 or Bcl-x(L). *The Journal of cell biology* **149:** 623-634

Haustein E, Schwille P (2004) Single-molecule spectroscopic methods. *Current opinion in structural biology* **14:** 531-540

Hawe A, Friess W, Sutter M, Jiskoot W (2008a) Online fluorescent dye detection method for the characterization of immunoglobulin G aggregation by size exclusion chromatography and asymmetrical flow field flow fractionation. *Analytical biochemistry* **378:** 115-122

Hawe A, Sutter M, Jiskoot W (2008b) Extrinsic fluorescent dyes as tools for protein characterization. *Pharmaceutical research* **25:** 1487-1499

He CH, Waxman AB, Lee CG, Link H, Rabach ME, Ma B, Chen Q, Zhu Z, Zhong M, Nakayama K, Nakayama KI, Homer R, Elias JA (2005) Bcl-2-related protein A1 is an endogenous and cytokine-stimulated mediator of cytoprotection in hyperoxic acute lung injury. *The Journal of clinical investigation* **115:** 1039-1048

He K, Ludtke SJ, Worcester DL, Huang HW (1996) Neutron scattering in the plane of membranes: structure of alamethicin pores. *Biophysical journal* **70:** 2659-2666

Heath-Engel HM, Chang NC, Shore GC (2008) The endoplasmic reticulum in apoptosis and autophagy: role of the BCL-2 protein family. *Oncogene* **27:** 6419-6433

Heimlich G, McKinnon AD, Bernardo K, Brdiczka D, Reed JC, Kain R, Kronke M, Jurgensmeier JM (2004) Bax-induced cytochrome c release from mitochondria depends on alpha-helices-5 and -6. *The Biochemical journal* **378:** 247-255

Heit B, Yeung T, Grinstein S (2011) Changes in mitochondrial surface charge mediate recruitment of signaling molecules during apoptosis. *American journal of physiology Cell physiology* **300:** C33-41

Hekman M, Albert S, Galmiche A, Rennefahrt UE, Fueller J, Fischer A, Puehringer D, Wiese S, Rapp UR (2006) Reversible membrane interaction of BAD requires two C-terminal lipid binding domains in conjunction with 14-3-3 protein binding. *The Journal of biological chemistry* **281:** 17321-17336

Herman MD, Nyman T, Welin M, Lehtio L, Flodin S, Tresaugues L, Kotenyova T, Flores A, Nordlund P (2008) Completing the family portrait of the anti-apoptotic Bcl-2 proteins: crystal structure of human Bfl-1 in complex with Bim. *FEBS letters* **582:** 3590-3594

Heuck AP, Hotze EM, Tweten RK, Johnson AE (2000) Mechanism of membrane insertion of a multimeric beta-barrel protein: perfringolysin O creates a pore using ordered and coupled conformational changes. *Molecular cell* **6:** 1233-1242

Heuck AP, Johnson AE (2002) Pore-forming protein structure analysis in membranes using multiple independent fluorescence techniques. *Cell biochemistry and biophysics* **36:** 89-101

Hinds MG, Smits C, Fredericks-Short R, Risk JM, Bailey M, Huang DC, Day CL (2007) Bim, Bad and Bmf: intrinsically unstructured BH3-only proteins that undergo a localized conformational change upon binding to prosurvival Bcl-2 targets. *Cell death and differentiation* **14:** 128-136

Hollville E, Martin SJ (2012) Greasing the path to BAX/BAK activation. *Cell* **148:** 845-846

Hope MJ, Bally MB, Webb G, Cullis PR (1985) Production of large unilamellar vesicles by a rapid extrusion procedure: characterization of size distribution, trapped volume and ability to maintain a membrane potential. *Biochimica et biophysica acta* **812:** 55-65

Horvath SE, Daum G (2013) Lipids of mitochondria. *Progress in lipid research* **52:** 590-614

Hsu YT, Wolter KG, Youle RJ (1997) Cytosol-to-membrane redistribution of Bax and Bcl-X(L) during apoptosis. *Proceedings of the National Academy of Sciences of the United States of America* **94:** 3668-3672

Huang HW (2000) Action of antimicrobial peptides: two-state model. *Biochemistry* **39:** 8347-8352

Huhn AJ, Guerra RM, Harvey EP, Bird GH, Walensky LD (2016) Selective Covalent Targeting of Anti-Apoptotic BFL-1 by Cysteine-Reactive Stapled Peptide Inhibitors. *Cell chemical biology* **23:** 1123-1134

Irvine RA, Adachi N, Shibata DK, Cassell GD, Yu K, Karanjawala ZE, Hsieh CL, Lieber MR (2005) Generation and characterization of endonuclease G null mice. *Molecular and cellular biology* **25:** 294-302

Ishikawa-Ankerhold HC, Ankerhold R, Drummen GP (2012) Advanced fluorescence microscopy techniques--FRAP, FLIP, FLAP, FRET and FLIM. *Molecules* **17:** 4047-4132

Jalmar O, Francois-Moutal L, Garcia-Saez AJ, Perry M, Granjon T, Gonzalvez F, Gottlieb E, Ayala-Sanmartin J, Klosgen B, Schwille P, Petit PX (2013) Caspase-8 binding to cardiolipin in giant unilamellar vesicles provides a functional docking platform for bid. *PloS one* **8:** e55250

Janmey PA, Kinnunen PK (2006) Biophysical properties of lipids and dynamic membranes. *Trends in cell biology* **16:** 538-546

Jayasinghe S, Hristova K, White SH (2001) Energetics, stability, and prediction of transmembrane helices. *Journal of molecular biology* **312:** 927-934

Jeong SY, Gaume B, Lee YJ, Hsu YT, Ryu SW, Yoon SH, Youle RJ (2004) Bcl-x(L) sequesters its C-terminal membrane anchor in soluble, cytosolic homodimers. *The EMBO journal* **23:** 2146-2155

Jiang J, Huang Z, Zhao Q, Feng W, Belikova NA, Kagan VE (2008) Interplay between bax, reactive oxygen species production, and cardiolipin oxidation during apoptosis. *Biochemical and biophysical research communications* **368:** 145-150

Johnson CK, Osborn KD, Allen MW, Slaughter BD (2005) Single-molecule fluorescence spectroscopy: new probes of protein function and dynamics. *Physiology* **20:** 10-14

Kagan VE, Borisenko GG, Tyurina YY, Tyurin VA, Jiang J, Potapovich AI, Kini V, Amoscato AA, Fujii Y (2004) Oxidative lipidomics of apoptosis: redox catalytic interactions of cytochrome c with cardiolipin and phosphatidylserine. *Free radical biology & medicine* **37:** 1963-1985

Kagan VE, Tyurin VA, Jiang J, Tyurina YY, Ritov VB, Amoscato AA, Osipov AN, Belikova NA, Kapralov AA, Kini V, Vlasova, II, Zhao Q, Zou M, Di P, Svistunenko DA, Kurnikov IV, Borisenko GG (2005) Cytochrome c acts as a cardiolipin oxygenase required for release of proapoptotic factors. *Nature chemical biology* **1:** 223-232

Kahya N (2006) Targeting membrane proteins to liquid-ordered phases: molecular self-organization explored by fluorescence correlation spectroscopy. *Chemistry and physics of lipids* **141:** 158-168

Karatekin E, Sandre O, Guitouni H, Borghi N, Puech PH, Brochard-Wyart F (2003) Cascades of transient pores in giant vesicles: line tension and transport. *Biophysical journal* **84:** 1734-1749

Karbowski M, Lee YJ, Gaume B, Jeong SY, Frank S, Nechushtan A, Santel A, Fuller M, Smith CL, Youle RJ (2002) Spatial and temporal association of Bax with mitochondrial fission sites, Drp1, and Mfn2 during apoptosis. *The Journal of cell biology* **159:** 931-938

Karsan A, Yee E, Harlan JM (1996a) Endothelial cell death induced by tumor necrosis factor-alpha is inhibited by the Bcl-2 family member, A1. *The Journal of biological chemistry* **271:** 27201-27204

Karsan A, Yee E, Kaushansky K, Harlan JM (1996b) Cloning of human Bcl-2 homologue: inflammatory cytokines induce human A1 in cultured endothelial cells. *Blood* **87:** 3089-3096

Kater AP, Evers LM, Remmerswaal EB, Jaspers A, Oosterwijk MF, van Lier RA, van Oers MH, Eldering E (2004) CD40 stimulation of B-cell chronic lymphocytic leukaemia cells enhances the anti-apoptotic profile, but also Bid expression and cells remain susceptible to autologous cytotoxic T-lymphocyte attack. *British journal of haematology* **127:** 404-415

Kathania M, Raje CI, Raje M, Dutta RK, Majumdar S (2011) Bfl-1/A1 acts as a negative regulator of autophagy in mycobacteria infected macrophages. *The international journal of biochemistry & cell biology* **43:** 573-585

Kathpalia VP, Mussak EN, Chow SS, Lam PH, Skelley N, Time M, Markelewicz RJ, Jr., Kanduc D, Lomas L, Xiang Z, Sinha AA (2006) Genome-wide transcriptional profiling in human squamous cell carcinoma of the skin identifies unique tumor-associated signatures. *The Journal of dermatology* **33:** 309-318

Kaufmann T, Schlipf S, Sanz J, Neubert K, Stein R, Borner C (2003) Characterization of the signal that directs Bcl-x(L), but not Bcl-2, to the mitochondrial outer membrane. *The Journal of cell biology* **160:** 53-64

Kawai F, Shoda M, Harashima R, Sadaie Y, Hara H, Matsumoto K (2004) Cardiolipin domains in Bacillus subtilis marburg membranes. *Journal of bacteriology* **186:** 1475-1483

Kenny JJ, Knobloch TJ, Augustus M, Carter KC, Rosen CA, Lang JC (1997) GRS, a novel member of the Bcl-2 gene family, is highly expressed in multiple cancer cell lines and in normal leukocytes. *Oncogene* **14:** 997-1001

Kessel A, Shental-Bechor D, Haliloglu T, Ben-Tal N (2003) Interactions of hydrophobic peptides with lipid bilayers: Monte Carlo simulations with M2delta. *Biophysical journal* **85:** 3431-3444

Killian JA (1998) Hydrophobic mismatch between proteins and lipids in membranes. *Biochimica et biophysica acta* **1376:** 401-415

Killian JA, Koorengevel MC, Bouwstra JA, Gooris G, Dowhan W, de Kruijff B (1994) Effect of divalent cations on lipid organization of cardiolipin isolated from Escherichia coli strain AH930. *Biochimica et biophysica acta* **1189:** 225-232

Kim H, Kim YN, Kim H, Kim CW (2005) Oxidative stress attenuates Fas-mediated apoptosis in Jurkat T cell line through Bfl-1 induction. *Oncogene* **24:** 1252-1261

Kim H, Tu HC, Ren D, Takeuchi O, Jeffers JR, Zambetti GP, Hsieh JJ, Cheng EH (2009) Stepwise activation of BAX and BAK by tBID, BIM, and PUMA initiates mitochondrial apoptosis. *Molecular cell* **36:** 487-499

Klein RA (1970) The detection of oxidation in liposome preparations. *Biochimica et biophysica acta* **210:** 486-489

Ko JK, Choi KH, Pan Z, Lin P, Weisleder N, Kim CW, Ma J (2007) The tail-anchoring domain of Bfl1 and HCCS1 targets mitochondrial membrane permeability to induce apoptosis. *Journal of cell science* **120:** 2912-2923

Ko JK, Lee MJ, Cho SH, Cho JA, Lee BY, Koh JS, Lee SS, Shim YH, Kim CW (2003) Bfl-1S, a novel alternative splice variant of Bfl-1, localizes in the nucleus via its C-terminus and prevents cell death. *Oncogene* **22:** 2457-2465

Kokoszka JE, Waymire KG, Levy SE, Sligh JE, Cai J, Jones DP, MacGregor GR, Wallace DC (2004) The ADP/ATP translocator is not essential for the mitochondrial permeability transition pore. *Nature* **427:** 461-465

Kolluri SK, Zhu X, Zhou X, Lin B, Chen Y, Sun K, Tian X, Town J, Cao X, Lin F, Zhai D, Kitada S, Luciano F, O'Donnell E, Cao Y, He F, Lin J, Reed JC, Satterthwait AC, Zhang XK (2008) A short Nur77-derived peptide converts Bcl-2 from a protector to a killer. *Cancer cell* **14:** 285-298

Korsmeyer SJ, Shutter JR, Veis DJ, Merry DE, Oltvai ZN (1993) Bcl-2/Bax: a rheostat that regulates an anti-oxidant pathway and cell death. *Seminars in cancer biology* **4:** 327-332

Kotschy A, Szlavik Z, Murray J, Davidson J, Maragno AL, Le Toumelin-Braizat G, Chanrion M, Kelly GL, Gong JN, Moujalled DM, Bruno A, Csekei M, Paczal A, Szabo ZB, Sipos S, Radics G, Proszenyak A, Balint B, Ondi L, Blasko G, Robertson A, Surgenor A, Dokurno P, Chen I, Matassova N, Smith J, Pedder C, Graham C, Studeny A, Lysiak-Auvity G, Girard AM, Grave F, Segal D, Riffkin CD, Pomilio G, Galbraith LC, Aubrey BJ, Brennan MS, Herold MJ, Chang C, Guasconi G, Cauquil N, Melchiore F, Guigal-Stephan N, Lockhart B, Colland F, Hickman JA, Roberts AW, Huang DC, Wei AH, Strasser A, Lessene G, Geneste O (2016) The MCL1 inhibitor S63845 is tolerable and effective in diverse cancer models. *Nature* **538:** 477-482

Kozlov MM, Campelo F, Liska N, Chernomordik LV, Marrink SJ, McMahon HT (2014) Mechanisms shaping cell membranes. *Current opinion in cell biology* **29:** 53-60

Krieger C, Duchen MR (2002) Mitochondria, Ca2+ and neurodegenerative disease. *European journal of pharmacology* **447:** 177-188

Kroemer G, El-Deiry WS, Golstein P, Peter ME, Vaux D, Vandenabeele P, Zhivotovsky B, Blagosklonny MV, Malorni W, Knight RA, Piacentini M, Nagata S, Melino G, Nomenclature Committee on Cell D (2005) Classification of cell death: recommendations of the Nomenclature Committee on Cell Death. *Cell death and differentiation* **12 Suppl 2:** 1463-1467

Kroemer G, Galluzzi L, Brenner C (2007) Mitochondrial membrane permeabilization in cell death. *Physiological reviews* **87:** 99-163

Kroemer G, Galluzzi L, Vandenabeele P, Abrams J, Alnemri ES, Baehrecke EH, Blagosklonny MV, El-Deiry WS, Golstein P, Green DR, Hengartner M, Knight RA, Kumar S, Lipton SA, Malorni W, Nunez G, Peter ME, Tschopp J, Yuan J, Piacentini M, Zhivotovsky B, Melino G, Nomenclature Committee on Cell D (2009) Classification of cell death: recommendations of the Nomenclature Committee on Cell Death 2009. *Cell death and differentiation* **16:** 3-11

Kucharczak JF, Simmons MJ, Duckett CS, Gelinas C (2005) Constitutive proteasome-mediated turnover of Bfl-1/A1 and its processing in response to TNF receptor activation in FL5.12 pro-B cells convert it into a prodeath factor. *Cell death and differentiation* **12:** 1225-1239

Kudla G, Montessuit S, Eskes R, Berrier C, Martinou JC, Ghazi A, Antonsson B (2000) The destabilization of lipid membranes induced by the C-terminal fragment of caspase 8-cleaved bid is inhibited by the N-terminal fragment. *The Journal of biological chemistry* **275:** 22713-22718

Kushnareva Y, Andreyev AY, Kuwana T, Newmeyer DD (2012) Bax activation initiates the assembly of a multimeric catalyst that facilitates Bax pore formation in mitochondrial outer membranes. *PLoS biology* **10:** e1001394

Kutik S, Stroud DA, Wiedemann N, Pfanner N (2009) Evolution of mitochondrial protein biogenesis. *Biochimica et biophysica acta* **1790:** 409-415

Kuwana T, Bouchier-Hayes L, Chipuk JE, Bonzon C, Sullivan BA, Green DR, Newmeyer DD (2005) BH3 domains of BH3-only proteins differentially regulate Bax-mediated mitochondrial membrane permeabilization both directly and indirectly. *Molecular cell* **17:** 525-535

Kuwana T, Mackey MR, Perkins G, Ellisman MH, Latterich M, Schneiter R, Green DR, Newmeyer DD (2002) Bid, Bax, and lipids cooperate to form supramolecular openings in the outer mitochondrial membrane. *Cell* **111:** 331-342

Kuwana T, Olson NH, Kiosses WB, Peters B, Newmeyer DD (2016) Pro-apoptotic Bax molecules densely populate the edges of membrane pores. *Scientific reports* **6:** 27299

Kyrychenko A, Ladokhin AS (2013) Molecular dynamics simulations of depth distribution of spin-labeled phospholipids within lipid bilayer. *The journal of physical chemistry B* **117:** 5875-5885

Ladokhin AS, Wimley WC, Hristova K, White SH (1997) Mechanism of leakage of contents of membrane vesicles determined by fluorescence requenching. *Methods in enzymology* **278:** 474-486

Laemmli UK (1970) Cleavage of structural proteins during the assembly of the head of bacteriophage T4. *Nature* **227:** 680-685

Lalier L, Cartron PF, Juin P, Nedelkina S, Manon S, Bechinger B, Vallette FM (2007) Bax activation and mitochondrial insertion during apoptosis. *Apoptosis : an international journal on programmed cell death* **12:** 887-896

Landeta O, Garcia Valero J, Flores-Romero H, Bustillo-Zabalbeitia I, Landajuela A, Garcia-Porras M, Terrones O, Basanez G (2014) Lipid-dependent bimodal MCL1 membrane activity. *ACS chemical biology* **9:** 2852-2863

Landeta O, Landajuela A, Garcia-Saez A, Basanez G (2015) Minimalist Model Systems Reveal Similarities and Differences between Membrane Interaction Modes of MCL1 and BAK. *The Journal of biological chemistry* **290:** 17004-17019

Landeta O, Landajuela A, Gil D, Taneva S, Di Primo C, Sot B, Valle M, Frolov VA, Basanez G (2011) Reconstitution of proapoptotic BAK function in liposomes reveals a dual role for mitochondrial lipids in the BAK-driven membrane permeabilization process. *The Journal of biological chemistry* **286:** 8213-8230

Langmuir I (1917) The Shapes of Group Molecules Forming the Surfaces of Liquids. *Proceedings of the National Academy of Sciences of the United States of America* **3:** 251-257

Lauber K, Bohn E, Krober SM, Xiao YJ, Blumenthal SG, Lindemann RK, Marini P, Wiedig C, Zobywalski A, Baksh S, Xu Y, Autenrieth IB, Schulze-Osthoff K, Belka C, Stuhler G, Wesselborg S (2003) Apoptotic cells induce migration of phagocytes via caspase-3-mediated release of a lipid attraction signal. *Cell* **113:** 717-730

Leber B, Lin J, Andrews DW (2007) Embedded together: the life and death consequences of interaction of the Bcl-2 family with membranes. *Apoptosis : an international journal on programmed cell death* **12:** 897-911

Leber B, Lin J, Andrews DW (2010) Still embedded together binding to membranes regulates Bcl-2 protein interactions. *Oncogene* **29:** 5221-5230

Lee EF, Grabow S, Chappaz S, Dewson G, Hockings C, Kluck RM, Debrincat MA, Gray DH, Witkowski MT, Evangelista M, Pettikiriarachchi A, Bouillet P, Lane RM, Czabotar PE, Colman PM, Smith BJ, Kile BT, Fairlie WD (2016) Physiological restraint of Bak by Bcl-xL is essential for cell survival. *Genes & development* **30:** 1240-1250

Lee MT, Chen FY, Huang HW (2004) Energetics of pore formation induced by membrane active peptides. *Biochemistry* **43:** 3590-3599

Lee MT, Hung WC, Chen FY, Huang HW (2008) Mechanism and kinetics of pore formation in membranes by water-soluble amphipathic peptides. *Proceedings of the National Academy of Sciences of the United States of America* **105:** 5087-5092

Lee MT, Sun TL, Hung WC, Huang HW (2013) Process of inducing pores in membranes by melittin. *Proceedings of the National Academy of Sciences of the United States of America* **110:** 14243-14248

Lei X, Chen Y, Du G, Yu W, Wang X, Qu H, Xia B, He H, Mao J, Zong W, Liao X, Mehrpour M, Hao X, Chen Q (2006) Gossypol induces Bax/Bak-independent activation of apoptosis and cytochrome c release via a conformational change in Bcl-2. *FASEB journal : official publication of the Federation of American Societies for Experimental Biology* **20:** 2147-2149

Leshchiner ES, Braun CR, Bird GH, Walensky LD (2013) Direct activation of full-length proapoptotic BAK. *Proceedings of the National Academy of Sciences of the United States of America* **110:** E986-995

Letai A, Bassik MC, Walensky LD, Sorcinelli MD, Weiler S, Korsmeyer SJ (2002) Distinct BH3 domains either sensitize or activate mitochondrial apoptosis, serving as prototype cancer therapeutics. *Cancer cell* **2:** 183-192

Lewis J, Oyler GA, Ueno K, Fannjiang YR, Chau BN, Vornov J, Korsmeyer SJ, Zou S, Hardwick JM (1999) Inhibition of virus-induced neuronal apoptosis by Bax. *Nature medicine* **5:** 832-835

Li H, Zhu H, Xu CJ, Yuan J (1998) Cleavage of BID by caspase 8 mediates the mitochondrial damage in the Fas pathway of apoptosis. *Cell* **94:** 491-501

Li LY, Luo X, Wang X (2001) Endonuclease G is an apoptotic DNase when released from mitochondria. *Nature* **412:** 95-99

Li P, Nijhawan D, Budihardjo I, Srinivasula SM, Ahmad M, Alnemri ES, Wang X (1997) Cytochrome c and dATP-dependent formation of Apaf-1/caspase-9 complex initiates an apoptotic protease cascade. *Cell* **91:** 479-489

Lin EY, Kozak CA, Orlofsky A, Prystowsky MB (1997) The bcl-2 family member, Bcl2a1, maps to mouse chromosome 9 and human chromosome 15. *Mammalian genome : official journal of the International Mammalian Genome Society* **8:** 293-294

Lindsay J, Esposti MD, Gilmore AP (2011) Bcl-2 proteins and mitochondria--specificity in membrane targeting for death. *Biochimica et biophysica acta* **1813:** 532-539

Lithgow T, van Driel R, Bertram JF, Strasser A (1994) The protein product of the oncogene bcl-2 is a component of the nuclear envelope, the endoplasmic reticulum, and the outer mitochondrial membrane. *Cell growth & differentiation : the molecular biology journal of the American Association for Cancer Research* **5:** 411-417

Liu J, Chen J, Dai Q, Lee RM (2003a) Phospholipid scramblase 3 is the mitochondrial target of protein kinase C delta-induced apoptosis. *Cancer research* **63:** 1153-1156

Liu J, Durrant D, Yang HS, He Y, Whitby FG, Myszka DG, Lee RM (2005) The interaction between tBid and cardiolipin or monolysocardiolipin. *Biochemical and biophysical research communications* **330:** 865-870

Liu J, Epand RF, Durrant D, Grossman D, Chi NW, Epand RM, Lee RM (2008) Role of phospholipid scramblase 3 in the regulation of tumor necrosis factor-alpha-induced apoptosis. *Biochemistry* **47:** 4518-4529

Liu Q, Leber B, Andrews DW (2012) Interactions of pro-apoptotic BH3 proteins with anti-apoptotic Bcl-2 family proteins measured in live MCF-7 cells using FLIM FRET. *Cell cycle* **11:** 3536-3542

Liu X, Dai S, Zhu Y, Marrack P, Kappler JW (2003b) The structure of a Bcl-xL/Bim fragment complex: implications for Bim function. *Immunity* **19:** 341-352

Liu X, Kim CN, Yang J, Jemmerson R, Wang X (1996) Induction of apoptotic program in cell-free extracts: requirement for dATP and cytochrome c. *Cell* **86:** 147-157

Losonczi JA, Olejniczak ET, Betz SF, Harlan JE, Mack J, Fesik SW (2000) NMR studies of the anti-apoptotic protein Bcl-xL in micelles. *Biochemistry* **39:** 11024-11033

Lovell JF, Billen LP, Bindner S, Shamas-Din A, Fradin C, Leber B, Andrews DW (2008) Membrane binding by tBid initiates an ordered series of events culminating in membrane permeabilization by Bax. *Cell* **135:** 1074-1084

Lucken-Ardjomande S, Montessuit S, Martinou JC (2008) Bax activation and stress-induced apoptosis delayed by the accumulation of cholesterol in mitochondrial membranes. *Cell death and differentiation* **15:** 484-493

Ludtke SJ, He K, Heller WT, Harroun TA, Yang L, Huang HW (1996) Membrane pores induced by magainin. *Biochemistry* **35:** 13723-13728

Lutter M, Fang M, Luo X, Nishijima M, Xie X, Wang X (2000) Cardiolipin provides specificity for targeting of tBid to mitochondria. *Nature cell biology* **2:** 754-761

Lutter M, Perkins GA, Wang X (2001) The pro-apoptotic Bcl-2 family member tBid localizes to mitochondrial contact sites. *BMC cell biology* **2:** 22

Llambi F, Moldoveanu T, Tait SW, Bouchier-Hayes L, Temirov J, McCormick LL, Dillon CP, Green DR (2011) A unified model of mammalian BCL-2 protein family interactions at the mitochondria. *Molecular cell* **44:** 517-531

Ma S, Hockings C, Anwari K, Kratina T, Fennell S, Lazarou M, Ryan MT, Kluck RM, Dewson G (2013) Assembly of the Bak Apoptotic Pore: A CRITICAL ROLE FOR THE BAK PROTEIN alpha6 HELIX IN THE MULTIMERIZATION OF HOMODIMERS DURING APOPTOSIS. *The Journal of biological chemistry* **288:** 26027-26038

Mahadevan D, Spier C, Della Croce K, Miller S, George B, Riley C, Warner S, Grogan TM, Miller TP (2005) Transcript profiling in peripheral T-cell lymphoma, not otherwise specified, and diffuse large B-cell lymphoma identifies distinct tumor profile signatures. *Molecular cancer therapeutics* **4:** 1867-1879

Malorni W, Giammarioli AM, Garofalo T, Sorice M (2007) Dynamics of lipid raft components during lymphocyte apoptosis: the paradigmatic role of GD3. *Apoptosis : an international journal on programmed cell death* **12:** 941-949

Manara A, Lindsay J, Marchioretto M, Astegno A, Gilmore AP, Esposti MD, Crimi M (2009) Bid binding to negatively charged phospholipids may not be required for its pro-apoptotic activity in vivo. *Biochimica et biophysica acta* **1791:** 997-1010

Mandal T, Shin S, Aluvila S, Chen HC, Grieve C, Choe JY, Cheng EH, Hustedt EJ, Oh KJ (2016) Assembly of Bak homodimers into higher order homooligomers in the mitochondrial apoptotic pore. *Scientific reports* **6:** 30763

Mannella CA (2006a) The relevance of mitochondrial membrane topology to mitochondrial function. *Biochimica et biophysica acta* **1762:** 140-147

Mannella CA (2006b) Structure and dynamics of the mitochondrial inner membrane cristae. *Biochimica et biophysica acta* **1763:** 542-548

Mari M, Colell A, Morales A, Caballero F, Moles A, Fernandez A, Terrones O, Basanez G, Antonsson B, Garcia-Ruiz C, Fernandez-Checa JC (2008) Mechanism of mitochondrial glutathione-dependent hepatocellular susceptibility to TNF despite NF-kappaB activation. *Gastroenterology* **134:** 1507-1520

Marsh D (1996) Lateral pressure in membranes. *Biochimica et biophysica acta* **1286:** 183-223

Martinez-Abundis E, Correa F, Rodriguez E, Soria-Castro E, Rodriguez-Zavala JS, Pacheco-Alvarez D, Zazueta C (2011) A CRAC-like motif in BAX sequence: relationship with protein insertion and pore activity in liposomes. *Biochimica et biophysica acta* **1808:** 1888-1895

Martinez-Caballero S, Dejean LM, Kinnally MS, Oh KJ, Mannella CA, Kinnally KW (2009) Assembly of the mitochondrial apoptosis-induced channel, MAC. *The Journal of biological chemistry* **284:** 12235-12245

Martinou JC, Youle RJ (2011) Mitochondria in apoptosis: Bcl-2 family members and mitochondrial dynamics. *Developmental cell* **21:** 92-101

Matsuzaki K, Murase O, Fujii N, Miyajima K (1996) An antimicrobial peptide, magainin 2, induced rapid flip-flop of phospholipids coupled with pore formation and peptide translocation. *Biochemistry* **35:** 11361-11368

Mayer LD, Hope MJ, Cullis PR (1986) Vesicles of variable sizes produced by a rapid extrusion procedure. *Biochimica et biophysica acta* **858:** 161-168

McDonnell JM, Fushman D, Milliman CL, Korsmeyer SJ, Cowburn D (1999) **Solution structure of the proapoptotic molecule BID: a structural basis for apoptotic agonists and antagonists**. *Cell* **96:** 625-634

McIntosh TJ, Simon SA (2006) Roles of bilayer material properties in function and distribution of membrane proteins. *Annual review of biophysics and biomolecular structure* **35:** 177-198

Megyesi J, Tarcsafalvi A, Seng N, Hodeify R, Price PM (2016) Cdk2 phosphorylation of Bcl-xL after stress converts it to a pro-apoptotic protein mimicking Bax/Bak. *Cell death discovery* **2**

Menoret E, Gomez-Bougie P, Surget S, Trichet V, Oliver L, Pellat-Deceunynck C, Amiot M (2010) Mcl-1(128-350) fragment induces apoptosis through direct interaction with Bax. *FEBS letters* **584:** 487-492

Michels J, O'Neill JW, Dallman CL, Mouzakiti A, Habens F, Brimmell M, Zhang KY, Craig RW, Marcusson EG, Johnson PW, Packham G (2004) Mcl-1 is required for Akata6 B-lymphoma cell survival and is converted to a cell death molecule by efficient caspase-mediated cleavage. *Oncogene* **23:** 4818-4827

Mikhailov V, Mikhailova M, Pulkrabek DJ, Dong Z, Venkatachalam MA, Saikumar P (2001) Bcl-2 prevents Bax oligomerization in the mitochondrial outer membrane. *The Journal of biological chemistry* **276:** 18361-18374

Mileykovskaya E, Dowhan W (2000) Visualization of phospholipid domains in Escherichia coli by using the cardiolipin-specific fluorescent dye 10-N-nonyl acridine orange. *Journal of bacteriology* **182:** 1172-1175

Miura M (2011) Active participation of cell death in development and organismal homeostasis. *Development, growth & differentiation* **53:** 125-136

Modjtahedi N, Giordanetto F, Madeo F, Kroemer G (2006) Apoptosis-inducing factor: vital and lethal. *Trends in cell biology* **16:** 264-272

Moldoveanu T, Follis AV, Kriwacki RW, Green DR (2014) Many players in BCL-2 family affairs. *Trends in biochemical sciences* **39:** 101-111

Moldoveanu T, Grace CR, Llambi F, Nourse A, Fitzgerald P, Gehring K, Kriwacki RW, Green DR (2013) BID-induced structural changes in BAK promote apoptosis. *Nature structural & molecular biology*

Moldoveanu T, Liu Q, Tocilj A, Watson M, Shore G, Gehring K (2006) The X-ray structure of a BAK homodimer reveals an inhibitory zinc binding site. *Molecular cell* **24:** 677-688

Montero J, Mari M, Colell A, Morales A, Basanez G, Garcia-Ruiz C, Fernandez-Checa JC (2010) Cholesterol and peroxidized cardiolipin in mitochondrial membrane properties, permeabilization and cell death. *Biochimica et biophysica acta* **1797:** 1217-1224

Montero J, Morales A, Llacuna L, Lluis JM, Terrones O, Basanez G, Antonsson B, Prieto J, Garcia-Ruiz C, Colell A, Fernandez-Checa JC (2008) Mitochondrial cholesterol contributes to chemotherapy resistance in hepatocellular carcinoma. *Cancer research* **68:** 5246-5256

Montessuit S, Somasekharan SP, Terrones O, Lucken-Ardjomande S, Herzig S, Schwarzenbacher R, Manstein DJ, Bossy-Wetzel E, Basanez G, Meda P, Martinou JC (2010) Membrane remodeling induced by the dynamin-related protein Drp1 stimulates Bax oligomerization. *Cell* **142:** 889-901

Morales A, Lee H, Goni FM, Kolesnick R, Fernandez-Checa JC (2007) Sphingolipids and cell death. *Apoptosis : an international journal on programmed cell death* **12:** 923-939

Morgan RK, Kingham PJ, Walsh MT, Curran DR, Durcan N, McLean WG, Costello RW (2004) Eosinophil adhesion to cholinergic IMR-32 cells protects against induced neuronal apoptosis. *Journal of immunology* **173:** 5963-5970

Mouritsen OG (2011) Lipids, curvature, and nano-medicine. *European journal of lipid science and technology : EJLST* **113:** 1174-1187

Muchmore SW, Sattler M, Liang H, Meadows RP, Harlan JE, Yoon HS, Nettesheim D, Chang BS, Thompson CB, Wong SL, Ng SL, Fesik SW (1996) X-ray and NMR structure of human Bcl-xL, an inhibitor of programmed cell death. *Nature* **381:** 335-341

Munoz-Pinedo C (2012) Signaling pathways that regulate life and cell death: evolution of apoptosis in the context of self-defense. *Advances in experimental medicine and biology* **738:** 124-143

Munoz-Pinedo C, Guio-Carrion A, Goldstein JC, Fitzgerald P, Newmeyer DD, Green DR (2006) Different mitochondrial intermembrane space proteins are released during apoptosis in a manner that is coordinately

initiated but can vary in duration. *Proceedings of the National Academy of Sciences of the United States of America* **103:** 11573-11578

Nakagawa T, Shimizu S, Watanabe T, Yamaguchi O, Otsu K, Yamagata H, Inohara H, Kubo T, Tsujimoto Y (2005) Cyclophilin D-dependent mitochondrial permeability transition regulates some necrotic but not apoptotic cell death. *Nature* **434:** 652-658

Nasu Y, Benke A, Arakawa S, Yoshida GJ, Kawamura G, Manley S, Shimizu S, Ozawa T (2016) In Situ Characterization of Bak Clusters Responsible for Cell Death Using Single Molecule Localization Microscopy. *Scientific reports* **6:** 27505

Nechushtan A, Smith CL, Hsu YT, Youle RJ (1999) Conformation of the Bax C-terminus regulates subcellular location and cell death. *The EMBO journal* **18:** 2330-2341

Nechushtan A, Smith CL, Lamensdorf I, Yoon SH, Youle RJ (2001) Bax and Bak coalesce into novel mitochondria-associated clusters during apoptosis. *The Journal of cell biology* **153:** 1265-1276

Nehls S, Snapp EL, Cole NB, Zaal KJ, Kenworthy AK, Roberts TH, Ellenberg J, Presley JF, Siggia E, Lippincott-Schwartz J (2000) Dynamics and retention of misfolded proteins in native ER membranes. *Nature cell biology* **2:** 288-295

New RRC (1990) Liposomes, a practical approach. *IRL Press at Oxford University Press, Oxford*

Nieva JL, Goni FM, Alonso A (1989) Liposome fusion catalytically induced by phospholipase C. *Biochemistry* **28:** 7364-7367

Nishibori A, Kusaka J, Hara H, Umeda M, Matsumoto K (2005) Phosphatidylethanolamine domains and localization of phospholipid synthases in Bacillus subtilis membranes. *Journal of bacteriology* **187:** 2163-2174

O'Neill JW, Manion MK, Maguire B, Hockenbery DM (2006) BCL-XL dimerization by three-dimensional domain swapping. *Journal of molecular biology* **356:** 367-381

O'Neill KL, Huang K, Zhang J, Chen Y, Luo X (2016) Inactivation of prosurvival Bcl-2 proteins activates Bax/Bak through the outer mitochondrial membrane. *Genes & development* **30:** 973-988

Obeid LM, Linardic CM, Karolak LA, Hannun YA (1993) Programmed cell death induced by ceramide. *Science* **259:** 1769-1771

Oh KJ, Singh P, Lee K, Foss K, Lee S, Park M, Lee S, Aluvila S, Park M, Singh P, Kim RS, Symersky J, Walters DE (2010) Conformational changes in BAK, a pore-forming proapoptotic Bcl-2 family member, upon membrane insertion and direct evidence for the existence of BH3-BH3 contact interface in BAK homo-oligomers. *The Journal of biological chemistry* **285:** 28924-28937

Okada H, Suh WK, Jin J, Woo M, Du C, Elia A, Duncan GS, Wakeham A, Itie A, Lowe SW, Wang X, Mak TW (2002) Generation and characterization of Smac/DIABLO-deficient mice. *Molecular and cellular biology* **22:** 3509-3517

Opydo-Chanek M, Gonzalo O, Marzo I (2017a) Multifaceted anticancer activity of BH3 mimetics: Current evidence and future prospects. *Biochemical pharmacology* **136:** 12-23

Opydo-Chanek M, Rak A, Cierniak A, Mazur L (2017b) Combination of ABT-737 and resveratrol enhances DNA damage and apoptosis in human T-cell acute lymphoblastic leukemia MOLT-4 cells. *Toxicology in vitro : an international journal published in association with BIBRA* **42:** 38-46

Orlofsky A, Berger MS, Prystowsky MB (1991) Novel expression pattern of a new member of the MIP-1 family of cytokine-like genes. *Cell regulation* **2:** 403-412

Ortiz A, Killian JA, Verkleij AJ, Wilschut J (1999) Membrane fusion and the lamellar-to-inverted-hexagonal phase transition in cardiolipin vesicle systems induced by divalent cations. *Biophysical journal* **77:** 2003-2014

Osellame LD, Blacker TS, Duchen MR (2012) Cellular and molecular mechanisms of mitochondrial function. *Best practice & research Clinical endocrinology & metabolism* **26:** 711-723

Osman C, Voelker DR, Langer T (2011) Making heads or tails of phospholipids in mitochondria. *The Journal of cell biology* **192:** 7-16

Ostolaza H, Goni FM (1995) Interaction of the bacterial protein toxin alpha-haemolysin with model membranes: protein binding does not always lead to lytic activity. *FEBS letters* **371:** 303-306

Ott M, Robertson JD, Gogvadze V, Zhivotovsky B, Orrenius S (2002) Cytochrome c release from mitochondria proceeds by a two-step process. *Proceedings of the National Academy of Sciences of the United States of America* **99:** 1259-1263

Palsdottir H, Hunte C (2004) Lipids in membrane protein structures. *Biochimica et biophysica acta* **1666:** 2-18

Peng J, Lapolla SM, Zhang Z, Lin J (2009) The cytosolic domain of Bcl-2 forms small pores in model mitochondrial outer membrane after acidic pH-induced membrane association. *Sheng wu yi xue gong cheng xue za zhi = Journal of biomedical engineering = Shengwu yixue gongchengxue zazhi* **26:** 130-137

Peng J, Tan C, Roberts GJ, Nikolaeva O, Zhang Z, Lapolla SM, Primorac S, Andrews DW, Lin J (2006) tBid elicits a conformational alteration in membrane-bound Bcl-2 such that it inhibits Bax pore formation. *The Journal of biological chemistry* **281:** 35802-35811

Petit PX, Dupaigne P, Pariselli F, Gonzalvez F, Etienne F, Rameau C, Bernard S (2009) Interaction of the alpha-helical H6 peptide from the pro-apoptotic protein tBid with cardiolipin. *The FEBS journal* **276:** 6338-6354

Petit PX, Lecoeur H, Zorn E, Dauguet C, Mignotte B, Gougeon ML (1995) Alterations in mitochondrial structure and function are early events of dexamethasone-induced thymocyte apoptosis. *The Journal of cell biology* **130:** 157-167

Petros AM, Nettesheim DG, Wang Y, Olejniczak ET, Meadows RP, Mack J, Swift K, Matayoshi ED, Zhang H, Thompson CB, Fesik SW (2000) Rationale for Bcl-xL/Bad peptide complex formation from structure, mutagenesis, and biophysical studies. *Protein science : a publication of the Protein Society* **9:** 2528-2534

Petros AM, Olejniczak ET, Fesik SW (2004) Structural biology of the Bcl-2 family of proteins. *Biochimica et biophysica acta* **1644:** 83-94

Peyerl FW, Dai S, Murphy GA, Crawford F, White J, Marrack P, Kappler JW (2007) Elucidation of some Bax conformational changes through crystallization of an antibody-peptide complex. *Cell death and differentiation* **14:** 447-452

Phair RD, Misteli T (2000) High mobility of proteins in the mammalian cell nucleus. *Nature* **404:** 604-609

Pinchuk I, Schnitzer E, Lichtenberg D (1998) Kinetic analysis of copper-induced peroxidation of LDL. *Biochimica et biophysica acta* **1389:** 155-172

Piva R, Pellegrino E, Mattioli M, Agnelli L, Lombardi L, Boccalatte F, Costa G, Ruggeri BA, Cheng M, Chiarle R, Palestro G, Neri A, Inghirami G (2006) Functional validation of the anaplastic lymphoma kinase signature identifies CEBPB and BCL2A1 as critical target genes. *The Journal of clinical investigation* **116:** 3171-3182

Placzek WJ, Wei J, Kitada S, Zhai D, Reed JC, Pellecchia M (2010) A survey of the anti-apoptotic Bcl-2 subfamily expression in cancer types provides a platform to predict the efficacy of Bcl-2 antagonists in cancer therapy. *Cell death & disease* **1:** e40

Plati J, Bucur O, Khosravi-Far R (2011) Apoptotic cell signaling in cancer progression and therapy. *Integrative biology : quantitative biosciences from nano to macro* **3:** 279-296

Polster BM, Basanez G, Etxebarria A, Hardwick JM, Nicholls DG (2005) Calpain I induces cleavage and release of apoptosis-inducing factor from isolated mitochondria. *The Journal of biological chemistry* **280:** 6447-6454

Pritz JR, Wachter F, Lee S, Luccarelli J, Wales TE, Cohen DT, Coote P, Heffron GJ, Engen JR, Massefski W, Walensky LD (2017) Allosteric sensitization of proapoptotic BAX. *Nature chemical biology* **13:** 961-967

Puthalakath H, Huang DC, O'Reilly LA, King SM, Strasser A (1999) The proapoptotic activity of the Bcl-2 family member Bim is regulated by interaction with the dynein motor complex. *Molecular cell* **3:** 287-296

Puthalakath H, Villunger A, O'Reilly LA, Beaumont JG, Coultas L, Cheney RE, Huang DC, Strasser A (2001) Bmf: a proapoptotic BH3-only protein regulated by interaction with the myosin V actin motor complex, activated by anoikis. *Science* **293:** 1829-1832

Qi B, Hardwick JM (2008) Bcl-2 turns deadly. *Nature chemical biology* **4:** 722-723

Qian S, Wang W, Yang L, Huang HW (2008a) Structure of the alamethicin pore reconstructed by x-ray diffraction analysis. *Biophysical journal* **94:** 3512-3522

Qian S, Wang W, Yang L, Huang HW (2008b) Structure of transmembrane pore induced by Bax-derived peptide: evidence for lipidic pores. *Proceedings of the National Academy of Sciences of the United States of America* **105:** 17379-17383

Ramachandran R, Heuck AP, Tweten RK, Johnson AE (2002) Structural insights into the membrane-anchoring mechanism of a cholesterol-dependent cytolysin. *Nature structural biology* **9:** 823-827

Ramachandran R, Schmid SL (2008) Real-time detection reveals that effectors couple dynamin's GTP-dependent conformational changes to the membrane. *The EMBO journal* **27:** 27-37

Rautureau GJ, Yabal M, Yang H, Huang DC, Kvansakul M, Hinds MG (2012) The restricted binding repertoire of Bcl-B leaves Bim as the universal BH3-only prosurvival Bcl-2 protein antagonist. *Cell death & disease* **3:** e443

Reeves JP, Dowben RM (1969) Formation and properties of thin-walled phospholipid vesicles. *Journal of cellular physiology* **73:** 49-60

Rehm M, Dussmann H, Prehn JH (2003) Real-time single cell analysis of Smac/DIABLO release during apoptosis. *The Journal of cell biology* **162:** 1031-1043

Reichert AS, Neupert W (2002) Contact sites between the outer and inner membrane of mitochondria-role in protein transport. *Biochimica et biophysica acta* **1592:** 41-49

Ries J, Petrasek Z, García-Sáez A, Schwille P (2010) A Comprehensive Framework for Fluorescence Cross-Correlation Spectroscopy. *New Journal of Physics* **12:** 113009 (113032pp)

Ries J, Yu SR, Burkhardt M, Brand M, Schwille P (2009) Modular scanning FCS quantifies receptor-ligand interactions in living multicellular organisms. *Nature methods* **6:** 643-645

Rippo MR, Malisan F, Ravagnan L, Tomassini B, Condo I, Costantini P, Susin SA, Rufini A, Todaro M, Kroemer G, Testi R (2000) GD3 ganglioside directly targets mitochondria in a bcl-2-controlled fashion. *FASEB journal : official publication of the Federation of American Societies for Experimental Biology* **14:** 2047-2054

Rizzuto R, Pinton P, Carrington W, Fay FS, Fogarty KE, Lifshitz LM, Tuft RA, Pozzan T (1998) Close contacts with the endoplasmic reticulum as determinants of mitochondrial Ca2+ responses. *Science* **280:** 1763-1766

Roucou X, Rostovtseva T, Montessuit S, Martinou JC, Antonsson B (2002) Bid induces cytochrome c-impermeable Bax channels in liposomes. *The Biochemical journal* **363:** 547-552

Saelens X, Festjens N, Vande Walle L, van Gurp M, van Loo G, Vandenabeele P (2004) Toxic proteins released from mitochondria in cell death. *Oncogene* **23:** 2861-2874

Saito M, Korsmeyer SJ, Schlesinger PH (2000) **BAX-dependent transport of cytochrome c reconstituted in pure liposomes**. *Nature cell biology* **2:** 553-555

Saksena S, Wahlman J, Teis D, Johnson AE, Emr SD (2009) Functional reconstitution of ESCRT-III assembly and disassembly. *Cell* **136:** 97-109

Salvador-Gallego R, Mund M, Cosentino K, Schneider J, Unsay J, Schraermeyer U, Engelhardt J, Ries J, Garcia-Saez AJ (2016) Bax assembly into rings and arcs in apoptotic mitochondria is linked to membrane pores. *The EMBO journal* **35:** 389-401

Sandra F, Degli Esposti M, Ndebele K, Gona P, Knight D, Rosenquist M, Khosravi-Far R (2005) Tumor necrosis factor-related apoptosis-inducing ligand alters mitochondrial membrane lipids. *Cancer research* **65:** 8286-8297

Sattler M, Liang H, Nettesheim D, Meadows RP, Harlan JE, Eberstadt M, Yoon HS, Shuker SB, Chang BS, Minn AJ, Thompson CB, Fesik SW (1997) Structure of Bcl-xL-Bak peptide complex: recognition between regulators of apoptosis. *Science* **275:** 983-986

Scaffidi C, Fulda S, Srinivasan A, Friesen C, Li F, Tomaselli KJ, Debatin KM, Krammer PH, Peter ME (1998) Two CD95 (APO-1/Fas) signaling pathways. *The EMBO journal* **17:** 1675-1687

Scorrano L, Ashiya M, Buttle K, Weiler S, Oakes SA, Mannella CA, Korsmeyer SJ (2002) A distinct pathway remodels mitochondrial cristae and mobilizes cytochrome c during apoptosis. *Developmental cell* **2:** 55-67

Schafer B, Quispe J, Choudhary V, Chipuk JE, Ajero TG, Du H, Schneiter R, Kuwana T (2009) Mitochondrial outer membrane proteins assist Bid in Bax-mediated lipidic pore formation. *Molecular biology of the cell* **20:** 2276-2285

Schellenberg B, Wang P, Keeble JA, Rodriguez-Enriquez R, Walker S, Owens TW, Foster F, Tanianis-Hughes J, Brennan K, Streuli CH, Gilmore AP (2013) Bax exists in a dynamic equilibrium between the cytosol and mitochondria to control apoptotic priming. *Molecular cell* **49:** 959-971

Schenk RL, Tuzlak S, Carrington EM, Zhan Y, Heinzel S, Teh CE, Gray DH, Tai L, Lew AM, Villunger A, Strasser A, Herold MJ (2017) Characterisation of mice lacking all functional isoforms of the pro-survival BCL-2 family member A1 reveals minor defects in the haematopoietic compartment. *Cell death and differentiation* **24:** 534-545

Schinzel A, Kaufmann T, Borner C (2004) Bcl-2 family members: integrators of survival and death signals in physiology and pathology [corrected]. *Biochimica et biophysica acta* **1644:** 95-105

Schlame M (2008) Cardiolipin synthesis for the assembly of bacterial and mitochondrial membranes. *Journal of lipid research* **49:** 1607-1620

Schlame M, Ren M (2006) Barth syndrome, a human disorder of cardiolipin metabolism. *FEBS letters* **580:** 5450-5455

Schlame M, Ren M (2009) The role of cardiolipin in the structural organization of mitochondrial membranes. *Biochimica et biophysica acta* **1788:** 2080-2083

Schlame M, Rua D, Greenberg ML (2000) The biosynthesis and functional role of cardiolipin. *Progress in lipid research* **39:** 257-288

Schlattner U, Tokarska-Schlattner M, Ramirez S, Tyurina YY, Amoscato AA, Mohammadyani D, Huang Z, Jiang J, Yanamala N, Seffouh A, Boissan M, Epand RF, Epand RM, Klein-Seetharaman J, Lacombe ML, Kagan VE (2013) Dual function of mitochondrial Nm23-H4 protein in phosphotransfer and intermembrane lipid transfer: a cardiolipin-dependent switch. *The Journal of biological chemistry* **288:** 111-121

Schnitzer E, Pinchuk I, Bor A, Fainaru M, Samuni AM, Lichtenberg D (1998) Lipid oxidation in unfractionated serum and plasma. *Chemistry and physics of lipids* **92:** 151-170

Schnitzer E, Pinchuk I, Lichtenberg D (2007) Peroxidation of liposomal lipids. *European biophysics journal : EBJ* **36:** 499-515

Schon P, Garcia-Saez AJ, Malovrh P, Bacia K, Anderluh G, Schwille P (2008) Equinatoxin II permeabilizing activity depends on the presence of sphingomyelin and lipid phase coexistence. *Biophysical journal* **95:** 691-698

Schug ZT, Gottlieb E (2009) Cardiolipin acts as a mitochondrial signalling platform to launch apoptosis. *Biochimica et biophysica acta* **1788:** 2022-2031

Schwille P (2001) Fluorescence correlation spectroscopy and its potential for intracellular applications. *Cell biochemistry and biophysics* **34:** 383-408

Selzner M, Bielawska A, Morse MA, Rudiger HA, Sindram D, Hannun YA, Clavien PA (2001) Induction of apoptotic cell death and prevention of tumor growth by ceramide analogues in metastatic human colon cancer. *Cancer research* **61:** 1233-1240

Semisotnov GV, Rodionova NA, Razgulyaev OI, Uversky VN, Gripas AF, Gilmanshin RI (1991) Study of the "molten globule" intermediate state in protein folding by a hydrophobic fluorescent probe. *Biopolymers* **31:** 119-128

Shamas-Din A, Kale J, Leber B, Andrews DW (2013) Mechanisms of action of Bcl-2 family proteins. *Cold Spring Harbor perspectives in biology* **5:** a008714

Shepard LA, Heuck AP, Hamman BD, Rossjohn J, Parker MW, Ryan KR, Johnson AE, Tweten RK (1998) Identification of a membrane-spanning domain of the thiol-activated pore-forming toxin Clostridium perfringens perfringolysin O: an alpha-helical to beta-sheet transition identified by fluorescence spectroscopy. *Biochemistry* **37:** 14563-14574

Shim YH, Byun EK, Lee MJ, Huh J, Kim CW (2000) Anti-apoptotic role of Bfl-1 in staurosporine-treated B-lymphoblastic cells. *International journal of hematology* **72:** 484-490

Simbeni R, Pon L, Zinser E, Paltauf F, Daum G (1991) Mitochondrial membrane contact sites of yeast. Characterization of lipid components and possible involvement in intramitochondrial translocation of phospholipids. *The Journal of biological chemistry* **266:** 10047-10049

Simonen M, Keller H, Heim J (1997) The BH3 domain of Bax is sufficient for interaction of Bax with itself and with other family members and it is required for induction of apoptosis. *European journal of biochemistry* **249:** 85-91

Siskind LJ (2005) Mitochondrial ceramide and the induction of apoptosis. *Journal of bioenergetics and biomembranes* **37:** 143-153

Siskind LJ, Kolesnick RN, Colombini M (2002) Ceramide channels increase the permeability of the mitochondrial outer membrane to small proteins. *The Journal of biological chemistry* **277:** 26796-26803

Siskind LJ, Mullen TD, Romero Rosales K, Clarke CJ, Hernandez-Corbacho MJ, Edinger AL, Obeid LM (2010) The BCL-2 protein BAK is required for long-chain ceramide generation during apoptosis. *The Journal of biological chemistry* **285:** 11818-11826

Smith PK, Krohn RI, Hermanson GT, Mallia AK, Gartner FH, Provenzano MD, Fujimoto EK, Goeke NM, Olson BJ, Klenk DC (1985) Measurement of protein using bicinchoninic acid. *Analytical biochemistry* **150:** 76-85

Smits C, Czabotar PE, Hinds MG, Day CL (2008) Structural plasticity underpins promiscuous binding of the prosurvival protein A1. *Structure* **16:** 818-829

Snider C, Jayasinghe S, Hristova K, White SH (2009) MPEx: a tool for exploring membrane proteins. *Protein science : a publication of the Protein Society* **18:** 2624-2628

Soloaga A, Ramirez JM, Goni FM (1998) Reversible denaturation, self-aggregation, and membrane activity of Escherichia coli alpha-hemolysin, a protein stable in 6 M urea. *Biochemistry* **37:** 6387-6393

Sorice M, Manganelli V, Matarrese P, Tinari A, Misasi R, Malorni W, Garofalo T (2009) Cardiolipin-enriched raft-like microdomains are essential activating platforms for apoptotic signals on mitochondria. *FEBS letters* **583:** 2447-2450

Sreerama N, Woody RW (2004a) Computation and analysis of protein circular dichroism spectra. *Methods in enzymology* **383:** 318-351

Sreerama N, Woody RW (2004b) On the analysis of membrane protein circular dichroism spectra. *Protein science : a publication of the Protein Society* **13:** 100-112

Steringer JP, Bleicken S, Andreas H, Zacherl S, Laussmann M, Temmerman K, Contreras FX, Bharat TA, Lechner J, Muller HM, Briggs JA, Garcia-Saez AJ, Nickel W (2012) Phosphatidylinositol 4,5-bisphosphate (PI(4,5)P2)-dependent oligomerization of fibroblast growth factor 2 (FGF2) triggers the formation of a lipidic membrane pore implicated in unconventional secretion. *The Journal of biological chemistry* **287:** 27659-27669

Stiban J, Fistere D, Colombini M (2006) Dihydroceramide hinders ceramide channel formation: Implications on apoptosis. *Apoptosis : an international journal on programmed cell death* **11:** 773-780

Stone SJ, Vance JE (2000) Phosphatidylserine synthase-1 and -2 are localized to mitochondria-associated membranes. *The Journal of biological chemistry* **275:** 34534-34540

Strasser A, Cory S, Adams JM (2011) Deciphering the rules of programmed cell death to improve therapy of cancer and other diseases. *The EMBO journal* **30:** 3667-3683

Strauss JF, 3rd, Kishida T, Christenson LK, Fujimoto T, Hiroi H (2003) START domain proteins and the intracellular trafficking of cholesterol in steroidogenic cells. *Molecular and cellular endocrinology* **202:** 59-65

Subburaj Y, Cosentino K, Axmann M, Pedrueza-Villalmanzo E, Hermann E, Bleicken S, Spatz J, Garcia-Saez AJ (2015) Bax monomers form dimer units in the membrane that further self-assemble into multiple oligomeric species. *Nature communications* **6:** 8042

Sung TC, Li CY, Lai YC, Hung CL, Shih O, Yeh YQ, Jeng US, Chiang YW (2015) Solution Structure of Apoptotic BAX Oligomer: Oligomerization Likely Precedes Membrane Insertion. *Structure* **23:** 1878-1888

Susin SA, Lorenzo HK, Zamzami N, Marzo I, Snow BE, Brothers GM, Mangion J, Jacotot E, Costantini P, Loeffler M, Larochette N, Goodlett DR, Aebersold R, Siderovski DP, Penninger JM, Kroemer G (1999) Molecular characterization of mitochondrial apoptosis-inducing factor. *Nature* **397:** 441-446

Suzuki M, Youle RJ, Tjandra N (2000) Structure of Bax: coregulation of dimer formation and intracellular localization. *Cell* **103:** 645-654

Szegezdi E, Logue SE, Gorman AM, Samali A (2006) Mediators of endoplasmic reticulum stress-induced apoptosis. *EMBO reports* **7:** 880-885

Tait SW, Parsons MJ, Llambi F, Bouchier-Hayes L, Connell S, Munoz-Pinedo C, Green DR (2010) Resistance to caspase-independent cell death requires persistence of intact mitochondria. *Developmental cell* **18:** 802-813

Tamba Y, Yamazaki M (2009) Magainin 2-induced pore formation in the lipid membranes depends on its concentration in the membrane interface. *The journal of physical chemistry B* **113:** 4846-4852

Tamura Y, Endo T, Iijima M, Sesaki H (2009) Ups1p and Ups2p antagonistically regulate cardiolipin metabolism in mitochondria. *The Journal of cell biology* **185:** 1029-1045

Terrones O, Antonsson B, Yamaguchi H, Wang HG, Liu J, Lee RM, Herrmann A, Basanez G (2004) Lipidic pore formation by the concerted action of proapoptotic BAX and tBID. *The Journal of biological chemistry* **279:** 30081-30091

Terrones O, Etxebarria A, Landajuela A, Landeta O, Antonsson B, Basanez G (2008) BIM and tBID are not mechanistically equivalent when assisting BAX to permeabilize bilayer membranes. *The Journal of biological chemistry* **283:** 7790-7803

Thomas LW, Lam C, Clark RE, White MR, Spiller DG, Moots RJ, Edwards SW (2012) Serine 162, an essential residue for the mitochondrial localization, stability and anti-apoptotic function of Mcl-1. *PloS one* **7:** e45088

Thuduppathy GR, Craig JW, Kholodenko V, Schon A, Hill RB (2006a) Evidence that membrane insertion of the cytosolic domain of Bcl-xL is governed by an electrostatic mechanism. *Journal of molecular biology* **359:** 1045-1058

Thuduppathy GR, Terrones O, Craig JW, Basanez G, Hill RB (2006b) The N-terminal domain of Bcl-xL reversibly binds membranes in a pH-dependent manner. *Biochemistry* **45:** 14533-14542

Tilley SJ, Orlova EV, Gilbert RJ, Andrew PW, Saibil HR (2005) Structural basis of pore formation by the bacterial toxin pneumolysin. *Cell* **121:** 247-256

Todt F, Cakir Z, Reichenbach F, Emschermann F, Lauterwasser J, Kaiser A, Ichim G, Tait SW, Frank S, Langer HF, Edlich F (2015) Differential retrotranslocation of mitochondrial Bax and Bak. *The EMBO journal* **34:** 67-80

Todt F, Cakir Z, Reichenbach F, Youle RJ, Edlich F (2013) The C-terminal helix of Bcl-x(L) mediates Bax retrotranslocation from the mitochondria. *Cell death and differentiation* **20:** 333-342

Tsujimoto Y, Nakagawa T, Shimizu S (2006) Mitochondrial membrane permeability transition and cell death. *Biochimica et biophysica acta* **1757:** 1297-1300

Tuzlak S, Schenk RL, Vasanthakumar A, Preston SP, Haschka MD, Zotos D, Kallies A, Strasser A, Villunger A, Herold MJ (2017) The BCL-2 pro-survival protein A1 is dispensable for T cell homeostasis on viral infection. *Cell death and differentiation* **24:** 523-533

Tyurin VA, Tyurina YY, Osipov AN, Belikova NA, Basova LV, Kapralov AA, Bayir H, Kagan VE (2007) Interactions of cardiolipin and lyso-cardiolipins with cytochrome c and tBid: conflict or assistance in apoptosis. *Cell death and differentiation* **14:** 872-875

Ugarte-Uribe B, Garcia-Saez AJ (2017) Apoptotic foci at mitochondria: in and around Bax pores. *Philosophical transactions of the Royal Society of London Series B, Biological sciences* **372**

Unsay JD, Cosentino K, Subburaj Y, Garcia-Saez AJ (2013) Cardiolipin effects on membrane structure and dynamics. *Langmuir : the ACS journal of surfaces and colloids* **29:** 15878-15887

Uren RT, O'Hely M, Iyer S, Bartolo R, Shi MX, Brouwer JM, Alsop AE, Dewson G, Kluck RM (2017) Disordered clusters of Bak dimers rupture mitochondria during apoptosis. *eLife* **6**

Valcarcel CA, Dalla Serra M, Potrich C, Bernhart I, Tejuca M, Martinez D, Pazos F, Lanio ME, Menestrina G (2001) Effects of lipid composition on membrane permeabilization by sticholysin I and II, two cytolysins of the sea anemone Stichodactyla helianthus. *Biophysical journal* **80:** 2761-2774

Valentijn AJ, Upton JP, Bates N, Gilmore AP (2008) Bax targeting to mitochondria occurs via both tail anchor-dependent and -independent mechanisms. *Cell death and differentiation* **15:** 1243-1254

Valero JG, Cornut-Thibaut A, Juge R, Debaud AL, Gimenez D, Gillet G, Bonnefoy-Berard N, Salgado J, Salles G, Aouacheria A, Kucharczak J (2012) micro-Calpain conversion of antiapoptotic Bfl-1 (BCL2A1) into a prodeath factor reveals two distinct alpha-helices inducing mitochondria-mediated apoptosis. *PloS one* **7:** e38620

Valero JG, Sancey L, Kucharczak J, Guillemin Y, Gimenez D, Prudent J, Gillet G, Salgado J, Coll JL, Aouacheria A (2011) Bax-derived membrane-active peptides act as potent and direct inducers of apoptosis in cancer cells. *Journal of cell science* **124:** 556-564

Van Brocklyn JR, Williams JB (2012) The control of the balance between ceramide and sphingosine-1-phosphate by sphingosine kinase: oxidative stress and the seesaw of cell survival and death. *Comparative biochemistry and physiology Part B, Biochemistry & molecular biology* **163:** 26-36

van Meer G, Voelker DR, Feigenson GW (2008) Membrane lipids: where they are and how they behave. *Nature reviews Molecular cell biology* **9:** 112-124

Vance JE (1990) Phospholipid synthesis in a membrane fraction associated with mitochondria. *The Journal of biological chemistry* **265:** 7248-7256

Vela L, Gonzalo O, Naval J, Marzo I (2013) Direct interaction of Bax and Bak proteins with Bcl-2 homology domain 3 (BH3)-only proteins in living cells revealed by fluorescence complementation. *The Journal of biological chemistry* **288:** 4935-4946

Vela L, Marzo I (2015) Bcl-2 family of proteins as drug targets for cancer chemotherapy: the long way of BH3 mimetics from bench to bedside. *Current opinion in pharmacology* **23:** 74-81

Vogler M (2012) BCL2A1: the underdog in the BCL2 family. *Cell death and differentiation* **19:** 67-74

Walensky LD (2013) Direct BAKtivation. *Nature structural & molecular biology* **20:** 536-538

Walensky LD, Gavathiotis E (2011) BAX unleashed: the biochemical transformation of an inactive cytosolic monomer into a toxic mitochondrial pore. *Trends in biochemical sciences* **36:** 642-652

Wang CY, Guttridge DC, Mayo MW, Baldwin AS, Jr. (1999) NF-kappaB induces expression of the Bcl-2 homologue A1/Bfl-1 to preferentially suppress chemotherapy-induced apoptosis. *Molecular and cellular biology* **19:** 5923-5929

Wang K, Yin XM, Chao DT, Milliman CL, Korsmeyer SJ (1996) BID: a novel BH3 domain-only death agonist. *Genes & development* **10:** 2859-2869

Weber K, Harper N, Schwabe J, Cohen GM (2013) BIM-Mediated Membrane Insertion of the BAK Pore Domain Is an Essential Requirement for Apoptosis. *Cell reports*

Wei MC, Lindsten T, Mootha VK, Weiler S, Gross A, Ashiya M, Thompson CB, Korsmeyer SJ (2000) tBID, a membrane-targeted death ligand, oligomerizes BAK to release cytochrome c. *Genes & development* **14:** 2060-2071

Westphal D, Dewson G, Czabotar PE, Kluck RM (2011) Molecular biology of Bax and Bak activation and action. *Biochimica et biophysica acta* **1813:** 521-531

Westphal D, Dewson G, Menard M, Frederick P, Iyer S, Bartolo R, Gibson L, Czabotar PE, Smith BJ, Adams JM, Kluck RM (2014a) Apoptotic pore formation is associated with in-plane insertion of Bak or Bax central helices into the mitochondrial outer membrane. *Proceedings of the National Academy of Sciences of the United States of America* **111:** E4076-4085

Westphal D, Kluck RM, Dewson G (2014b) Building blocks of the apoptotic pore: how Bax and Bak are activated and oligomerize during apoptosis. *Cell death and differentiation* **21:** 196-205

Whelan RS, Kaplinskiy V, Kitsis RN (2010) Cell death in the pathogenesis of heart disease: mechanisms and significance. *Annual review of physiology* **72:** 19-44

Whelan RS, Konstantinidis K, Wei AC, Chen Y, Reyna DE, Jha S, Yang Y, Calvert JW, Lindsten T, Thompson CB, Crow MT, Gavathiotis E, Dorn GW, 2nd, O'Rourke B, Kitsis RN (2012) Bax regulates primary necrosis through mitochondrial dynamics. *Proceedings of the National Academy of Sciences of the United States of America* **109:** 6566-6571

White J, Stelzer E (1999) Photobleaching GFP reveals protein dynamics inside live cells. *Trends in cell biology* **9:** 61-65

Wilfling F, Weber A, Potthoff S, Vogtle FN, Meisinger C, Paschen SA, Hacker G (2012) BH3-only proteins are tail-anchored in the outer mitochondrial membrane and can initiate the activation of Bax. *Cell death and differentiation* **19:** 1328-1336

Wilson-Annan J, O'Reilly LA, Crawford SA, Hausmann G, Beaumont JG, Parma LP, Chen L, Lackmann M, Lithgow T, Hinds MG, Day CL, Adams JM, Huang DC (2003) Proapoptotic BH3-only proteins trigger membrane integration of prosurvival Bcl-w and neutralize its activity. *The Journal of cell biology* **162:** 877-887

Willis SN, Chen L, Dewson G, Wei A, Naik E, Fletcher JI, Adams JM, Huang DC (2005) Proapoptotic Bak is sequestered by Mcl-1 and Bcl-xL, but not Bcl-2, until displaced by BH3-only proteins. *Genes & development* **19:** 1294-1305

Xiang Z, Ahmed AA, Moller C, Nakayama K, Hatakeyama S, Nilsson G (2001) Essential role of the prosurvival bcl-2 homologue A1 in mast cell survival after allergic activation. *The Journal of experimental medicine* **194:** 1561-1569

Xu XP, Zhai D, Kim E, Swift M, Reed JC, Volkmann N, Hanein D (2013) Three-dimensional structure of Bax-mediated pores in membrane bilayers. *Cell death & disease* **4:** e683

Yang L, Harroun TA, Weiss TM, Ding L, Huang HW (2001) Barrel-stave model or toroidal model? A case study on melittin pores. *Biophysical journal* **81:** 1475-1485

Yethon JA, Epand RF, Leber B, Epand RM, Andrews DW (2003) Interaction with a membrane surface triggers a reversible conformational change in Bax normally associated with induction of apoptosis. *The Journal of biological chemistry* **278:** 48935-48941

Yeung T, Terebiznik M, Yu L, Silvius J, Abidi WM, Philips M, Levine T, Kapus A, Grinstein S (2006) Receptor activation alters inner surface potential during phagocytosis. *Science* **313:** 347-351

Youle RJ, Strasser A (2008) The BCL-2 protein family: opposing activities that mediate cell death. *Nature reviews Molecular cell biology* **9:** 47-59

Zamzami N, Marchetti P, Castedo M, Decaudin D, Macho A, Hirsch T, Susin SA, Petit PX, Mignotte B, Kroemer G (1995) Sequential reduction of mitochondrial transmembrane potential and generation of reactive oxygen species in early programmed cell death. *The Journal of experimental medicine* **182:** 367-377

Zemel A, Ben-Shaul A, May S (2008) Modulation of the spontaneous curvature and bending rigidity of lipid membranes by interfacially adsorbed amphipathic peptides. *The journal of physical chemistry B* **112:** 6988-6996

Zhang T, Barclay L, Walensky LD, Saghatelian A (2015) Regulation of mitochondrial ceramide distribution by members of the BCL-2 family. *Journal of lipid research* **56:** 1501-1510

Zhang T, Saghatelian A (2013) Emerging roles of lipids in BCL-2 family-regulated apoptosis. *Biochimica et biophysica acta* **1831:** 1542-1554

Zhang Z, Lapolla SM, Annis MG, Truscott M, Roberts GJ, Miao Y, Shao Y, Tan C, Peng J, Johnson AE, Zhang XC, Andrews DW, Lin J (2004) Bcl-2 homodimerization involves two distinct binding surfaces, a topographic arrangement that provides an effective mechanism for Bcl-2 to capture activated Bax. *The Journal of biological chemistry* **279:** 43920-43928

Zhang Z, Subramaniam S, Kale J, Liao C, Huang B, Brahmbhatt H, Condon SG, Lapolla SM, Hays FA, Ding J, He F, Zhang XC, Li J, Senes A, Andrews DW, Lin J (2016) BH3-in-groove dimerization initiates and helix 9 dimerization expands Bax pore assembly in membranes. *The EMBO journal* **35:** 208-236

Zhang Z, Zhu W, Lapolla SM, Miao Y, Shao Y, Falcone M, Boreham D, McFarlane N, Ding J, Johnson AE, Zhang XC, Andrews DW, Lin J (2010) Bax forms an oligomer via separate, yet interdependent, surfaces. *The Journal of biological chemistry* **285:** 17614-17627

Zhao H, Kinnunen PK (2002) Binding of the antimicrobial peptide temporin L to liposomes assessed by Trp fluorescence. *The Journal of biological chemistry* **277:** 25170-25177

Zhou L, Chang DC (2008) Dynamics and structure of the Bax-Bak complex responsible for releasing mitochondrial proteins during apoptosis. *Journal of cell science* **121:** 2186-2196

Zhou LL, Zhou LY, Luo KQ, Chang DC (2005) Smac/DIABLO and cytochrome c are released from mitochondria through a similar mechanism during UV-induced apoptosis. *Apoptosis : an international journal on programmed cell death* **10:** 289-299

Zhu W, Cowie A, Wasfy GW, Penn LZ, Leber B, Andrews DW (1996) Bcl-2 mutants with restricted subcellular location reveal spatially distinct pathways for apoptosis in different cell types. *The EMBO journal* **15:** 4130-4141

Zong WX, Edelstein LC, Chen C, Bash J, Gelinas C (1999) The prosurvival Bcl-2 homolog Bfl-1/A1 is a direct transcriptional target of NF-kappaB that blocks TNFalpha-induced apoptosis. *Genes & development* **13:** 382-387

Zong WX, Lindsten T, Ross AJ, MacGregor GR, Thompson CB (2001) BH3-only proteins that bind pro-survival Bcl-2 family members fail to induce apoptosis in the absence of Bax and Bak. *Genes & development* **15:** 1481-1486

Zou H, Henzel WJ, Liu X, Lutschg A, Wang X (1997) Apaf-1, a human protein homologous to C. elegans CED-4, participates in cytochrome c-dependent activation of caspase-3. *Cell* **90:** 405-413